Earthquake Swarm Studies in the Central Rio Grande Rift: Specific and General Results

by

Robert S. Balch

Submitted in Partial Fulfillment of

the Requirements for the Degree of

Doctor of Philosophy

New Mexico Institute of Mining and Technology

Socorro, New Mexico, 87801

April, 1997

Preface

My dissertation project has covered two major topics: first, the use of reflection phases on microearthquake swarms to map the geographic extent of an inflating midcrustal magma body beneath the central Rio Grande rift; and second, the determination of the spatial, temporal and faulting characteristics of several significant earthquakes sequences in the crust overlying the midcrustal magma body. The two topics are loosely related since an accurate description of the midcrustal magma body is essential to understanding the concentration of earthquake activity in the Socorro area and the swarm type earthquake sequences which have occurred. In this dissertation I have dealt with the two research topics separately and as a result this paper is in two parts. Part I is the transcript of a published paper [*Balch et al.*, 1997] and describes the research pertaining to the lateral extent of the midcrustal magma body. Part II contains the results of my research on significant earthquake sequences and their relationship to the tectonics of central New Mexico.

Acknowledgments

A number of individuals have contributed to the success of this study. First, my advisor, Allan Sanford. His extensive knowledge and our numerous constructive dialogues were indispensable. Further discussions with my other committee members Rick Aster, Larry Teufel, Steve Cather and Al Smoake have led to a more complete dissertation. I thank Hans Hartse for the use of his inverse package **SEISMOS**, which has revolutionized earthquake studies at New Mexico Tech. I also thank Kuo-wan Lin, Mitch Withers and other Geophysics graduate students for numerous productive discussions related to this study. Many of the figures in this dissertation were produced using the XMAP8 GIS software [*Lees*, 1995] and the majority of the data used in this study was accumulated with support from the Los Alamos National Laboratory Institute of Geophysics and Planetary Physics (IGPP), grants 349 and 349R.

For the first part of this dissertation, which is the transcript of a published paper, I would like to acknowledge the contributions of the co-authors - Hans Hartse, Allan Sanford and Kuo-wan Lin. The paper benefitted from careful reviews and helpful comments by Tom Brocher and Larry Brown.

The completion of this course of study was due in no small part to the patience and understanding of my wife, Darlene.

Table of Contents

List of Figures

Part I: New Map of the Socorro Magma Body

Part II: Analysis of Microearthquake Swarms

List of Tables

Part II: New Map of The Socorro Magma Body

Part I

New Map of the Socorro Magma Body

Abstract

For 35 years, strong reflected phases from the sill-like, midcrustal Socorro Magma Body (SMB) have been observed on microearthquake seismograms recorded in the central Rio Grande rift, New Mexico. In 1979 the lateral extent of the SMB was estimated at 1700 km^2 by mapping reflection points for 220 observed S_zS arrivals. We have remapped the magma body using 697 P_zP, 2169 S_zP, and 2589 S_zS reflections observed on seismograms recorded between 1975 and 1995 by New Mexico Tech seismic networks.

These data indicate that the SMB covers an area greater than 3400 km^2. By comparing the distribution of observed reflection points with the distribution of all possible reflection points, limits can be set for the northern and southern boundaries of the SMB. The ~80 km north-south extent of the SMB falls just inside an ~100 km north-south range of enhanced seismicity near Socorro. This area, the Socorro Seismic Anomaly (SSA), covers ~5000 km^2 and has the same elliptical shape as the outline of the SMB based on observed reflection points. The close spatial relation between the SSA and the midcrustal magma body along their northern and southern boundaries suggests that the observed seismicity can be used to place limits on the eastern and western boundaries of the magma body. Using the distribution of earthquakes within the SSA over the last 34 years, the maximum east-west extent of the SMB is <60 km, our reflection based value is ~50 km.

Our data indicates that the upper surface of the magma body displays no regional dip. Considering timing errors, maximum possible relief on the magma body surface is ±0.50 km.

1. Introduction

The Socorro, New Mexico area of the Rio Grande rift (Figure 1) is known for seismic reflections from an extensive midcrustal magma body near 19 km depth [*Sanford et al.*, 1977]. The reflections, appearing as the clear, sharp secondary arrivals, P_zP, S_zP, and S_zS on microearthquake seismograms [*Sanford and Long*, 1965; *Sanford et al.*, 1973, 1977; *Rinehart et al.*, 1979; *Ake and Sanford*, 1988 and *Hartse*, 1991], have been used in a variety of seismic studies. *Sanford et al.* [1977] were the first investigators to estimate the lateral extent of the magma body by calculating the reflection-point positions of 142 S_zS arrivals. *Rinehart et al.* [1979] estimated the lateral extent of the magma body using 220 S_zS reflection-point positions and the Socorro COCORP profiles [*Brown et al.*, 1979]. *Hartse* [1991] mapped the magma body using 406 reflections of all three phase types from 75 microearthquakes.

Overlaying the Socorro Magma Body is a $\sim$5000 km^2 region of accentuated seismicity in the central Rio Grande rift of New Mexico [*Sanford et al.*, 1995] which has been designated the Socorro Seismic Anomaly (SSA) (Figure 1). The SSA covers only 1.6 percent of the total area of the state but accounts for $\sim$36 percent of the state's seismicity above magnitude 2.5. The lateral extent of the SSA is defined by the existence of an aseismic halo surrounding the area of intense seismic activity (Figure 1).

In this paper we present a new map of the geographic extent of the Socorro magma body. Our map is constructed using all three commonly identified reflected phases. We used over 5400 reflections, 24 times the number of reflection points used by *Rinehart et al.* [1979]. We have found that the magma body extends farther south, southeast, and northwest than had been previously mapped, and its

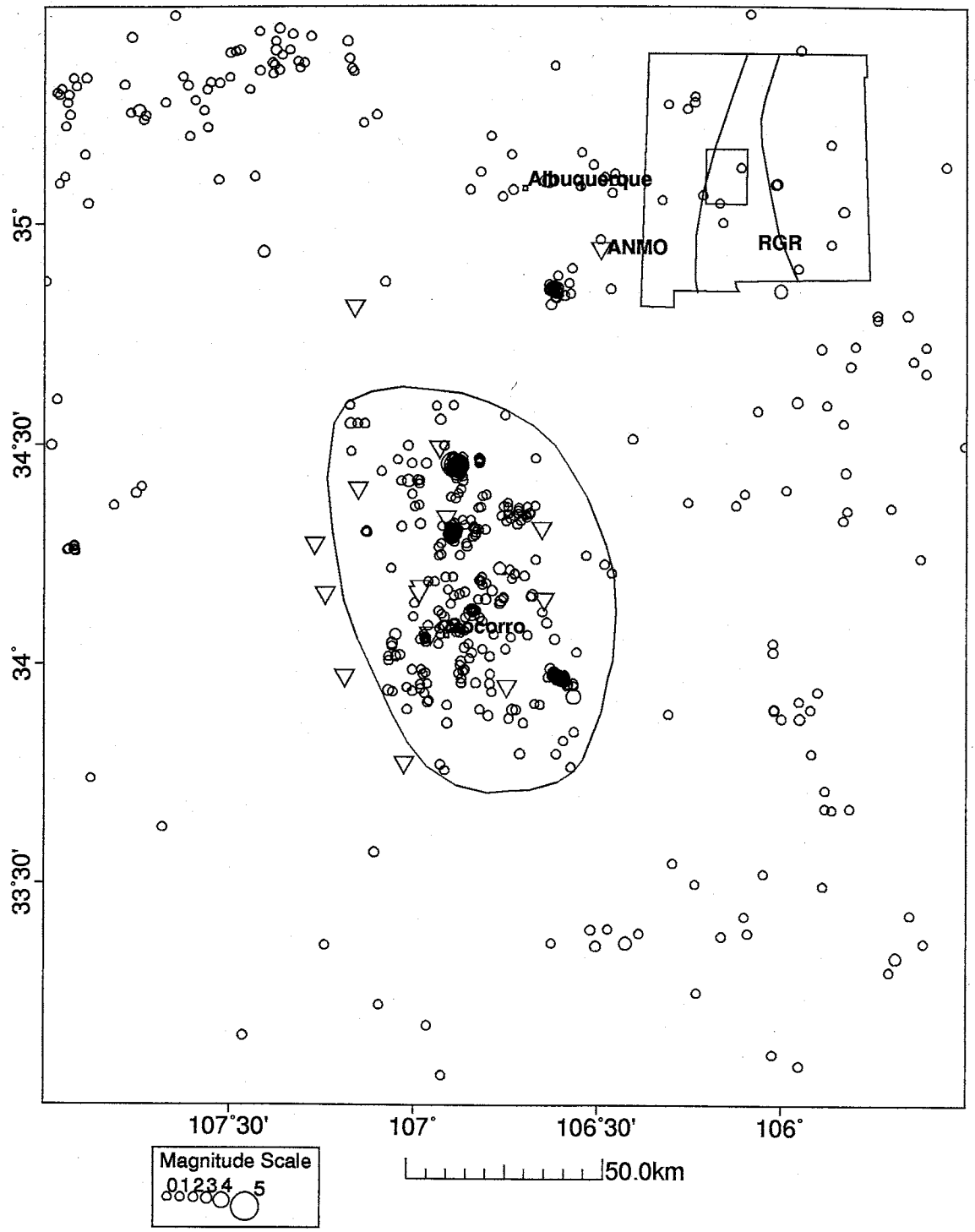

Figure 1. Earthquake epicenters ($M_d \geq 1.3$) 1962-1995 defining the Socorro Seismic Anomaly. Also shown are permanent seismograph station sites (triangles) in the vicinity of Socorro, NM. The inset map shows the study area for subsequent figures and generalized boundaries of the Rio Grande rift (RGR) after *Chapin* [1971].

northern limit has been well constrained for the first time. The western and eastern boundaries are less well known, primarily due to the recording geometry dictated by the station configuration of the Socorro seismic network. We have also found that the upper surface of the magma body displays no measurable dip, or regional variations in depth. Below, we summarize previous magma body studies, describe the data and method we use to find reflection-point positions, present our new magma body map and evidence for flatness, and compare our map with the findings of *Rinehart et al.* [1979].

2. Previous Magma Body Studies

Our work builds on the accomplishments of many previous Socorro-area researchers. *Sanford and Holmes* [1961] first noted the presence of unusual secondary phases on microearthquake seismograms recorded at Socorro, and suggested that the phases could be reflections. *Sanford and Long* [1965] identified two strong phases arriving after direct S as the reflections S_zP and S_zS from a crustal discontinuity at a depth of near 18 km. From amplitude comparisons between S_zP and S_zS, *Sanford et al.* [1973] attributed these phases to an interface between rigid and non-rigid crust. *Sanford et al.* [1977] concluded this interface was the top of a sill-like magma body near 19 km depth and estimated its lateral extent by calculating the reflecting positions of 142 S_zS arrivals. With an expanded data set of 220 arrivals, *Rinehart et al.* [1979] remapped the magma body and estimated its lateral extent at a minimum of 1700 km^2 (Figure 2). Their map is the most recently published outline of the magma body. The minimum areal extent was updated to 2000 km^2 by *Hartse* [1991] using 406 reflection points of all three phases (P_zP, S_zP and S_zS), though no map was published in a journal. Preliminary constraints on the northern margin of the magma body were applied by *Balch* [1992], while remapping the magma body using an independent data set.

By cross correlating digital microearthquake waveforms, *Ake and Sanford* [1988] further demonstrated that the reflector is an interface between rigid and non-rigid crust. Using several events from an earthquake swarm located 15 km southwest of Socorro, they found large correlation coefficients ($\sim$0.80) between S and S_zS, and small correlation coefficients ($\sim$0.45) between P and P_zP. The similarity between S and S_zS indicates that shear energy does not penetrate the reflection interface, while the poor match between P and P_zP indicates some compressional energy does penetrate the interface and reverberates within the magma body. Furthermore, the

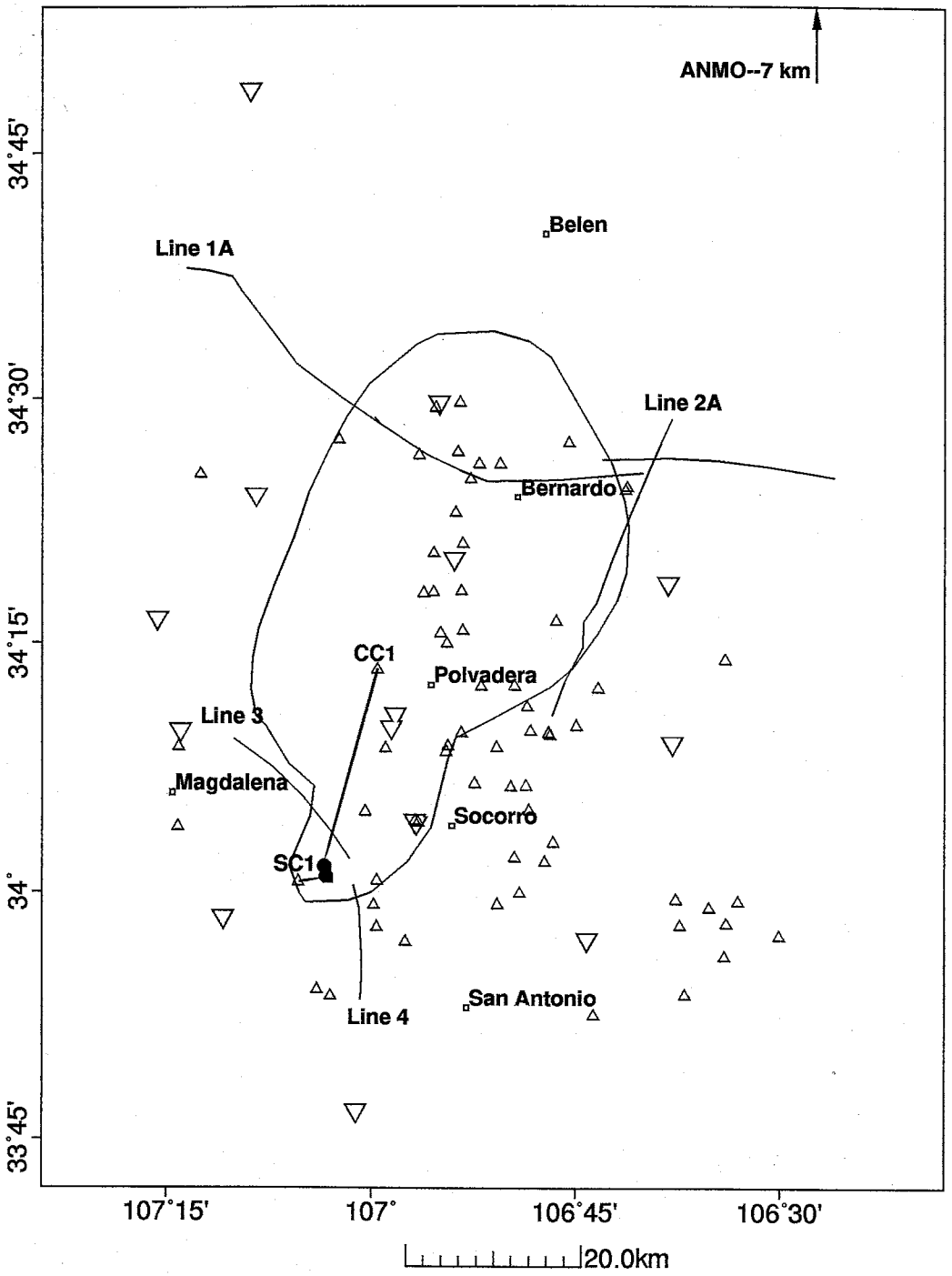

Figure 2. Seismic network near Socorro, NM. Large triangles indicate permanent station sites, and small triangles indicate temporary station sites. Also shown are COCORP profile lines [*Brown et al.*, 1980] and the last published outline of the Socorro midcrustal magma body [*Rinehart et al.*, 1979]. The two earthquakes shown in Figure 3 are represented by small filled circles and each event is connected to the recording station by a line.

signs of the correlation coefficients indicated a phase reversal occurs at the interface. They used the P_zP waveform to model the internal structure of the magma body, finding a best-fitting model of 70 m of magma overlaying 60 m of partial melt or crystalline mush.

Rinehart and Sanford [1981] used S_zS travel times to estimate a velocity model and a depth to the magma body. *Hartse et al.* [1992] simultaneously inverted direct P, direct S, P_zP, S_zP and S_zS, arrival times to jointly solve for hypocenters, velocities, Poisson's ratios, magma body depth, and station corrections. We use the velocity model obtained by *Hartse et al.* to calculate reflection-point positions used in this study. The 75 event data set used in their inversion is included in our data.

In 1975 and 1976 COCORP acquired 155 kilometers of Vibroseis (Trademark of Continental Oil Company) data in the Socorro area (Figure 2). The seismic sections from Lines 1A and 2A reveal unusually strong reflections from near 19 km depth. *Brown et al.* [1979] and *Brown et al.* [1980] present details of the initial interpretations of these lines. *Brocher* [1981] used the COCORP data to model the internal structure of the magma body.

In 1976 a 40 station seismic refraction profile 350 km in length was recorded using chemical explosions at the White Sands Missile Range [*Olsen et al.*, 1980]. Seismometers were deployed from 40 km southeast of Socorro to the New Mexico-Colorado border. Near the southeast end of the line *Olsen et al.* report a series of strong P-wave reflections from a discontinuity at about 21 km depth, where the P-wave velocity changes from 6.0 to 6.4 km/s. *Olsen et al.*, [1982] report additional wide angle P_zP reflections 70 km northeast of Socorro. Strong midcrustal P_zP reflections, particularly at wide angles, do not necessarily imply the existence of magma. For this reason, we have not used *Olsen et al.* [1980] or *Olsen et al.* [1982] reflection data to define the boundaries of the magma body.

3. Mapping Procedure and Data

The data we used were the reflected phases identified on seismograms (Figure 3) recorded with a variety of seismic networks (Figure 2) between 1975 and 1995. The majority of this data was recorded from 1982 through 1995 on a permanent radio telemetered short-period vertical component network operated into the New Mexico Tech seismic observatory. The analog signals were recorded continuously on helicorders revolving at 1mm/sec. The timing was controlled at the observatory with a quartz-controlled clock synchronized with WWV. Since 1992 the network has also been recorded digitally on a PC using XDETECT [*Lee*, 1992]. For significant swarms additional stations were deployed following the main shocks at sites near the epicenter. New Mexico Tech has Sprengnether MEQ-800 seismic recording systems which provided the bulk of temporary station data, but some additional analog data was recorded on Geotech Portacorders. Two Sprengnether DR-100 portable 12-bit digital seismic recorders were also used as temporary stations.

The Seismograms in Figure 3 were produced by the DR-100 digital recorders. These recorders were generally located at remote sites and produced better than average data quality. The relative amplitudes of the direct and reflected phases, however, are comparable between the digital and analog records.

The identification of reflected phases (P_zP, S_zP and S_zS) has been routine for some time in Socorro area microearthquake studies. This process is aided by the use of theoretical arrival time curves based on the best known crustal model. As explained in detail by *Hartse et al.* [1992], correct phase identification is nearly always possible because most seismograms have reflection pairs (S_zP-S_zS, S_zP-P_zP, or S_zS-P_zP) which, for a given earthquake, will only match theoretical curves over a narrow depth range.

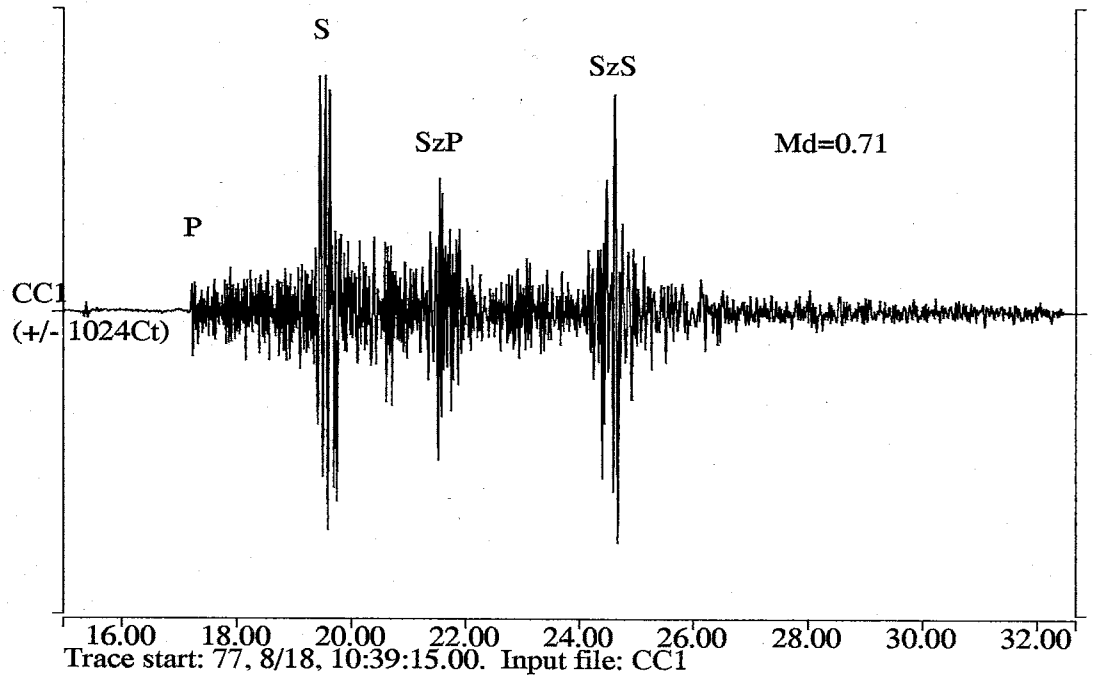

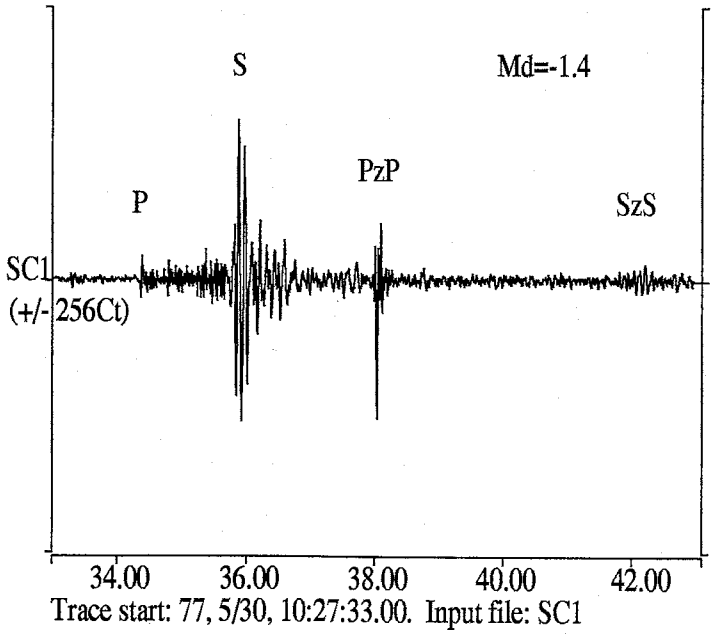

Figure 3. Digitally recorded seismograms with midcrustal magma body reflected phases. These events are somewhat better than average, but adequately represent relative amplitudes of direct and reflected phases on analog as well as digital records.

Timing of the paper records was done on a light table using a magnifying eyepiece which contains a graticle with 0.1 millimeter gradations. When read this way, reading errors for a clear, impulsive P pick is small, less than 0.1 second. The highest quality pick, weight of 0, was assigned a standard error of 0.075 second. Weights of 1 through 9 were also applied by adding 0.075 second for each additional weight factor. A weight of 1 was applied to a P arrival if the onset was clear, but the direction of first motion was somewhat uncertain. Secondary arrivals S, P_zP, S_zP, and S_zS of very high quality were occasionally assigned a weight of 1. A weight of 2 was given for good picks, a weight of 3 for fairly good picks, and larger weights for increasingly poor picks.

An indication that reading errors were accurately estimated for the analog records is demonstrated by exceptional matching of travel-time residuals with timing error, as discussed in the **Evidence For Flatness** section of this paper.

Utilizing the *Hartse et al.* [1992] velocity model (Figure 4) we traced rays between earthquake hypocenters and the stations which recorded reflections to find reflection-point positions. Plotting the reflection-point positions in map view provides an estimate of the magma body's lateral extent.

Figure 5 shows the epicenters of the 1181 events in our data set. The majority of events detected within the SSA occur in swarms, which appear as clusters of epicenters on Figure 5. Between five and 16 stations recorded each earthquake. Hypocenters were determined using the computer program SEISMOS [*Hartse*, 1991; *Hartse et al.*, 1992] which incorporates arrival times of reflections off the midcrustal magma body as well as direct P and S. Inclusion of reflected phases in the location process can decrease depth error by a factor of three [*Hartse et al.*, 1992]. All of the events in the data set have latitude, longitude and depth errors $\leq$ 1.0 km at one standard deviation; the average errors are 0.31 km, 0.37 km and 0.46 km,

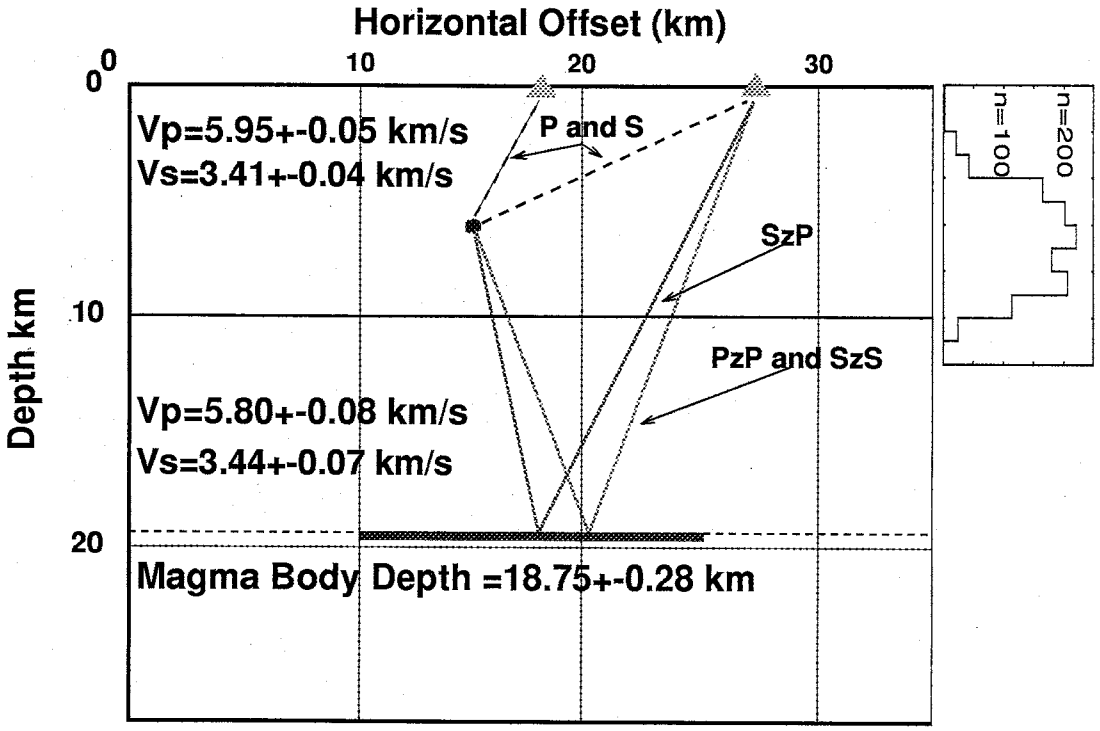

Figure 4. Velocity model and sample raypaths for a hypothetical earthquake. Triangles indicate seismic stations and the reflecting layer represents the Socorro Magma Body. For details on the inversion that produced this crustal model, see *Hartse et al.* [1992]. The seismogenic zone for this study is defined on the right of the figure by a histogram of number of events versus depth for the 1181 earthquakes in the data set.

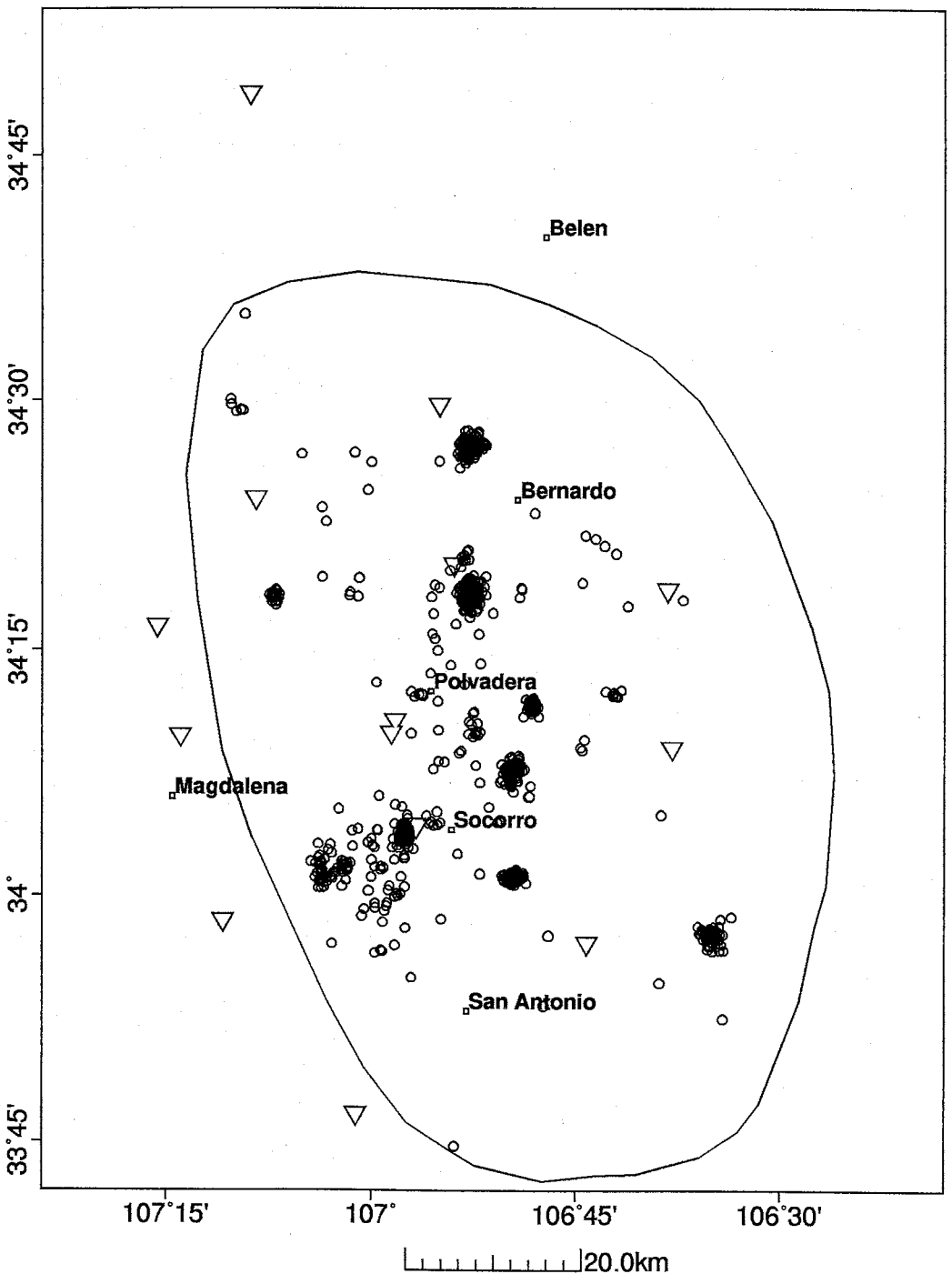

Figure 5. Epicenters of the 1181 earthquakes used in this study. Also shown is the outline of the Socorro Seismic Anomaly.

respectively. Magnitudes (M_d) range between -0.8 and 2.6.

Our final reflected phase data set consisted of 697 P_zP, 2169 S_zP, and 2589 S_zS arrivals identified on the seismograms of 1181 earthquakes. An average earthquake produced between 4 and 5 observed reflections. The maximum number of reflections from a single event was 15.

4. Lateral Extent of the Socorro Magma Body

We estimate the lateral extent of the SMB by computing the reflection-point positions of the observed S_zP and S_zS arrivals (Figure 6). P_zP reflections are used only to fill in the region defined by the S_zP and S_zS reflections and to obtain additional constraints on hypocenter estimates. Because most earthquakes occur within the seismic array, the concentration of these reflection-point positions diminishes as the periphery of the permanent network is approached.

The segments of the COCORP lines marked with bold lines on Figure 6 denote locations along the profiles where the magma body is clearly imaged. The microearthquake reflection points plotted along these lines are from S_zP and S_zS reflections. *Brocher* [1981] demonstrated that the characteristics of strong reflections near 19 km depth on the COCORP profiles support the interpretation that they are from a thin intrusive molten magma complex. We therefore are confident in identifying the bold segments of the COCORP lines as indicating magma body reflections. Other portions of the lines do not clearly show reflections, even where we observe many microearthquake reflections, such as near Lines 3 and 4. This is probably the result of poor signal penetration as Lines 3 and 4 traverse a buried caldera with thick tuff deposits [*de Voogd et al.*, 1988].

The outline surrounding the reflection-point positions shown in Figure 6 is our new map of the Socorro magma body. This map indicates that the minimum lateral extent of the magma body is >3400 km^2. To better determine which borders of the magma are well constrained we plotted hypothetical reflection-point positions (Figure 7). That is, we assumed that every station which recorded a direct arrival from each of the 1181 events could also have recorded P_zP, S_zP, and S_zS arrivals. The outline in Figure 7 is taken from Figure 6 If hypothetical reflection-point positions in

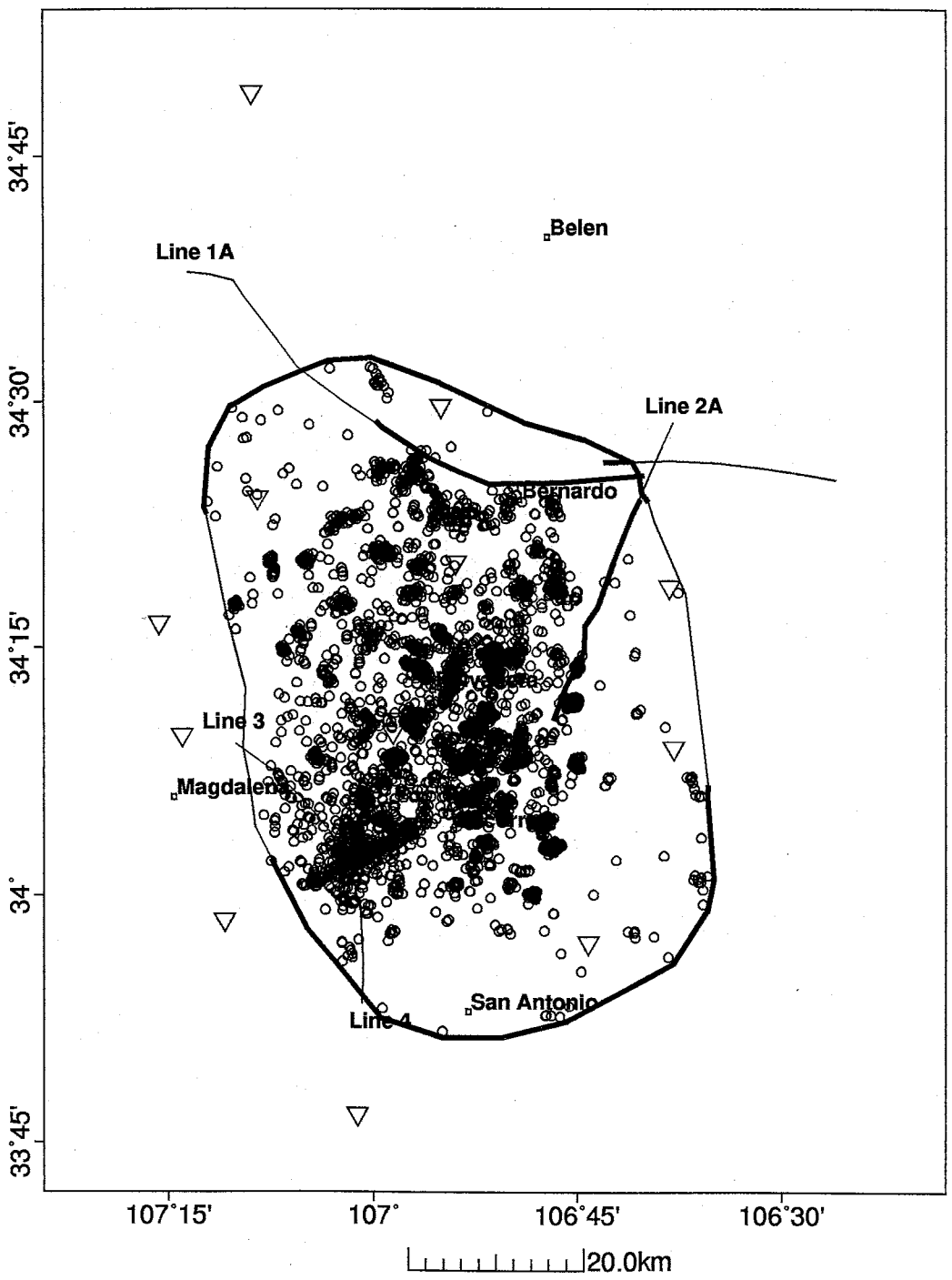

Figure 6. Reflection-point positions associated with the P_zP, S_zP and S_zS phases and the new map of the outline of the Socorro magma body. Heavy solid lines indicate portions of the COCORP profiles which image the magma body clearly and boundary segments of the magma body constrained by this study.

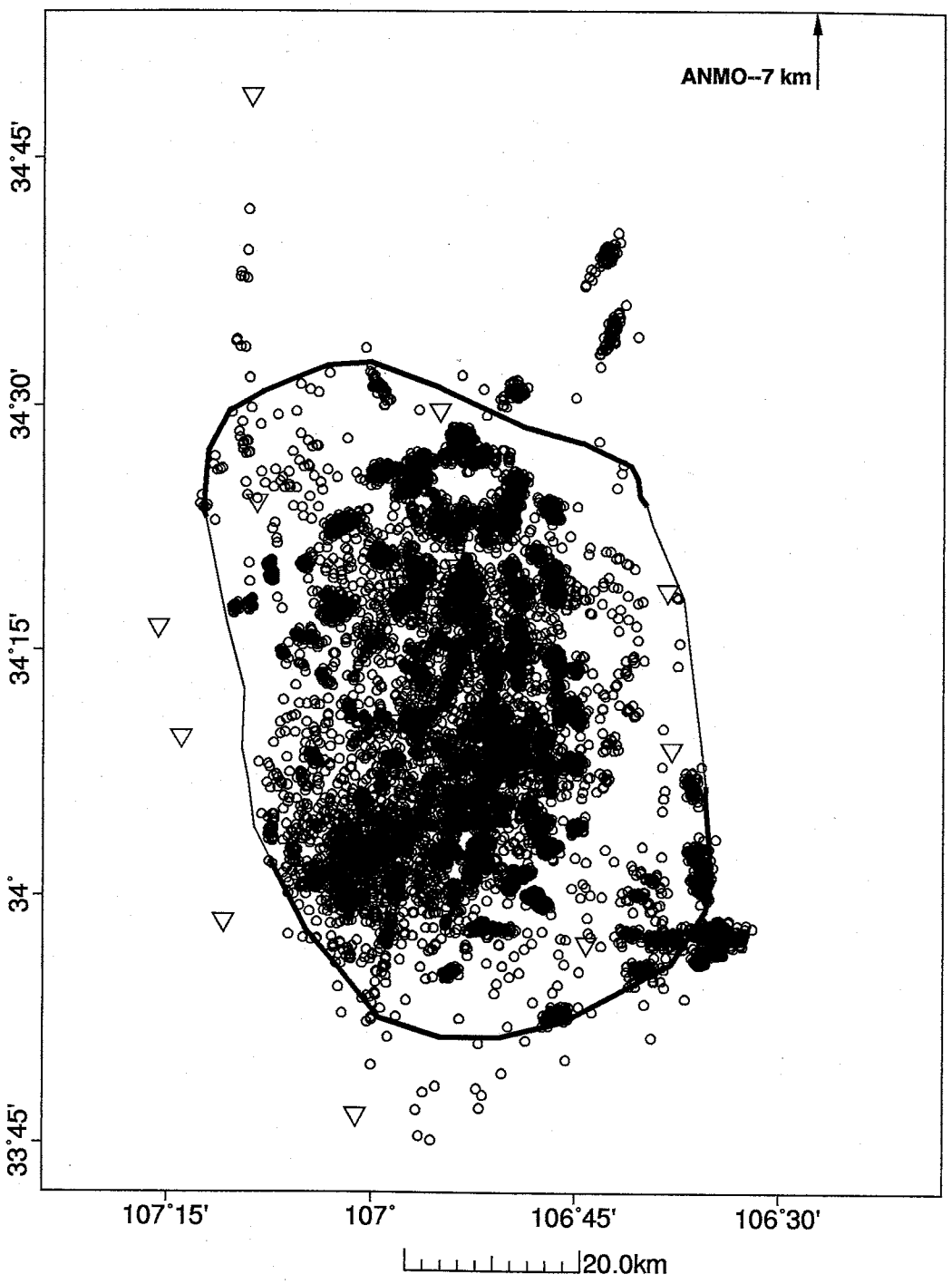

Figure 6. Hypothetical reflection point positions. We assumed that every station that recorded a direct arrival could have also recorded S_zP and S_zS arrivals. The outline of the magma body is from Figure 6, but the solid segments of the boundary are based on the distributions of hypothetical reflection points relative to observed reflection points.

Figure 7 are found just outside the boundary and opposite observed reflection points in Figure 6, then we assume the boundary is constrained by our data. Thus, our microearthquake reflection data constrain the south, southeast, north, and northwest sides of the magma body.

The primary limitation of our data is that most earthquakes in the SSA occur inside the network (Figure 2), limiting the lateral extent of possible reflection-point positions and contributing to the sparseness of data as the perimeter of the magma body is approached, particularly in the south and east. One result of this sparseness is that we cannot confirm the continuity of the magma body in these regions. Close examination of Figures 6 and 7 reveals areas which contain possible reflection points yet have no observed reflections. These observed unreflective regions need not imply no magma. Whether reflections are observed or not depends on the focal mechanism, rupture direction and, azimuth and inclination of raypaths from the focal region to the stations. Also, in the south and east where this problem is most pronounced the majority of hypothetical reflection points are due to temporary stations deployed near the epicentral regions of earthquake swarms. The strength of the P and S codas for near stations coupled with earlier arrival times for reflected phases often obscure reflections for these stations. A larger network aperture would generate more data and better constraints along the borders. Selecting events outside the network would provide more opportunities to define the magma body limits, but an apparently aseismic halo surrounds the SSA and few events would be available.

The northern boundary of the magma body is primarily limited by an absence of observed reflections at the Albuquerque Seismic Lab stations ALQ and ANMO, $\sim$110 km northeast of Socorro. Two swarms are responsible for the clusters of possible reflection points north of the magma body outline (Figure 7). The San Acacia swarm events [*Balch et al.*, 1994, 1995] show no reflected phases of any kind

at the Albuquerque stations; and the Bernardo swarm events [*Sanford et al.*, 1993] have no midcrustal reflections, but a matched pair of P and S Moho reflections are observed. The existence of these shear wave reflections is further evidence that midcrustal magma is not present northeast of our boundary, because S-waves must have traveled through the midcrust before reflecting off the Moho.

Figure 8 compares the magma body outline estimated by *Rinehart et al.* [1979] to the outline we have found. The new outline clearly indicates the minimum lateral extent of the magma body is much greater than had been previously estimated. The new northwest and especially the southeast limits account for the primary differences between the two maps. These portions of the magma body were not imaged by *Rinehart et al.* because they had a more limited data set. Stations deployed in the 1970's did not extend as far south and southeast as the current network, and they used 220 S_zS reflections while we used all three phases and 5455 reflections. Further, the data of *Rinehart et al.* was gathered in a three year period, a relatively short time span to record seismicity in the Socorro Seismic Anomaly. Our data covers 20 years and has a more complete sampling of the overall pattern of seismicity.

Only the northernmost part of the magma body map presented by *Rinehart et al.* [1979] extends beyond the new boundaries. In this region, *Rinehart et al.* did not observe any reflections and this part of their outline was originally interpolated and displayed with a dashed line.

A strong spatial correlation exists between our map of the midcrustal magma body and the extent of the Socorro Seismic Anomaly (Figure 8), suggesting that the seismicity is causally related to the magma body. The ~80 km north-south extent of the magma body falls just inside the ~100 km north-south range of the SSA, which covers about 5000 km^2 and has the same elliptical shape as the outline of the 3400 km^2 magma body. The close spatial relation between the SSA and

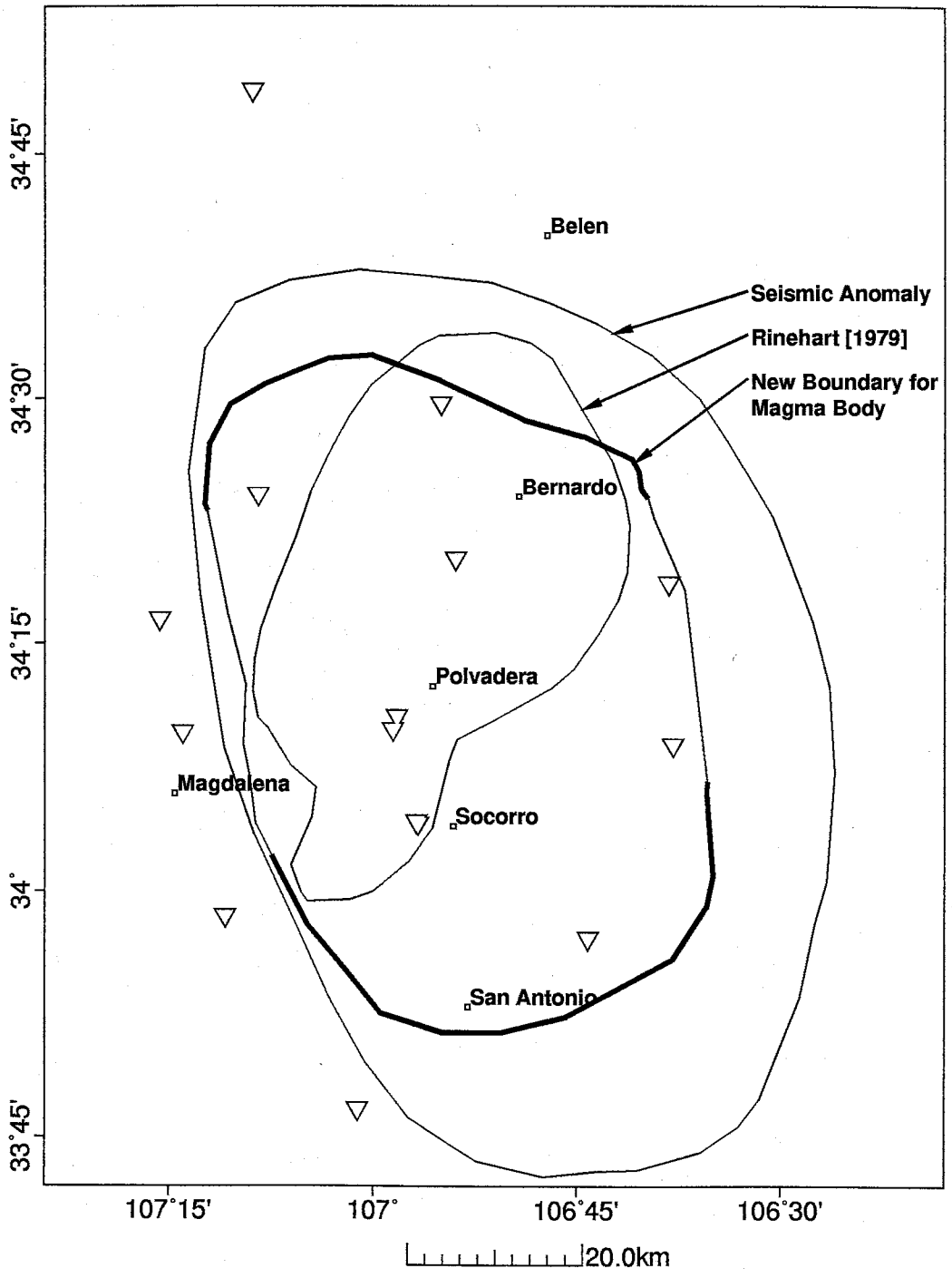

Figure 8. Comparison of the lateral extent of the magma body obtained by *Rinehart et al.* [1979] with the results of this paper. The northern section of the *Rinehart et al.* map was interpolated from the COCORP profiles. Also shown is the outline of the Socorro Seismic Anomaly and permanent stations in the New Mexico Tech Network.

the midcrustal magma body along their northern and southern boundaries suggests that the observed seismicity can be used to place limits on the eastern and western boundaries. Using the distribution of earthquakes within the SSA over the last 34 years, the maximum east-west extent of the SMB is <60 km, our observed value from the map of reflection points is ~50 km.

5. Evidence for Flatness

Below, we discuss two factors that strongly indicate the upper surface of the magma body is nearly flat. We consider how well observed reflected phase arrival times fit assumed timing errors and we present reflection point maps displaying nearly identical geographical distributions of positive and negative arrival time residuals.

Because *Hartse et al.* [1992] assumed a flat reflector when inverting for a velocity model, arrival time residuals which do not fit assumed timing errors can indicate dip or significant relief. *Jackson* [1972] quantifies how well residuals match timing error by:

$$R = \left[\frac{1}{n}\sum_{i=1}^{n}\left(\frac{\Delta y_i}{\phi_i}\right)^2\right]^{\frac{1}{2}}$$

where Δy_i is the difference between an observed arrival time and a model arrival time, ϕ_i is the assumed measurement error, and a total of n data are used in the inversion. If R is much greater than 1.0, then assumed picking errors are too small, or the assumed model is too simple. If R is much less than 1.0, then the assumed picking errors are too large, or the assumed model is too complex. For the 5455 reflected phases we found R=1.06, indicating that the reflected phase residuals are very similar to the assumed timing errors. If dip or any relief were significant, then residuals should exceed assumed timing error, and hence, R for reflections should be large. This is especially true when considering that the reflection-point positions (Figure 7) are from such a wide geographic distribution and are associated with both large and small source-receiver distances.

An argument could be made that R ~1.0 for the 1181 event data set because

event focal depths are being adjusted within the inversion to compensate for reflector dip or relief. However, each event has up to 15 phases which sample the reflecting surface at different geographic positions. Assuming dip or any significant relief, it is unlikely that focal depth adjustments could compensate for several different reflector depths at once and still fit a velocity model which matches the observations so well. Furthermore, *Hartse et al.* [1992] demonstrated that when the S_zP and S_zS arrival times from a single station can be included in the earthquake location problem, the two arrivals define a unique reflector depth and focal depth. Because we are holding the velocity model (and reflector depth) fixed, any dip or unevenness on the reflector should force a poor fit between the S_zP - S_zS observations and the S_zP - S_zS arrival times predicted by the fixed velocity model. Clearly, $R \sim 1.0$ for the reflected phases indicates that this is not happening, even though we use 1328 S_zP - S_zS pairs in our data set.

The other way we tested for dip was to examine the distribution of the residuals associated with the reflection-point positions. Figure 9 shows the positions of reflection points that have negative and positive reflection time residuals. If the magma body displayed a regional dip, then the positive and negative residuals should display roughly separated geographic distributions. For instance, if dip were down to the north, then positive residuals should be more prevalent to the north and negative residuals more prevalent to the south (positive residuals imply later observed arrival times). No such patterns are apparent. Instead, the positive and negative residuals each cover the same areas. This implies random timing errors, rather than a complicated model, are responsible for the residual patterns.

Summarizing, the evidence for flatness comes from the fact that the reflected phase residuals fit an assumed flat model, and positive and negative reflected phase residuals are evenly distributed across the entire imaged portion of the magma body.

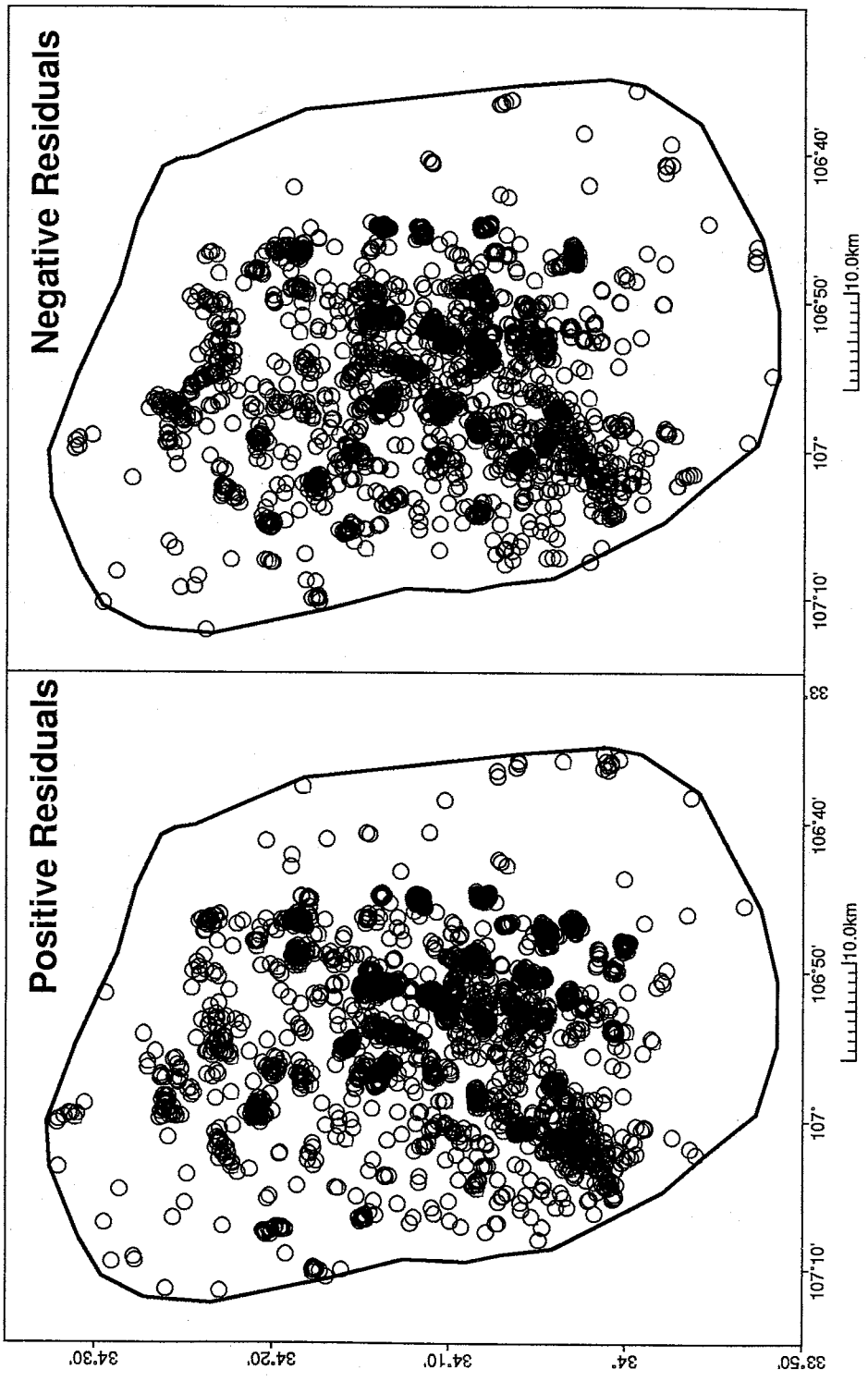

Figure 9. Comparison of the distribution of positive and negative travel-time residuals. There are 2752 positive and 2703 negative residuals.

The question remains: how much dip or relief could be present, but not resolvable, considering data quality?

Typical timing errors for the reflections are between 0.225 and 0.300 s. For the short-offset (10 to 15 km) reflected phases, reflector depths which differ by ± 0.50 km from the assumed 18.75 km flat model will produce S_zS travel-times which will differ by 0.25 to 0.30 seconds from the times of the assumed model. Thus short and long wavelength relief of up to ± 0.50 km is possible on the upper surface of the magma body. If the true relief exceeds ± 0.50 km then segregated patterns of positive and negative residuals should become apparent. Assuming a maximum depth variation of about 1 km (18.75 ± 0.50 km) over an 80 km distance, this allows for a maximum north-south dip on the upper surface of the magma body of less than 1^o. A width of 50 km limits east-west dip to a maximum of about 1^o.

6. Conclusions

We have re-estimated the lateral extent of the Socorro magma body based on calculating the reflection-point positions of 5455 P_zP, S_zP, and S_zS reflected phases identified on the seismograms of 1181 microearthquakes. Additional constraints on the northeast limit of the magma body were obtained from COCORP profiles recorded in the Socorro area in 1975 and 1976. Our map indicates that the magma body extends farther to the south, southeast, and northwest than had been previously mapped, and we have found that the minimum size of the magma body is around 3400 km^2. A maximum possible extent of the midcrustal magma body may be the size of the Socorro Seismic Anomaly, which occupies a somewhat larger area of 5000 km^2 and includes our magma body outline.

Our study indicates the upper surface of the magma body is relatively flat. The primary reasons for this conclusion are the exceptionally good fit between observed and theoretical reflection times and the even distribution of reflection-point positions associated with positive and negative reflected-phase residuals across the entire mapped surface of the magma body. The timing errors associated with our data allow for maximum relief on the magma's upper surface of about ± 0.50 km, which translates to a maximum north-south dip of $< 1^o$ and a maximum east-west dip of about 1^o.

7. References

Ake, J. P., and A. R. Sanford (1988). New evidence for the existence and internal structure of a thin layer of magma at mid-crustal depths near Socorro, New Mexico. *Bull. Seismol. Soc. Am.*, **78**, 1335-1359.

Balch, R. S., (1992). New constraints on the Socorro Magma Body based on improved hypocenter estimates, Geophysics Open-file Report 63, New Mexico Tech, Socorro, 120 pp.

Balch, R. S., A. R. Sanford, L. H. Jaksha, H. E. Hartse, and L. S. House (1994). Non-Double-Couple Focal Mechanisms Observed in the central Rio Grande Rift of New Mexico, abstract, *EOS*, **75 no. 44**, p. 446.

Balch, R. S., A. R. Sanford, L. H. Jaksha, H. E. Hartse and L. S. House (1995). Exotic Seismic Sources Observed in the Central Rio Grande Rift, abstract, *Seis. Res. Letters*, **66 no. 2.**, p 25.

Brocher, T. M. (1981). Geometry and physical properties of the Socorro, New Mexico, magma bodies, *J. Geophys. Res.*, **86**, 9420-9432.

Brown, L. D., C. E. Chapin, A. R. Sanford, S. Kaufman, and J. Oliver (1980). Deep structure of the Rio Grande rift from seismic reflection profiling, *J. Geophys. Res.*, **85**, 4773-4800.

Brown, L. D., P. A. Krumhansl, C. E. Chapin, A.R. Sanford, F. A. Cook, S. Kaufman, J. Oliver, and F. S. Schilt (1979). COCORP seismic reflection studies of the Rio Grande rift, in *Rio Grande Rift: Tectonics and Magmatism*, edited by R. E. Riecker, AGU, Washington, D.C., 169-184.

Chapin, C. E. (1971). The Rio Grande rift; Modifications and additions, *New Mexico Geological Society 22nd Annual Field Conference Guidebook*, 191-201.

de Voogd, B., L. Serpa, and L. Brown (1988). Crustal extension and magmatic processes: COCORP profiles from Death Valley and the Rio Grande rift, *Geol. Soc. Am. Bull.*, **100**, 1550-1567.

Hartse, H. E. (1991). Simultaneous hypocenter and velocity model estimation using direct and reflected phases from microearthquakes recorded within the central Rio Grande rift, New Mexico, *Ph.D. Dissertation*, New Mexico Institute of Mining and Technology, Socorro, New Mexico, 251 pp.

Hartse, H. E., A. R. Sanford, and J. S. Knapp (1992). Incorporating Socorro Magma Body reflections into the earthquake location process, *Bull. Seismol. Soc. Am.* **82**, 2511-2532.

Jackson, D. D. (1972). Interpretation of inaccurate, insufficient, and inconsistent data, *Geophys. J. Roy. Astron. Soc.*, **28**, 97-109.

Lee, W. H. K. (1992) The Xdetect program: A course on PC-based Networks, *U.S.G.S. Open-File Report*, **92-441**, edited by W. H. K. Lee and D. A. Dodge, 138-151.

Lees, J. M. (1995). Xmap8: Three-dimensional GIS for geology and geophysics, *Seismol. Res. Let.*, **66**, 33-37.

Olsen, K. H., G. R. Keller, and J.N. Stewart (1980). Crustal structure along the Rio Grande rift from seismic refraction profiles, in *Rio Grande Rift: Tectonics and Magmatism*, edited by R. E. Riecker, AGU, Washington, D.C., 127-143.

Olsen, K. H., D. J. Cash, and J. N. Stewart (1982). Mapping the northern and eastern extent of the Socorro Midcrustal Magma body by wide-angle seismic reflections, New Mexico Geological Society guidebook **33**, 179-185.

Rinehart, E. J., and A. R. Sanford (1981). Upper crustal structure of the Rio

Grande rift near Socorro, New Mexico, from inversion of microearthquake S-wave reflections, *Bull. Seismol. Soc. Am.*, **71**, 437-450.

Rinehart, E. J., A. R. Sanford, and R. M. Ward (1979). Geographic extent and shape of an extensive magma body at mid-crustal depths in the Rio Grande rift near Socorro, New Mexico, in *Rio Grande Rift: Tectonics and Magmatism*, edited by R. E. Riecker, AGU, Washington, D.C., 237-251.

Sanford, A. R., and C. R. Holmes (1961). Note on the July 1960 earthquakes in central New Mexico, *Bull. Seismol. Soc. Am.*, **51**, 311-314.

Sanford, A. R., and L. T. Long (1965). Microearthquake crustal reflections, Socorro, New Mexico, *Bull. Seismol. Soc. Am.*, **55**, 579-586.

Sanford, A. R., O. Alptekin, and T. R. Toppozada (1973). Use of reflection phases on microearthquake seismograms to map an unusual discontinuity beneath the Rio Grande rift, *Bull. Seismol. Soc. Am.*, **63**, 2021-2034.

Sanford, A. R., R. S. Balch, J. A. Lakings, H. E. Hartse and L. S. House (1993). A Link Between Listric Faulting and Recent Seismicity in the central Rio Grande Rift of New Mexico, abstract *EOS*, **74 no. 43**, p. 417.

Sanford, A. R., R. S. Balch, K. Lin (1995). A seismic anomaly in the Rio Grande rift near Socorro, New mexico, abstract, *Seis. Res. Letters*, **66 no. 2**, p. 44.

Sanford, A. R., R. P. Mott, P. J. Shuleski, E. J. Rinehart, F. J. Caravella, R. M. Ward, and T. C. Wallace (1977). Geophysical evidence for a magma body in the vicinity of Socorro, New Mexico, in *The Earth's Crust: Its Nature and Physical Properties, Geophys. Monogr. Ser.*, **20**, edited by J. G. Heacock, AGU, Washington, D.C., 385-404.

Part II

Analysis of Microearthquake Swarms

Abstract

Microearthquake swarms have been observed in the central Rio Grande rift instrumentally since the 1960's and by felt reports since 1849. In this dissertation I undertake detailed studies of the seismic characteristics of five swarms (occurring in three sequences) and their relationship to regional tectonics. I analyzed 488 high quality hypocenters (latitude, longitude and depth errors $\leq$ 0.5 km) to describe swarm seismicity, with a 208 event subset of earthquakes for study of focal mechanisms.

The San Acacia swarm (February and March, 1983) occurred at shallow depths within the transfer zone between the Albuquerque-Belen and Socorro basins in the central Rio Grande rift. The 101 high quality events described an ellipsoidal volume with a 4.0 km major axis trending ENE and plunging 45^o and minor axes of 1.5 and 3.0 km. Ten of the 30 focal mechanisms computed for the swarm had reduced dilatational quadrants which I modeled as combination shear and tensile faults, possibly resulting from rapid fluid injection during shear failure. The existence of non-double couple (NDC) earthquake sources in the swarm forces the conclusion that less well-constrained double-couple events in the Socorro area may have unresolved NDC components.

The 78 high quality events of the Socorro Mountain sequence (May and July, 1983) defined a volume slightly greater than 1 km^3 at 8 km depth beneath Socorro Peak. Twenty-four north-striking normal fault mechanisms were computed with a wide range of fault dips, three at at very low angle. The distribution of seismicity and variety of fault dip-angles appear to represent reactivation of an Oligocene age fracture system developed through three episodes of domino-style faulting. Digital data recorded 1 km from the swarm epicenter defined 10 earthquake sub-types on

the basis of cross-correlation. I was unable to directly match the sub-types with hypocenter clusters as the dimensions of the active volume was similar to location errors.

The East Rift sequence occurred in three main swarms between August 1985 and May 1986. The sequence initiated with the Arroyo del Coyote swarm (ADC) followed by the Puertecito de Bowling Green (PBG) swarm one month later and 6 km to the north. Eight months later and 10 km south of the ADC swarm The Loma de las Cañas (LDC) swarm concluded the sequence. A total of 309 high quality locations were obtained from the three swarms. The 154 computed focal mechanisms (60, 39, and 55 events in the ADC, PBG, and LDC swarms, respectively) describe strike-slip solutions with two primary orientations. ADC events prior to the PBG swarm and PBG swarm events shared one orientation, while post PBG ADC events and LDC mechanisms shared the other. The strong spatial and temporal relationship between the three swarms implies that the sequence represents activity on as single buried fault with a bend at ADC, able to produce a M_d=6.5 earthquake without surface rupture.

An additional 693 well-located earthquakes (latitude, longitude and depth errors $\leq$ 1.0 km) from the five swarms and other studies were used to address the question of the lateral extent of the Socorro Magma Body (Part I) and to map the base of the seismogenic zone. The base of the seismogenic zone has considerable topography, though it tends to be deepest in a WSW to ENE trend, perhaps related to a known structural lineament, the the Socorro Fracture Zone.

The apparent absence of extension in the Rio Grande rift leaves inflation of the Socorro Magma body as responsible for the increased seismicity in the area. Earthquake swarms in the Socorro area have large volumes compared to the predicted rupture area of their strongest earthquakes. Two factors which may impact swarm

genesis, propagation and volume in the Socorro area are the apparent role of fluids in faulting in the studied swarms and the highly fractured nature of the seismogenic crust in the region.

The orientation of the maximum and minimum compressive stresses (P-T axes) for the studied swarms failed to show consistent values across the region, implying that a single contemporary source of stress does not dominate faulting in the Socorro area. Thus it is very difficult to predict what sort of activity might be observed in the future, as similarly paleo-stressed and fractured volumes could exist, with a variety of orientations in the subsurface. N-S striking normal faults appear to predominate, however.

1. Introduction

The purpose of this study is to reveal information fundamental to earthquake processes in the Socorro area of the Rio Grande rift (RGR). In the central RGR microearthquakes are common with most events related temporally and/or spatially to swarm sequences. Central RGR swarms are very similar to A-type volcanic earthquake sequences [*Minakami*, 1974] and may have similar source types. Swarms of this type are also noted in extensional regions in other parts of the world and source explanations of central RGR swarms may be portable.

I have selected five earthquake swarms covering discrete regions of the central RGR and containing characteristic event types. The Socorro Mountain swarms (SMS) occurred above the southern portion of the SMB, and was composed of normal fault events. The San Acacia Swarm (SAS) was located along the transfer zone between two basins of the central RGR and was situated above the geographic center of the SMB. Events in the San Acacia swarm were a mix of normal faults and events with reduced dilatational components which must have an additional source component to standard double-couple without moment (DCWM) sources. Three swarms which occurred along a linear trend on the eastern margin of the Socorro basin in the central RGR were examined: The Arroyo del Coyote swarm (ADC), the Puertecito de Bowling Green swarm (PBG) and the Loma de las Cañas swarm (LDC). The three swarms are characterized by strike-slip earthquakes and were temporally related to one another.

In addition to their strategic locations, the selected swarms represent the best recorded earthquake sequences in the central RGR, as temporary stations were deployed in the epicentral regions. Each swarm was closely analyzed to extract useful information in the following sequence:

1) Determination of accurate hypocenter locations.

2) Assignment of appropriate velocity models and computation of station corrections.

3) Computation of accurate focal mechanisms.

4) Relation of seismicity to known geologic and geophysical data.

5) Detailed descriptions of temporal and spatial variations of events and source mechanisms within the sequences.

A major question to be addressed in this study is the relationship of the central RGR swarms to active rifting processes and the SMB. An examination of a seismicity map for New Mexico (Figure 1.1) illustrates the elevated seismicity associated spatially with the SMB, which underlies a large portion of the central RGR. It seems likely that the SMB has some role in swarm genesis which needs to be explored.

Careful analysis of temporal and spatial changes in source type and hypocenter distributions throughout each swarm sequence may reveal processes related to swarm propagation. Often the largest events in a swarm sequence have rupture surfaces which cover only a small portion of the seismically active volume. For example, the San Acacia swarm (SAS) had a magnitude $\sim$4 main shock, which would allow for slip on a fault plane $\sim$1 km on a side. The hypocentral volume of the SAS was about 4 by 3 by 1.5 km. The accurate hypocenters available to researchers in the central RGR allows precise control of the time-history of the swarms sources and event locations, thus allowing studies of swarm genesis and propagation.

The five microearthquake swarms have been extensively studied during the course of this dissertation and each swarm has posed interesting questions related to source mechanisms and seismicity in the central Rio Grande rift.

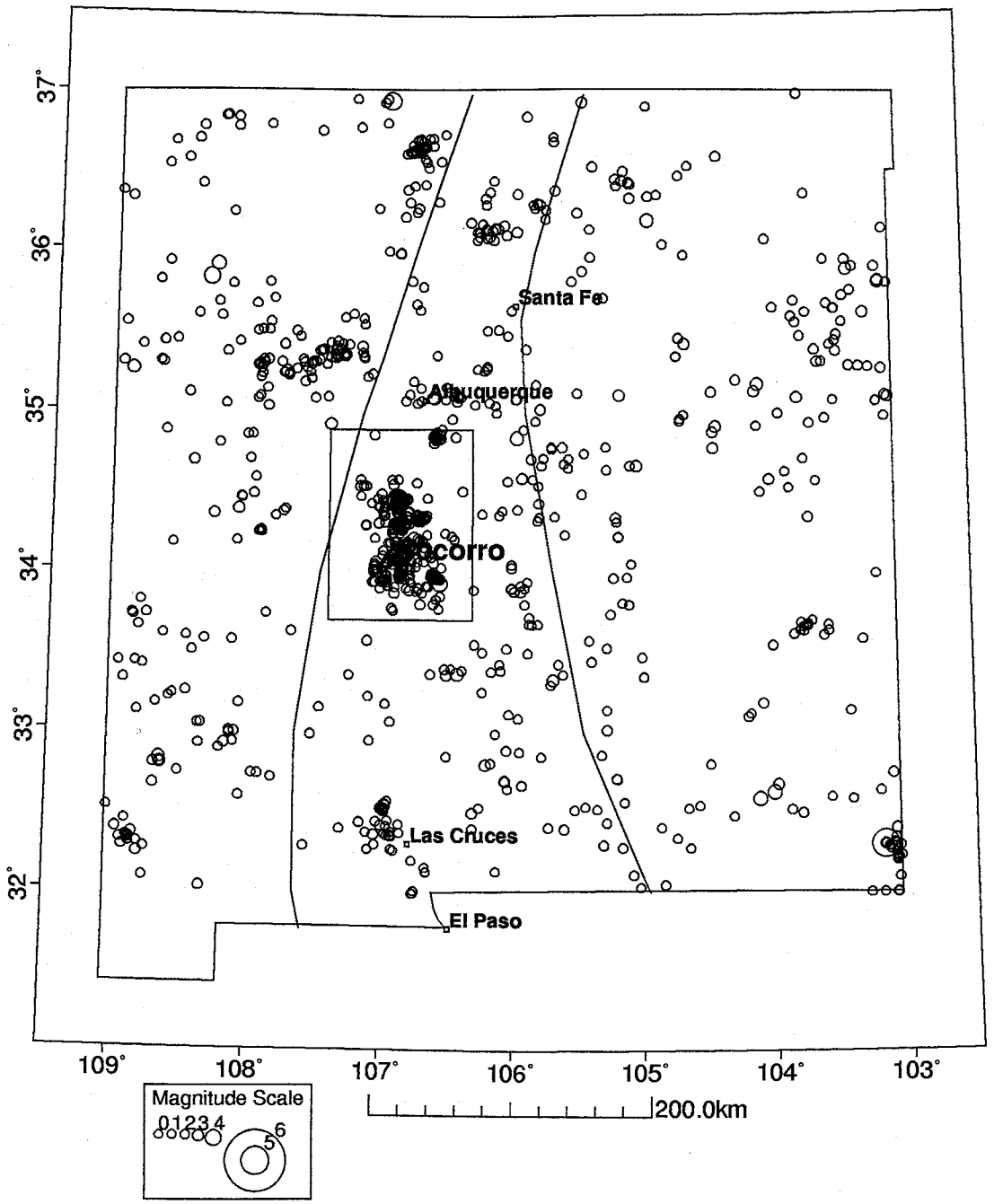

Figure 1.1. New Mexico seismicity $M_d > 1.3$. Note the concentration of activity near Socorro and the aseismic halo surrounding it. The events were recorded at New Mexico Tech from January 1962 through December 1995. A generalized outline of the Rio Grande rift (after *Chapin* [1971]) occupies the center of the state and the study area is restricted to the Socorro Seismic Anomaly [*Sanford et al.*, 1995[1]] (boxed region).

Applications

Several regions in the world have non-double-couple focal mechanisms similar to those observed for the San Acacia swarm, most notably Iceland and Japan. An adequate model for the SAS events could probably be applied to these locations. The possible quantification of changes in source (or near source path) for the Socorro Mountain swarms may lead to increased knowledge of the role of fluids in volcanic A-type sequences. Models for swarm genesis and propagation may be used in other extensional/volcanic regions to explain seismicity patterns (or the lack of). The existence of a hidden fault capable of producing a M_d 6.5 earthquake east of Socorro has implications for seismic hazards analysis in the region.

In the past, the majority of swarm studies in the central RGR have primarily addressed the orientation of fault planes of aftershocks and applications of reflected phases from the SMB. Generally, double-couple without moment (DCWM) sources have been assumed for all swarm earthquakes. I have studied the source characteristics of select swarms and examined relevant geophysical and geologic data in an attempt to compose a model to explain the origins of the volcanic-style earthquake swarms in the central Rio Grande rift.

Overview of the Dissertation

This section describes the content and organization of the remainder of this paper. First, in **Geophysical Setting**, I discuss the tectonic setting of the area with particular attention given to the Socorro Magma Body. Next, in **Previous Studies**, I describe in detail relevant previous studies in the Socorro area, with additional descriptions of studies in other parts of the world. In **Methods** I outline the methods and procedures used to analyze the swarms. In the four **Results**

sections I present my findings for the five studied swarms, a map of the base of the seismogenic zone, and a comparison of earth tides and seismicity. In **Discussion**, I address the broader questions of swarm genesis, swarm propagation, swarm volume, and the cause of the heightened seismicity in the Socorro area. I finish with **Summary and Conclusions** and **Suggestions for Further Studies**.

2. Geophysical Setting.

The central RGR is bounded by the Great Plains to the east, the Colorado Plateau to the northwest, and the Datil-Mogollon volcanic field to the southwest. Rifting of the central Rio Grande rift in the Socorro area began about 29 m.y. ago [*Chapin*, 1979]. Features of the study area include Tertiary calderas, observed crustal doming, and the Socorro Magma Body. The Socorro area also has the greatest amount of seismic activity of any area (Figure 1.1) within the Rio Grande rift [*Bagg*, 1904; *Reid*, 1911; *Northrop*, 1945, 1947; *Sanford et al.*, 1991], both in numbers and strengths. Most of the earthquakes in the Socorro area occur on normal faults with north-south strikes [*Sanford et al.*, 1991].

Crustal deformation in the Socorro area [*Larsen et al.*, 1986], as determined by releveling bench marks between 1911 and 1980 (uplift of over 120 mm was observed), is roughly centered on the study area. *Ouichi* [1983] presented geomorphic evidence for 1.8 mm/yr of uplift for the last 20,000 years in the area of maximum deformation, a number that agrees well with the rate from the releveling measurements. Based on the tilt of Rio Grande sand deposits [*Bachman and Mehnert*, 1978] and assuming the ancestral Rio Grande had the same gradient as the present river, *Sanford et al.* [1991] calculated that uplift in the Socorro area may have begun about 40,000 years ago.

Analysis of the SMB relies primarily on seismic data recorded during Socorro area earthquake swarms. These swarms, which account for most of the Socorro area earthquakes, may be related to the injection of small amounts of magma into the upper crust [*Sanford and Einarsson*, 1982]. The seismicity, like the crustal uplift, is centered over the magma body. This suggests a relationship between the seismicity and the localized uplift which may be the result of inflation of the SMB. Socorro

area earthquakes may also be occurring on faults reactivated by the stretching of the crust above the inflating body [*Sanford et al.* 1991].

Earthquake swarms have often struck the Socorro area. The earliest report is that of a U.S. Army surgeon who reported 22 felt shocks during a swarm that lasted from December 11, 1849 to February 8, 1850 [*Hammond*, 1966]. Earlier records may exist in Spanish and Mexican archives. Other notable swarms have occurred near Socorro including a vigorous swarm between July of 1906 and January of 1907 which produced felt events nearly daily, sometimes within hours of one another. The most recent strong earthquake swarm in the Socorro area was centered near the village of Bernardo, New Mexico, and had 45 magnitude 2.0 or greater events between November of 1989 and May of 1992 [*Sanford et al.*, 1993]. Four earthquakes of magnitude 4.0 or greater were recorded in the swarm during the same time period.

3. Previous Studies

Socorro Area Studies

Most microearthquake swarms in the central RGR undergo some analysis. Swarms with durations of only a few days, or no relatively strong events are assigned a location based on well recorded events and then filed. Larger swarms tend to become projects for graduate students and are looked at more closely. Studies of seismicity and upper crustal velocity structure of the region incorporate data from many swarms. Most microearthquakes in the central Rio Grande rift occur in clusters of at least a few similarly located events.

The internal structure of a small portion of the magma body was determined by *Ake and Sanford* [1988] using P_zP and S_zS reflected phases. The study was based on digital recordings of an earthquake swarm near station SC (South Canyon) that sampled approximately a 500 m length of the magma body surface. *Ake and Sanford* found that the S and S_zS phases correlated well (average correlation coefficient, +0.79), while the P and P_zP phases did not (average correlation coefficient, +0.45). For this swarm the S and S_zS phases left the focal region 180^o out of phase; because the correlation coefficient between these two phases was positive, the magma body surface must have produced a 180^o phase shift. A very high correlation coefficient between the S and S_zS phases for different swarm events demonstrated that the reflecting surface was a liquid in the study area. Variability in the P_zP phase (as indicated by low cross-correlation coefficients) implied that the internal structure of the magma body was not uniform. An average two layer magma body was proposed, a layer of full melt over a layer of partial melt. Comparisons between theoretical and observed spectra indicated a best fit for a 70 m layer of full melt over a 60 m thickness of partial melt. Spectral data from a COCORP study in the central RGR

[*Brown et al.*, 1980] were used to verify that these results were consistent for other portions of the SMB.

A study of strain across the rift [*Savage et al.* 1980 and 1985] was inconclusive regarding the amount (if any) of present day extension occurring in the central RGR near Socorro. Geologic maps show numbers of large normal faults exposed at the surface in the rift [e.g. *Machette*, 1982]. These faults often show large displacements which seem inconsistent with the recorded seismicity in the region. Generally the recorded swarms have had no spatial relationship to these surface exposures.

Hartse [1991] produced a new hypocenter location program **SEISMOS**, capable of utilizing the observed reflected phases from the magma body in the location process, and in inversions for crustal models. *Hartse et al.* [1992] found that the use of reflected phases improved hypocenter locations, in particular the depth estimate which was improved by about a factor of three. *Hartse* inverted jointly for 75 hypocenters, and a one dimensional velocity model using over 1000 direct arrivals and over 400 reflected arrivals. Important results of this undamped inversion were the first indication that the Socorro magma body appears to have no perceptible dip and that it is located at about 18.75 km depth ($\pm$0.28 km). In addition, it was found that Poissons ratio may be unusually low beneath the seismogenic zone (about 10 km depth). *Hartse* also analyzed the distribution of reflection points to place the lateral extent of the magma body at > 2000 km^2. A good average velocity model for the upper crust in the central RGR was developed in his study.

Until the development of **SEISMOS** in 1991 it was fairly difficult to obtain accurate hypocenter depths with the sparse New Mexico Tech seismic network. Good hypocentral control is essential to studies of source mechanisms since the distribution of first-motion incident angles are depth-dependant. Thus only recently did it become feasible to accurately survey source mechanisms in the RGR, though ade-

quate data have existed for years. Focal mechanisms for one other swarm have been examined using new hypocenters: the Bernardo swarm *Sanford et al.* [1993].

Volcanic Region Studies

There are similarities between microearthquakes in the central RGR and A-type volcanic earthquakes, therefore I have reviewed papers concerning various volcanic terrains. The regions most similar in earthquake types are in Iceland, Japan, and Kamchatka.

The Hengill triple junction in Iceland is the landward extension of the mid-Atlantic ridge and is centered in the active Hengill-Grensdalur volcanic complex. The region experiences A-type earthquake swarms which are located within known geothermal resevoirs. *Klein et al.* [1977] first noted swarm earthquakes for which orthogonal nodal planes were not possible. *Foulger* [1988] found 178 well-constrained events for a swarm of which 47% appeared to be non-double couple, in particular the dilatational quadrants covered unusually small areas on the focal sphere. A re-examination of the data with a more sophisticated velocity model still yielded 43% unusual sources. The greatest changes in mechanism occurred when the depth of the event changed substantially [*Foulger et al.* 1993]. The Hengill events appear similar to solutions found for the San Acacia swarm which may also be located near a geothermally active area [*Sanford*, 1996 personal comm.].

A study of the seismicity of Miyakejima island, Japan, was undertaken for one month following an eruption on October 3, 1983 [*Shimizu et al.*, 1987]. Two active regions were discerned using temporary and permanent stations: one area close to eruptive fissures had events which were primarily dilatational; the other area was characterized by A-type earthquakes with dominantly compressional first motions. The authors used a moment tensor representation of a tensile-shear crack to model

the latter earthquakes. The compressional events were thought to be due to sudden tensile opening of cracks due to excess pressure of intruding magma, with a small component of shear slip. Reduction of the magma pressure in the cracks and sudden closure was interpreted to be the cause of the dilatational events.

A study of 32 earthquake swarms in Kamchatka and the Commander Islands [*Zobin and Ivanova*, 1994] noted that the swarms primarily occurred in tensional areas such as trench slopes and volcanic complexes. The swarms tended to be unrelated to the type of faulting dominant in the epicentral region, though 24 of the swarms were located in areas with near horizontal tension. These observations are in accord with observations for the central RGR swarms.

These studies and others not mentioned demonstrate that earthquakes in volcanic regions have different distributions of activity, and in some cases, source mechanisms that are not strictly shear failures. The exact reasons for these differences are as yet unresolved. The data collected from earthquake swarms in the central RGR are of the necessary quality to explore the characteristics of some of these unusual volcanic/extensional-style events.

4. Methods

The examination of the five selected swarms followed a common method. The first step in each study was to locate as many hypocenters as was feasible using SEISMOS [*Hartse*, 1991]. The second step was to determine the best velocity model and compute swarm-specific station corrections using inverse modeling and checking them for realism by comparing them to local geology, as an example, a strong positive correction would be expected for a station site underlain by thick alluvial deposits. Third, fault plane mechanisms were examined using FPFIT [*Reasenberg and Oppenheimer*, 1985] to determine if reasonable DCWM mechanisms could be found. When non-standard mechanisms were found other methods were applied. The final step involved accurate characterization of the spatial and temporal history of the swarms. The analysis type was dependant on amounts and types of seismic and geologic data and varied between swarms.

Hypocenters

All hypocenters used in this study were located using SEISMOS with all available reflected phases (P_zP, S_zP and S_zS) since it was very important to accurately resolve depth for studies of focal and source mechanisms. All hypocenters used in this study had at least six recording stations distributed such that azimuthal gaps were less than 180^o.

Velocity Models

Velocity models for the central Rio Grande rift have been determined twice using all recorded phases in inversions for crustal models. *Hartse* [1991] determined two models, one with two layers in the upper crust and the other a single layer

upper crust model. *Hartse's* work provided good average velocity models over the whole extent of the magma body. The single layer model of *Balch* [1992] used the same programs (SEISMOS) as *Hartse's* studies, but the earthquakes in the data set were more commonly located over the southern portion of the magma body and is thus more appropriate for studies in that region. When studying microearthquake swarms in the central RGR, it has become apparent [*Sanford et al.*, 1993 and *Balch*, 1994[1,2]] that each swarm requires individual consideration for the most appropriate velocity model and site-specific station corrections. Station corrections (also known as station delays) account for velocity and thickness variations of Phanerozoic rocks. A positive correction generally indicates thick deposits of low-velocity material (relatively unconsolidated sediments) below a station. A negative or very small correction indicates that the station is sited where basement rocks are at (or very close to) the surface. Computed station corrections were validated by examination of geologic and geophysical data.

Other Geologic and Geophysical Data

As indicated previously, a good understanding of the geology and tectonics of the epicentral regions is necessary. Toward this end, previous work in the regions of interest was reviewed. Previous seismic studies were of particular interest as they yielded information on how best to approach the data. Additional insight was gained from examining regional geophysical data such as gravity maps when appropriate.

Fault Plane Solutions

Most fault plane solutions used in this study were computed using FPFIT [*Reasenberg and Oppenheimer* 1985]. The program calculates solutions for events assuming DCWM sources. FPFIT uses a grid-search method to fit nodal planes to

first motion data keeping nodal planes equidistant from first motion points. As the program is not aware of geologic and geophysical constraints for particular regions it is necessary to examine solutions carefully to determine if they are reasonable. In cases where standard DCWM sources did not appear feasible, forward modeling of moment tensors was applied.

Moment Tensor Analysis

Elastic media theory allows us to replace the displacements on a fault with equivalent body forces. These body forces are equivalent to the fault slip since they yield the same radiation patterns. Though not describing the actual fault process these body forces do describe a seismic source equivalent to the fault motion.

The body forces are described using force couples, which are simply two forces acting together similar to magnetic dipoles. There are two basic types of force couples (Figure 4.1): One is comprised of two forces of equal magnitude working in opposite directions on a segment of a given length perpendicular to the force vectors. The second is comprised of two forces of equal magnitude acting in opposite directions on a segment of some length parallel to the force vectors.

For three components of force able to act in any of three directions there are nine possible couples. Combinations of these nine couples can be used to describe any fault motion [*Aki and Richards*, 1980]. To describe slip on a fault it is necessary to use a superposition of two couples (a double couple), one for motion in the slip direction and the other perpendicular to slip in order to avoid rotation of the fault (conservation of angular momentum). The magnitude of these double-couples is simply the scalar seismic moment of the earthquake M_o:

$$M_o = \mu_h DS$$

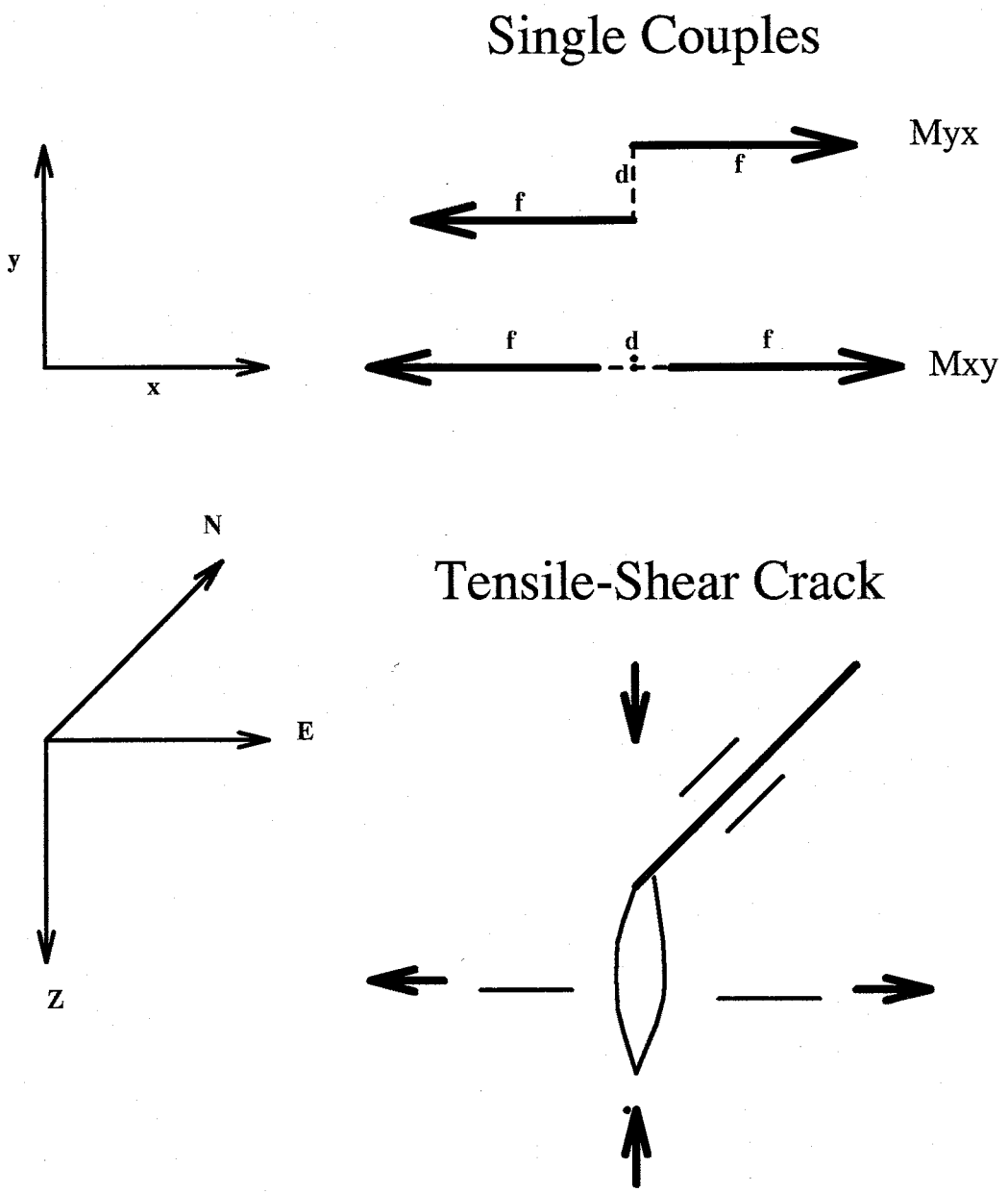

Figure 4.1. Example single couples and a model for a tensile-shear crack (after *Shimizu et al.* [1987]).

Where μ_h is the rigidity at the source depth, D is the average slip on the fault with surface area S. M_o is a scale factor describing the expected spectral amplitude for an earthquake.

For the nine mentioned force couples a moment tensor can be defined as follows.

$$M = \begin{pmatrix} M_{xx} & M_{xy} & M_{xz} \\ M_{yx} & M_{yy} & M_{yz} \\ M_{zx} & M_{zy} & M_{zz} \end{pmatrix} \tag{1}$$

This moment tensor would appear more complicated if the fault and slip were not oriented with the coordinate system.

Shimizu et al. [1987] used a moment tensor approach to model a tensile-shear crack (Figure 4.1) to explain anomalous focal mechanisms. The usefulness of their technique is in gaining information on the orientation of fractures for this type of non-double-couple (NDC) fault mechanism. A thorough description of their technique is summarized in **Appendix II** for completeness.

The program (**MOMTEN**) [*Julian*, 1995] which allows the computation of moment tensors for Double-Couple, Tensile and Concentrated Linear Vector Dipole sources was used to estimate separate moment tensors for shear and tensile components. The principle of superposition was then used to combine shear fault moment tensors with tensile fault moment tensors in order to obtain a composite solution. Another program **BWNODE** [*Julian*, 1995] was then used to compute P-wave nodal plane data. This data was converted to a form appropriate for plotting on standard Schmidt stereonets and plotted, using programs I developed

Temporal and Spatial analysis

An important component of this study was the thorough examination of the

temporal and spatial relationships of swarm events to one another and to known structures. Accurate descriptions of spatial and temporal variability within swarm sequences may provide information on swarm propagation, particularly when used with source and focal mechanism data. A major question for this study is the relationship of main shocks to other activity in the swarm volume.

Digital Data

Digital data allows more precise analyses, therefore the available digital data received extra attention. Two types of digital data were encountered for the five subject swarms. Three-component data recorded at the Albuquerque Seismological Laboratory was used for large events, yielding accurate arrival time and first motion data. Vertical component digital data obtained on event recorders (Sprengnether DR-100's) allowed a closer look at the spatial variability of events and better control of some source parameters as outlined in the following paragraphs.

Cross-Correlation

The Socorro Mountain swarm was well recorded by a Sprengnether DR-100 located in a mine within 1 km of the epicentral region. Events within the swarm were separated into groupings with similar full waveform characteristics using cross-correlation techniques.

Cross-correlation is a process by which two time series may be compared, for this study the similarities between earthquake time-series were examined. The equation for cross-correlation follows,

$$C(t) = \int_{-\infty}^{+\infty} x(t)y(t-\tau)d\tau$$

C(t) describes the similarity between x(t) and the equivalent portion of y(t), calculated at incremental lag times (τ). If C(t) is normalized by the cross-signal power,

$$c(t) = \frac{C(t)}{\int_{-\infty}^{+\infty} x(\tau)y(\tau)d\tau}$$

the result is the cross-covariance c(t), which describes the correlation between the time-series at different lag times. Often a *correlation coefficient* is given to describe this similarity. This coefficient is obtained by picking the peak value of the cross-covariance function. Of course real data is not comprised of infinite time-series and is discrete. However, the same method applies as long as you are careful to pad both series correctly to avoid wrap-around effects. In this study I elected to use **SAC2000** (Copyright 1987 the Regents of the University of California) to compute cross-correlations, using simple macros constructed of intrinsic **SAC2000** functions.

5. Data

The Socorro Network

In 1982 a network of short-period seismic stations was installed in the central RGR. The network is a permanent, radio-telemetered network whose data are transmitted into the New Mexico Tech Seismic Observatory. Field components include vertical component seismometers operating at 1.0 Hz natural frequency, preamplifier-VCO's and transmitters. In the observatory are receivers and discriminators for each channel. The analog signals from the discriminators are recorded continuously on analog drums revolving at 1 mm/sec. Timing is controlled at the observatory with a quartz-controlled clock synchronized with the WWV radio signal transmitted from Colorado. The network has variously had between 8 to 10 stations in its configuration. Since 1992 data has also been digitized and recorded at the observatory using a PC running the event detection and recording software, **XDETECT** [*Lee*, 1992].

Additional stations were deployed at sites near the epicenters of main shocks for the more significant swarms. New Mexico Tech has Sprengnether MEQ-800 seismic recording systems which provided the bulk of the temporary station data, but some additional analog data was recorded on Geotech Portacorders. The MEQ-800 seismic stations record an analog signal onto a smoked paper drum revolving at 2 mm/sec with a diamond tipped stylus and the Geotech Portacorders record at the same speed with an ink writing stylus. Self-contained quartz-crystal chronometers are synchronized at the beginning of each recording period with WWV, and again at the end of the recording period in order to correct for clock drift. Mark Products vertical L4-C geophones (1.0 Hz natural frequency) were used as sensors for the stations. Two DR-100 portable 12-bit digital seismic recorders were also used as

temporary stations. The DR-100 continuously samples the seismic signal until triggered using standard STA/LTA values (larger short-term average (by a set amount) than the long-term average). The triggering signal is recorded on magnetic tape at 100 samples per second. Mark Products vertical L4-C geophones were used with these systems also.

A third source of data was the 3-component digital recordings from the Albuquerque Seismic Laboratory recorded at 20 samples per second since 1974.

Identification, Timing, and Weighting of Arrival Times

The identification of reflected phases (P_zP, S_zP and S_zS) has been routine for some time in Socorro area microearthquake studies. Often, theoretical arrival time curves based on the best known crustal model are used in the identification of phases on seismic records. These travel time curves are generated for 1 km intervals of focal depth covering the entire thickness of the seismogenic zone (2-12 km).

Timing of the paper records is done on a light table using a magnifying eyepiece which contains a graticle with 0.1 millimeter gradations. Overall, a standard error for a clear, impulsive P pick is assumed to be 0.075 seconds, corresponding to an assigned weight of 0. Weights of 1 through 9 are also applied by adding 0.075 s for each additional weight factor. A weight of 1 is applied to a P arrival if it is impulsive but the direction of first motion is questionable. Secondary arrivals of very high quality such as S, P_zP, S_zP, and S_zS picks are occasionally assigned a weight of 1. A weight of 2 is given for good picks, a weight of 3 for fairly good picks, and larger weights for increasingly poor picks.

Socorro area microearthquake seismograms typically exhibit five phases - direct P and S, and P_zP, S_zP, and S_zS phases reflected from the magma body surface (Figure 5.1), though not all phases are likely to be observed on the seismogram from

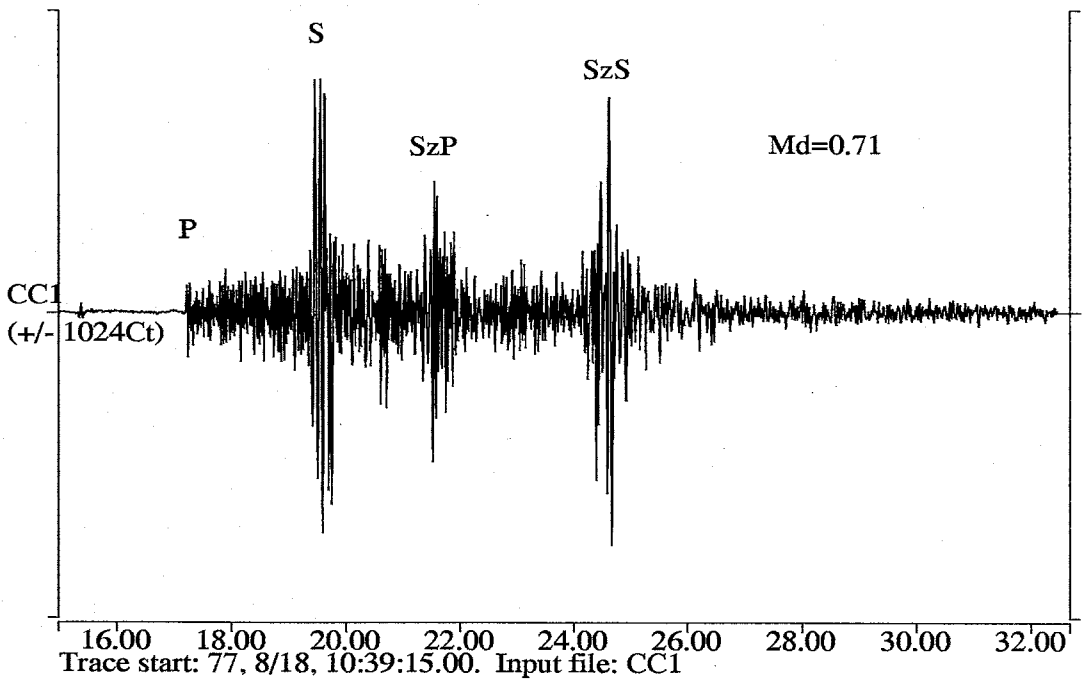

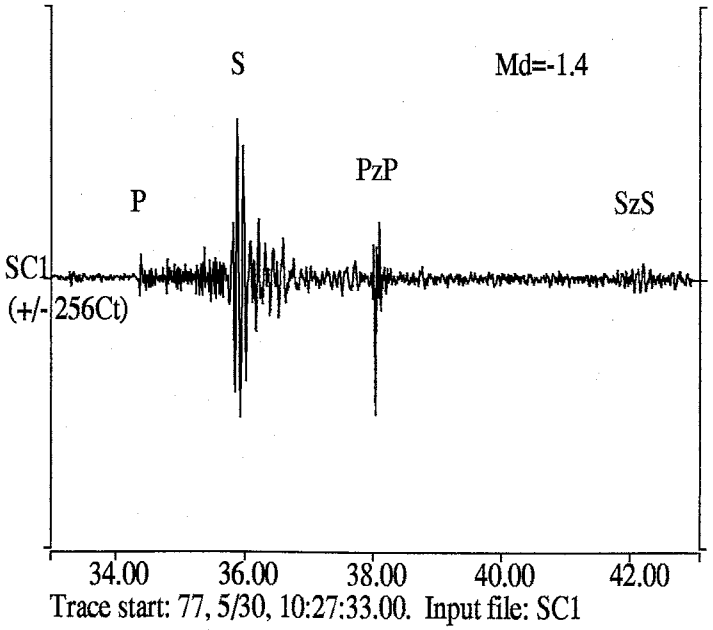

Figure 5.1. Digitally recorded seismograms with midcrustal magma body reflected phases.

a single station, particularly the reflected phases. A schematic diagram showing the crustal model of *Balch* [1992] and sample raypaths of phases used in this study is given in Figure 5.2. The frequency of occurrence and characteristics of each phase is discussed in detail in two references [*Hartse*, 1991 and *Balch*, 1992].

Microearthquake Swarms

Five separate swarms covering distinct geologic settings were examined (Figure 5.3). All of these swarms were recorded by both the permanent Socorro seismic network and temporary stations deployed following main shocks. In the following paragraphs brief descriptions of the five microearthquake swarms analyzed are given.

The **San Acacia swarm** occurred about 25 km north of Socorro, New Mexico, along the transfer zone between the Albuquerque-Belen and Socorro basins in the central RGR [*Balch et al.*, 1994[2]]. The swarm commenced on February 25, 1983, had a magnitude 4.2 main shock on March 2nd and ended on March 17, 1983. Permanent station recordings were supplemented with three to five temporary stations occupying 12 sites in the epicentral region for 10 days following the M_d=4.2 main shock. This swarm was first studied by *Jarpe* [1984] who first noted the possibility of unusual focal mechanisms.

The **Socorro Mountain Swarms** occurred in May and July of 1983 beneath the mountains a few kilometers west of Socorro, NM. The first sequence occurred between May 10-14 and the second between July 14-21. During both swarms digital recordings using a DR100 were taken at the nearest permanent station, WTX, which is located in a mine at the base of Socorro Peak. Over 400 events were recorded at WTX, most with $M_d < 0.0$ [Ake, 1986]. Hypocenters for 78 events with $M_d < 2.1$ were calculated with errors in latitude, longitude and depth ≤ 0.5 km [*Balch et al.*, 1994[1]]. The average hypocenter locations for the May and July sequences were not

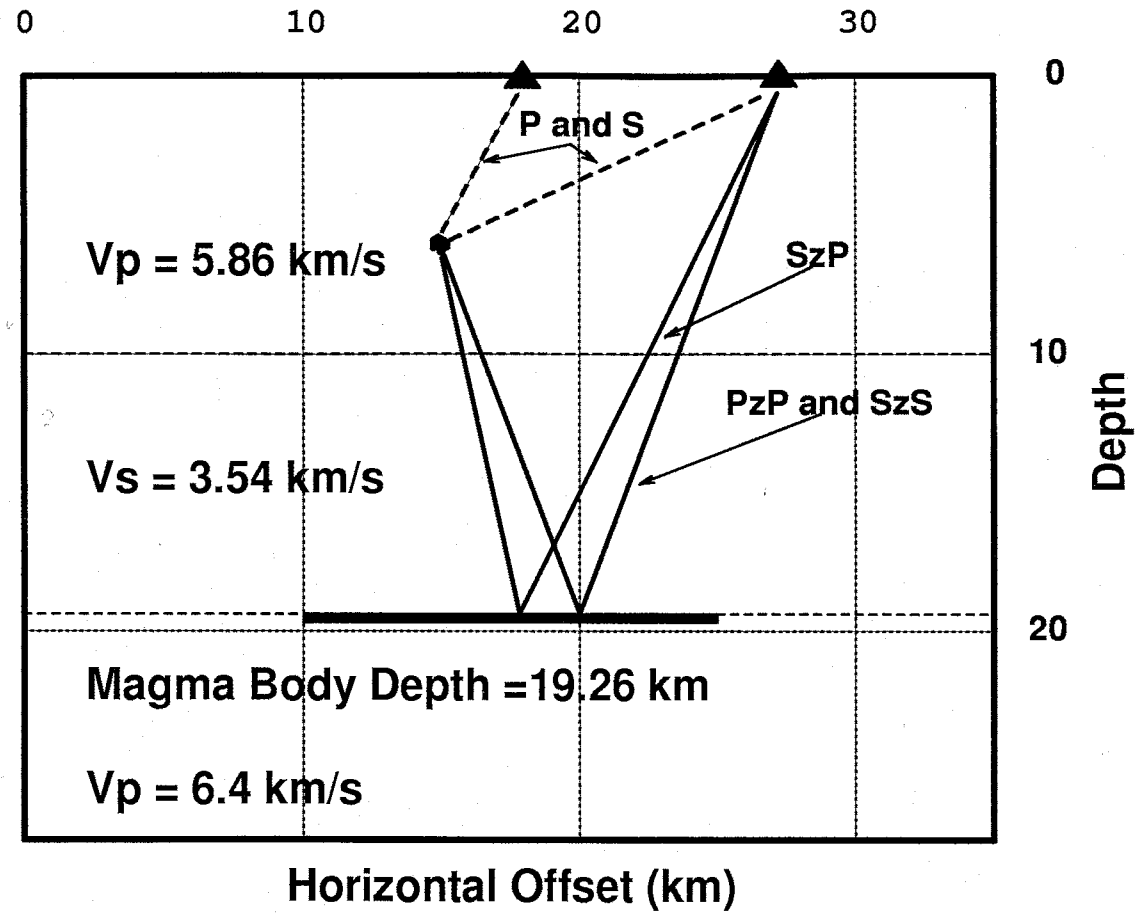

Figure 5.2. Velocity model and sample raypaths for a hypothetical earthquake. Triangles indicate seismic stations and the reflecting layer represents the Socorro Magma Body. Velocity model from *Balch* [1992].

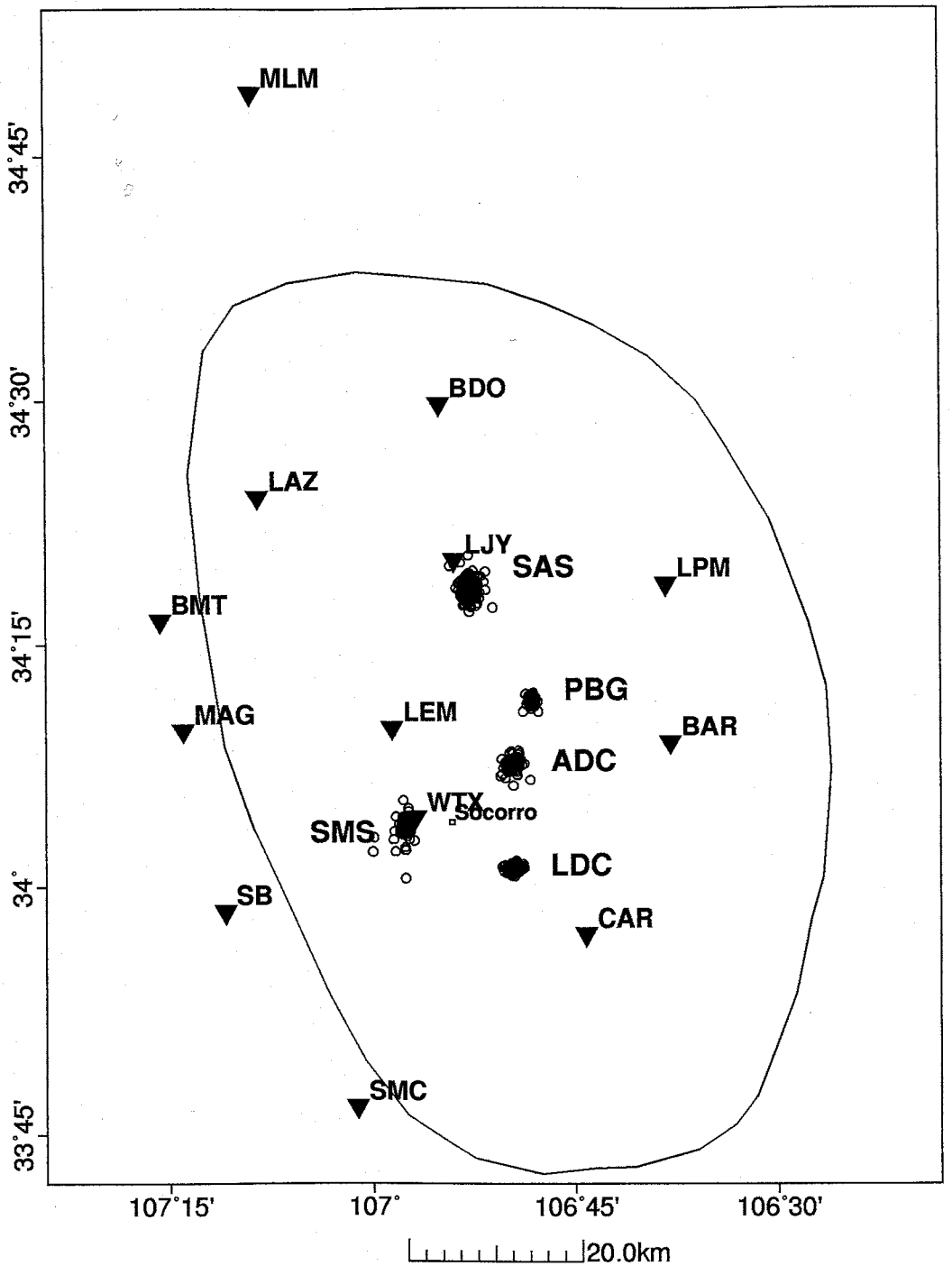

Figure 5.3. Epicenters from the five studied swarms. Also shown is the outline of the Socorro Seismic Anomaly and permanent stations operated in the region by New Mexico Tech.

statistically different. The average hypocentral depth for the 78 events was 8.4 km with a standard deviation of 0.5 km.

During the mid-1980's three swarms occurred along a linear trend on the eastern margin of the central graben of the RGR and lasted for 8 months. The Arroyo del Coyote (ADC) swarm (August 16, 1985 to May 8, 1986) had a M_d=4.0 main shock 12 hours into the sequence. The Puertecito de Bowling Green (PBG) swarm (September 17-20, 1985) had three events with M_d=2.73, 2.52 and 2.57 on September 19, 1985. The Loma de las Cañas (LDC) swarm (April 16 to May 23, 1986) had a main shock of M_d=3.1 on April 28, 1986. The swarms in spatial order from north to south were PBG, ADC, and LDC. Preliminary studies were performed on these swarms by *Petrilla* [1987].

6. Results – San Acacia Swarm

The San Acacia swarm (SAS) occurred 25 km north of Socorro, New Mexico, along the transfer zone between the Albuquerque-Belen and Socorro basins of the central Rio Grande rift. The swarm commenced on February 25, 1983, had a magnitude 4.2 main shock on March 2nd and ended on March 17, 1983. The San Acacia swarm was centered near the point of maximum geodetic uplift thought to be due to inflation of the Socorro Magma Body. Maximum surface uplift rates of 2 mm/yr over the SMB in the epicentral area have been reported by *Larsen et al.* [1986].

Hypocenters

The velocity model estimated by *Hartse* [1991] for the central Rio Grande rift was used in this study, with computed station corrections that are specific to the San Acacia swarm. To test that the calculated station corrections are geologically reasonable, gravity data for the San Acacia area were examined. Most of the gravity measurements were made by previous investigators, but some measurements to supplement the earlier studies were made by an undergraduate assistant and myself using a Worden gravimeter. The Bouguer gravity map (Figures 6.1 and 6.2) clearly shows a gravity low associated with the rift. However, along the low, a local gravity high forms a saddle between the Albuquerque-Belen and Socorro basins. The gravity saddle identifies an area where basement rocks are close to the surface. The smallest station corrections estimated are from sites that are over this gravity saddle, while the largest corrections correspond to sites in the basins to the north and south. Thus, the gravity and seismic data are in agreement.

Hypocenters for 204 events in the swarm were computed, of which 101 were considered high quality (latitude, longitude and depth errors of $\leq$ 0.5 km). For

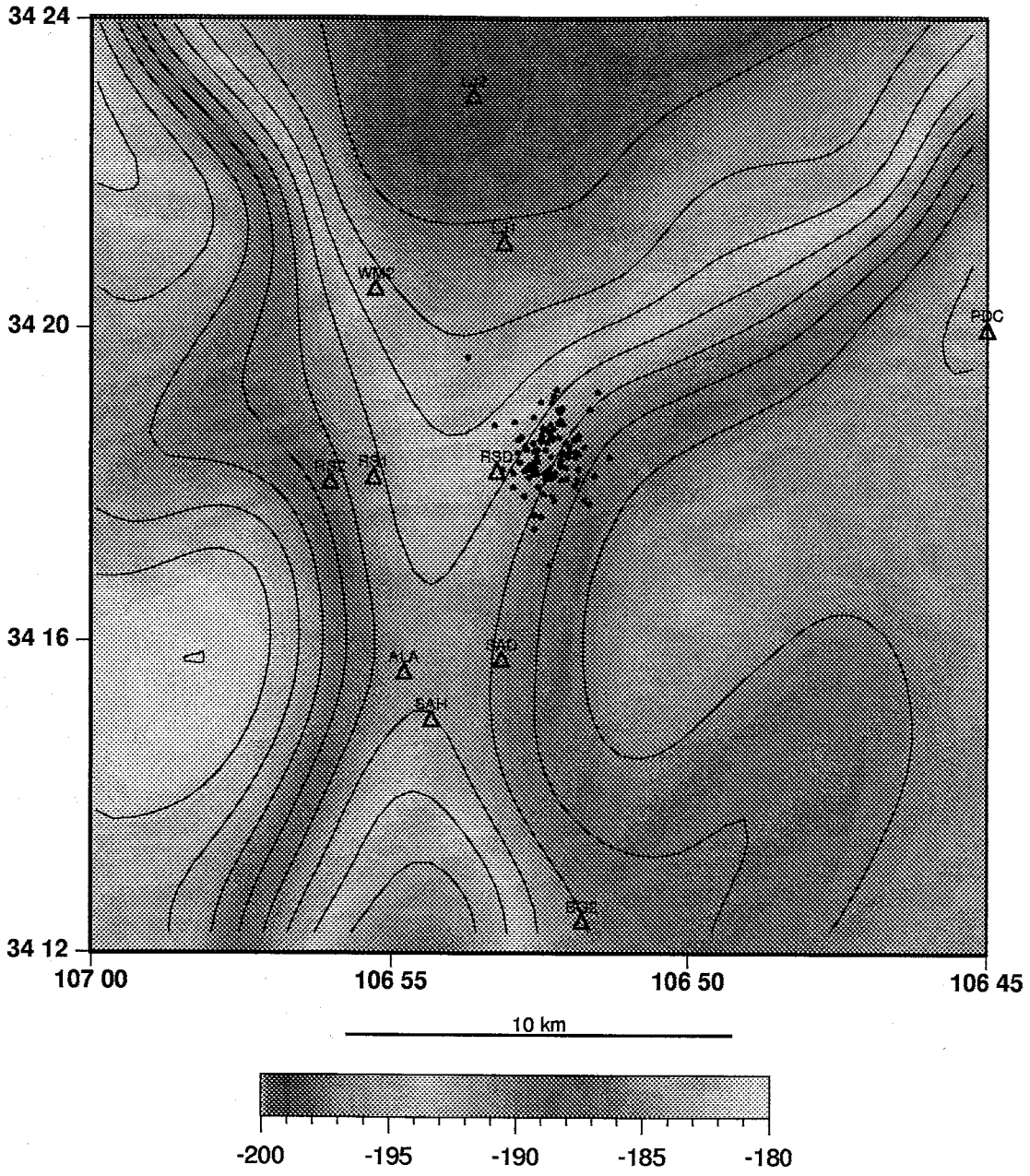

Figure 6.1. Bouguer anomaly contour map (mgals) for the San Acacia, New Mexico area. Also shown are the locations of temporary station sites (triangles) and the 101 best epicenters (black circles).

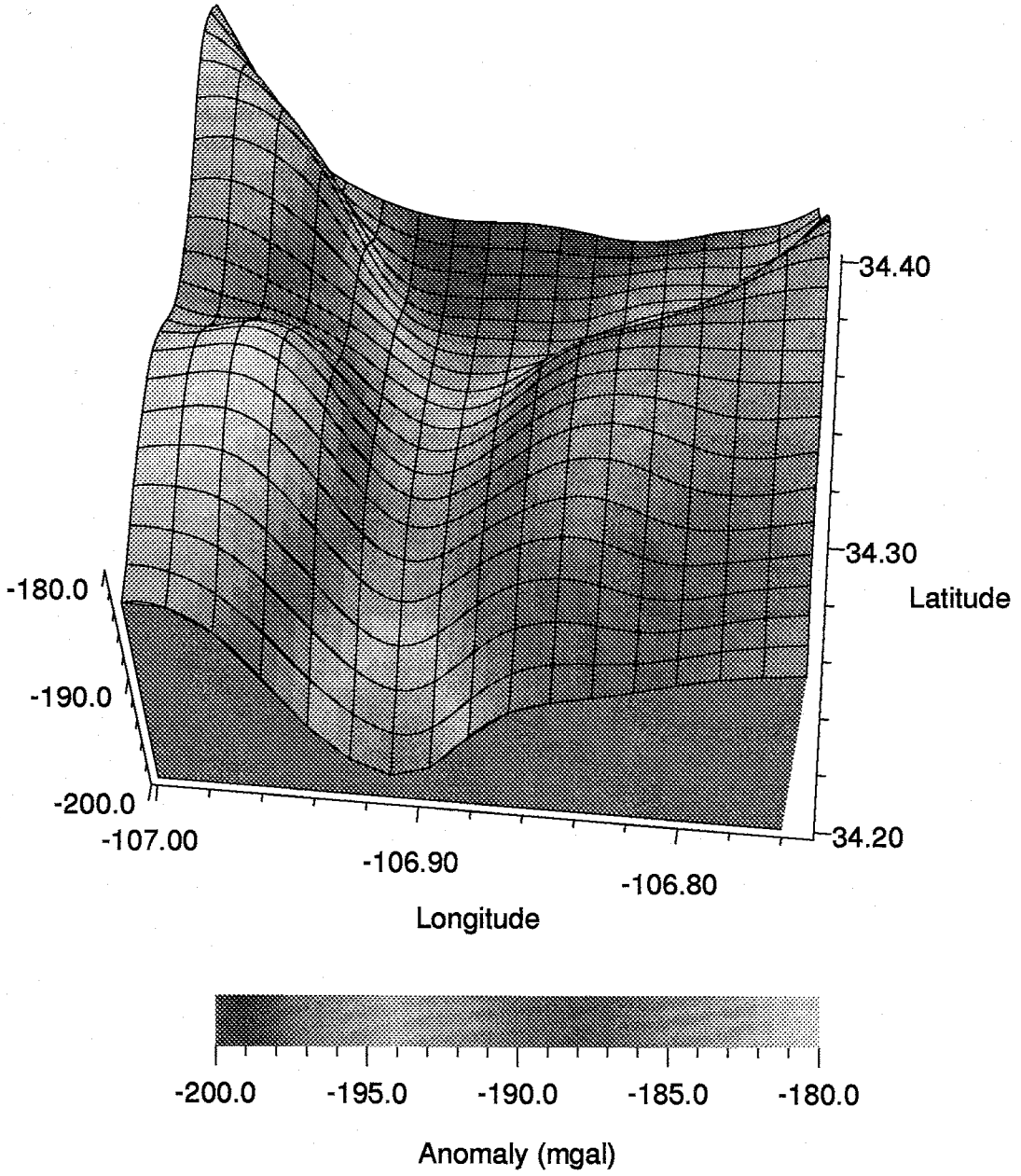

Figure 6.2. Three-dimensional representation of the contour plot in Figure 6.1, further illustrating the saddle between two RGR basins.

the well-constrained data set (Figure 6.3), the focal depths were evenly distributed between 3.3 and 6.3 km depth. Because the swarm was located on the saddle between the two basins, the shallowest hypocenters were below the Phanerozoic-Precambrian interface. Therefore the standard model with station corrections is an adequate velocity model for location and fault mechanism analysis of swarm events.

Cross sections of the earthquake hypocenters roughly define an ellipsoid with the major axis striking ENE and plunging 45^o along strike (the cross-sections shown in Figure 6.4 are samples of several cross sections that were examined). The lengths of the major and minor axes of the ellipsoid are about 4.0 and 1.5 km, respectively. The seismicity does not appear to define a tectonic foreshock-aftershock sequence, as the active volume is much larger than the rupture area of the magnitude 4.0 mainshock.

Focal Mechanisms.

Using the computer program FPFIT [*Reasenberg and Oppenheimer*, 1985] I obtained fault mechanisms for 30 earthquakes in the San Acacia swarm which had seven or more first motion readings and latitude, longitude and depth errors $\leq$ 0.5 km. Twenty mechanisms exhibit primarily normal slip on fault planes striking roughly north (Figure 6.5). First motions for ten of the events did not fit any standard double-couple source model (Figure 6.6). The ten events appear to have reduced dilatational quadrants, which may indicate rapid tensile opening as well as shear motions during faulting. I speculate that movement of groundwater in a geothermal reservoir could account for these observations.

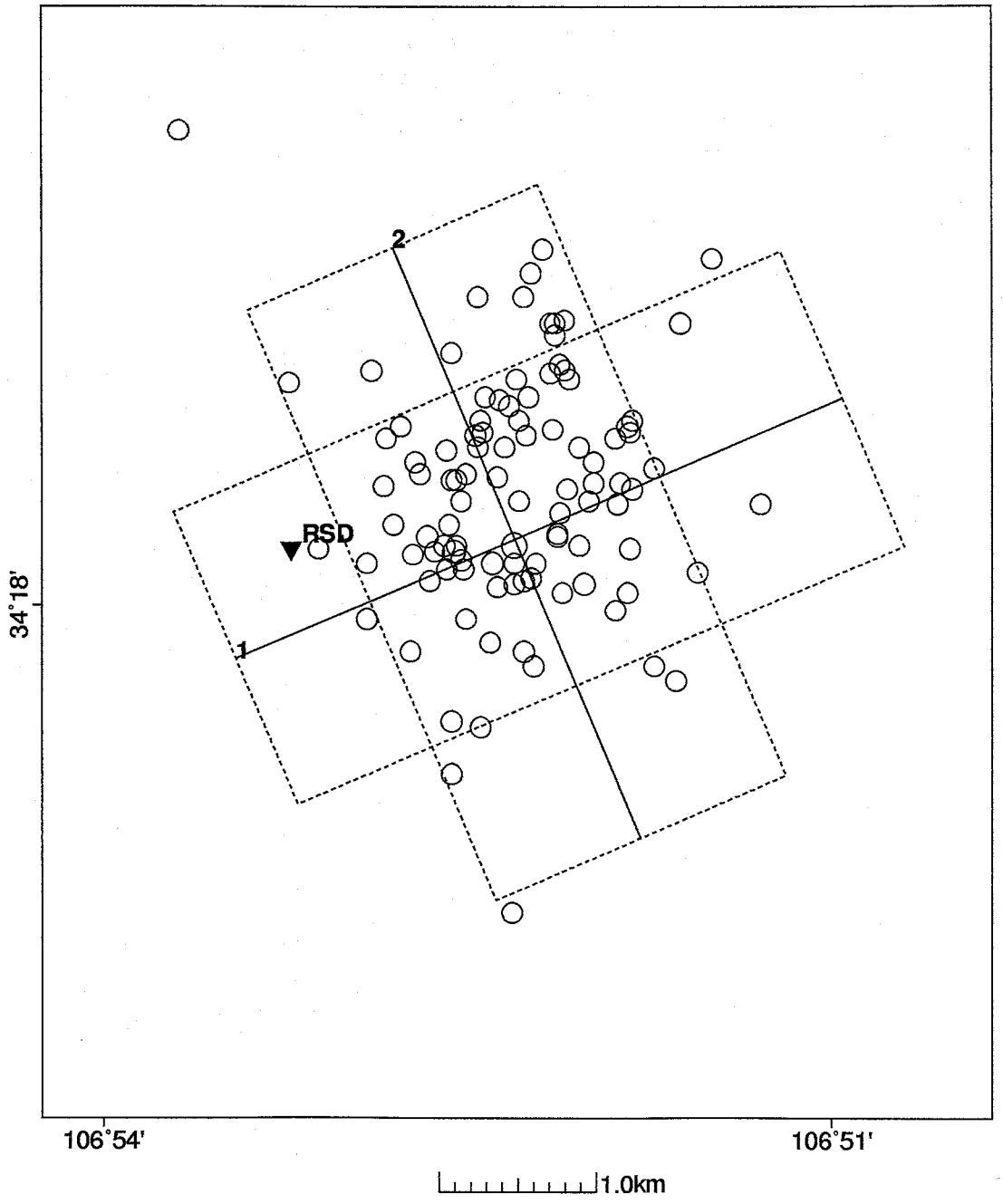

Figure 6.3. Epicenters for earthquakes in the San Acacia swarm. The map is restricted to the 101 events that have errors in latitude, longitude and depth ≤ 0.5 km.

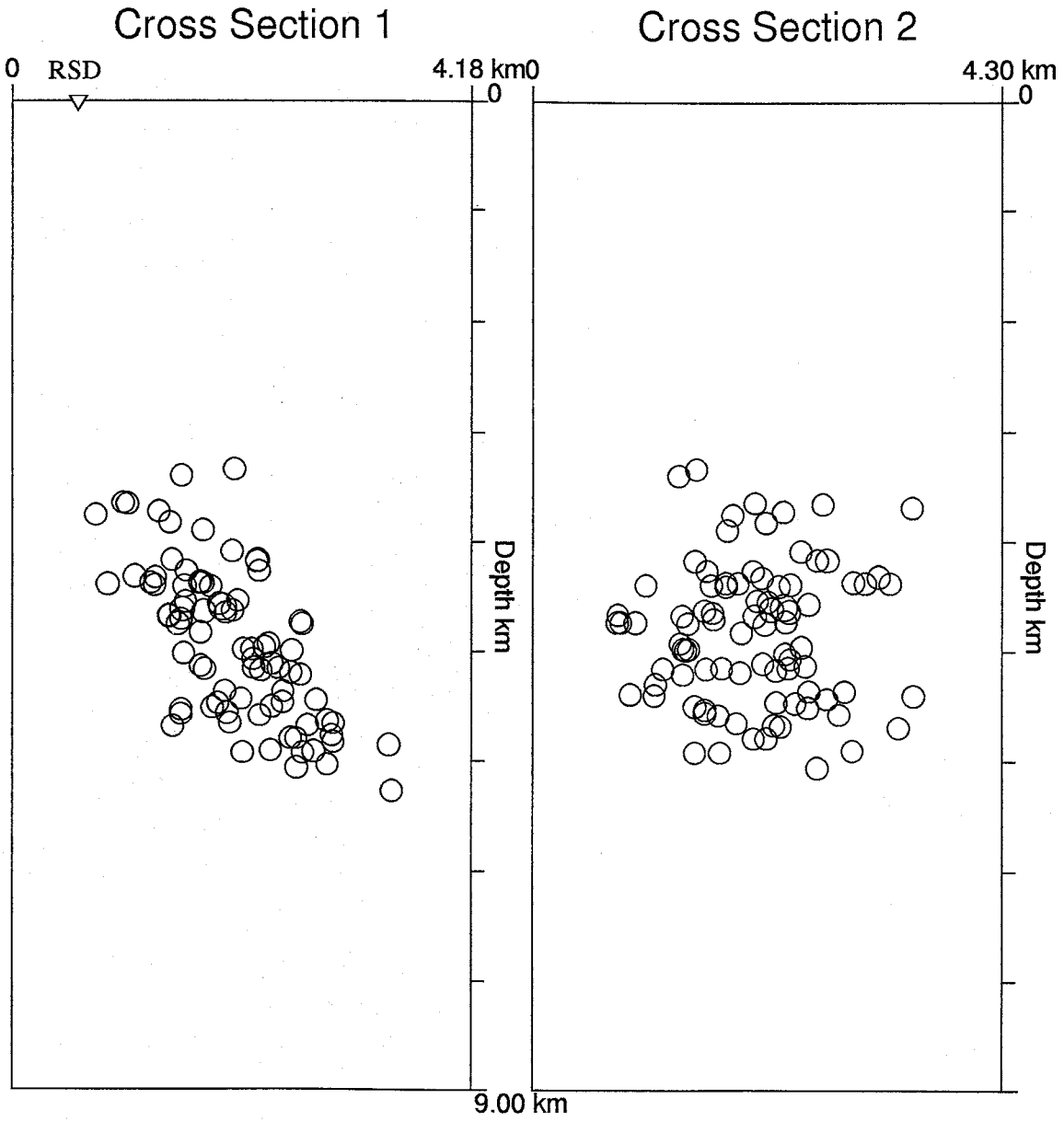

Figure 6.4. Cross-Sections 1 and 2 from Figure 6.3.

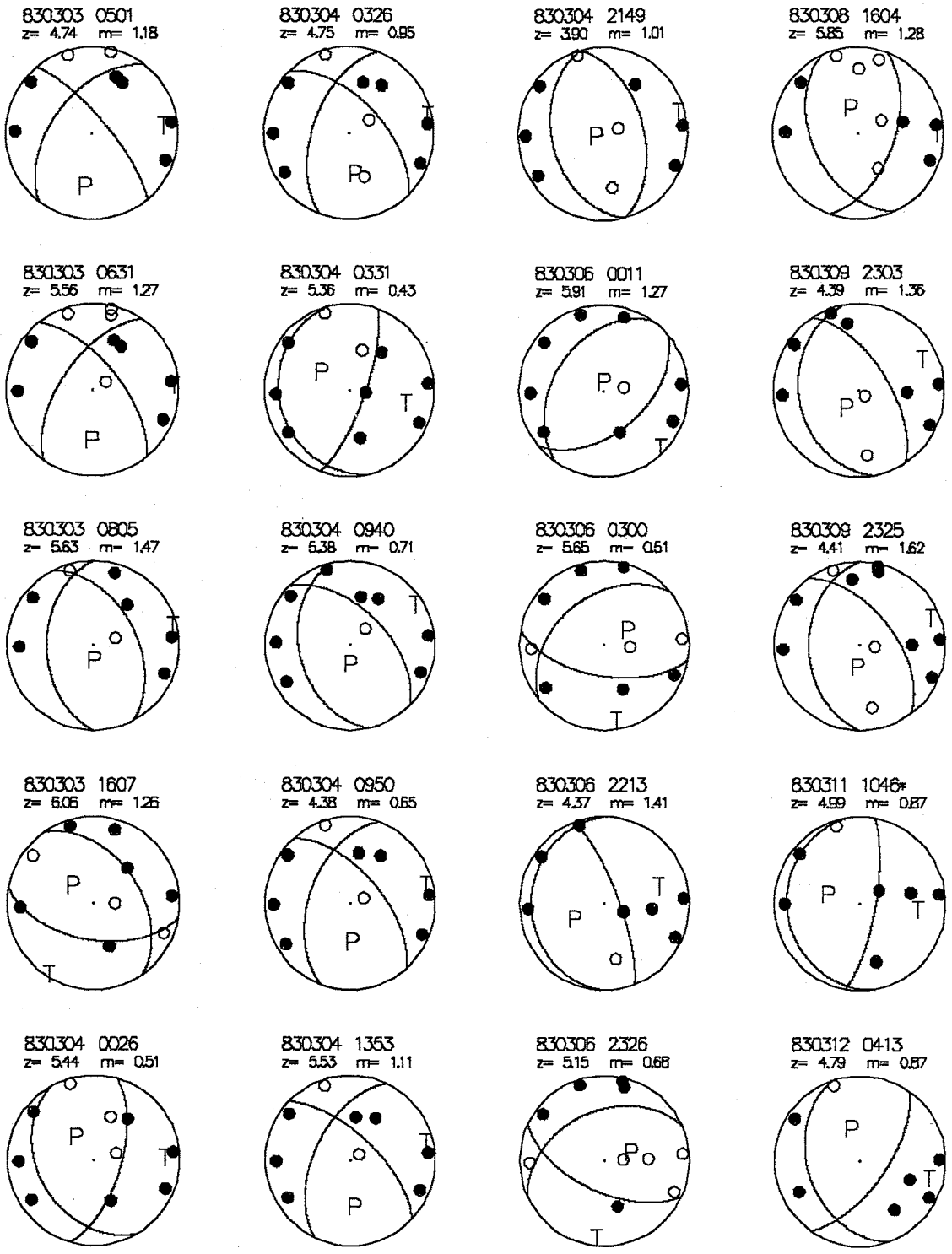

Figure 6.5. Fault mechanisms which fit double-couple sources. Most can be constrained as normal faults striking roughly north.

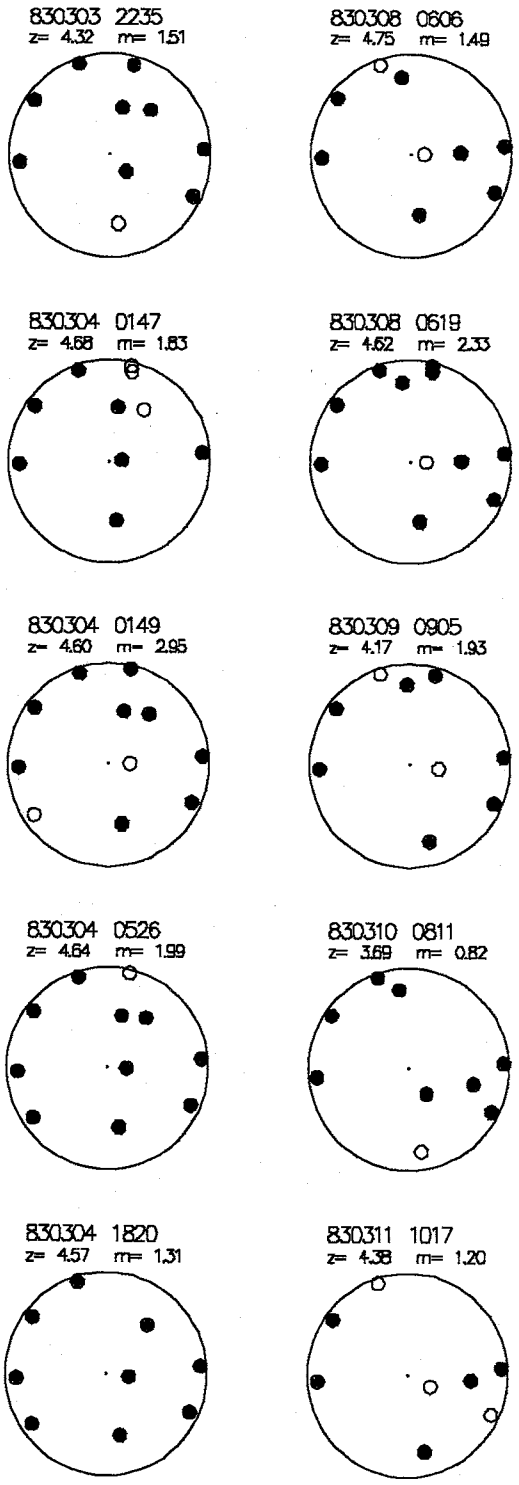

Figure 6.6. Focal mechanisms which do not fit standard double-couple sources. Note the reduced dilatational quadrants.

Non-Double Couple Focal Mechanisms.

Can groundwater circulating in cracks in heated rocks account for the disparate focal mechanisms plotted in Figure 6.6? Some additional component to the standard double-couple without moment (DCWM) source mechanism is necessary to explain the reduction in the dilatational quadrants for one-third of the well-constrained focal mechanisms. It is interesting to note that hypocenter plots (Figures 6.7 and 6.8) for the two types of events show that the NDC events occupy a distinct sub-volume of the swarm as a whole.

The observed distributions of first motion data for the ten event subset in Figure 6.6 was the first indication that some NDC events had occurred. I was unable to fit any double-couple mechanisms to the ten event subset using FPFIT; examination of the misfit nodal curves indicated that the problem was caused by a reduction in the dilatational quadrants. It is possible to adjust the position of first motion intersections on the focal sphere by altering hypocenter parameters, particularly depth. In the *Hypocenter* discussion of this chapter, evidence is given that the velocity model and station corrections are reasonable and that the earthquakes occurred in the basement rocks. This, coupled with the observation that the unusual focal mechanisms were located in a sub-volume of the swarm, supports the unique character of the cluster and favors the selection of a NDC interpretation.

Several options were available for forward modeling of these NDC mechanisms. First, an isotropic source with compressive first motions in all directions (consistent with an explosive source) would fit one event (Figure 6.6; 830304 1820); however, explosive (and implosive sources) do not generate S-waves, and strong direct and reflected S-waves were observed for the NDC events. Second, the less well understood concentrated linear vector dipole (CLVD) model which describes uniform outward motion in a plane due to normal shortening (opposite motions along polar

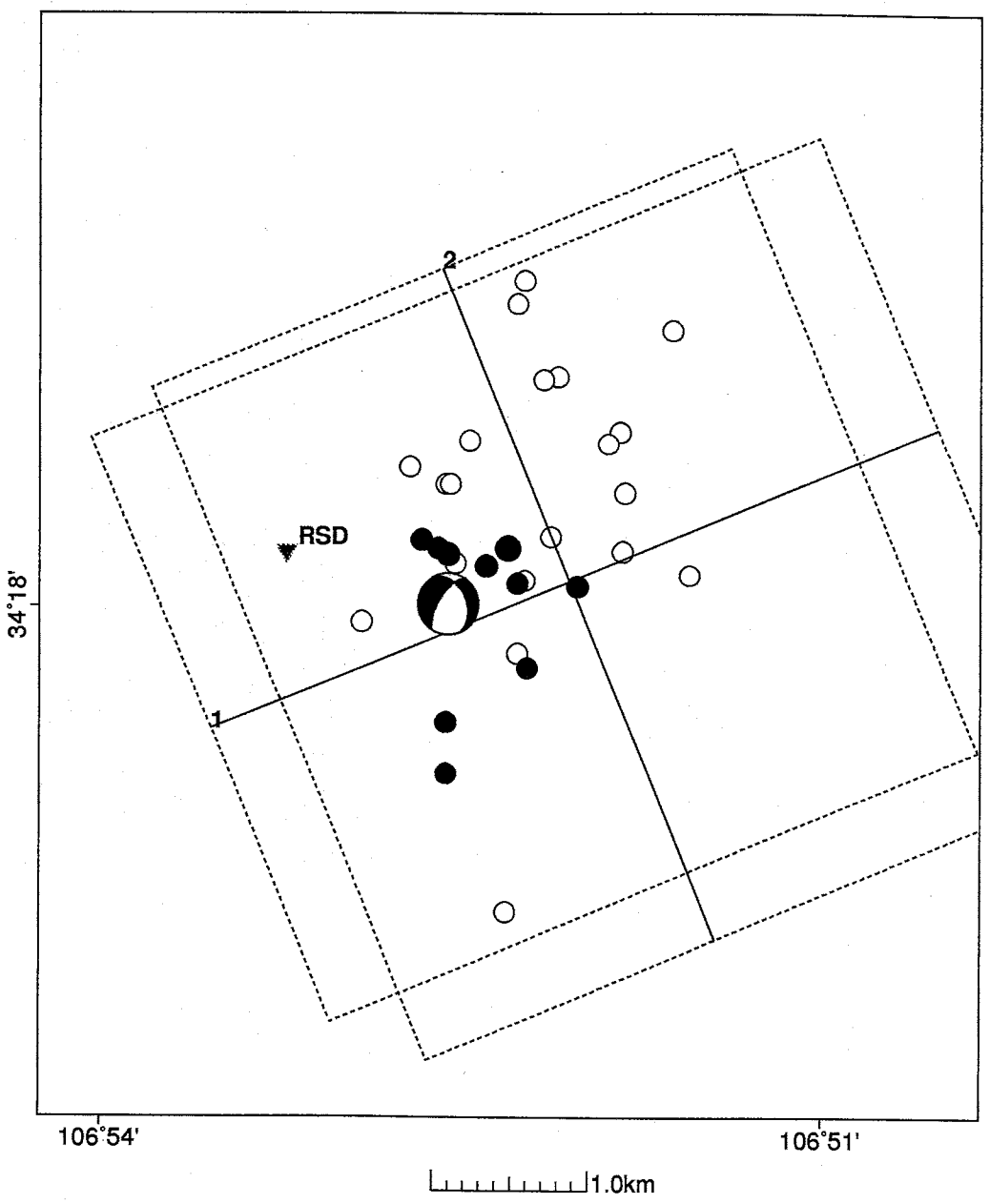

Figure 6.7. Epicenters for earthquakes in the San Acacia swarm for which focal mechanisms were computed. Filled circles represent the 10 events with NDC focal mechanisms. The plotted focal mechanism is for the $M_d = 4.2$ main shock.

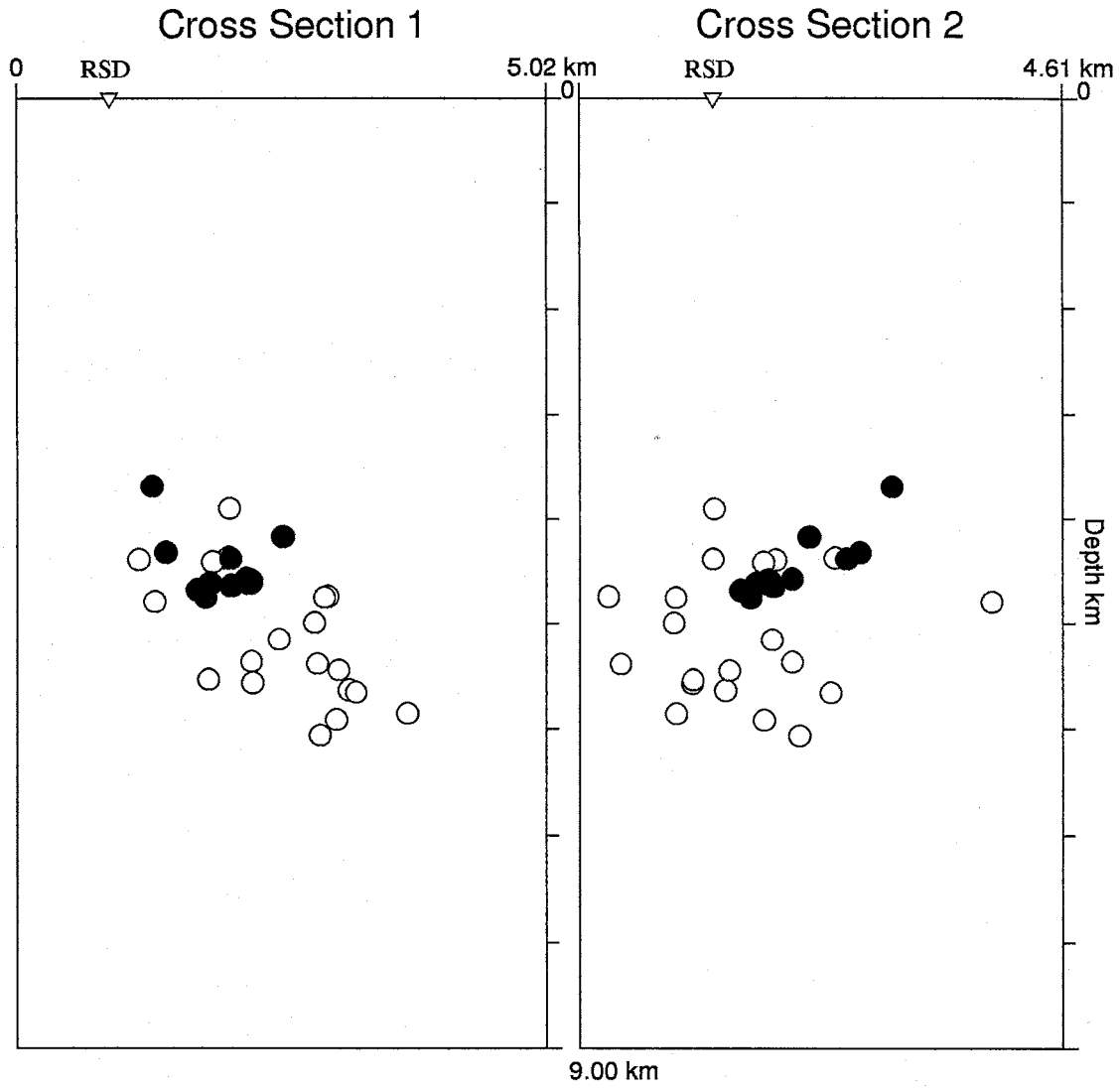

Figure 6.8. Cross-Sections 1 and 2 from Figure 6.7.

and equatorial axes) [*Frohlich*, 1994] was considered. To fit all ten observed events would require a large variability in both fault plane orientation and the corresponding "normal shortening". It seems unlikely that such disparate directions of normal shortening could occur over such a small volume of the crust, in a region otherwise characterizable consistently by N-S oriented normal faults. Third, tensile cracks have been considered to be a source of seismic radiation in rocks under tension. A tensile crack model was used by *Chouet*, [1979] to describe seismic events which occurred in a cooling lava lake on Kilauea Iki, Hawaii. While the first motion pattern of P-waves radiated from a tensile crack is compressive in all directions, in theory equivalent S-wave energy is also released [*Sato*, 1978]. Thus the radiation pattern of tensile cracks can explain some characteristics of these primarily compressive earthquakes.

The observed reduced dilatational components of the San Acacia NDC events require an additional component of shear to make them consistent with other mechanisms in the swarm, thus I used combinations of shear and tensile faults to model the NDC mechanisms as discussed in the **Methods** section of this dissertation. The moment of the shear component ranged from 2-7 times that of the tensile component, consistent with the observation that the events were primarily shear faults with an added component of tensile motion. The computed nodal curves for the NDC events are plotted in Figure 6.9 while the shear and tensile fault combinations are listed in Table 6.1. Figure 6.10 shows the shear component of the composite events overlaid on the observed first motion data for the NDC events illustrating the reduction in dilatation. Cursory examination of the double-couple events (Figure 6.5) indicates that some mechanisms could also have a tensile component, though the distribution of first motion directions narrowly allow double-couple solutions. Having successfully modeled the NDC events I attempt to relate them to the tectonic framework in the next sections.

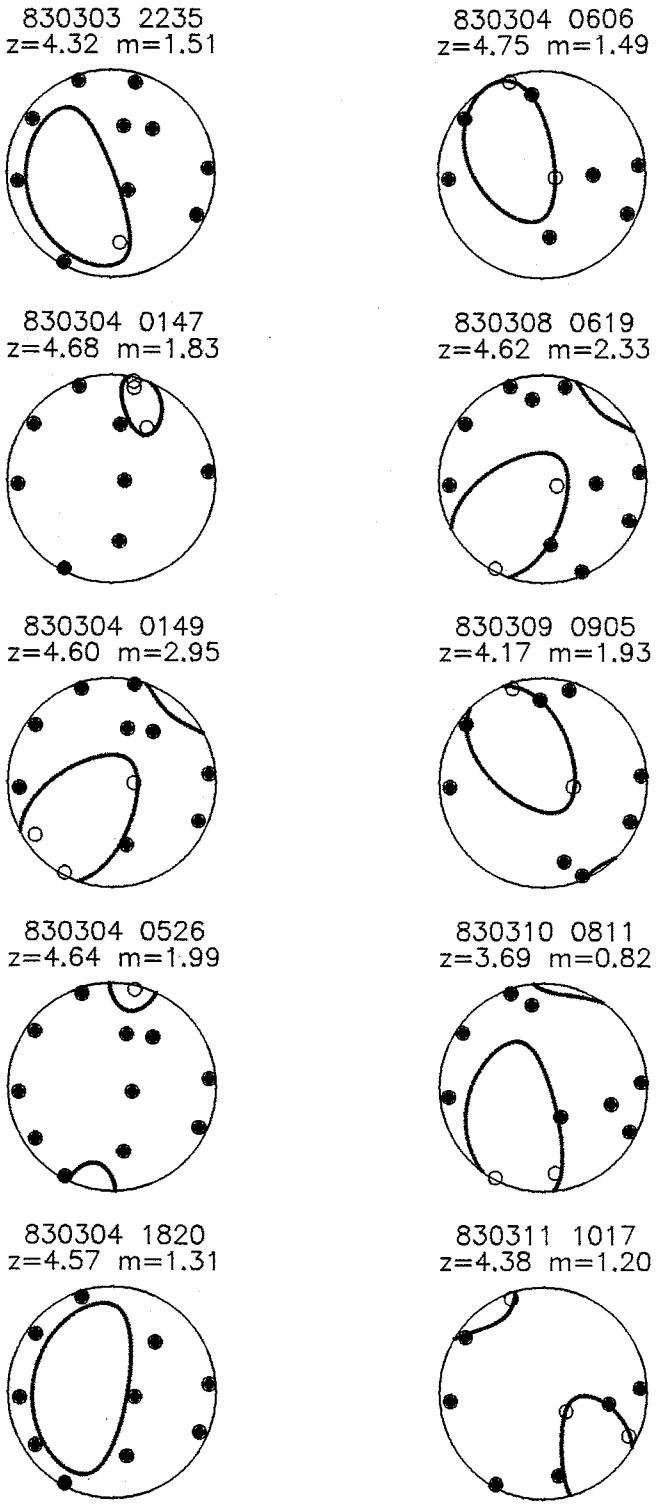

Figure 6.9. Nodal curve models for the non-double-couple events. Curves were modeled to maximize the shear component.

Modeled sources for NDC events				
Date	Strike	Dip	Rake	Shear/Tensile
830303 2235	180	15	-70	7
830304 0147	345	85	150	2
830304 0149	250	60	-40	6
830304 0526	340	90	-180	2
830304 1820	20	75	-80	3
830308 0606	127	40	-135	5
830308 0619	250	60	-40	6
830309 0905	122	60	-130	5
830310 0811	345	80	-120	7
830311 2235	288	60	-170	3

Table 6.1. Focal mechanism parameters strike, dip and rake measured in degrees. The tensile components share strike and dip with the shear components, and the multiplier indicates the ratio of shear to tensile moment.

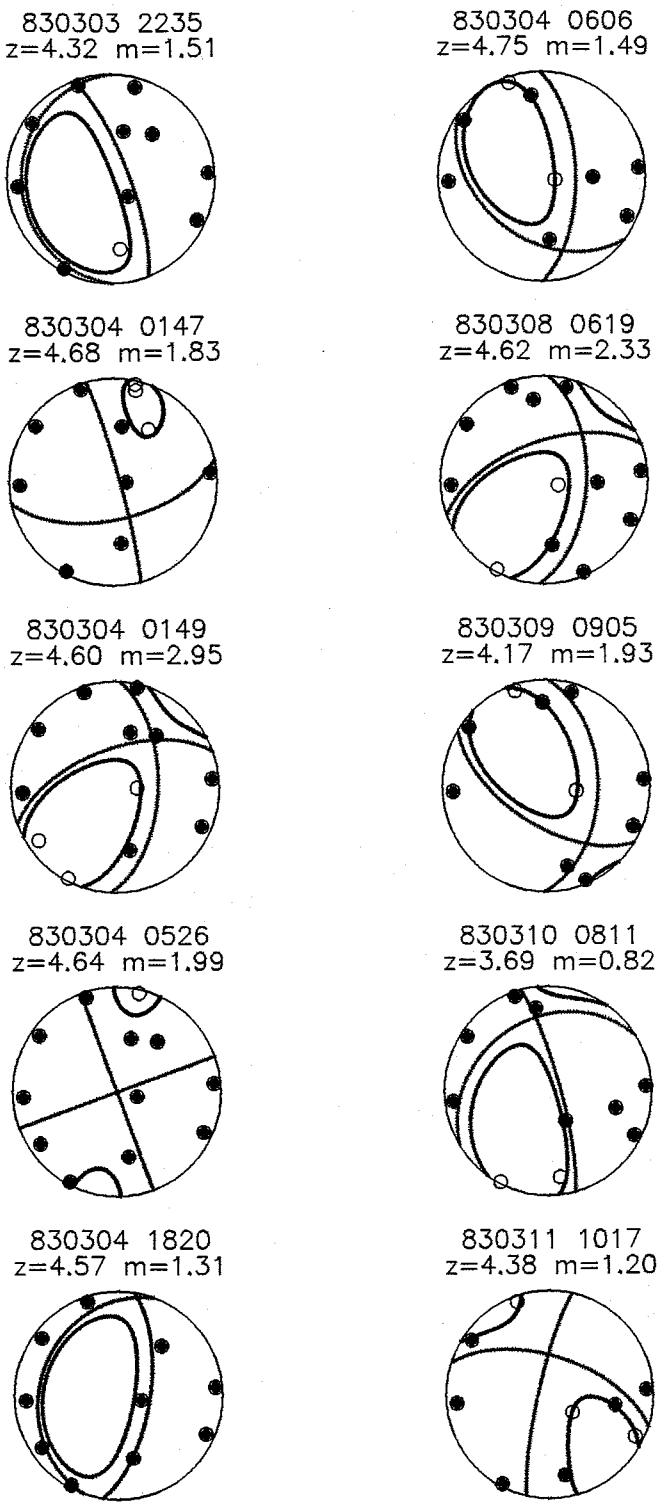

Figure 6.10. Shear components of modeled NDC events (full nodal curves). Also shown are modeled tensile-shear solutions from Figure 6.9 and observed first motion data.

Geology

The San Acacia swarm occurred in a region of the upper crust which is experiencing a variety of tectonic forces. Because the region is located within the RGR rift it experiences normal, rift-related stresses. Further, the region is identified as a transfer zone between two basins in the central Rio Grande rift. Transfer zones are transverse shear features which compensate for differentials in extension rates between two basins. *Chapin and Cather* [1994] believe that transverse features in the central RGR were formed as a result of rotation of the Colorado Plateau with respect to the stable craton about its Miocene euler pole. The swarm epicenter is also located near the center of the Socorro Magma Body and its associated maximum geodetic uplift of 1.8 mm/yr [*Larsen et al.*, 1986], thus the maximum amount of uplift induced stress is focused on the swarm region. Further, the region a few kilometers northwest of the epicentral region has a mapped normal fault at the surface [*Machette*, 1978] which though buried in an active dune field in the epicentral region, would trend through the swarm volume. It seems likely that a pre-existing pattern of N-S oriented shear cracks exists in the hypocentral volume.

One symptom of this complex geology is that the focal mechanisms computed for the San Acacia swarm (Figures 6.5 and 6.6) have the greatest amount of diversity of the swarms studied, particularly in the existence of NDC events and the variable strike orientations of the predominantly normal fault double-couple events (Figure 6.5). A thermal spring has been reported about 3 km south of the epicentral region [*Summers*, 1965; *Sanford,* 1996] in a pond alongside railroad tracks paralleling the Rio Grande. The closeness of this thermal spring to the river indicates a strong heat source, since significant masking of the heat source should occur due to subsurface flow of the Rio Grande. A thermal spring only 3 km from the epicentral region enhances the argument for involvement of heated fluids in producing the observed

NDC events.

Time History.

Figure 6.11 shows an event histogram for all events recorded at station BAR for the San Acacia swarm (SAS). These 288 events represent events with $M_d \geq$ -0.25 and illustrates two features of Socorro area swarms. The strongest event was located toward the temporal center of the swarm as is common for Socorro area swarms. Events are also temporally clustered; except for the most active periods (close to main event) events occurred in bursts of activity followed by periods of quiescence. The earthquakes with NDC mechanisms started 24 hours after the main shock of March 2, 1983 (Julian Day 63) and concluded on Julian Day 71. The swarm sequence as a whole lasted for 20 days. Because the NDC events occurred in the vicinity of the $M_d = 4.2$ main shock (Figure 6.7) and did not commence until after that rupture, the NDC events may have been causally related to the main shock rupture process. The main event most likely occurred on a normal fault oriented roughly N-S, consistent with observed surface faults northwest of the epicentral region [*Machette*, 1978].

Interpretation.

The existence of what have been modeled as tensile-shear failures poses an interesting question: What was the physical cause of the NDC events? *Shimizu et al.* [1987] believe that tensile-shear ruptures modeled for earthquakes recorded following a volcanic eruption on Miyakejima Island were the result of sudden tensile opening of shear cracks resulting from excessive pressure of intrusive magma. Though magma may not be present in the upper crust near San Acacia, the shallow nature of the earthquakes, when combined with the observed thermal spring near the epicentral region, indicates that ground water is circulating at depth. The highly fractured

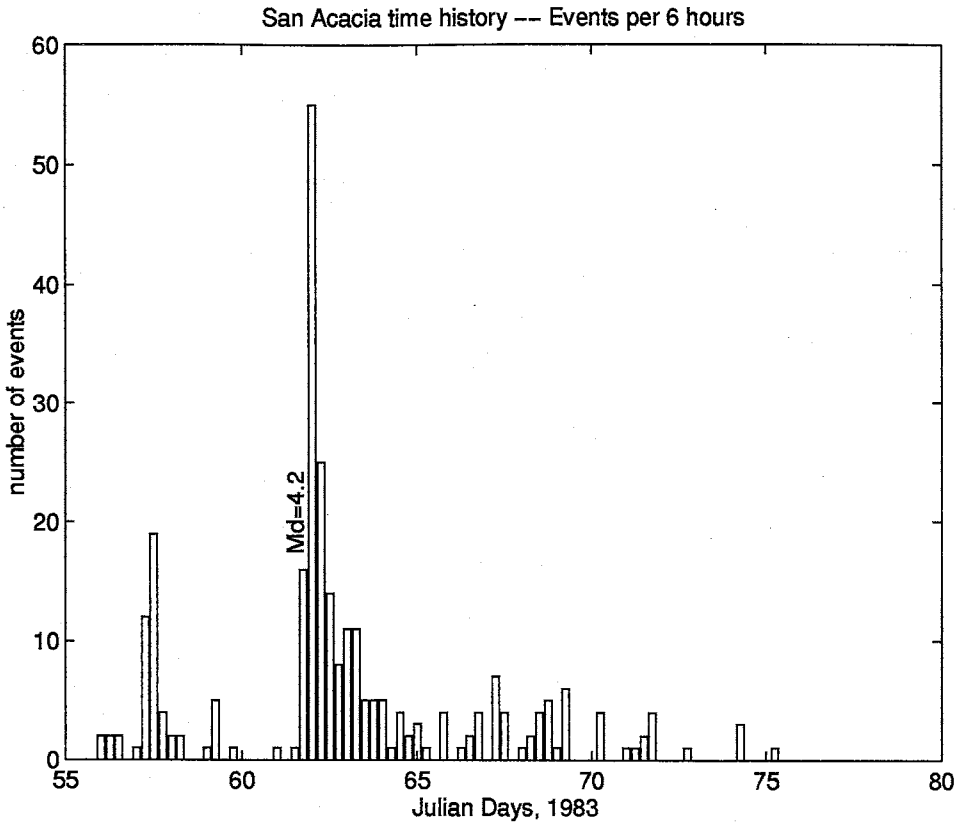

Figure 6.11. Event histogram for the San Acacia Swarm. The plot contains 288 events above M_d=-0.25 in six hour bins. Note the temporal clustering of the earthquakes.

nature of the hypocentral volume, as evidenced by variable focal mechanisms and complex geology, could provide adequate conduits for movement of groundwater. It seems possible that pressurized water acting on the fault planes could account for the relatively small tensile motions associated with the NDC earthquake mechanisms – perhaps as a result of rapid fluid injection into a crack as it begins shear failure.

7. Results – Socorro Mountain Swarms

Introduction

The Socorro Mountain swarms occurred in May and July, 1983. Hypocenters were determined using the computer program **SEISMOS** [*Hartse*, 1991] with a crustal model consisting of a single constant velocity layer from the surface to the top of the Socorro Magma Body (SMB) at a depth of 19.26 km (Figure 5.2). A total of 108 events with $M_d < 2.1$ were located, of which 78 had errors in latitude, longitude and depth ≤ 0.5 km. The average hypocenter locations for the May and July sequences were not statistically different. The average hypocenter depth for the 78 events was 8.4 km with a standard deviation of 0.5 km.

Fault Plane Solutions

Focal mechanisms for 24 of the largest events were determined using FPFIT [*Reasenberg and Oppenheimer*, 1985]; 11 events from the May swarm and 13 from the July swarm (Figure 7.1). Both sequences contained dominantly normal-fault earthquakes with the P axes near-vertical and nearly all T axes oriented from west to northwest. The first 10 mechanisms in the May sequence had an average T axis azimuth and dip of $316^0 \pm 5.6^0$ (1 s.d.) and $11.5^0 \pm 4.9^0$ (1 s.d.), respectively. These fault-plane solutions have a small component of strike-slip motion. The first 11 mechanisms for the July sequence describe two distinct focal mechanisms: the first has T axes which average $297^0 \pm 5.6^0$ (1 s.d.) in azimuth and $2.8^0 \pm 0.8^0$ (1 s.d.) in dip; the second has T axes which average $254^0 \pm 2.9^0$ (1 s.d.) in azimuth and $1.7^0 \pm 0.0^0$ (1 s.d.) in dip. The dominantly normal-fault mechanisms in the July swarm have a larger component of strike-slip motion than those of the May swarm. The last mechanism found for the May swarm and last two mechanisms

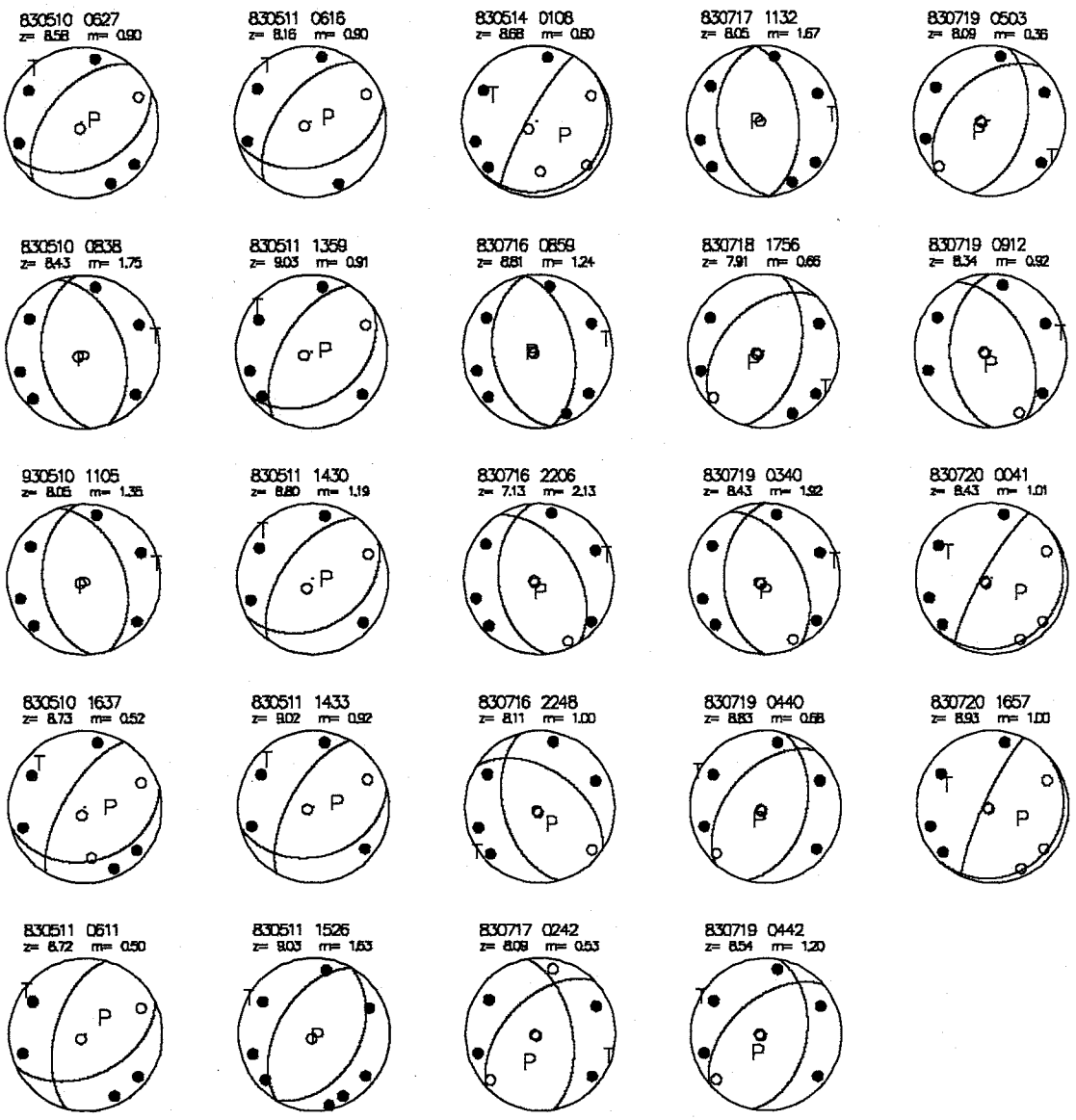

Figure 7.1. Unconstrained FPFIT fault-plane solutions for 24 of the largest swarm events.

determined for the July swarm may indicate a different mode of crustal movement than the other events. One nodal plane for these three events strikes $\sim$N30^{0}E and dips $\sim$80^0 to the WNW, the other nodal plane strikes $\sim$N50^{0}E and dips $\sim$10^0 to the ESE.

A simplification can be made to the computed SMS fault plane solutions by applying constraints to the grid FPFIT uses to compute the solutions [*Reasenberg and Oppenheimer*, 1985]. By constraining the strike range between N5°E and N35°E and allowing rake and dip the complete range, all events but one event were fit. The constraints were chosen to make nodal planes pass close to two stations which frequently exhibited alternating directions of first motion during the swarms. FPFIT on the other hand attempts to keep the nodal planes as far as possible from all first motions. The new fault plane solutions (Figure 7.2) show varying degrees of dip on nodal planes striking NNE, dipping shallowly to the ESE or steeply WNW. The greatest error in the original fault plane solutions occurred in the strike, so these solutions are considered reasonable.

Geology

A study of the surface geology in the Socorro Mountains has been completed by *Chamberlin* [1980]. The crest of Socorro Mountain is the remnant of the rim of an Oligocene caldera complex. The cauldron formed during early extension of the Rio Grande rift, and has ring fractures which trend WNW and dip toward the southwest in the vicinity of Socorro Peak [*Chamberlin*, 1980]. Three phases of extension were identified by *Chamberlin*, two phases of domino-style faulting (32-20 ma and 12-7 ma) followed by the current horst and graben style faulting.

Domino-style faulting is most common in regions with high heat flow and results from progressive necking of the lithosphere which grades into upper crustal exten-

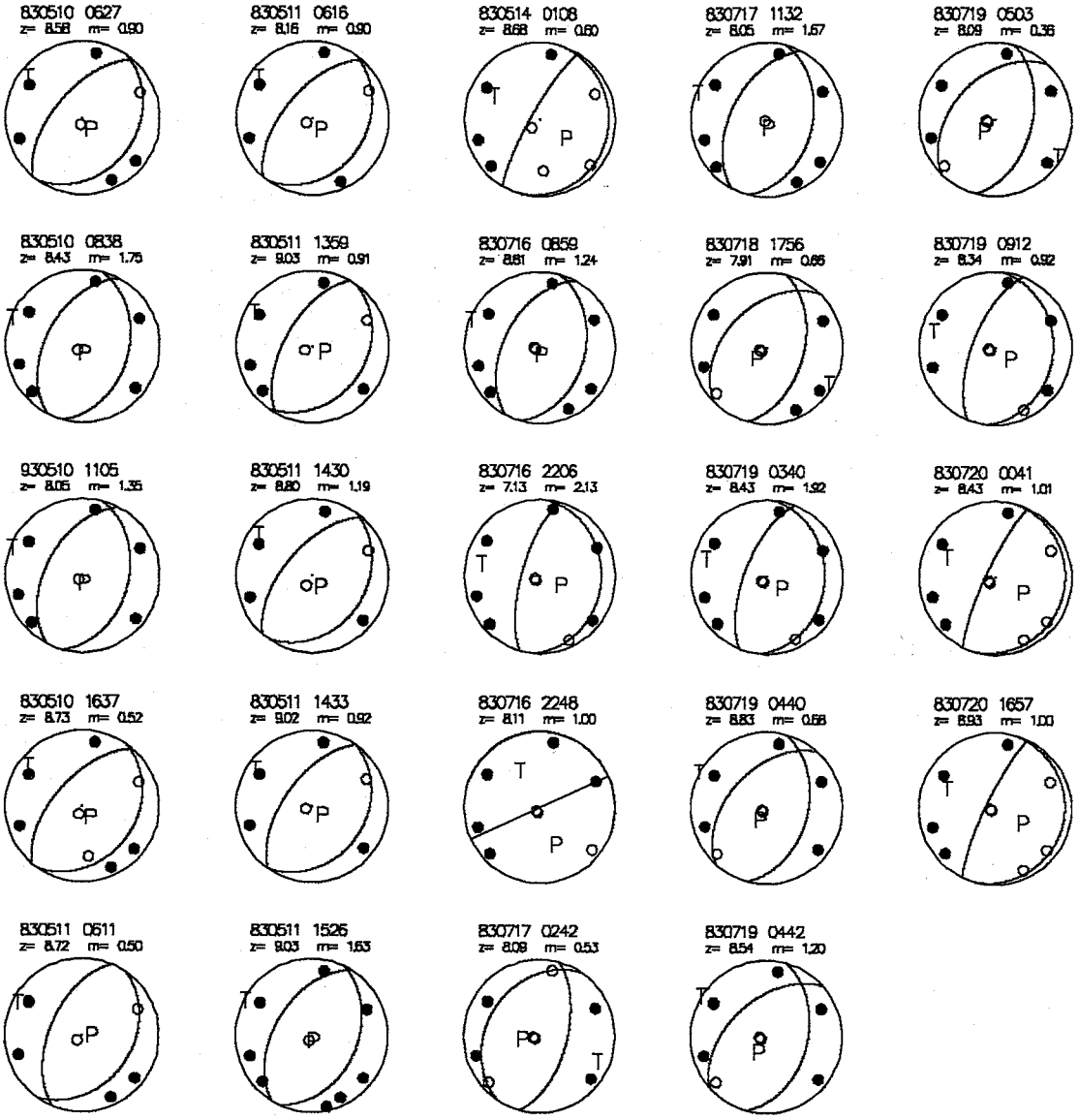

Figure 7.2. Constrained FPFIT fault-plane solutions for the 24 events in Figure 7.1.

sion. Extension is accommodated by rotation of large blocks along normal faults [*Morton and Black*, 1975]. After the blocks rotate 20-30 degrees new normal faults develop as in Figure 7.3. The Spears formation, a thick bed of volcanic sediments deposited during pre-Oligocene erosion of earlier volcanic centers, are tilted 50-60 degrees westward in the Lemitar Mountains, a few kilometers to the north of the swarm epicenter. *Chamberlin* notes that post-Oligocene rotation of domino-style blocks in the Socorro Peak area approaches 40 degrees.

Interpretation

Close examination of *Chamberlin's* geologic map and associated cross-sections reveals that the only large surface faults near the epicentral region are the caldera rim faults and the Socorro fault zone (Figure 7.4). The rim faults do not correlate spatially with the swarm events at hypocentral depths, nor do any of the possible nodal planes share the WNW trend and southwestward dip of the rim faults. The Socorro fault zone is a major basin-bounding fault system separating the Socorro Mountain horst block from the deeply offset basin to the east of the mountains [*Sanford*, 1968]. This eastward dipping fault zone fails to intersect the hypocentral region.

Since the surface geology fails to explain the fault planes computed for the swarm earthquakes, an alternate tectonic explanation is proposed below. The epicentral map (Figure 7.5) shows the constrained FPFIT solutions for 24 of the largest events in the swarms. Two interpretations can be made from these lower hemisphere projections: dominantly shallow normal faults striking NNE and dipping to the ESE, or dominantly steeply dipping normal faults striking NNE and dipping WNW. A wide range of dips is observed, and no one single fault plane seems to contain all of the events in cross-section (Figure 7.6).

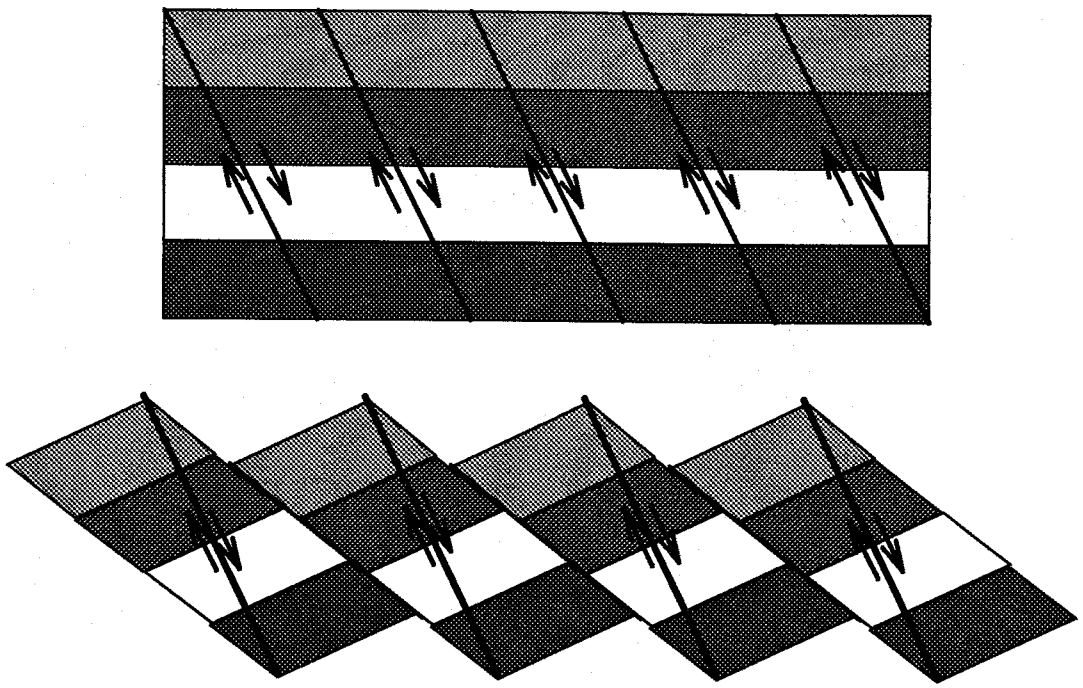

Figure 7.3. Schematic diagram depicting domino-style faulting. The upper figure depicts initial extensional faulting. The lower figure depicts 25° of rotation in the original fault blocks and formation of new normal faults.

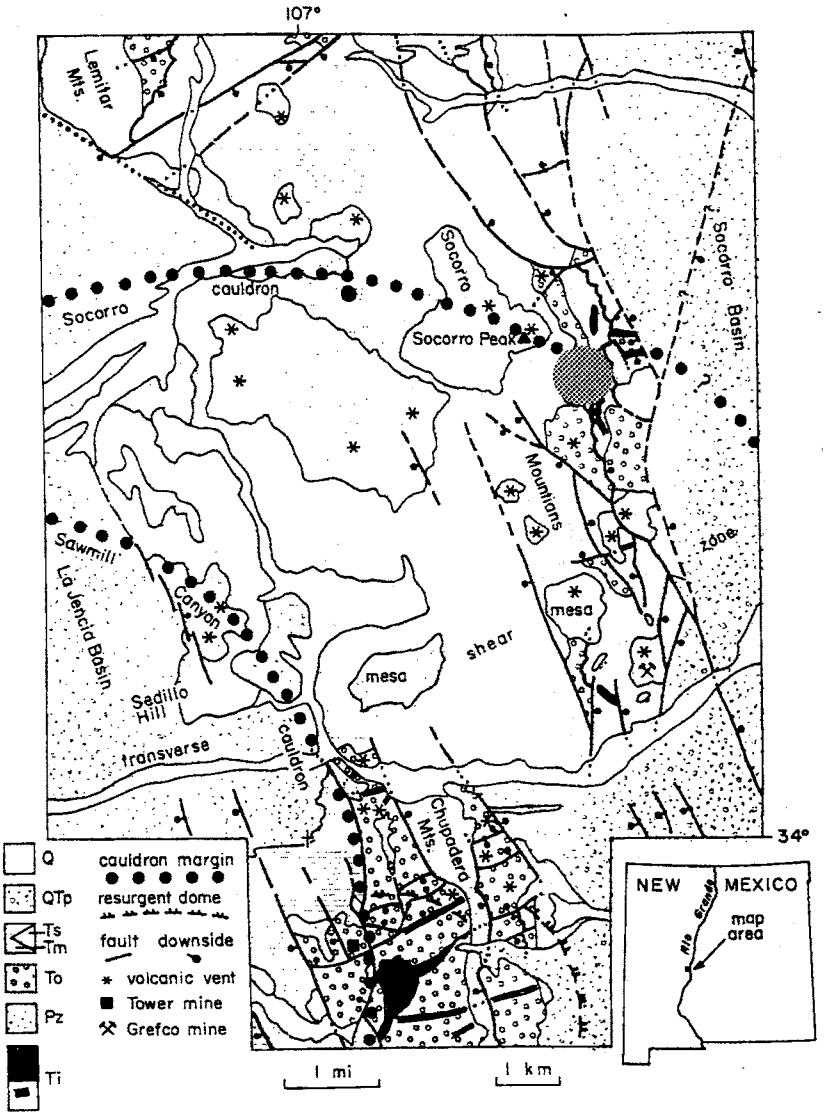

Figure 7.4. Geology of the Socorro Mountain volcanic center. Faults are indicated by thick lines. The epicentral region is indicated by a circle. Figure modified from *Chamberlin* [1981].

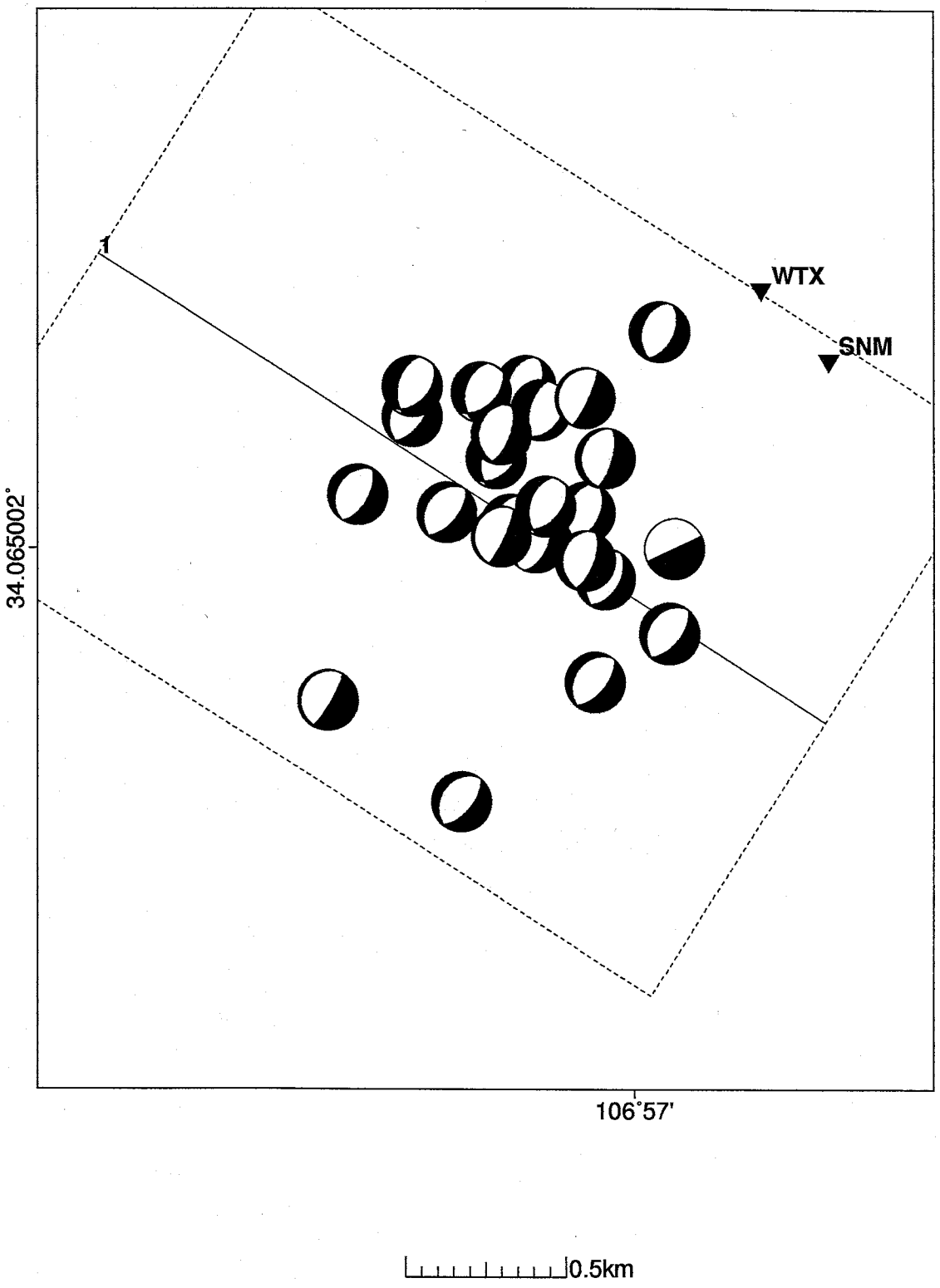

Figure 7.5. Epicenter map for the FPFIT constrained focal mechanisms. The 24 constrained focal mechanisms are plotted.

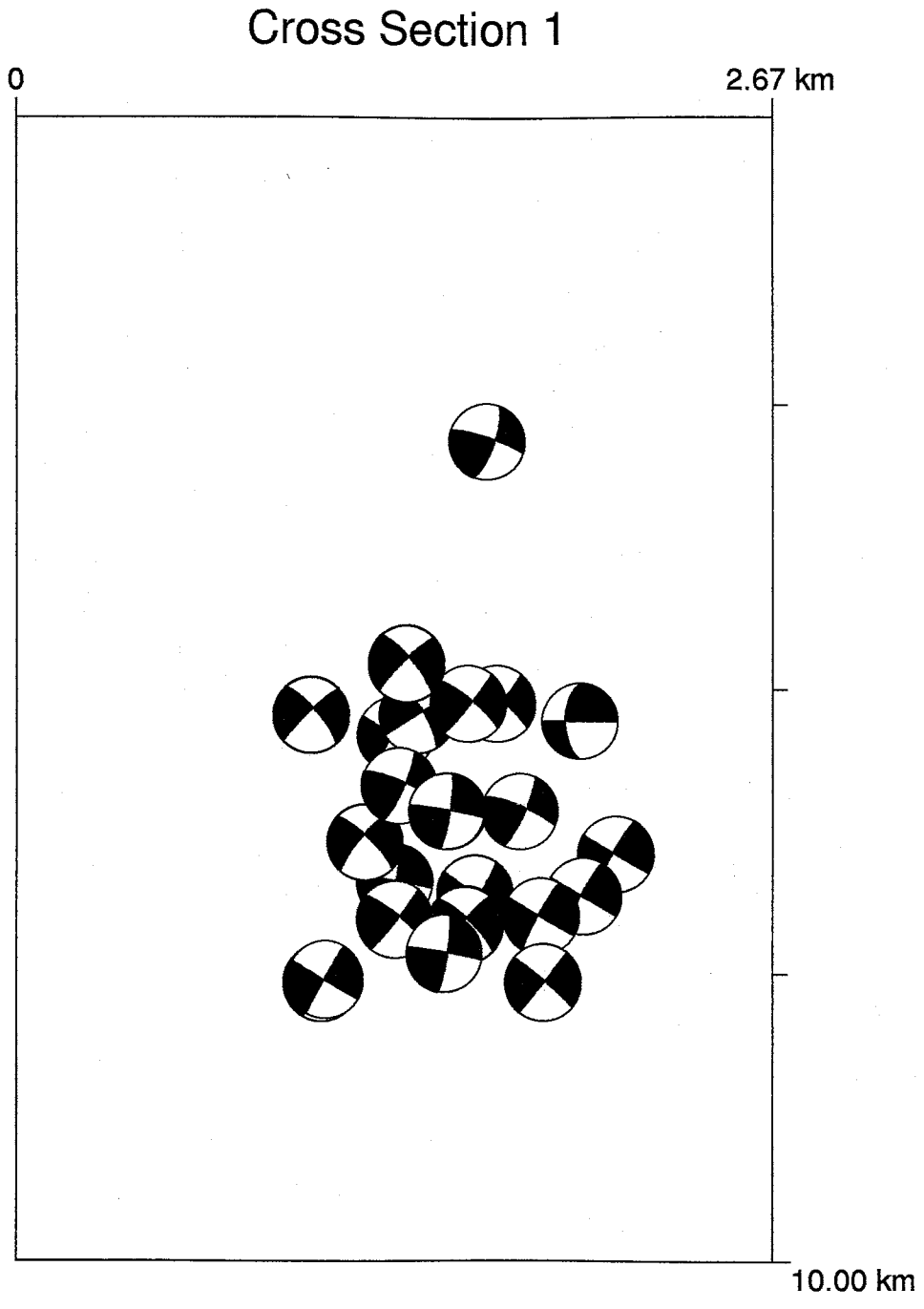

Figure 7.6. Cross-section from Figure 7.5. No single fault plane contains all of the swarm events.

One possible tectonic explanation is that the events occurred on a system of shallow-angle, east-dipping faults that were formed during the post-Oligocene domino-style faulting. The two or three identified episodes of domino faulting may explain the observed variety of fault dips, as well as the closely spaced fault planes.

A recurrent problem in analysis of Socorro area microearthquake swarms is the lack of correlation of fault-plane solutions with mapped Quaternary and/or Pliocene faults at the surface. The 1983 Socorro Mountain swarms described here are an example of this problem. One mechanism we may invoke is reactivation of older fault systems at depth. The fault-plane solutions for these swarms appear to fit an Oligocene fault pattern developed through several phases of domino-style faulting. Post-Oligocene rotation of 40^o could lead to dips of 20^o or less on the oldest normal faults. Reactivation of old faults at low angle could result from a reduction of stresses normal to the fault resulting from the presence of fluids within the fault plane. Groundwater circulation beneath the Socorro Mountains has been reported [*Barroll and Reiter*, 1990].

Digital Data and Time History

Digital data recorded at WTX during both swarm sequences opened questions about the dynamics of swarm processes. Both sequences shared the same statistical location and fault type, however some anomalies in the codas for the two sequences warranted further study. The relative amplitudes of the P-wave was highly variable between events within each swarm, even those separated by minutes, and though sample events within each sequence correlated well [*Ake* 1986], a closer look at the digital data demonstrated that a number of swarm subtypes existed, particularly during the longer July sequence.

The digital data for the May and July SMS swarm was reduced to 4 second win-

dows for events between May and July and examined using cross-correlation. The cross-correlations were accomplished using **SAC2000** (Copyright 1987 the Regents of the University of California) with simple scripts and programs. The events were recorded on a Sprengnether DR100 digital recorder at station WTX, located in a mine tunnel within one kilometer of the epicentral region. The recording began 4 days into the May swarm (on May 14, 1983), so it is uncertain if the lower variability in waveforms for the May sequence is a meaningful observation. However, examination of analog recordings from WTX for the May swarm indicates that the codas were less variable than those of the July sequence.

The master events for the sub-types which occurred in the May and July sequences are shown in Figure 7.7. **Appendix III** contains plots of all events by subtype, including correlation coefficients. Examination of Figure 7.7 reveals that most of the apparent differences in waveforms (amplitude independent) occur in the S-phase. In fact the 120 digitally recorded events which occurred during the main May and July sequences have an average P-wave (0.3 second window) (Figure 7.8) correlation coefficient of 0.75; the corresponding overall correlation coefficient (4.0 second window) is only 0.51. The most likely cause of this variability between relative amplitudes of the P and S phases is that small changes in fault plane orientation, particularly dip, affected the P and S wave radiation patterns throughout the swarm sequence.

The swarm sequence as a whole occupied a volume about one kilometer on a side at a depth of 8.0 km. The small size of the swarm volume makes it impossible to statistically tie swarm event sub-types based on cross-correlation to hypocenter locations since the acceptable hypocentral error was 0.5 km in latitude, longitude and depth (1 std.). The subdivision of the swarm into event sub-types with apparently variable fault plane orientations is supported by the computed focal mechanisms

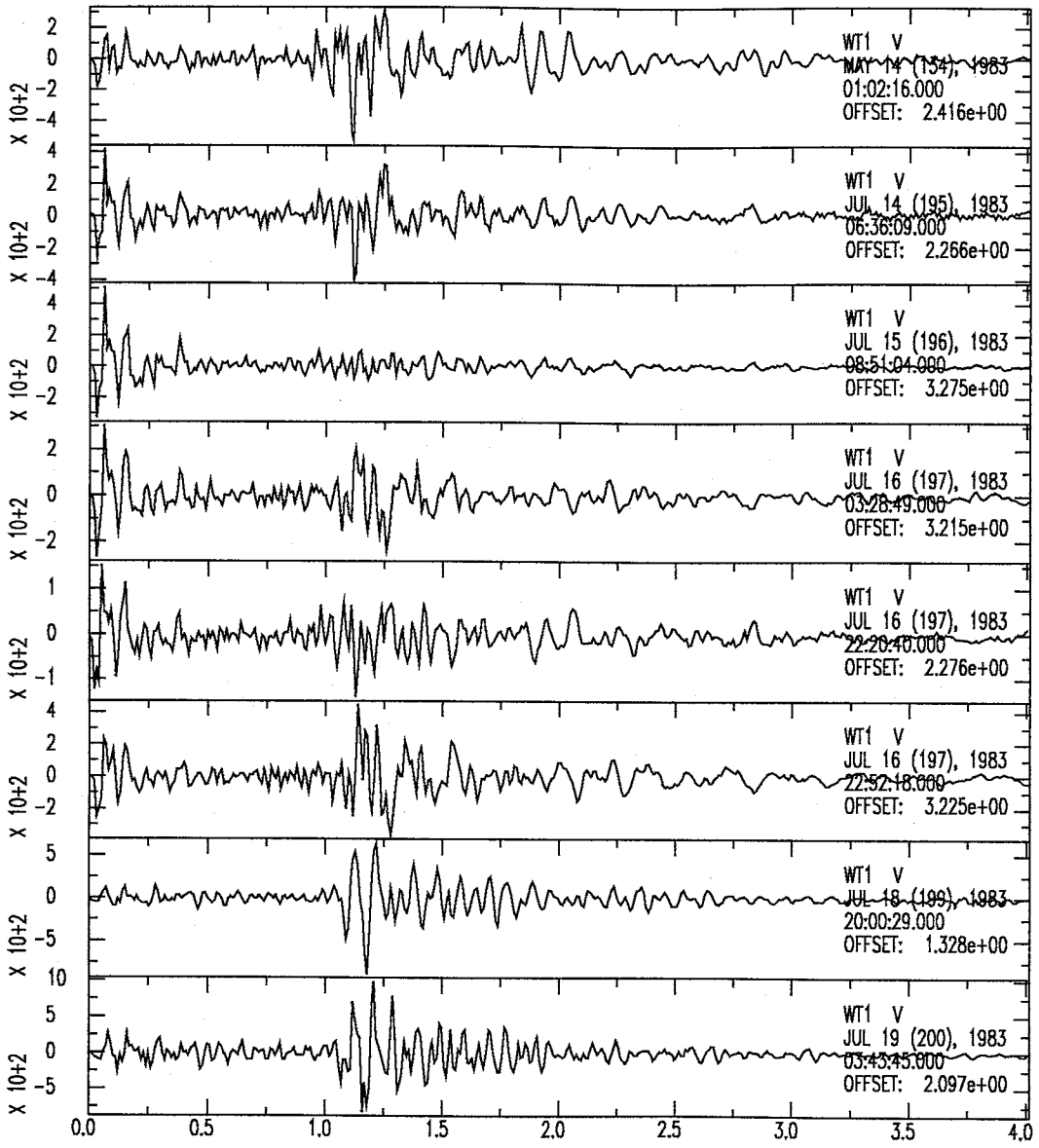

Figure 7.7. Master events defining Socorro Mountain swarm sub-types.

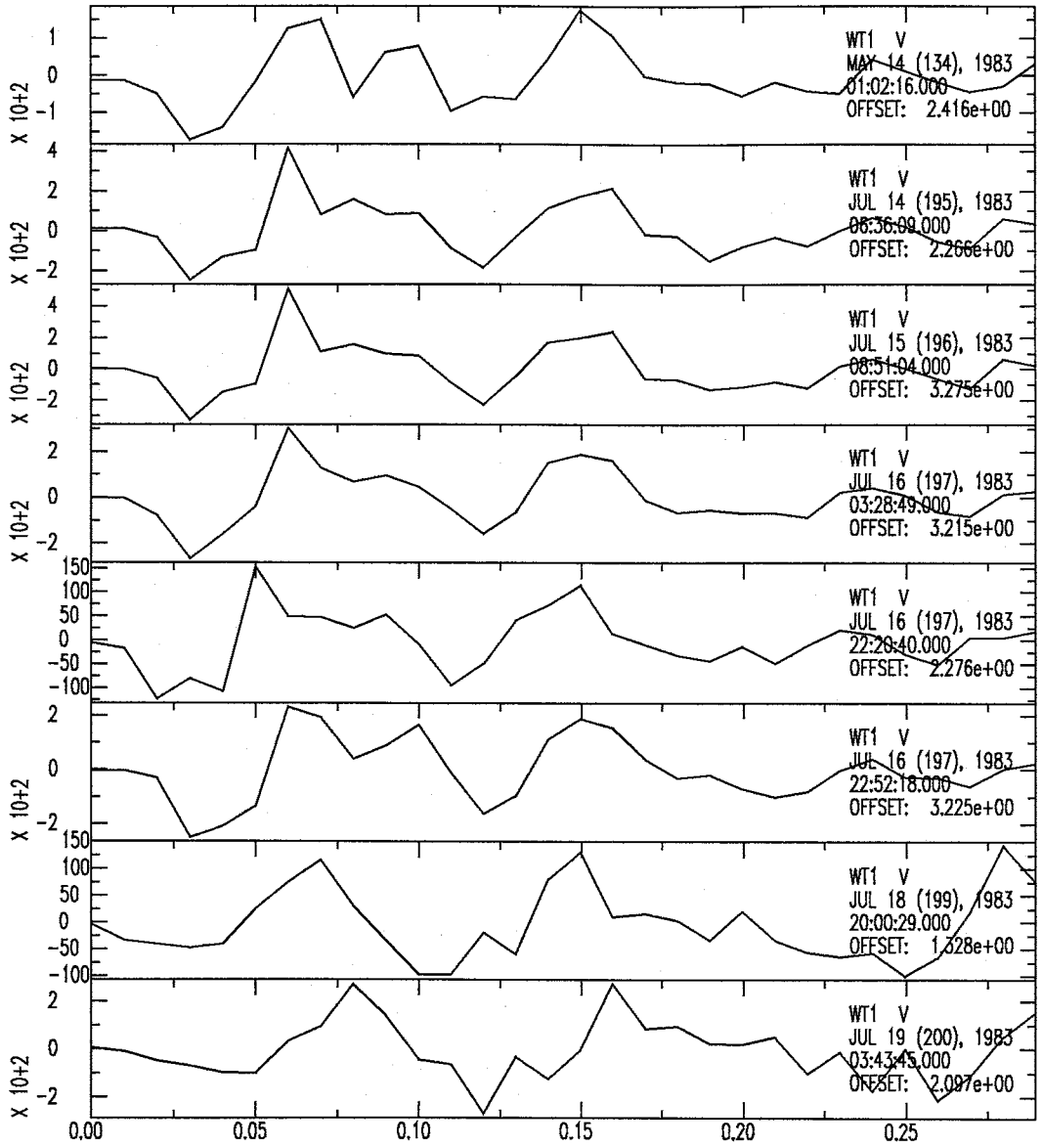

Figure 7.8. P-wave window for master events in Figure 7.7. Windows are 30 samples (0.3 seconds) in length.

(Figures 7.1 and 7.2), which show a wide variety of dip angles. This further supports the geologic interpretation of recurrent earthquakes on a reactivated Oligocene fault system, developed through several episodes of domino-style faulting.

It was initially hoped that examination of pulse broadening could provide some determination of the near source changes as a result of propagation of the swarm through time. Ideally, observed pulse broadening (of the first cycle) would indicate progressive fracturing of rock in the source volume. The perceived pulse broadening was not quantifiable, however, due to limitations in the data. With a sample rate of 100 samples per second, the high-frequency first arrivals provided only three to four sample points in the first half-cycle; hence, the first pulse was insufficiently sampled to separate pulse broadening from possible errors associated with interpolating the time series.

8. Results – East Rift Swarms

The East Rift swarms occurred along a linear trend east of Socorro NM, and were oriented North-South, parallel to rift related structures. The East Rift sequence can be divided into three distinct sub-swarms related by time history and focal mechanisms. The swarm sequence had an interesting chronological order. The sequence commenced on August 16, 1985, with the Arroyo del Coyote (ADC) swarm. Most activity at ADC tapered off within two weeks, but periodic bursts of activity continued for eight months. The second swarm was the Puertecito de Bowling Green (PBG) swarm, which occurred between September 17 and 20, 1985, about 6 km to the north of the ADC swarm. Six months later the Loma de las Cañas (LDC) swarm (April 16 to May 23, 1986) occurred about 10 km south of the ADC epicentral region.

Hypocenters

Each of the three East Rift swarms (ERS) had several portable stations deployed following the first strong events. For best locations I elected to use the velocity model of *Hartse* [1991] with specific station corrections computed for each individual swarm. The application of these delays has significantly improved hypocenter locations, as illustrated in **Appendix IV**, for all studied swarms.

High quality hypocenters were computed for 309 events; latitude, longitude and depth errors were all less than 0.5 km at 1 std. Of these 309 events, 138, 65, and 106 events were from the ADC, PBG, and LDC swarms, respectively. Figure 8.1 shows the relative positions of the epicenters of the three swarms in the sequence. An interesting observation can be made concerning the distribution of events in the ADC swarm; the events from the onset of the ADC swarm through the onset of the

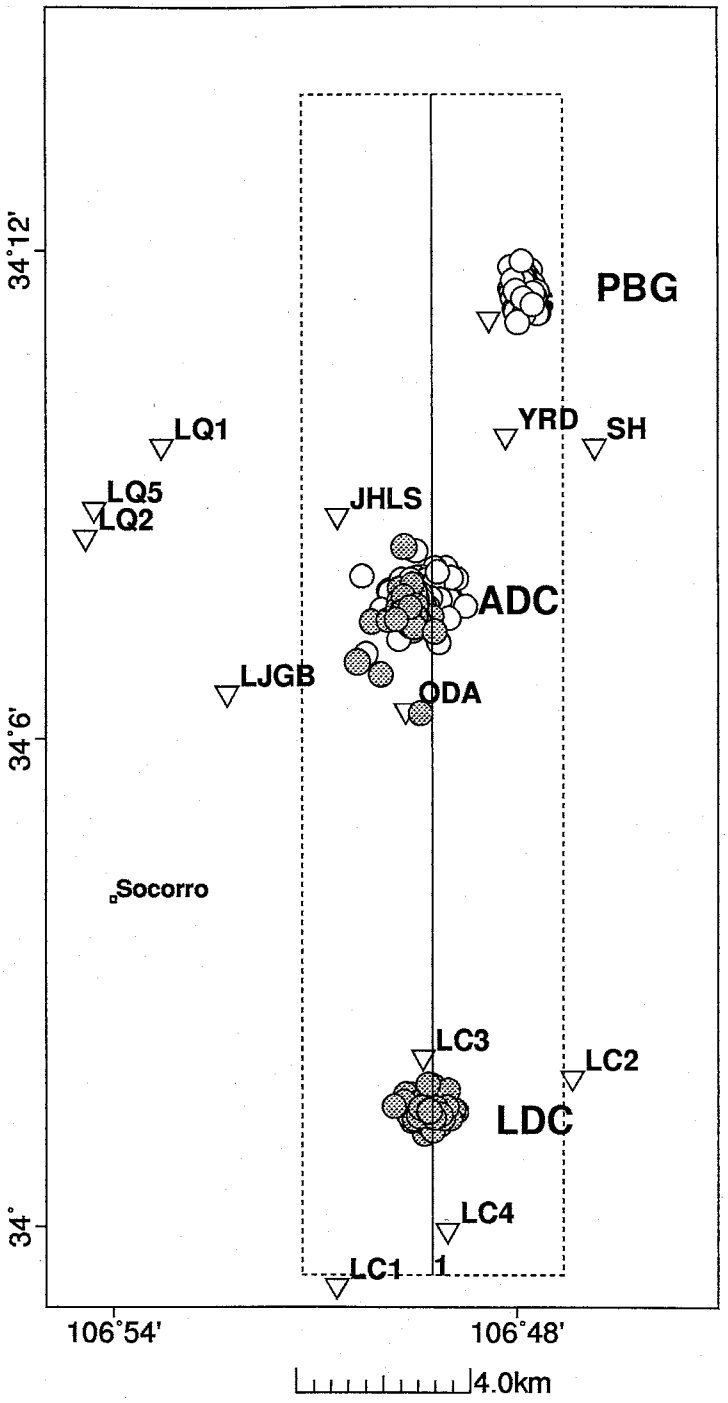

Figure 8.1. 309 epicenters for earthquakes in the East Rift sequence that have errors in latitude, longitude and depth ≤ 0.5 km. Swarms are labeled as follows: Puertecito de Bowling Green (PBG), Arroyo del Coyote (ADC), and Loma de las Cañas (LDC). Events in the ADC swarm are further subdivided into Type 1 (open circles) and Type 2 (filled circles) as discussed in the text. Also shown are temporary station locations (triangles).

PBG swarm (one month later) occupied a distinct sub-volume from the ADC events following the PBG swarm and preceding the LDC swarm. The ADC events preceding the PBG swarm (hereafter Type 1 ADC events) were on average located more to the north (closer to the PBG epicentral region), while ADC events following the PBG swarm and prior to the LDC swarm (hereafter Type 2 ADC events) occurred further south and closer to the LDC epicentral region. The spatial clustering of ADC Type 1 events nearer to the PBG swarm and that of the ADC Type 2 events closer to the LDC swarm, combined with the apparent temporal associations, suggests a strong causal link between the three swarm and justified combining them into one overall sequence for analysis.

In cross-section (Figure 8.2), the swarms occupied a slab-like volume 2 to 3 km thick dipping 10^o to the north with an upper surface ranging in depth between 5.0 and 8.5 km. It is important to note (Figures 8.1 and 8.2) that these swarms occupy large volumes compared to the presumed fault plane of their strongest individual events. The largest event on these figures was located in the ADC swarm and had a magnitude of 4.2, consistent with a fault plane roughly 1.3 square kilometers [*Wells and Coppersmith*, 1994]. The hypocentral cloud of the ADC swarm had dimensions of 3 km on a side, substantially larger in every dimension than the rupture area of its strongest event. The PBG and LDC swarms had maximum event magnitudes of 2.7 and 3.1 respectively.

Fault Mechanisms

I used FPFIT [*Reasenberg and Oppenheimer*, 1985] to compute fault mechanisms for 154 of the best located events, with 60, 39 and 55 events in the ADC, PBG and LDC swarms, respectively. For ADC events, focal mechanisms were primarily distributed between two types. Type 1 (31 events) consisted of strike slip

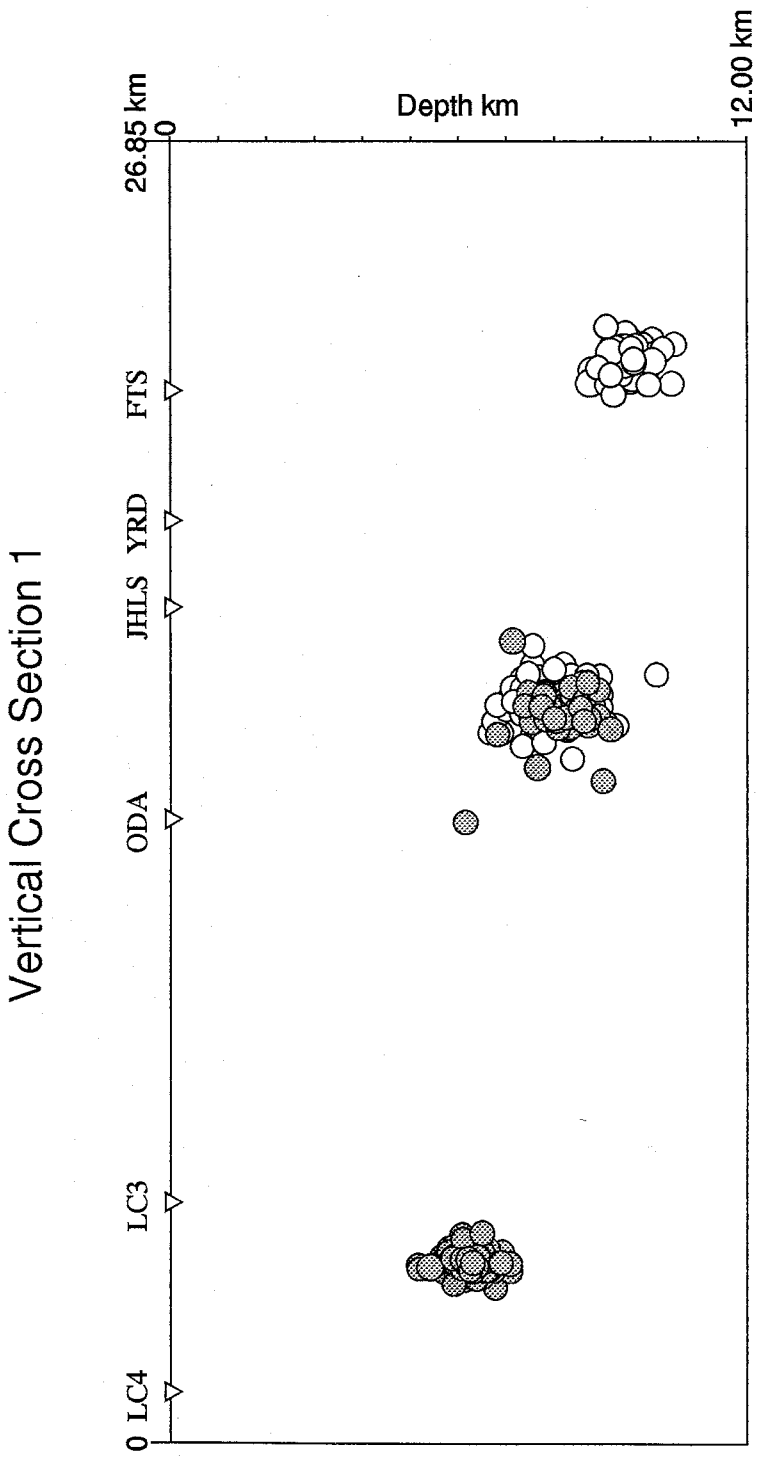

Figure 8.2. Cross-section from Figure 8.1. All labels and hypocenter designations are the same as in Figure 8.1.

events with an average T-axis of 247.6 ±9.5. Type 2 (22 events) consisted of strike slip events with an average T-axis of 214.4 ± 8.5. Seven other events had normal fault mechanisms. Type 1 focal mechanisms were most common prior to and during the PBG swarm, while Type 2 events were more common after the PBG swarm. The PBG and LDC swarms both exhibited strike-slip focal mechanisms. The average T-axis for the PBG swarm was 236.8 ±4.7, and the average T-axis of the LDC swarm was 219.6 ±8.0. Figure 8.3 shows the P and T based on the 154 focal mechanisms. To first order, it appears that ADC Type 1 events closely resemble PBG events while Type 2 ADC events are more similar to LDC events. As previously noted, Type 1 ADC epicenters average slightly to the north and east of Type 2 events, closer to the PBG swarm. Figure 8.4 shows the average focal mechanisms for the three swarms.

It seems likely that these three swarms represent activity on a single strike-slip fault which has a sharp bend at the location of the ADC swarm (Figure 8.5). The distinct spatial separation of the different Type 1 and 2 strike-slip mechanisms narrowly constrain the location of the kink for the proposed fault. Other evidence for a kink in the fault at the site of the ADC swarm includes the occurrence of the largest overall event of the three swarms (M_d=4.2) near the kink, where higher stress accumulation would be expected. In addition, the ADC swarm has greater complexity when compared to the PBG and LDC swarms, suggesting a more complicated stress regime in the vicinity of the ADC swarm.

Geology

Cather [1996] was mapping the geology of the upper Cenozoic deposits in the epicentral regions during the course of this study. *Cather's* maps showed surface exposures of faults in the region occupied by the postulated sub-surface strike-slip

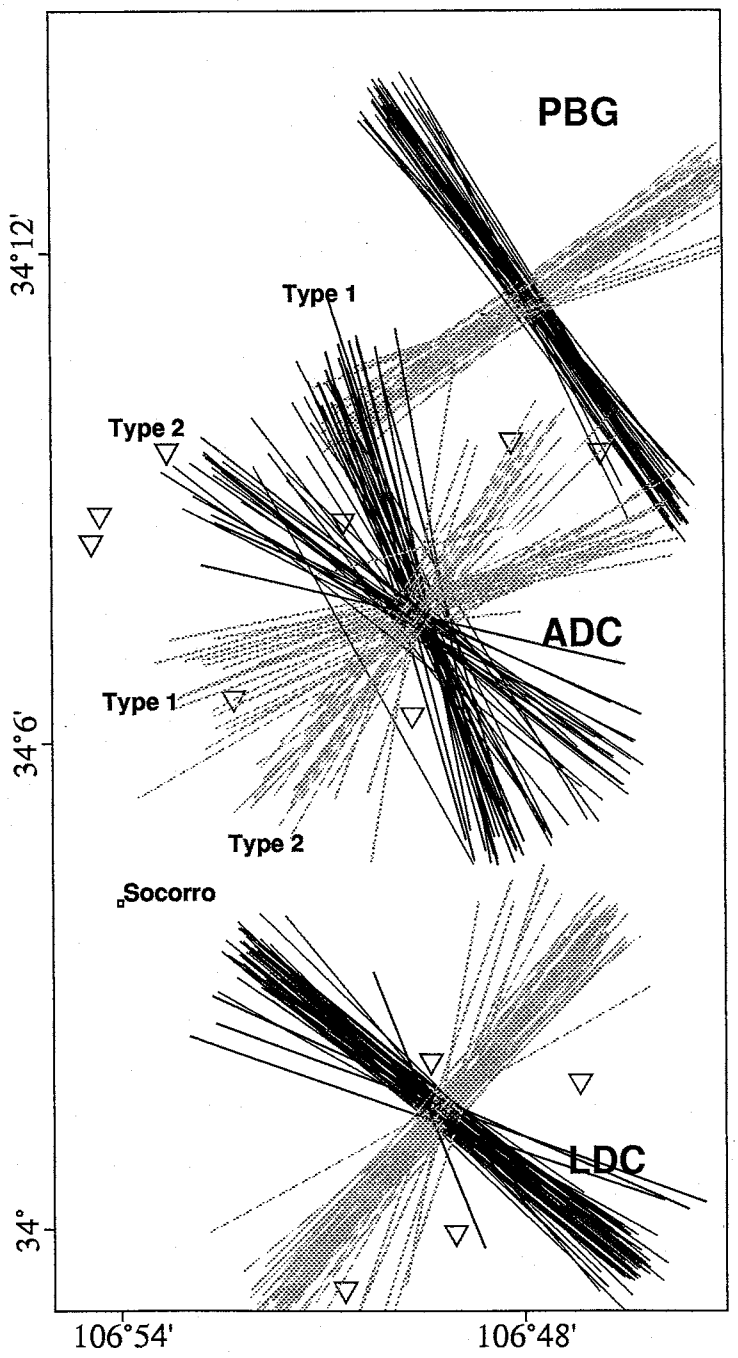

Figure 8.3. P and T axis for the 154 events with computed focal mechanisms. Note that the ADC swarm divides into two separate types.

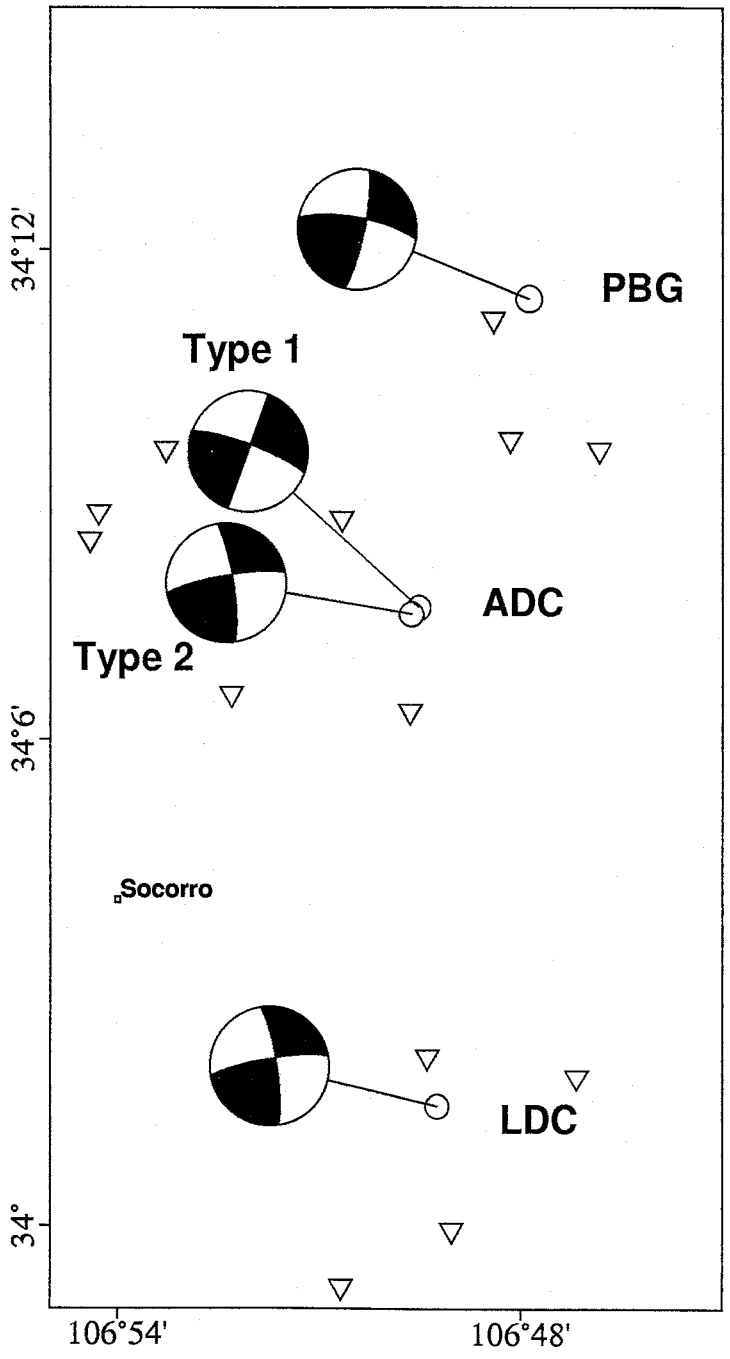

Figure 8.4. Representative focal mechanisms for the three swarms, with ADC mechanisms labeled Type 1 and 2.

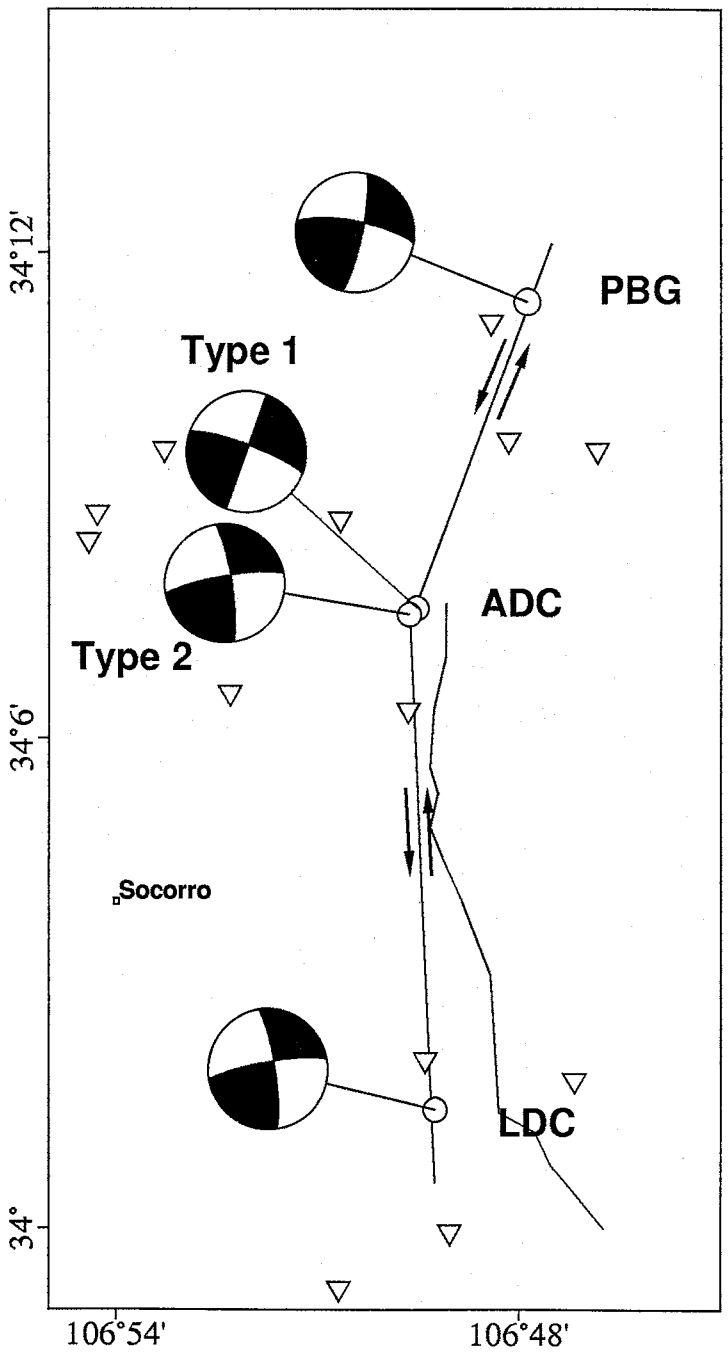

Figure 8.5. Representative focal mechanisms for the three swarms. Also shown is the proposed left-lateral strike-slip fault with a sharp bend at the location of the ADC swarm, and the Coyote fault mapped by *Cather* [1996].

fault. *Cather* has mapped a fault (the Coyote) which has surface exposures sub-parallel to, but several kilometers east of, the LDC swarm; it intersects the ADC epicentral region before disappearing, no mapping was done in the area of the PBG swarm. The existence of this 40-50^o west dipping normal fault in the ADC epicentral region may explain the existence of the seven normal fault earthquakes observed during the main swarm, as well as similar earthquake activity which occurred immediately south of the epicentral region and at shallower depths in 1995 (Figure 8.6 and Figure 8.7). This is consistent with the earlier noted geologic complexity in the ADC epicentral region.

Interpretation

Older structures in the east rift region may be found on another geologic map [*Osburn*, 1984]. Examination of *Osburn's* map indicates that the trend of the proposed fault while having no surface expression, closely mimics structural grain in exposed rocks two kilometers to the east. This suggests that if a fault exists at depth, linking the three swarms in the sequence, it may be a reactivation of a pre-existing fracture system. It is easy to imagine a large, buried, rift-bounding fault; it is more difficult to explain the observation of left-lateral strike-slip motion on that fault within the context of continental rifting. A reasonable explanation could involve stresses imposed by the clockwise rotation of the Colorado Plateau during the Miocene as described by *Chapin and Cather*, [1994] with respect to the stable craton. The observed strike-slip faults may be an indication that stresses imposed on the region due to the Miocene rotation of the Colorado Plateau are still relaxing.

Temporal and Spatial Analysis

The East rift sequence may have the most interesting time-history of any of

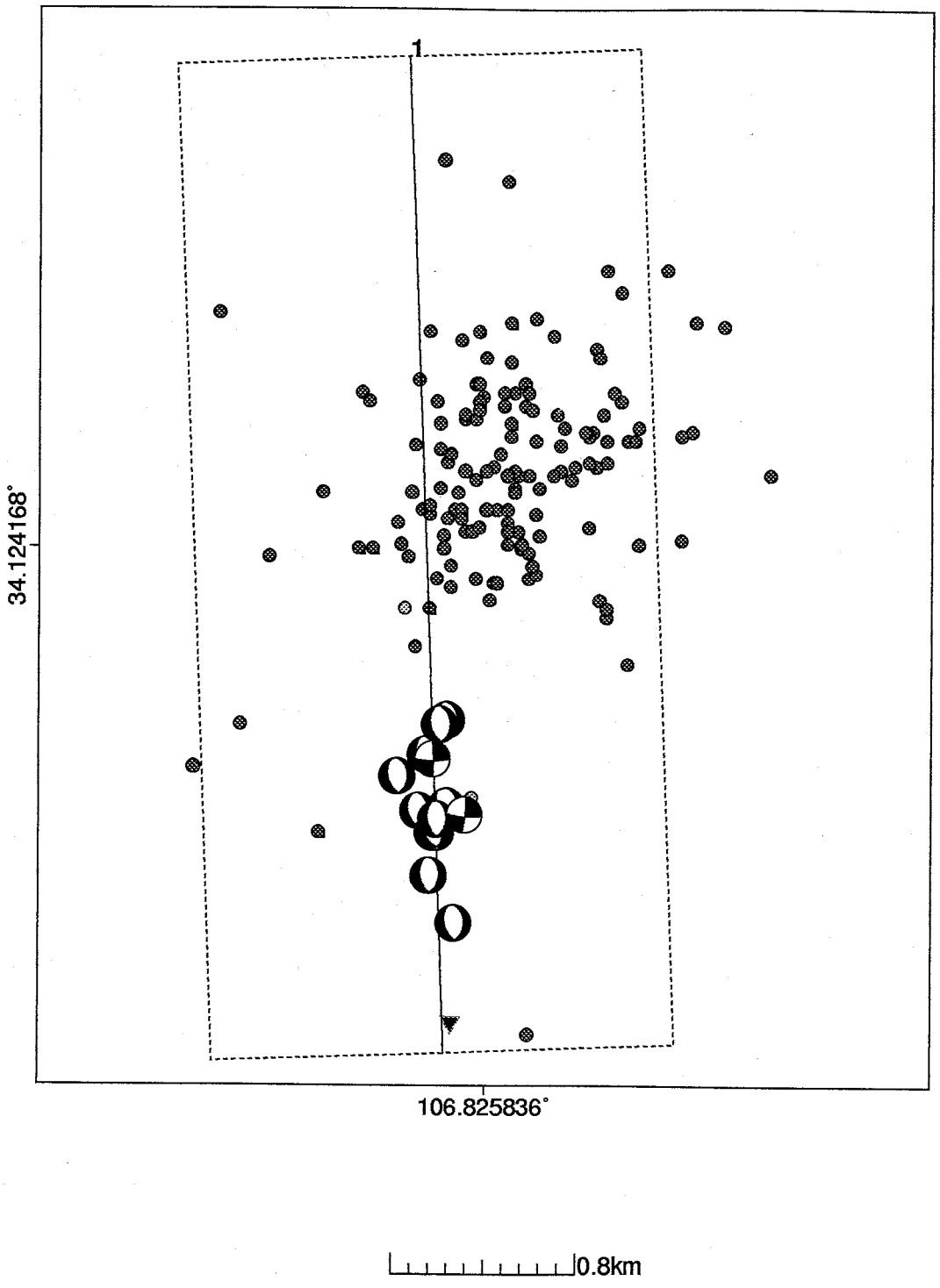

Figure 8.6. Arroyo del Coyote swarm best 101 epicenters. Also shown are events from September 1995 in the epicentral region (lighter color and focal mechanisms).

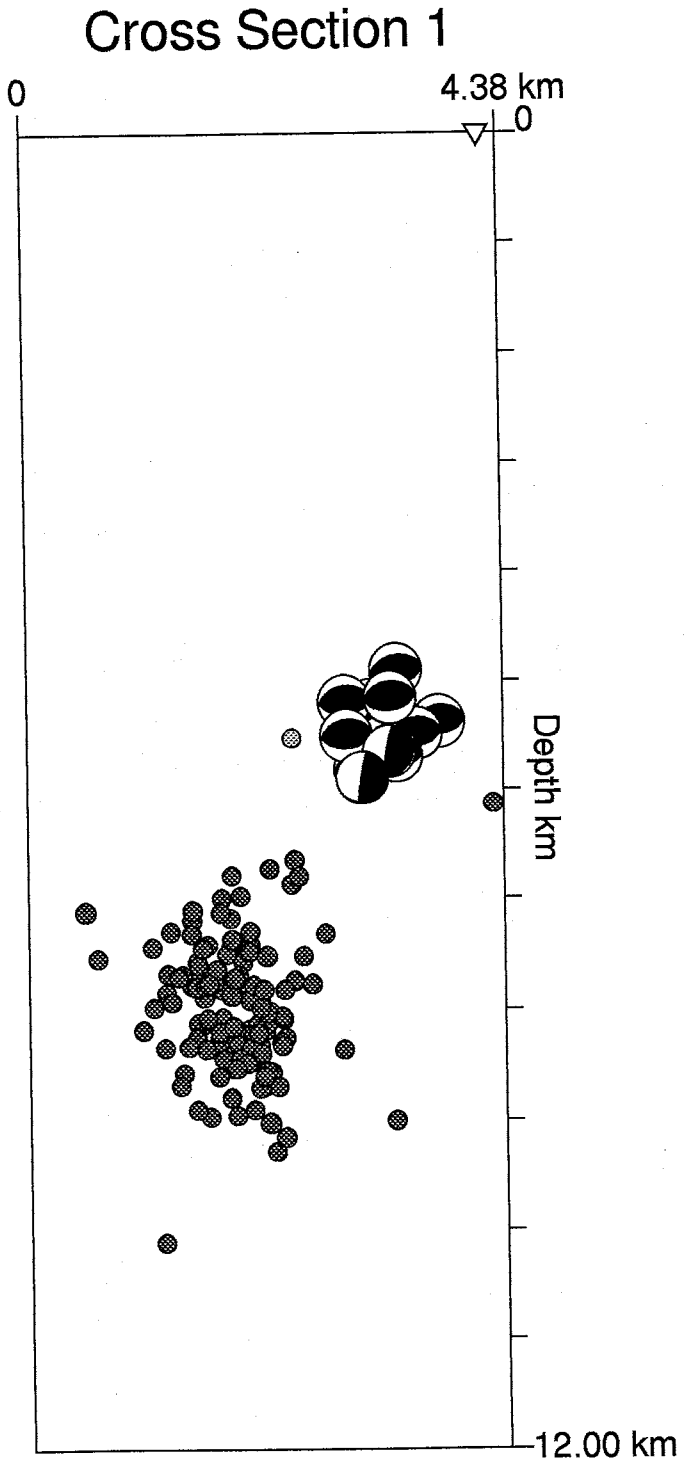

Figure 8.7. Cross-section 1 from Figure 8.6. Note the two strike-slip solutions for the 1995 events are at the base of the active volume.

the studied swarms. Figure 8.8 (upper) shows an events/day histogram of ADC events with magnitudes greater than 1.0. For this swarm the events usually occur in clusters of weak microearthquakes in association with one or two stronger (M_d greater than 1.0) events. Figure 8.8 (lower) shows the same histogram with the PBG and LDC swarm histograms superposed. Activity in the ADC swarm area continued for nearly 300 days ending just before the final earthquakes of the LDC swarm. This continued activity may imply some mechanism for communication of stresses along the sub-surface fault(s) proposed earlier. The periodic nature of the activity in the ADC swarm inspired an investigation of possible relations to earth tides discussed in the next chapter.

The apparent causal link between the three swarms of the East Rift sequence implies some method of communication between the pivotal ADC swarm and the PBG and LDC swarms. Is this the result of seismic energy propagating through the crust and inducing earthquakes at a distance? This phenomenon is well documented for the M_d=7.3 Landers, California earthquake of June 28, 1992 [*Hill et al.*, 1993]. Earthquakes were triggered in areas of persistent seismicity at distances of up to 1250 km, with onsets often during the passage of the surface wave train. *Hill et al.* [1993] conclude that these were most likely caused by the effects on crustal fluids of dynamic strains accompanying seismic waves from the main shock. It seems unlikely that this model explains the triggering of the PBG and LDC swarms by earthquakes in the ADC swarm; the largest event was only M_d=4.2 and occurred one month and eight months prior to the PBG and LDC swarm onsets, respectively. Static stress changes as a result of elastic deformation in the crust also seems an unlikely candidate, as they usually induce earthquakes within only one or two fault dimensions [*Hill et al.*, 1993] (in this case about 1 km) and the PBG and LDC swarms were 6 and 10 km distant, respectively. One possible explanation involves fault creep, or slow aseismic fault motion, with most of the fault failing aseismically

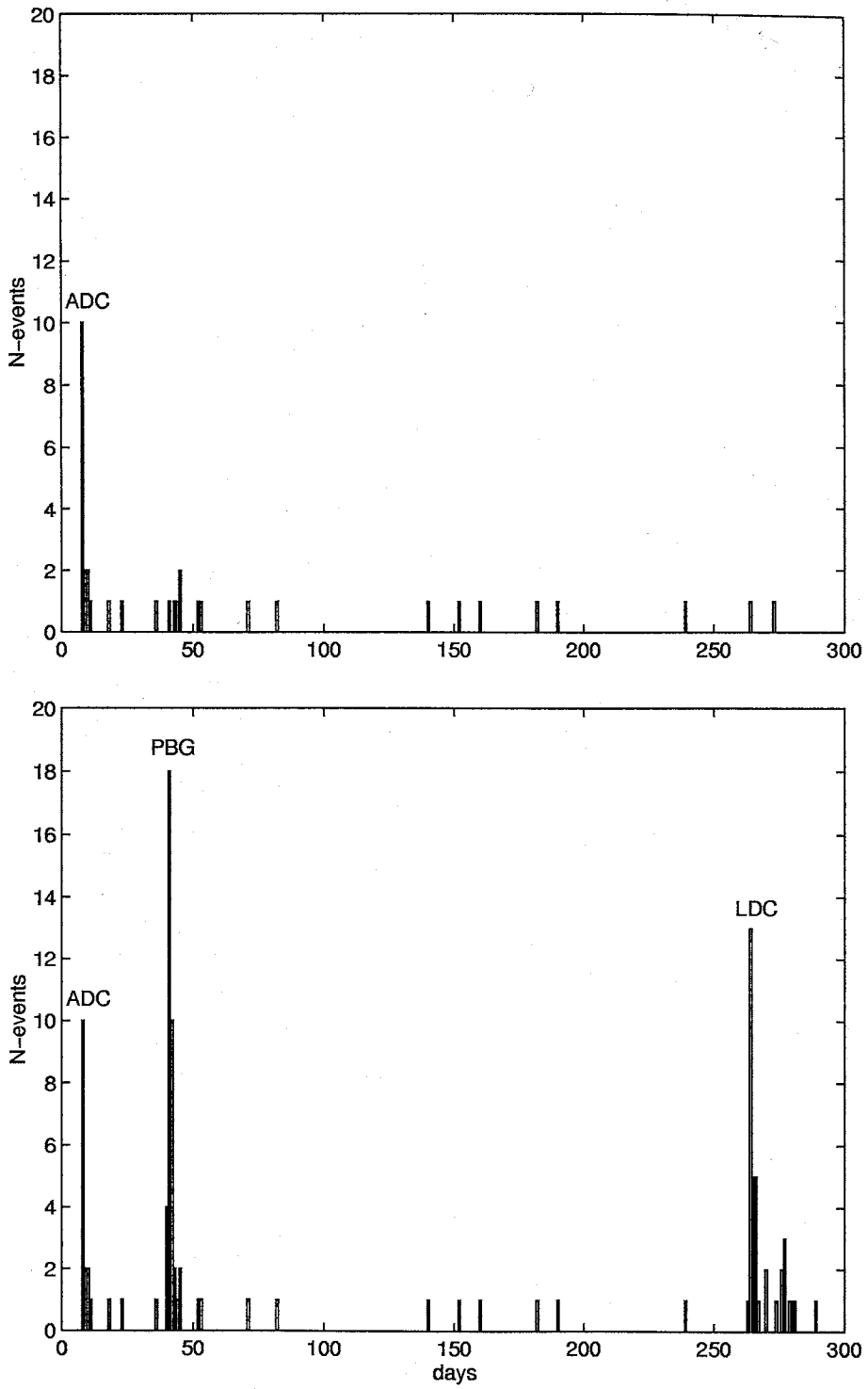

Figure 8.8. Counts of magnitude 1.0 or greater events for the East Rift sequence. The upper figure shows events from the Arroyo del Coyote swarm. The lower figure contains events from all three sequences. Swarm sequences are labeled with abbreviations.

and brittle failure occurring at points of high stress (the three swarms).

9. Results – General

Several general questions were addressed using the data gathered from the five studied swarms in conjunction with other data not specifically examined during the course of this study. This combined data set contains data from a number of in-house and published studies for a total of 1181 earthquake locations with associated reflected phases. The majority of the data was analyzed by myself or by undergraduate assistants under my direction. Seventy-three events, however, were taken from hypocenters located by Hans Hartse for use in evaluating a local velocity model [*Hartse*, 1991; *Hartse et al.*, 1992]. Three major questions were addressed using this combined data set: (1) The lateral extent of the Socorro Magma Body, (2) the base of the seismogenic zone in the Socorro Seismic Anomaly, and (3) the relation (if any) between earth tides and swarm seismicity.

New Map of the Socorro Magma Body

The study of the lateral extent of the Socorro Magma Body has been published [*Balch et al.*, 1997] and a complete transcript of the journal paper comprises Part I of this dissertation. A thorough description of the general data set is contained in **Part I**, and all events used in this study are listed in **Appendix VI**.

Base of the Seismogenic Zone

The distribution of hypocenters in the combined data set provides the possibility of mapping a portion of the base of the seismogenic zone in the Socorro area. Figure 9.1 shows the 1181 events of the general data set relative to the extent of the Socorro Seismic Anomaly. An 8 by 11 grid was superimposed on the data and the deepest hypocenter depth for a given block was selected. While many of the blocks contained

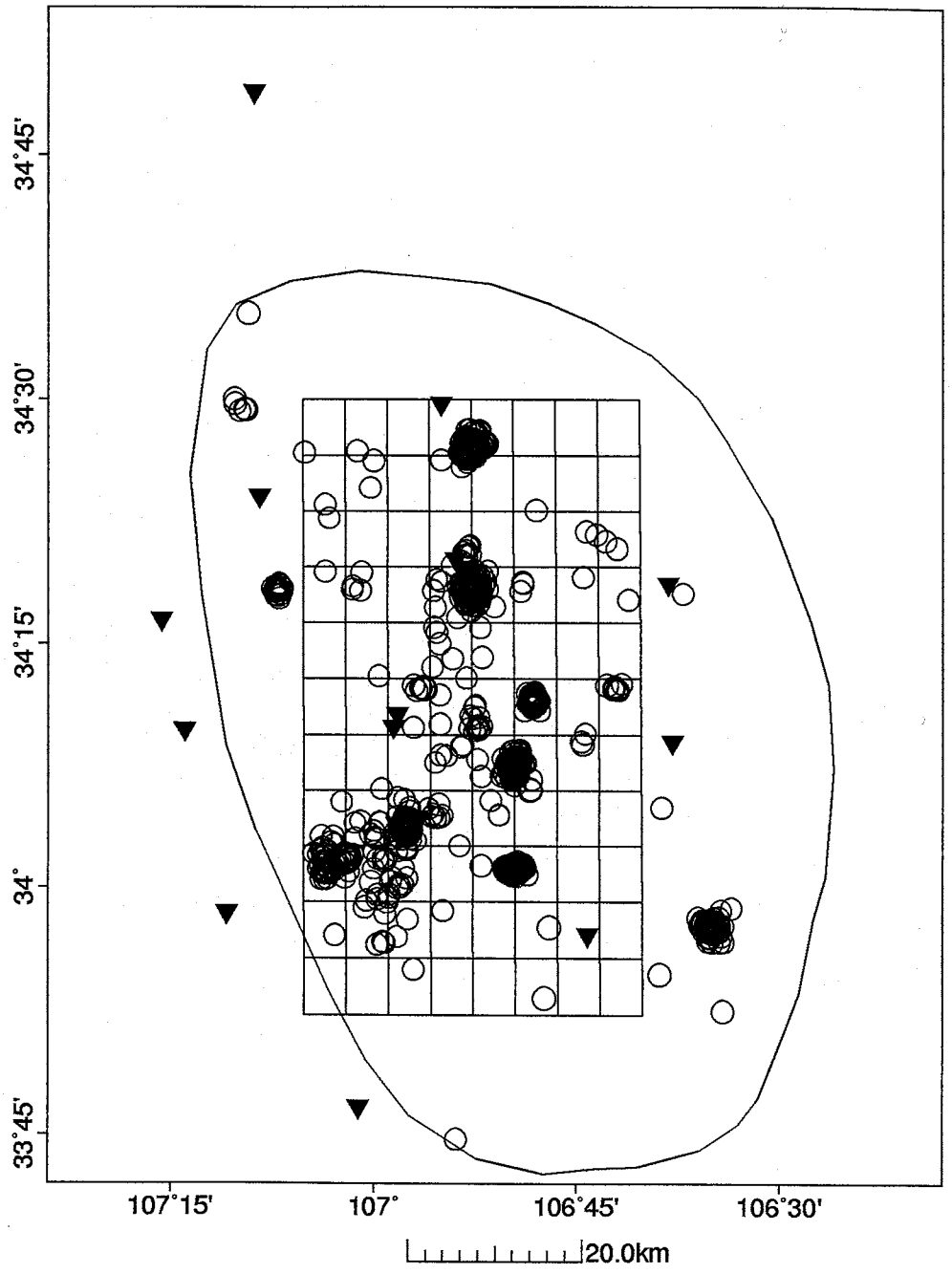

Figure 9.1. The 1181 earthquakes in the general data set. Also shown are the Socorro Seismic Anomaly (thin line), permanent stations in the New Mexico Tech Network, and the 8x11 grid used for binning hypocenter depths.

swarm data which may have events representing the both upper and lower bounds, a greater number of blocks contained only a few events. Therefore I elected to use only the deepest hypocenters in order to construct a "minimum depth" map of the base of the local seismogenic zone.

Table 9.1 (upper) contains the selected data for each grid block. Note that depths are with respect to station SNM which is at an elevation of 1511 meters above sea-level. Examination of Table 9.1 (upper) shows that about 1/3 of the grid blocks are empty. Many of the empty blocks are contained within the body of the grid; these were filled by interpolation using the *Kernel Smoothing* function of **Spyglass Transform** (copyright 1993 Spyglass Inc.). The resulting interpolated data set is given in Table 9.1 (lower). The effect of the interpolation process is "blurry" or smoothed data, which while not directly representing the observed values, does give an adequate sense of the relative depths and variation in depth of the base of the seismogenic zone.

A depth contour map covering the area of the grid in Figure 9.1 and using the data from Table 9.1 (lower) is shown in Figure 9.2 and a 3-D version of the same map in Figure 9.3. The maps show a considerable variability in the depth to the base of the seismogenic zone. A notable trend of deeper activity runs from the WSW to the ENE corner, perhaps as a subsurface expression of the Socorro Fracture Zone [*Sanford et al.*, 1995[2]].

Periodic Seismicity and Earth Tides

The pulse-like distribution of earthquakes within the studied swarms raised the issue of an external driving force, perhaps earth tides. The term "earth tides" describes the gravitational effect of the Moon and the Sun on the shape of the earth and results in a bulging of the earth's crust of ~20 cm maximum height. The

(a) Observed maximum depth by bin								
Lat/Lon	107.09	107.03	106.97	106.91	106.85	106.79	106.73	106.67
34.50	-4.00	-4.93	-0.00	-4.49	-4.49	-0.00	-0.00	-0.00
34.44	-3.31	-4.36	-0.00	-5.52	-0.00	-0.00	-0.00	-0.00
34.37	-9.04	-0.00	-0.00	-7.86	-0.00	-5.57	-9.85	-8.71
34.31	-8.04	-7.09	-6.61	-7.86	-8.06	-7.72	-4.38	-0.00
34.25	-0.00	-4.91	-0.00	-7.01	-6.45	-0.00	-0.00	-0.00
34.19	-0.00	-0.00	-4.43	-7.07	-7.00	-10.5	-7.76	-10.1
34.12	-0.00	-0.00	-0.00	-6.28	-8.86	-9.12	-8.23	-0.00
34.06	-9.26	-9.56	-7.37	-7.97	-4.91	-0.00	-0.00	-6.97
34.00	-9.40	-9.65	-10.5	-9.03	-8.04	-7.22	-0.00	-0.00
33.93	-5.97	-10.1	-7.79	-5.65	-0.00	-2.62	-0.00	-0.00
33.87	-0.00	-0.00	-4.58	-0.00	-0.00	-8.98	-0.00	-0.00

(b) Smoothed maximum depth by bin								
Lat/Lon	107.09	107.03	106.97	106.91	106.85	106.79	106.73	106.67
34.50	-4.35	-4.72	-4.93	-4.92	-5.01	-5.65	-7.16	-8.42
34.44	-5.06	-5.14	-5.62	-5.88	-5.97	-6.55	-7.76	-8.19
34.37	-6.74	-6.36	-6.50	-6.85	-6.90	-6.93	-7.60	-8.20
34.31	-7.24	-6.72	-6.80	-7.20	-7.35	-7.20	-7.02	-7.50
34.25	-6.65	-6.21	-6.47	-7.03	-7.30	-7.77	-7.67	-8.32
34.19	-6.82	-6.23	-6.28	-6.90	-7.55	-8.33	-8.42	-8.86
34.12	-8.59	-7.98	-7.17	-7.27	-7.66	-8.33	-8.33	-8.46
34.06	-9.08	-8.79	-8.19	-7.61	-7.22	-7.45	-7.66	-7.51
34.00	-8.82	-9.00	-8.62	-7.94	-7.24	-6.69	-6.76	-6.95
33.93	-8.10	-8.52	-7.94	-7.28	-6.57	-5.84	-5.68	-6.26
33.87	-7.65	-7.60	-6.78	-6.66	-6.94	-6.95	-6.98	-6.39

Table 9.1. Upper: Raw maximum hypocenter depth data by bin. Lower: Data from upper table after application of a Kernel Smoothing.

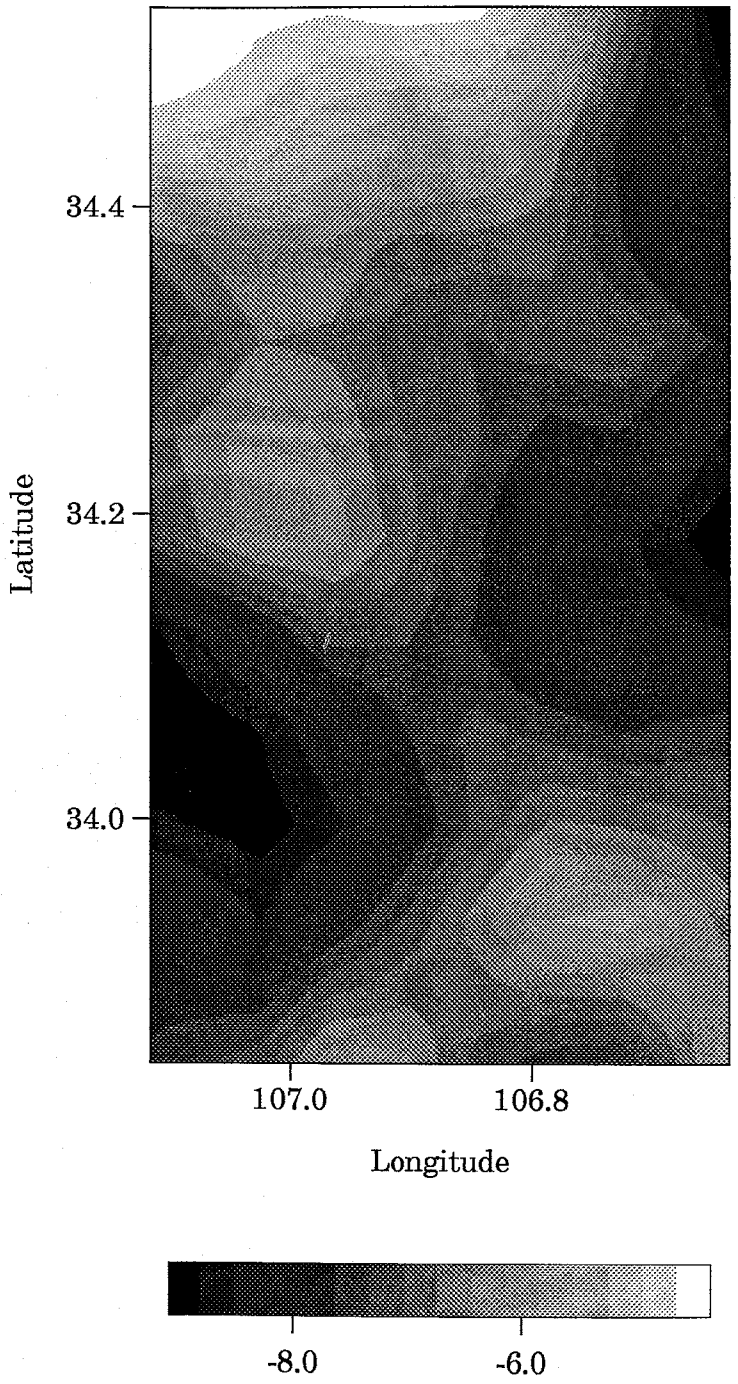

Figure 9.2. Depth contours of the base of the seismogenic zone from the Kernel smoothed depth data. Contour depth is in km.

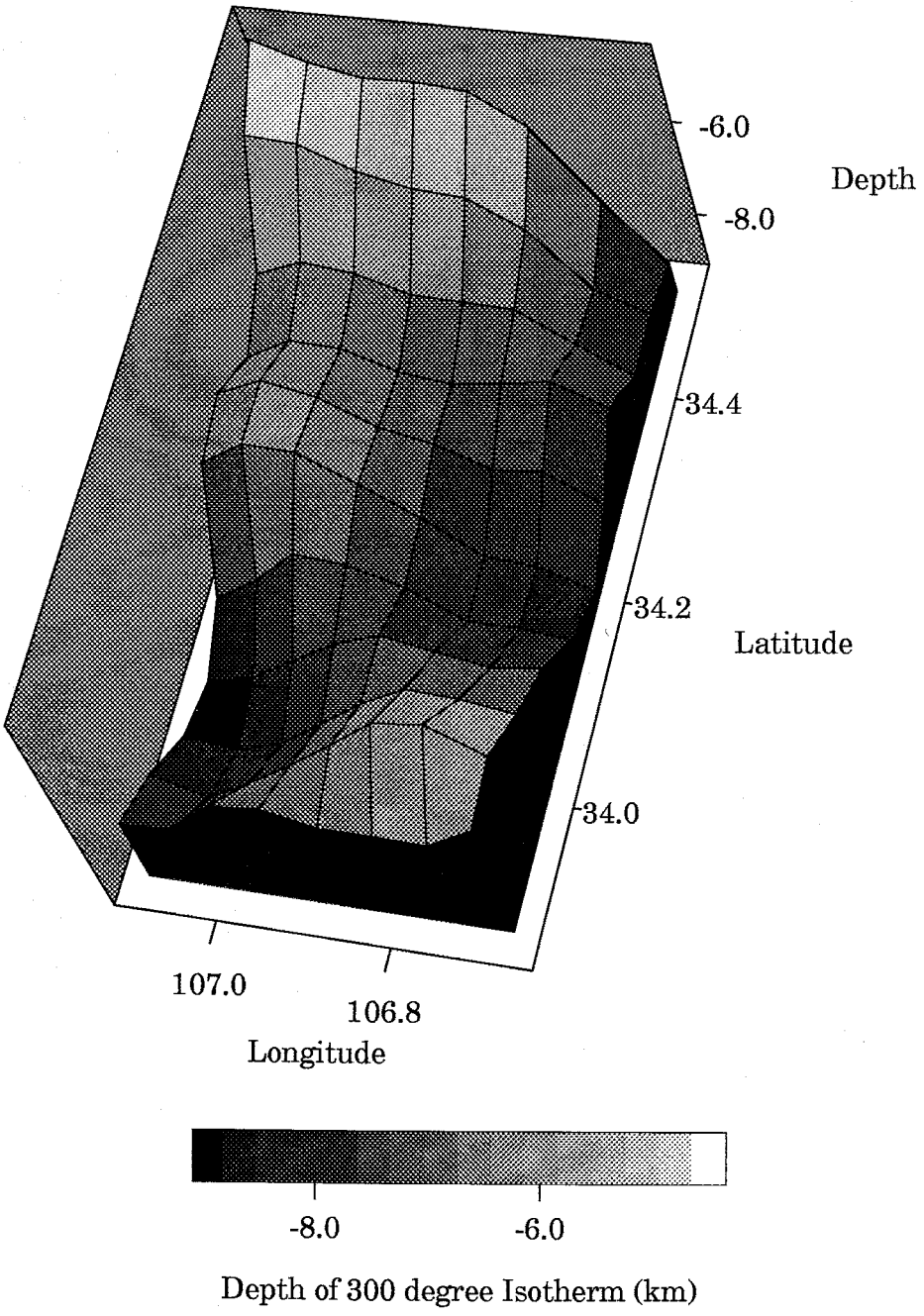

Figure 9.3. Three dimensional representation of the contour map in Figure 9.2.

geophysics of earth tides is well understood. A recent, concise, summary can be found in *Withers* [1993], thus a thorough description is not given in this dissertation. Figure 9.4 shows a sample of predicted gravity variations at a specific site as a result of tides. Note the daily diurnal variations as well as peaks at about 8 and 22 days when the effects of the the sun and the moon reinforce one another (full and new moon). The plot was generated using the **TAMURA GRAVITATIONAL TIDE** computation program (developed by NOAA). Subsequent figures showing predicted gravity variations also use data generated by this program.

The primary question to be addressed is whether or not a noticeable correlation exists between the local earth tides and the observed temporal periodicity of events within swarms. In order to address this question histograms of event counts with two hour bins were made for each of the studied sequences. These histograms were superimposed upon plots of predicted gravity variations for the epicentral region over the same time period. The composite figures are addressed in chronological order in the following paragraphs.

Figure 9.5 shows predicted microgravity variations in the epicentral region of the San Acacia swarm and the associated histogram of observed events. Please note that activity does not appear as an even distribution through time, but rather as series of pulses of somewhat irregular periodicity. The events in this swarm did not correlate directly with daily variations, in fact the distribution appears somewhat random. Though the the initial events in the swarm occurred near a new or full moon, the strongest event (M_d=4.2) occurred near a low in the earth tide.

The Socorro Mountain sequence was split into two time periods for analysis. Figure 9.6 has the May event histogram superimposed on predicted tidal gravity variations. An argument might be made that the periodic bursts of seismicity did occur at peaks in microgravity, with some variance. The initial activity, however,

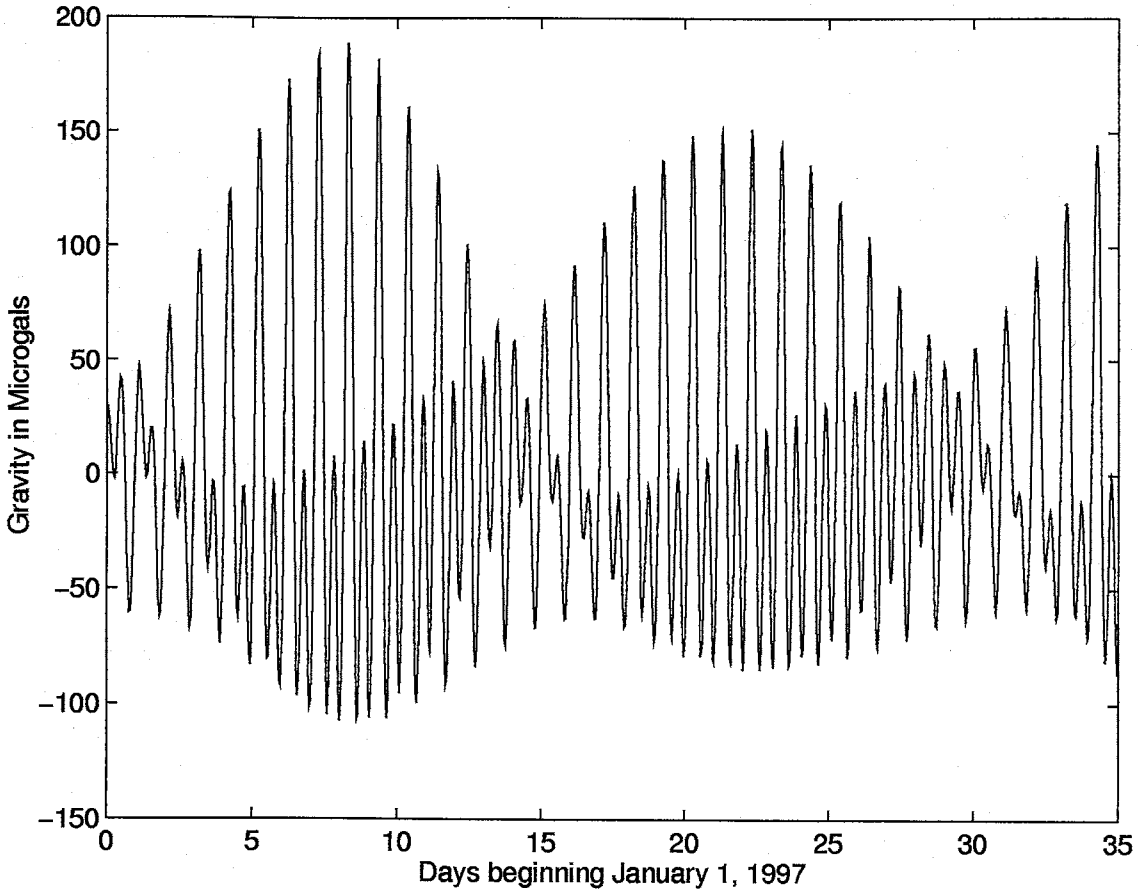

Figure 9.4. Sample of predicted microgravity variations due to earth tides. Note the diurnal component as well as the peaks around day 8 and day 22 (full and new moon) when the fields of the Sun and the Moon reinforce each other.

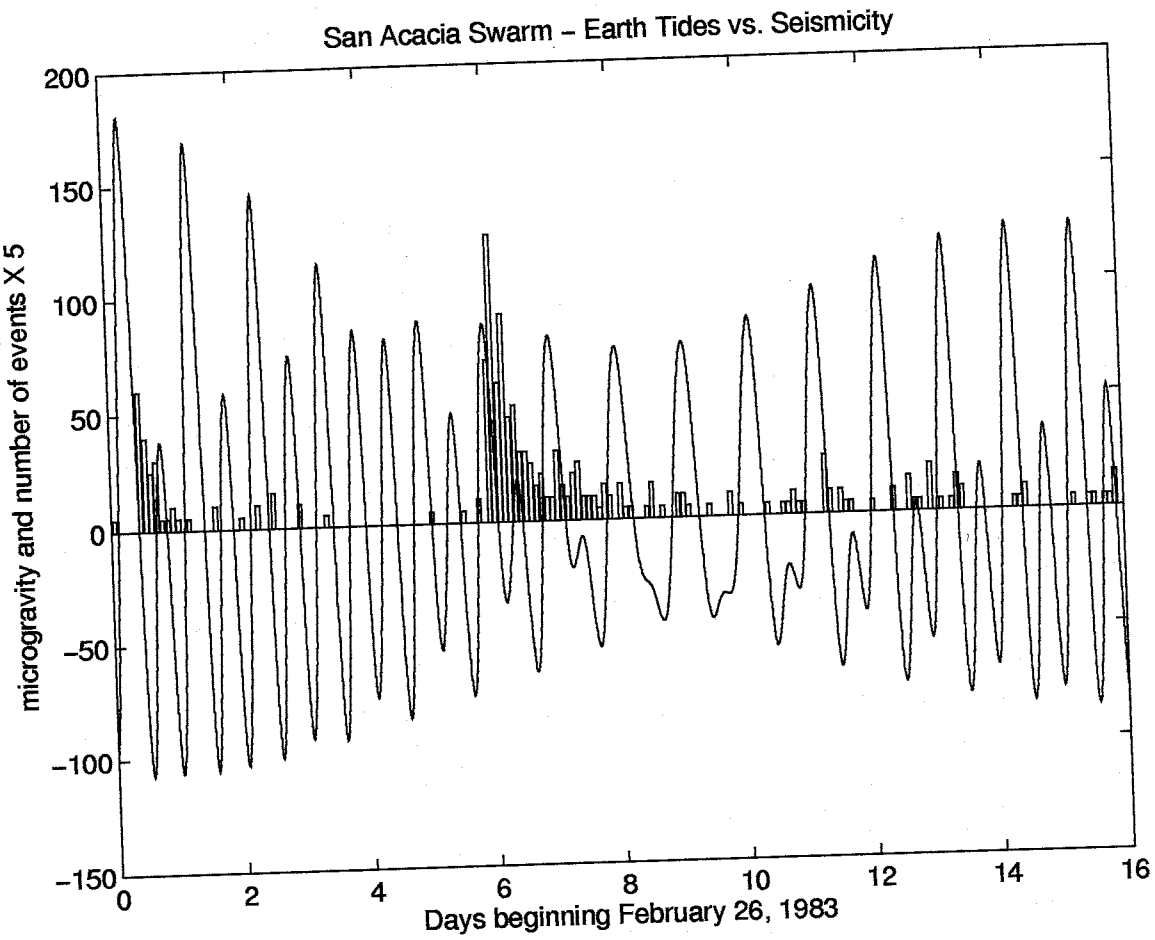

Figure 9.5. Event histogram and predicted microgravity variations for the San Acacia swarm.

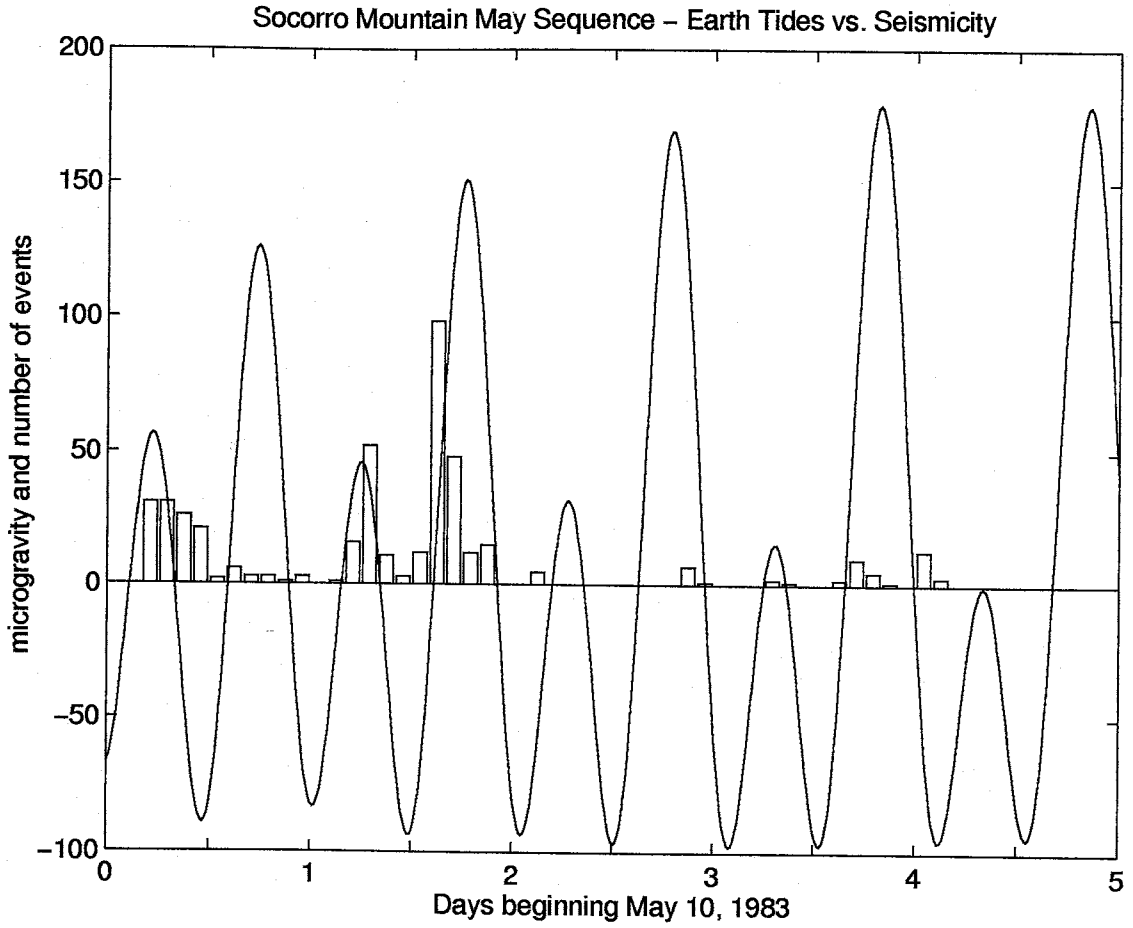

Figure 9.6. Event histogram and predicted microgravity variations for the May 1983, Socorro Mountain sequence.

begins near a twice monthly low in the earth tide. In Figure 9.7, data for the July sequence is portrayed. In contrast to the fair fit for the May sequence, the July sequence has a more random pattern of events vs. fluctuations in the tidal gravity. The July swarm as a whole was roughly centered on one of the twice monthly lows in the overall earth tide.

The East Rift sequence was studied in three time periods corresponding to the three sub-swarms (ADC, PBG and LDC). Predicted gravity and an event histogram for the Arroyo del Coyote swarm is presented in Figure 9.8. Except for a small precursory cluster, the swarm started with a magnitude 4.0 event. The distribution of event clusters when compared to peaks in the earth tide appears random, though the swarm initiated during a new or full moon. Figure 9.9 shows the event histogram and earth tides for the Puertecito de Bowling Green swarm. The swarm as a whole was centered on one of the twice monthly highs in microgravity due to earth tides. Event clusters, however, do not appear to match short period fluctuations. Earthquakes in the Loma de las Cañas swarm deviated from the other four swarms in that the distribution of activity was more uniform, with less significant clustering. No discernible pattern was found between the temporal variations in LDC activity and predicted gravity variations due to earth tides (Figure 9.10). Consistent with the other East Rift swarms, the LDC swarm started near a peak in overall gravity (new or full moon).

With the possible exception of the May 1983, Socorro Mountain swarm the data indicates that the pulses, or periodic bursts of activity within the swarms, were not directly related to variations in microgravity caused by earth tides.

Is it possible to relate the occurrence of swarm activity to earth tidal effects on a larger scale? Figure 9.11 shows an event histogram (events per day above M_d=1.0) for the entire East Rift sequence. All of the events between the main

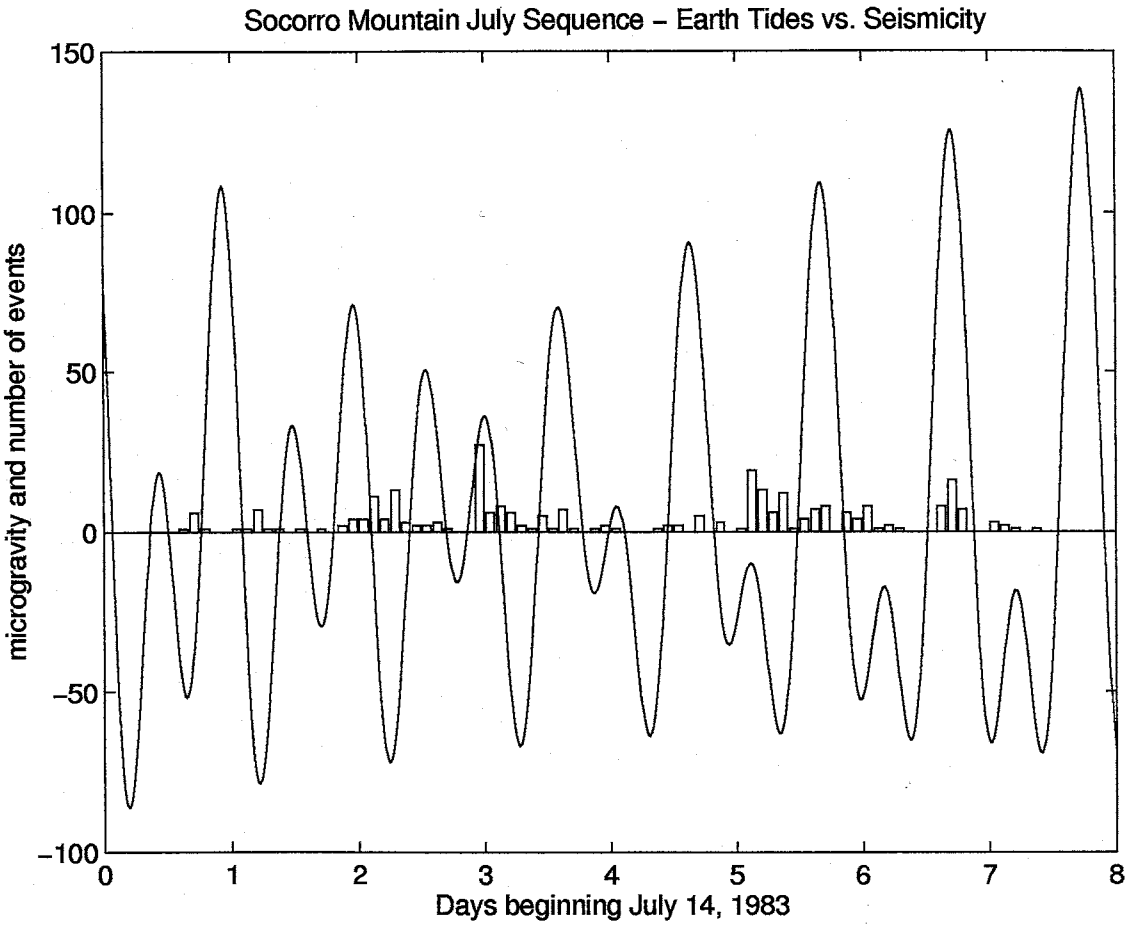

Figure 9.7. Event histogram and predicted microgravity variations for the July 1983, Socorro Mountain sequence.

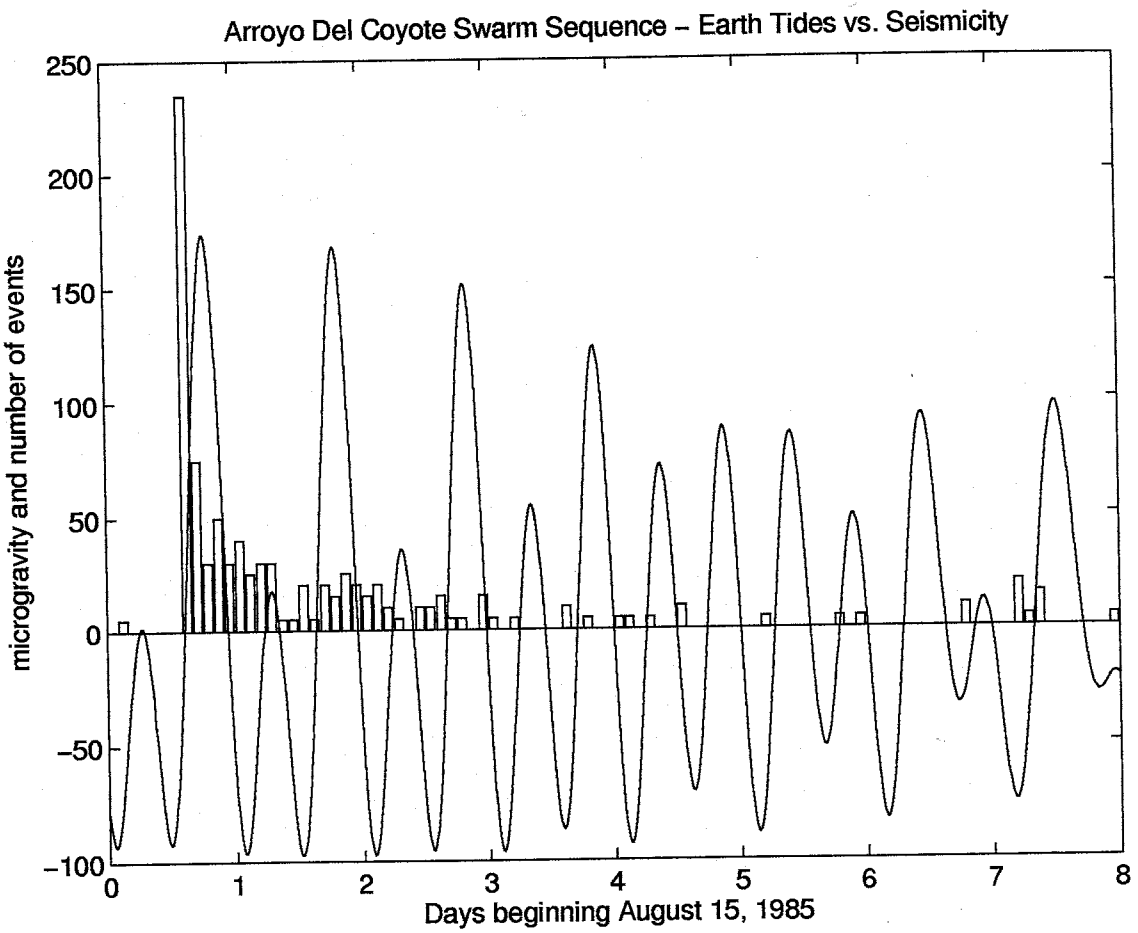

Figure 9.8. Event histogram and predicted microgravity variations for the Arroyo del Coyote Swarm.

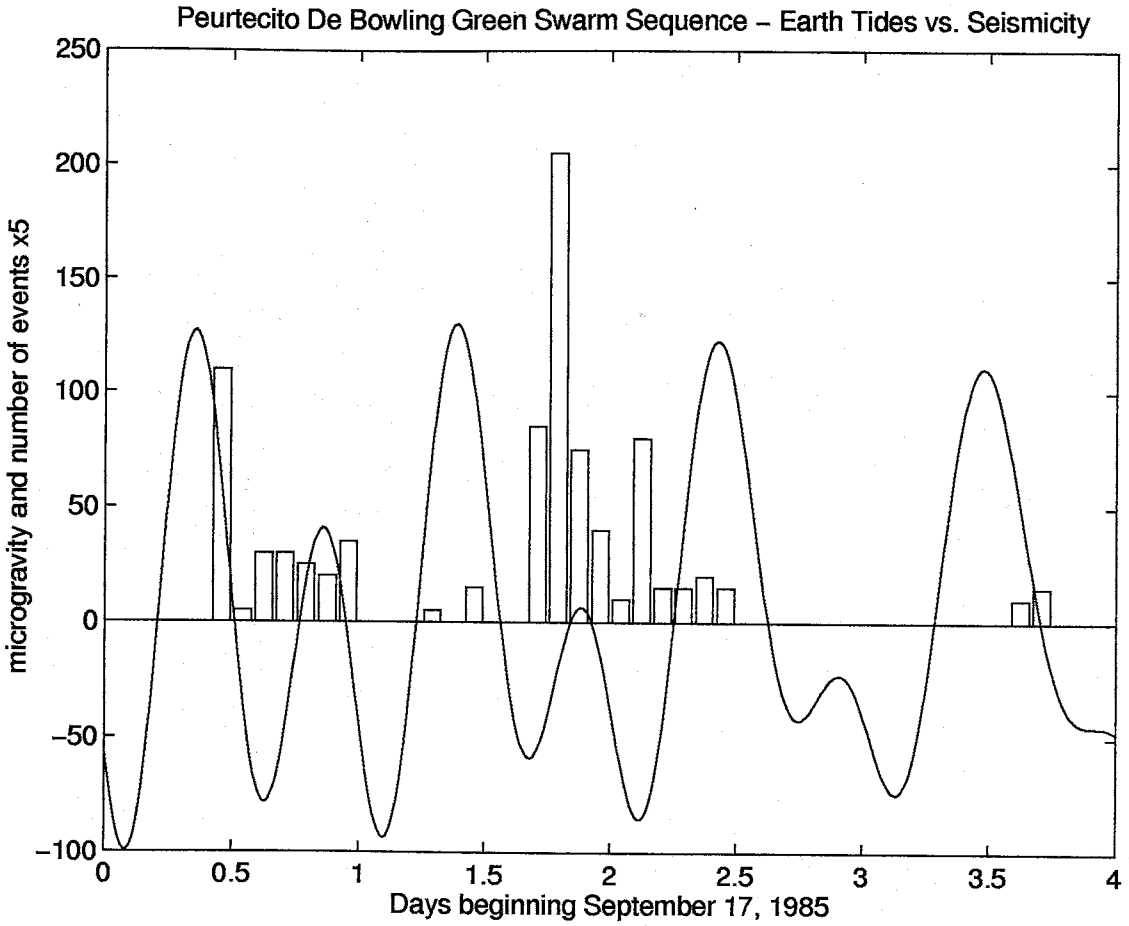

Figure 9.9. Event histogram and predicted microgravity variations for the Puertecito de Bowling Green swarm.

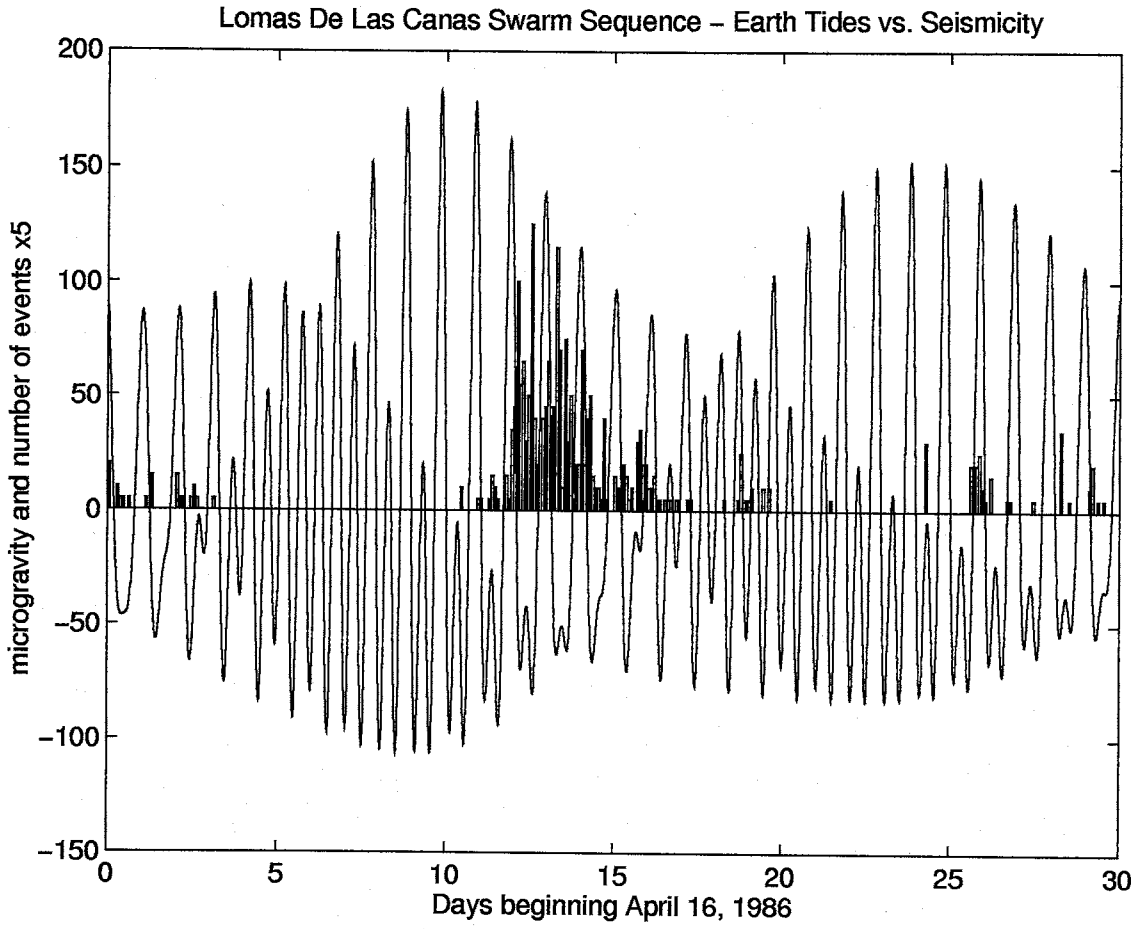

Figure 9.10. Event histogram and predicted microgravity variations for the Loma de las Cañas swarm.

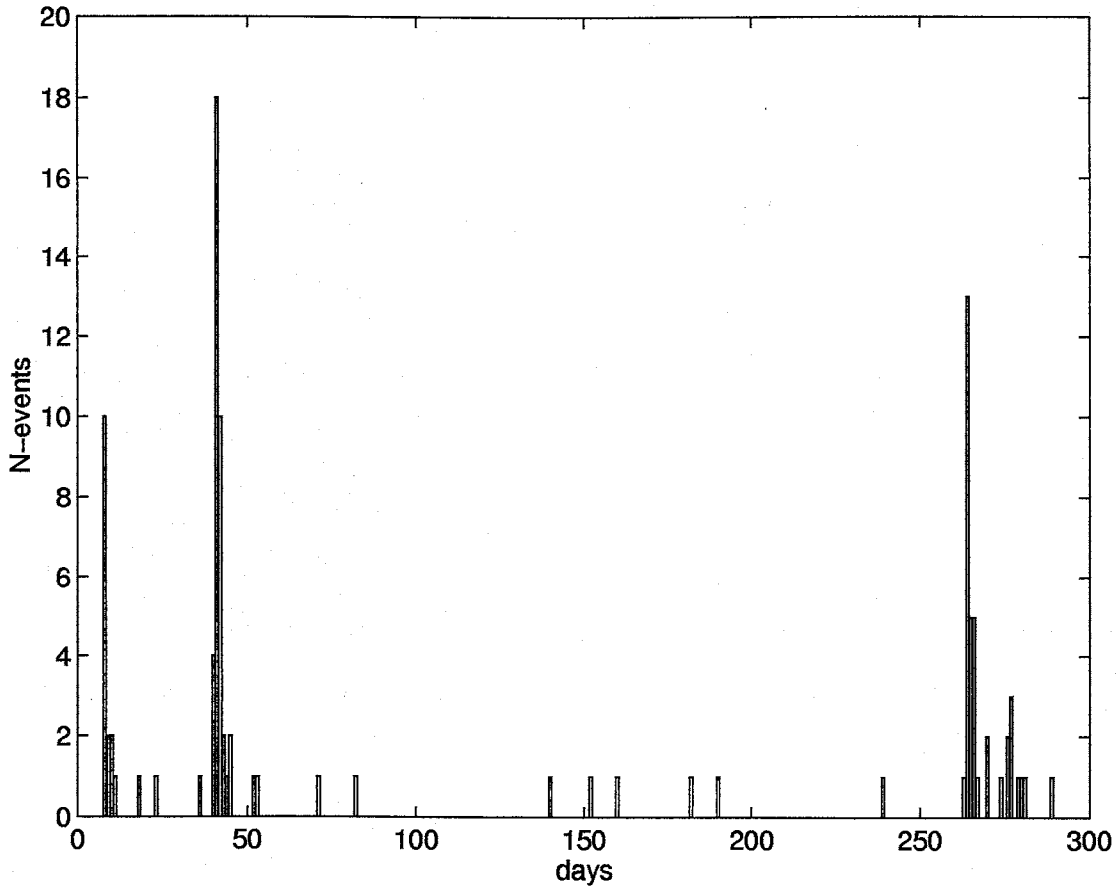

Figure 9.11. Histogram of events per day for the East Rift Sequence. Periodic bursts of activity are indicated by single events above M$-d$=1.0 on this plot.

swarms occurred in the epicentral region of the ADC swarm as a series of minor swarms (several events with one event near magnitude 1.0). Examination of Figure 9.11 shows periodicity or pulsing of events, though on a much longer time scale. The three panels in Figure 9.12 compare the events per day histogram of Figure 9.11 with predicted gravity variation due to earth tides. All three of the main sequences, and the largest sub swarm (near day 60) all initiated during new or full moons (at the peak of gravitational variance). The smaller sub-swarms, however, tended to initiate at or near lows in the lunar cycle. This phenomenon is evident on all three panels, though the center panel illustrates it best. It seems unlikely that this is a complete coincidence, yet a relationship between lows in the earth tide and swarm initiation seems tenuous, perhaps there is a time-lag between extremes in local microgravity due to earth tides and subsequent swarm initiation.

The majority of the earthquakes in the East Rift sequence occurred on left-lateral strike-slip faults and the major swarms all initiated during New or Full moons. A macro-scale look at the San Acacia swarm (Figure 9.13) shows that the swarm commenced during a new or full moon, though the main sequence did not start until a week later when microgravity fluctuations due to earth tides were at a low. The Socorro Mountain swarms (Figure 9.14) both commenced during lows in the earth tide. The San Acacia swarm and the Socorro Mountain sequence were both dominated by earthquakes occurring on normal faults.

From this notably small sample of three strike-slip and three normal fault swarms a tentative conclusion may be drawn. Strike-slip swarms initiated during new or full moons at the peak in microgravity variations due to earth tides. Swarms dominated by normal faulting, however, appeared to nucleate during lows in the earth tide effect.

Another possible explanation for the periodic bursts of seismicity in the swarms

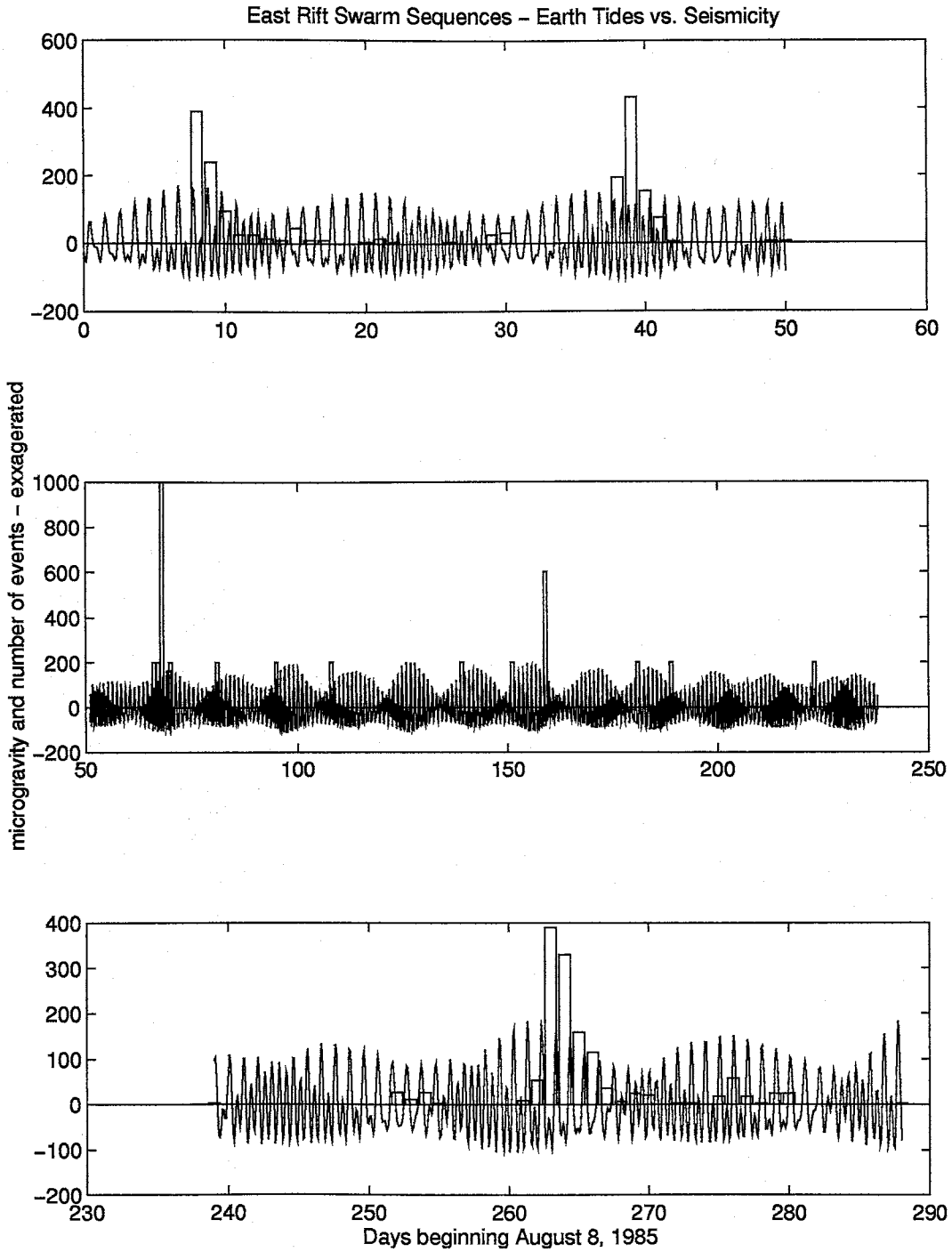

Figure 9.12. Event histogram and macro-scale microgravity variations for the East Rift sequence. The histograms come from Figure 9.11.

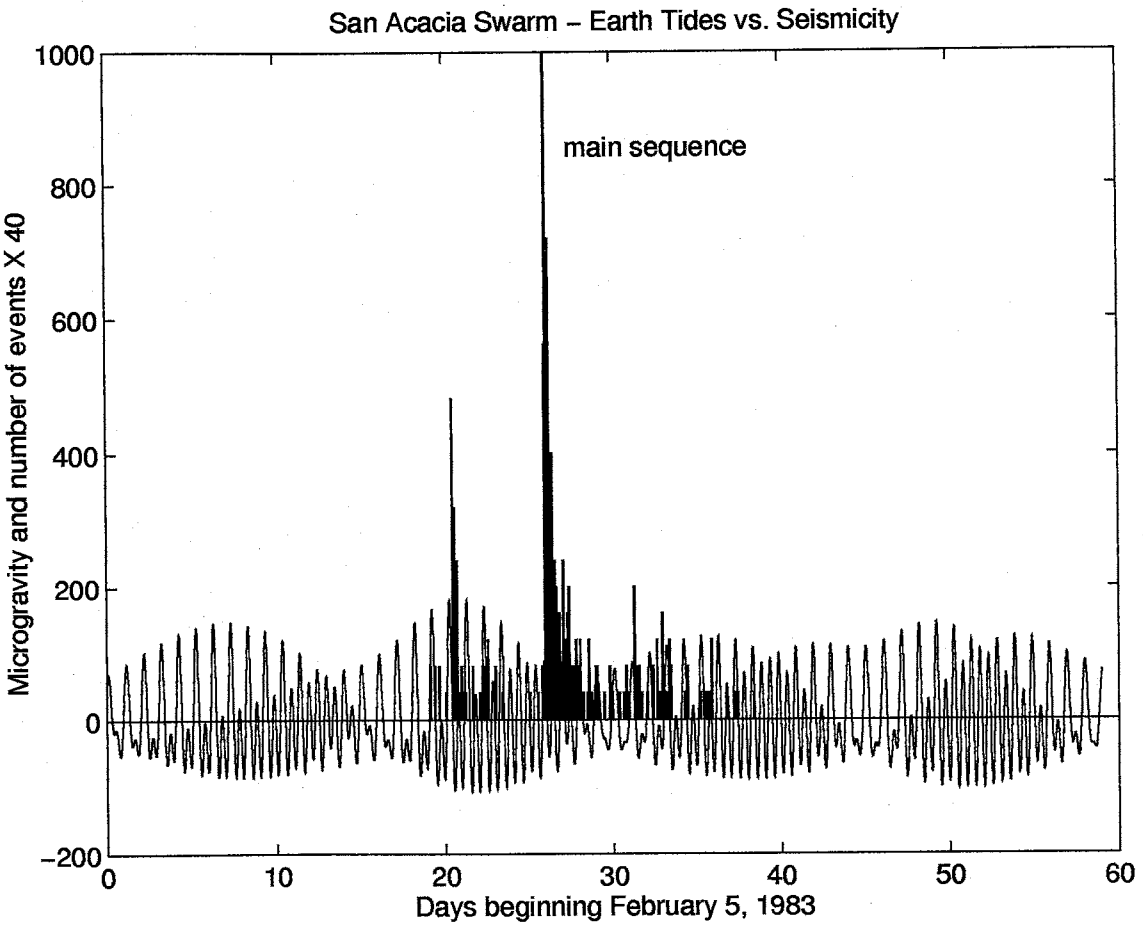

Figure 9.13. Event histogram and macro-scale microgravity variations for the San Acacia Swarm.

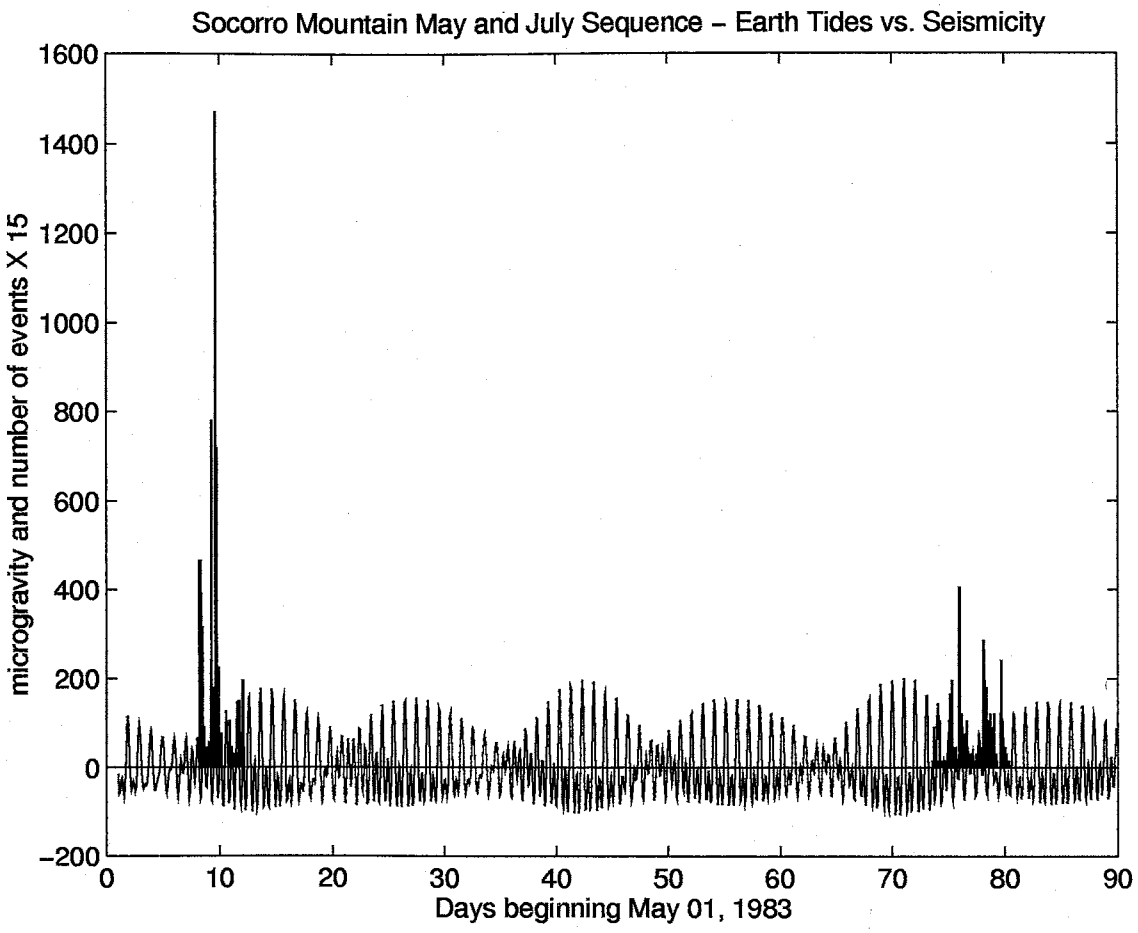

Figure 9.14. Event histogram and macro-scale microgravity variations for the Socorro Mountain sequence.

could be irregular injections of fluid into the crust. High pressure injection of chemical waste water into fractured basement rock at the Rocky Mountain arsenal [*Evans*, 1966] was correlated with 710 earthquakes in the Denver, Colorado area. A clear match between pulses of earthquakes and periods of fluid injection was found. Other examples of seismicity caused by fluid injection include Rangley Field, Colorado [*Raleigh et al.*, 1976] and oil fields in west Texas [*Sanford and Toppozada*, 1974; and *Davis and Pennington*, 1989]. For the Socorro area, spasmatic movement of magma or water in the seismogenic crust could be the potential driving force behind the bursts of seismicity.

10. Discussion

In the **Introduction** section of this paper a number of general questions were presented. In this discussion those questions are addressed in two subdivisions: *The Relationship of Swarms to the Magma Body and Rio Grande Rift*; and *Characteristics of Socorro Area Microearthquake Swarms.*

The Relationship of Swarms to the Magma Body and Rio Grande Rift

One of the most important questions to be addressed by this study is the relationship between the observed seismic activity and the local tectonic framework. Two major seismotectonic features exist in the Socorro area, of which the Rio Grande rift is the dominant feature and at least overprints older features with its stress field. Crosscutting the Rio Grande rift in the Socorro area is a wide band of increased seismicity related to a topographic lineament [*Sanford et al.*, 1995[2]]. This lineament, identified as the Socorro Fracture Zone (SFZ), appears to be a large scale crustal feature which has affected the morphology of the RGR in the Socorro area. Other relevant features of the Socorro area include the Socorro Magma Body which is a young feature with measurable uplift beginning about 50,000 years ago [*Ouichi*, 1983; *Sanford et al.*, 1991] and a contemporary uplift rate of ~2 mm/yr [*Larsen et al.*, 1986]. As previously noted, the Socorro Seismic Anomaly (SSA) is a region of enhanced seismicity in New Mexico [Sanford et al., 1995[1]]. The area of the SSA is similar in shape to the SMB though slightly larger (Figure 8 in part I) [*Balch et al.*, 1997]. Is it possible that any of these seismotectonic elements directly influence the increased local seismicity?

In a continental rift one would expect to see predominantly normal faulting with perhaps some strike-slip faults. Certainly the activity in the five studied swarms

fits well into this framework, and it could seem reasonable to relate contemporary seismic activity in the region to extension of the Rio Grande rift. However, *Savage et al.* [1980 and 1985] found from geodetic data, that measurements across a strain network located near Socorro were consistent with no deformation across the rift. The small strain rates required by the measured vertical uplift due to inflation of the magma body [*Larsen et al.*, 1986] could be accommodated by their measurements, however. A possible extension rate of 0.3 mm/yr was given by *Woodward* [1977] for Albuquerque, New Mexico, 100 km north of Socorro. Thus, extension of the rift near Socorro is either very slow (or non-existent) and probably could not provide the impetus for the enhanced seismicity. Also, if the increased seismicity was due to extension of the rift, one would expect similar distributions of earthquakes along other rift segments.

The Socorro Fracture Zone (SFZ) is a transverse ENE structural lineament paralleling the better known Jemez lineament to the north [*Sanford et al.*, 1995[2]]. The SFZ is characterized by prominent ENE trending topographic and structural features and enhanced seismicity above M_d=3.0 in eastern New Mexico and West Texas. *Sanford et al.* [1995[2]] found that the northern and southern boundaries of SFZ bracket the Socorro Magma Body (SMB). Therefore, they consider it likely that the SMB occurs in the Socorro area rather than elsewhere along the rift because of the additional weakness of the crust imposed by the SFZ. By comparison, the large Valles volcanic complex lies at the intersection of the Jemez lineament with the Rio Grande rift.

The final structural element in the region is the Socorro Magma Body. The magma body, by a process of elimination, must provide the driving force for the enhanced seismicity in the Socorro area. The magma body has the same basic outline and orientation as the SSA and falls just within its boundaries, providing

a strong causal link between the two. The enhanced seismicity of the SSA is likely a result of reactivation of earlier rift-related faults due to stresses imposed by the uplift associated with the magma body. The aseismic halo surrounding the Socorro Seismic Anomaly and the proposed fault reactivations may share a similar cause. Uplift from the inflation of the magma body would allow extension over the center of the uplift and compression beyond the bodies margins (Figure 10.1). Normal and strike-slip faults over the extending portion of the crust would experience a reduction of normal stress across their fault planes, while corresponding faults in the aseismic halo would experience an increase in normal stress, thus tending to lock the faults. Modeling using sinusoidal vertical displacements at the base of an elastic homogeneous rock layer supports this argument [*Sanford*, 1959].

Characteristics of Socorro Area Microearthquake Swarms.

The primary expression of seismic activity in the Socorro Seismic Anomaly appears very similar to A-type volcanic swarms. A-type volcanic earthquake sequences take place beneath volcanoes at depths of 1 to 20 km; they generally have magnitudes less (often much less) than 6.0, follow a swarm pattern distinct from tectonic earthquake sequences, and are the result of shear faulting [*Minakami*, 1974]. Most earthquake sequences observed in the central RGR have a swarm temporal distribution, with the strongest events occurring a considerable time after the start of the activity. By comparison, tectonic sequences are often characterized by few if any precursors, followed by main shocks early in the sequence and with the majority of events being aftershocks. The hypocentral distribution of a tectonic aftershock sequence may define the rupture surface of the main shock.

For the RGR swarms I have studied, the distribution of hypocenters has not been useful in defining rupture surfaces as the longest two dimensions of the hypocentral

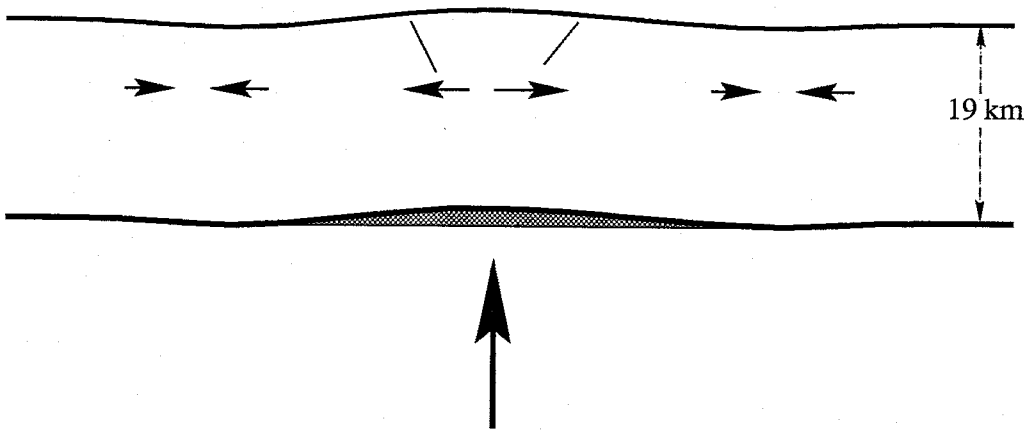

Figure 10.1. Cartoon illustrating reaction of a rigid plate to an applied force. In this case the force is magma injection at a depth of 19 km contributing to surface uplift of ~2 mm/yr.

cloud defines an area several times the size of the rupture surface of the strongest shock. I used an empirical relationship between moment magnitude and rupture area found in *Wells and Coppersmith* [1994] to calculate the rupture area for the strongest events in the studied swarms (their table 2A and normal and strike-slip regression relationships). The duration magnitude scale used for central New Mexico [*Ake et al.*, 1983] provides an estimate of M_L for magnitudes between 1.1 and 4.2. Since the local magnitude (M_L) is equivalent to moment magnitude (**M**) [*Hanks and Kanamori*, 1979] it is acceptable to use locally computed values of duration magnitude (M_d) in the *Wells and Coppersmith* formulations. Table 10.1 lists duration magnitudes and rupture area computed using their formulas, and approximate observed dimensions of the swarm volume. The dimensions of the fault plane of the main event in every swarm is dwarfed by the dimensions of the active volume. Curiously, focal mechanisms within these swarms are often quite consistent and must be occurring on systems of sub-parallel fractures.

Several other factors indicate that the upper crust in the Socorro area is highly fractured. First, P wave velocities determined in the rift in the Socorro area [*Rinehart et al.*, 1979; *Singer*, 1989; *Hartse et al.*, 1992; and *Balch*, 1992] are lower than off-rift values. In-rift Pg velocities average about 5.85 km/s while off-rift values average 6.15 km/s [*Stewart and Pakiser*, 1962; *Jaksha and Evans*, 1984; and *Sinno et al.*, 1986]. Exposed Paleozoic rocks on the eastern margin of the Rio Grande rift are highly fractured in contrast to similar formations outside of the rift [*Mozley, personal communication*, 1997]. The confluence of the RGR and SFZ probably produces additional fracturing in the Socorro area beyond that which characterizes the rest of the RGR. It seems certain that the seismogenic zone in the upper crust in the Socorro area is highly fractured.

There are some indications that fluid plays a role in faulting for Socorro area

Swarm Dimensions and Main Shock Rupture Area			
Swarm	M_d ($\sim$M)	Rupture Area	Swarm Dimensions
SAS	4.2	1.8	4.0 x 3.0 x 1.5
SMS	2.1	0.3	1.0 x 1.5 x 1.5
ADC	4.0	1.2	3.0 x 4.0 x 3.0
PBG	2.7	0.4	1.0 x 2.0 x 2.0
LDC	3.1	0.5	2.0 x 2.0 x 2.0

Table 10.1. Table comparing swarm dimensions to rupture area for the studied swarms. Rupture area is in km^2, swarm dimensions in km.

swarms. The San Acacia swarm had a number of non-double couple (NDC) earthquakes which may be the result of rapid injection of fluids into the fault plane during rupture propagation. The Socorro Mountain sequences are interpreted to have occurred on a reactivated Oligocene fracture system with some faults at very low angles. Reactivation of low-angle normal faults is more likely with the presence of fluid within the fault since it reduces the effective stress (lithostatic load) which otherwise acts to increase the coefficient of friction across low-angle faults. The presence of the Rio Grande and the fractured nature of the crust in central Rio Grande rift certainly would allow for transport of water into the subsurface and the existence of fluids may be fairly common in fractures at depth.

It seems reasonable that the time distribution of earthquakes (swarms), consistency of focal mechanisms, and the large observed hypocentral volumes occupied by Socorro area microearthquake swarms, must be explained in the context of three primary observations: (1) The highly fractured nature of the seismogenic crust, (2) the uplift induced reduction of normal stresses across normal and strike-slip faults within the seismic anomaly, and (3) the postulated presence of water in fractures at any depth of the seismogenic crust. Further, items (2) and (3) both imply that reactivation of pre-existing faults is the principle driving force for the swarms. The large hypocentral volumes and the commonly observed consistency of focal mechanisms within swarm sequences indicates that the fault reactivations occur in blocks of similarly faulted and stressed rock. Between the studied sequences, no consistent pattern of stress orientations were observed, though N-S striking faults were most common. Therefore, the seismicity of the region is not well characterized as the release of stress imposed by a single dominant stress field, such as those imposed by simple extension. Instead, isolated crustal blocks with consistent fracture patterns appear to be releasing previously imposed stresses during the earthquake swarms. The large volumes and consistent orientation of fault planes in the swarms can be

explained by this interpretation.

Finally, I attempt to relate the primary observations to the remaining characteristic of Socorro area seismicity – the swarm temporal distributions of otherwise tectonic earthquakes. Assume that a volume of the crust contains faults which are very close to failure. Initial earthquakes could perturb the balance of fluid pressures in nearby cracks by dynamic stress transfer [*Hill et al.*, 1993], or physical transfer of fluids, which could result in further fault reactivations. As an ongoing process this could result in a cascade of events towards the temporal center of the swarm, perhaps peaking just after the occurrence of the strongest quakes, with a subsequent reduction in activity as the number of critically stressed faults in the hypocentral volume decreases. Though speculative, I believe this is a reasonable model to describe the temporal distribution of events in Socorro earthquake swarms.

11. Summary and Conclusions

Microearthquake swarms have been recognized in the central Rio Grande rift for many years, both instrumentally since the 1960's and by felt reports since 1849. Though commonly observed, little previous work has been done to understand the genesis and propagation of the swarms and their relationship to the seismotectonic framework of the central Rio Grande rift. With the advent of **SEISMOS** [*Hartse*, 1991] more detailed studies of the swarm seismicity became possible. In this study five separate swarms were studied in great detail, to address not only specific problems but also some broader issues.

For my study of the San Acacia swarm (February and March 1983), I located 204 earthquakes of which 101 were defined to be "high quality" with latitude, longitude and depth errors of less than 0.5 km at 1 standard deviation. Focal mechanisms were computed for a subset of 30 events of the high quality data set which had seven or more first motion readings. Of the computed focal mechanisms, one third had distributions of first motions incompatible with standard double-couple models of faulting. I modeled these 10 events as tensile-shear faults using separate moment tensors for aligned shear and tensile faults and summing them using the principle of superposition. The modeled non-double-couple events are consistent with rapid fluid injection (opening the fault) while shear failure is occurring. The SAS occurred at shallow depths within the transfer zone between two basins in the central Rio Grande rift which may explain why the twenty double-couple earthquakes, while primarily occurring on N-S oriented normal faults, were more diverse in type than those for the other studied swarms.

The Socorro Mountain sequence occurred in two spatially related swarms in May and July of 1983. A total of 108 earthquakes were located of which 78 events were of high quality. Focal mechanisms were computed for 24 of the strongest events

from the high quality data set, with 11 events from the May swarm and 13 events from the July swarm. The focal mechanisms consisted of north-striking normal fault events with varying degrees of dip. The most geologically reasonable explanation for the distribution of seismicity in the sequence involves reactivation of an Oligocene age fracture system which had experienced 2-3 episodes of domino-style faulting. Three of the focal mechanisms exhibited possible low-angle fault planes, implying the presence of fluid in the hypocentral rocks. Digital seismograms were divided into eight sub-groups on the basis of full waveform cross-correlations, which compliments the observed variety in dip for the computed focal mechanisms. I was unable to directly match correlated earthquake sub-types with hypocenter clusters since the active volume was less than a cubic kilometer and acceptable errors were ± 0.5 km.

The East Rift sequence contained three swarms and was studied as a single sequence because of apparent temporal and spatial relationships between the swarms. The sequence was initiated in August, 1985 with the Arroyo del Coyote swarm, which continued to have periodic bursts of activity until the end of the entire sequence nearly 300 days later. In September, the Puertecito de Bowling Green swarm occurred about 6 kilometers north of the ADC epicentral region. Nearly eight months later, in April of 1986, the Loma de las Cañas swarm began about 10 kilometers south of the location of the ADC swarm. High quality hypocenters were found for 309 events with 138, 56, and 106 events from the ADC, PBG, and LDC swarms, respectively. Focal mechanisms were calculated from the high quality data set with 60, 39, and 55 events in the ADC, PBG, and LDC swarms, respectively. The focal mechanisms for the PBG and LDC swarms consisted of strike-slip faults and displayed a high degree of consistency of strike-direction within each swarm. The average T-axis azimuths for the PBG swarm was 236.8 ± 4.7^0 and for the LDC swarm 219.6 ± 8.0^o. The ADC swarm was more complex with events falling into two major and 1 minor categories. Type 3 ADC events consisted of seven north-striking

normal fault mechanisms. Type 1 ADC events, 87% of which occurred prior to the PBG swarm, had an average T-axis azimuth of 247.6±9.5°, very close to the average T-axis of the PBG swarm. Type 2 ADC events were more evenly distributed in time, with 59% occurring after the PBG swarm and prior to the LDC swarm. Their average T-axis azimuth of 214.4±8.5° was nearly identical to that observed for LDC swarm events. In addition to highly similar focal mechanisms, Type 1 events were clustered at the north end of the ADC swarm volume, closest to the PBG swarm, while Type 2 events were commonly located more to the south, closer to the LDC swarm. It seems likely that the three swarms indicate activity on a single fault or fault system with a well constrained bend at the location of the ADC swarm, and that some mechanism (possibly fault creep, or fluid transfer) communicated stress along the fault during the sequence.

A common feature of the temporal distributions of earthquakes in the studied swarms was bursts of activity punctuated by periods of inactivity. It is possible that a common driving force causes these bursts in activity in the swarms. I investigated the possibility that the earthquakes were sensitive to variations in microgravity caused by tidal effects of the Moon and Sun. The temporal distribution of earthquakes was compared to predicted local variations in microgravity due to the earth tides and no direct correlation was found. Another possibility, though unexplored, is that the pulses of activity in Socorro area swarms is caused by injection of fluids (magma?) into the active volume. Several examples of induced seismicity caused by fluid injection have been observed [*Evans*, 1966; *Raleigh et al.*, 1976; and *Davis and Pennington*, 1989].

The data from the five swarms were combined with all other hypocenters that have been located with **SEISMOS** in the Socorro area. This larger data set was used for two studies: To re-map the lateral extent of the Socorro Magma Body and

to map the base of the local seismogenic zone for the first time. The lateral extent of the Socorro Magma Body and the combined data set is described in **part I** of this dissertation (published paper).

The base of the seismogenic zone was mapped for the region from 33.9° to 34.5° N latitude and 106.7° to 107.1° W longitude. This region was subdivided into 88 cells and the maximum hypocenter depth for each cell was extracted. Since not all cells had a thorough sampling of activity the map should be considered a "minimum depth" map for the base of the seismogenic zone. In addition, the data was smoothed to fill in empty grid blocks, and thus best represents the shape and average depth of the base of the seismogenic zone, rather than an absolute definition. The base of the seismogenic zone is not flat in the Socorro area and is deepest (8 to 10 km) in a band running from the WSW corner to the ENE corner, perhaps as a subsurface expression of the Socorro Fracture zone.

The orientation of the maximum and minimum compressive stresses (P-T axes) for the studied swarms failed to show consistent values across the region. This means that a single contemporary source of stress does not dominate faulting and stress release in the Socorro area. Further, it makes it very difficult to predict what sort of activity might be observed in the future, as similarly paleo-stressed and fractured volumes could exist, with a variety of orientations in the subsurface. However, faults roughly oriented N-S seem to be most common and release of previously imposed stresses appear to make use of the pre-existing structural weaknesses presented by rift related fractures.

The distributions of P and T axes orientations within individual swarm sequences is fairly consistent. However, offsets of even a few kilometers appears to be sufficient to alter the distribution of stresses in the crust. It is possible to relate the various paleo-stress orientations, implied by observed fault reactivations, to past

geologic conditions. I have done this twice in this study. The Socorro Mountain sequence appears to be related to an Oligocene age fracture system developed through several episodes of domino-style faulting and the East Rift sequence appears to have released stress related to rotation of the Colorado Plateau in the Miocene.

The apparent absence of extension in the Rio Grande rift [*Savage et al.*, 1985] seems to indicate that the Socorro Magma Body is responsible for the heightened seismicity of the the region. Evidence for the magma body as a source of stresses for reactivation of faults comes from observed surface uplift of ~2 mm/yr [*Larsen et al.*, 1986] and the similarities in shape and centerpoint of the magma body and the Socorro Seismic Anomaly [*Balch et al.*, 1997].

The time distribution of earthquakes, consistency of focal mechanisms, and the large observed hypocentral volumes occupied by Socorro area swarms, needs to be explained in the context of three observations: (1) The highly fractured nature of the seismogenic crust, (2) the uplift induced reduction of normal stresses across normal and strike-slip faults within the seismic anomaly, and (3) the presumed presence of water in fractures at any depth of the seismogenic crust. These observations indicate that reactivation of pre-existing faults is the principle driving force for the swarms.

If we assume that a volume of the crust contains faults which are very close to failure, initial earthquakes in a swarm could perturb the balance of fluid pressures in nearby cracks by dynamic stress transfer [*Hill et al.*, 1993], or physical transfer of fluids, resulting in further fault reactivations. As a continuing process, this could result in an increase of events towards the temporal center of the swarm, perhaps peaking just after the occurrence of the strongest events, with a subsequent reduction in activity as the number of critically stressed faults in the active volume is diminished. Though speculative, I believe this is a reasonable model for swarm genesis and propagation in the Socorro area.

The existence of obvious non-double couple earthquake sources in the San Acacia NM area forces the conclusion that less well-constrained double-couple events near San Acacia, and in the Socorro area as a whole, may have NDC components. It seems likely that other NDC events could be found, if as I have alluded, water is pervasive in the highly fractured upper crust in the region.

The observation of a large sub-surface fault, capable of producing a "hidden" earthquake of magnitude 6.5, five km east of Socorro, could impact seismic hazards estimates for the region. For all of the studied swarms, no direct relationship to mapped surface faults was observed, so earthquakes on hidden faults appears to be the norm.

12. Suggestions for Further Studies

A comprehensive examination of focal mechanisms across the region could be the basis for a 2-D or 3-D map of stress distributions in the seismogenic crust. An ambitious study would attempt to relate the stress directions, implied by the focal mechanisms, to paleo-stress conditions in the past within the seismogenic zone.

Close examination of a catalog of focal mechanisms across the region may also be helpful in determining how common NDC events are in the Socorro Seismic Anomaly. However, unless portable stations are operated in the region of a swarm, the distribution and number of first motion directions may be inadequate to resolve NDC events. As the catalog of digitally recorded events increases it should be possible to use moment tensor analysis to examine focal mechanisms in more detail. If more NDC events are found, the arguments for the role of fluids in Socorro area seismicity would be strengthened

The apparent link between fluids and faulting in the Socorro area highlights the need for a better mechanistic understanding of the phenomena. Much work has been done on fractured resevoirs by people doing research for petroleum companies. Some of these advances could have relevance to swarm propagation and the observed large volumes for Socorro area earthquake swarms.

It should be possible to compute a 2-D finite element model portraying uplift induced stresses for the Socorro Seismic Anomaly, starting with the well-constrained magma body outline from this study and uplift rates from *Larsen et al.* [1986]. A model of this type would indicate areas of maximum and minimum crustal extension and assist seismic hazards analyses in the region.

13. References

Ake, J. P. (1983). A magnitude scale for central New Mexico based on signal duration, *Geophysics Open-file Report* **45**, New Mexico Tech, Socorro, New Mexico, 8 pp.

Ake, J. P. (1986). An analysis of the May and July, 1983 Socorro Mountain earthquake swarms, *Geophysics Open-file Report* **49**, New Mexico Tech, Socorro, New Mexico, 107 pp.

Ake, J. P. and A. R. Sanford (1988). New evidence for the existence and internal structure of a thin layer of magma at mid-crustal depths near Socorro, New Mexico, *Bull. Seismol. Soc. Am.* **78**, 1335-1359.

Aki, K. and P. G. Richards (1980). Quantitative Seismology, Theory and Methods. Freeman, San Francisco, Calif., 932 pp.

Bachman, G. O. and H. H. Mehnert (1978). New K-Ar dates and late Pliocene to Holocene geomorphic history of the Central Rio Grande region, *Geol. Soc. Am. Bull.* **89**, 283-293.

Bagg, R.M. (1904). Earthquakes in Socorro, New Mexico, *Am. Geologist* **34**, 102-104.

Balch, R. S., H. E. Hartse, A. R. Sanford, and K. Lin (1997). A new map of the geographic extent of the Socorro Magma Body, *Bull. Seism. Soc. Am.* **87**, 174-182.

Balch, R. S. (1992). New constraints on the Socorro Magma Body based on improved hypocenter estimates, *Geophysics Open-file Report* **63**, New Mexico Tech, Socorro, 120 pp.

Balch, R. S., A. R. Sanford, and H. E. Hartse, 1994[1]. Focal mechanisms for two microearthquake swarms beneath the Socorro Mountains, New Mexico, in May and

July 1983, *abstract Seismol. Res. Letters* **65**.

Balch, R. S., A. R. Sanford, L. H. Jaksha, H. E. Hartse, and L.S. House, 1994[2]. Non-Double-Couple Focal Mechanisms Observed in the Central Rio Grande Rift of New Mexico, *abstract EOS*, **75 no. 44**.

Barrol, M. W., and M. R. Reiter, (1990). Analysis of the Socorro hydro-geothermal system; central New Mexico, *J. Geophys. Res.* **95**, 21949-21963.

Burridge, R. and L. Knoppoff (1964). Body force equivalents for seismic dislocations, *Bull. Seism. Soc. Am.*, **54**, 1875-1888.

Brown, L. D., C. E. Chapin, A. R. Sanford, S. Kaufman, and J. Oliver (1980). Deep structure of the Rio Grande rift from seismic reflection profiling, *J. Geophys. Res.* **85**, 4773-4800.

Cather, S. M. (1996). Geologic Maps of upper Cenozoic deposits of the central Socorro basin, *New Mexico Bureau of Mines and Mineral Resources Open-file Report* **417**, preliminary.

Chamberlin, R. M. (1980). Cenozoic stratigraphy and structure of the Socorro Peak volcanic center, central New Mexico [Ph.D thesis]: *New Mexico Bureau of Mines and Mineral Resources Open-file Report* **118**, 2 Vols., 495 pp.

Chamberlin, R. M. (1981). Cenozoic stratigraphy and structure of the Socorro Peak volcanic center, central New Mexico: A summary, *New Mexico Geology* **3**, May 1981, 22-24.

Chapin, C. E. (1971). The Rio Grande rift; modifications and additions, *New Mexico Geol. Soc. 22nd Annual Field Conference Guidebook*, 191-201.

Chapin, C. E. and S. M. Cather (1994). Tectonic setting of the axial basins of the northern and central Rio Grande rift, in Keller, G. R. and Cather, S. M., eds.

Basins of the Rio Grande rift: Structure, stratigraphy, and tectonic setting. GSA Spec. Pub. **291**.

Chapin, C. E. (1979). Evolution of the Rio Grande rift - a summary, in *Rio Grande Rift: Tectonics and Magmatism*, edited by R. E. Reicker, 1-5.

Chouet, B. (1979). Sources of seismic events in the cooling lava lake of Kilauea Iki, Hawaii. *J. Geophys. Res.* **84** pp. 2315-2330.

Davis, S. D. and W. D. Pennington (1989). Induced seismic deformation in the Cogdell oil field of west Texas, *Bull. Seismol. Soc. Am.* **79**, 1477-1495.

Evans, M. E. (1966). The Denver area earthquakes and the Rocky Mountain Arsenal disposal well, *Mountain Geology* **3**, 23-36.

Foulger, G. R. (1988). Hengill triple junction, SW Iceland 2. Anomalous earthquake focal mechanisms and implications for process within the geothermal reservoir and at accretionary plate boundaries, *J. Geophys. Res.* **93**, 13507-13523.

Foulger, G. R. and B. R. Julian (1993). Non-double-couple earthquakes at the Hengill-Grensdalur volcanic complex, Iceland: Are they artifacts of crustal heterogeneity? *Bull. Seismol. Soc. Am.* **83**, 38-52.

Frankel, J. J. and H. Kanamori (1983). Determination of rupture duration and stress drop for earthquakes in Southern California, *Bull. Seismol. Soc. Am.* **73**, 1527-155.

Frohlich, C. (1994). Earthquakes with non-double-couple mechanisms, *Science* **264**, 804-809.

Hammond, J. F. (1966). *A Surgeon's Report on Socorro, New Mexico, 1852*, Sante Fe, New Mexico, Stagecoach Press.

Hanks, T. C. and H. Kanamori (1979). A moment magnitude scale, *J. Geophys.*

Res. **84**, 2348-2350.

Hartse, H. E. (1991). Simultaneous hypocenter and velocity model estimation using direct and reflected phases from microearthquakes recorded within the central Rio Grande rift, New Mexico, *Ph.D. Dissertation*, New Mexico Institute of Mining and Technology, Socorro, New Mexico, 251 pp.

Hartse, H. E., A. R. Sanford, and J. S. Knapp (1992). Incorporating Socorro Magma Body reflections into the earthquake location process, *Bull. Seism. Soc. Am.* **82**, 2511-2532.

Hill, D. P., R. A. Reasenburg, A. Michael, and 28 others, (1993). Seismicity remotely triggered by the magnitude 7.3 Landers, California, earthquake, *Science* **260**, 1617-1623.

Jaksha, L. H. and D. H. Evans (1984). Reconnaissance seismic refraction-reflection surveys in northwestern New Mexico, *Bull. Seismol. Soc. Am.* **74**, 1263-1274.

Jarpe, S. (1984). Characteristics and possible cause of an earthquake swarm in the central Rio Grande rift 28 km North of Socorro, New Mexico: February and March, 1983, *Masters I.S.*, New Mexico Institute of Mining and Technology, Socorro, New Mexico, 74 pp.

Julian, B. R. (1995). Personal Communication, software packages BWNODE and MOMTEN.

Kelly, V. C. (1952). Tectonics of the Rio Grande depression of central New Mexico, *New Mexico Geol. Soc. 3d Annual Field Conference Guidebook*, 93-105.

Klein, F. W., P. Einarsson, and M. Wyss (1977). The Reykjanes Peninsula, Iceland, earthquake swarm of September 1972 and its tectonic significance, *J. Geophys. Res.* **82**, 865-888.

Kluth, C. F. and P. J. Coney (1981). Plate tectonics of the Ancestral Rocky Mountains, *Geology* **9**, 10-15.

Lee, W. H. K. (1992) The Xdetect program: A course on PC-based Networks, *U.S.G.S. Open-File Report*, **92-441**, edited by W. H. K. Lee and D. A. Dodge, 138-151.

Lees, J. M. (1995). Xmap8: Three-dimensional GIS for geology and geophysics, *Seismol. Res. Let.*, **66**, 33-37.

Larsen, S., R. Reilenger, and L. Brown (1986). Evidence of ongoing crustal deformation related to magmatic activity near Socorro, New Mexico, *J. Geophys. Res.* **91**, 6283-6292.

Machette, M. N. (1978). Geologic map of the San Acacia Quadrangle, Socorro County, New Mexico, *USGS Map GQ-1415*.

Machette, M. N. (1982). Quaternary and Pliocene faults in the La Jencia and southern part of the Albuquerque-Belen basins, New Mexico: evidence of fault history from scarp morphology and Quaternary geology in *Albuquerque County II*, J. A. Grambling and S. G. Wells. eds., *New Mexico Geological Society, Guidebook* **33**, 161-169.

Minakami, T. (1974). Seismology of volcanoes in Japan, in *Physical Volcanology*, L. Civetta, P. Gasparini, G. Luongo and A. Rapolla eds., 1-27.

Morton, W. H. and R. Black (1975). Crustal attenuation in Afar; in Pilger, A. and Rosler, A., eds., *Afar Depression of Ethiopia: Inter-Union Commission on Geodynamics Scientific Report 14*, pp. 55-65.

Mozely, P. S. (1997). Personal Communication, fractures in exposed rocks east of Socorro, New Mexico.

Northrop, S. A. (1947). Seismology in New Mexico [abstract], *Geol. Soc. Am. Bull.* **58**, 1268.

Osburn, G. R. (1984). Geology of Socorro County, *New Mexico Bureau of Mines and Mineral Resources, Open-file Report* **238**.

Ouichi, S. (1983). Effects of uplift on the Rio Grande over the Socorro Magma Body, New Mexico, *Field Conference Guidebook N. M. Geol. Soc.* **34**, 54-56.

Petrilla, C. C. (1987). Analysis of recent swarm activity along the Hot Springs-Montosa Fault east of Socorro, New Mexico, *Geophysics Open-File Report* **58**, New Mexico Tech, Socorro, 215 pp.

Raleigh, C. B., J. H. Healy, and J. D. Bredehoeft (1976). An experiment in control at Rangely, Colorado, *Science* **191**, 1230-1237.

Reasenberg, P. and D. Oppenheimer (1985). FPFIT, FPPLOT, and FPPAGE: FORTRAN computer programs for calculating and displaying earthquake fault-plane solutions, *U.S. Geological Survey Open File Report* **85-739**, 109 pp.

Reid, H. F. (1911). Remarkable earthquakes in central New Mexico in 1906 and 1907, *Bull. Seism. Soc. Am.* **1**, 10-16.

Rinehart, E. J., A. R. Sanford, and R. M. Ward (1979). Geographic Extent and Shape of an Extensive Magma Body at Mid-Crustal Depths in the Rio Grande Rift Near Socorro, New Mexico, in *Rio Grande Rift: Tectonics and Magmatism*, edited by R. E. Reicker, 237-251.

Sanford, A. R. (1959). Analytical and experimental study of simple geologic structures, *Bull. Geol. Soc. Am.* **70**, 19-52.

Sanford, A.R. (1968). Gravity survey in central Socorro County, New Mexico, *New Mexico Bureau of Mines Circular* **91**, 14 pp.

Sanford, A. R. (1996). Personal Communication, Existence of hot springs near San Acacia, New Mexico.

Sanford, A. R., R. S. Balch, J. A. Lakings, H. E. Hartse, and L. S. House (1993). A Link Between Listric Faulting and Recent Seismicity in the Central Rio Grande Rift of New Mexico, *Abstract EOS*, **74 no. 43**.

Sanford, A. R., R. S. Balch, and K. Lin (1995[1]). A seismic anomaly in the Rio Grande rift near Socorro, New mexico, abstract, *Seis. Res. Letters*, **66 no. 2**, p. 44.

Sanford, A. R. and P. Einarsson (1982). Magma chambers in rifts, *Continental and Oceanic Rifts, A.G.U. Geodynamics Series* **8**, 147-168.

Sanford, A. R., L. H. Jaksha, and D. J. Cash (1991). Seismicity of the Rio Grande Rift in New Mexico, *The Geology of North America Decade Map* **1**, 229-244.

Sanford, A. R., K. Lin, I. Tsai and L. H. Jaksha (1995[2]). Seismicity along a segment of a prominent ENE trending topographic lineament in New Mexico and West Texas, *Geophysics Open-file Report* **63**, New Mexico Tech, Socorro, 15 pp.

Sanford, A. R. and T. R. Toppozada (1974). Seismicity of proposed radioactive waste disposal site in southeastern New Mexico, *New Mex. Bur. Mines Mineral resources Circular* **143**.

Sato, T. (1978). A note on body wave radiation from expanding tension crack. Sci. Rep. Tohoku Univ. Ser. 5, Geophysics. **25** pp. 1-10.

Savage, J. C., M. Lisowski, and W. H. Prescott (1980). Geodetic measurement of horizontal deformation across the Rio Grande rift near Socorro, New Mexico, *J. Geophys. Res.* **85**, 7215-7220.

Savage, J. C., M. Lisowski, and W. H. Prescott, (1985). Strain accumulation in the

Rocky Mountain states, *J. Geophys. Res.* **90**, 10310-10320.

Shimizu, H., S. Ueki and J. Koyama (1987). A tensile-shear crack model for the mechanism of volcanic earthquakes, *Tectonophysics* **144**, 287-300.

Singer. P. J. (1989). Crustal structure in the Socorro area of the Rio Grande rift from time-term analysis, *Ph.D. Dissertation*, New Mexico Institute of Mining and Technology, Socorro, New Mexico, 206 pp.

Sinno, Y. A., P. H. Dagget, G. R. Keller, P. Morgan, and S. H. Harder (1986). Crustal structure of the southern Rio Grande rift from seismic refraction profiling, *J. Geophys. Res.* **91**, 6143-6156.

Stewart, S. W. and L. C. Pakiser (1962). Crustal structure in eastern New Mexico interpreted from the GNOME explosion, *Bull. Seismol. Soc. Am.* **52**, 1017-1030.

Summers, W. K. (1965). A preliminary report on New Mexico's geothermal energy resources, *New Mex. Bur. Mines Mineral resources Circular* **80**.

Wells, D. L. and K. J. Coppersmith (1994). New emperical relationships among magnitude, rupture length, rupture width, rupture area, and surface displacement, Bull. Seismol. Soc. Am. **84**, 974-1002.

Withers, M. M. (1993). Why do tides exist? *The Phys. Teacher* **31**, p 394.

Woodward, L. A. (1977). Rate of crustal extension across the Rio Grande rift near Albuquerque, New Mexico, *Geology* bold 5, 269-272.

Zobin, V. M. and E. I. Ivanova (1994). Earthquake swarms in the Kamchatka-Commander region, *Geophys. J. Int.* **117**, 33-47.

Appendix I - Published Abstracts

The appendix contains published meeting abstracts directly related to this dissertation. The first abstract was written for the Spring 1994 Seismological Society of America Meeting and was published in *Seis. Res. Letters*, **65 no. 1**.

FOCAL MECHANISMS FOR TWO MICROEARTHQUAKE SWARMS BENEATH THE SOCORRO MOUNTAINS, NEW MEXICO, IN MAY AND JULY 1983

Balch, R.S., and Sanford, A.R., Geophysical Research Center, New Mexico Institute of Mining and Technology, Socorro, NM 87801, balch@nmt.edu; Hartse, H.E., Los Alamos National Laboratory, MS D-443, Los Alamos, NM 87545.

In May and July of 1983, two microearthquake swarms beneath the mountains a few kilometers west of Socorro NM were recorded by a local network of 10 stations. The first sequence occurred between May 10-14 and the second between July 14-21. The majority of swarm events had epicenters within 2 km of the nearest station, WTX, which is located in a mine at the base of Socorro Peak. Hypocenters were determined using the computer program SEISMOS with a crustal model consisting of a single constant velocity layer from the surface to the top of the Socorro Magma Body (SMB) at a depth of 19.26 km. When observed, reflected phases P_zP, S_zP, and S_zS from the SMB were used in conjunction with direct P and S phases to constrain hypocenters. Hypocenters for 78 events were found with error in latitude, longitude and depth $\leq$ 0.5 km. The average hypocenter locations for the May and July sequences were not statistically different. The average hypocenter depth for the 78 events was 8.4 km with a standard deviation of 0.5 km. Focal mechanisms for 24 of the largest events were determined, 11 from the May swarm and 13 from the July swarm. Both sequences contained dominantly normal-fault earthquakes with the P axes near vertical and T axes oriented west-northwest, thus the earthquake mechanisms are consistent with the regional stress field of the Rio Grande rift. The first 10 mechanisms in the May sequence have an average T axis azimuth and dip of $316^0 \pm 5.6^0$ (1 s.d.) and $11.5^0 \pm 4.9^0$ (1 s.d.), respectively. These fault-plane solutions have a small component of strike-slip motion. The first 11 mechanisms for the July sequence describe two distinct focal mechanisms: the first has T axes which average $297^0 \pm 5.6^0$ (1 s.d.) in azimuth and $2.8^0 \pm 0.8^0$ (1 s.d.) in dip; the second has T axes which average $254^0 \pm 2.9^0$ (1 s.d.) in azimuth and $1.7^0 \pm 0.0^0$ (1 s.d.) in dip. The dominantly normal-fault mechanisms in the July swarm have a larger component of strike-slip motion than the May swarm. The last mechanism found for the May swarm and last two mechanisms determined for the July swarm indicate a different mode of crustal movement than the other events. One nodal plane for these three events strikes $N30^0E$ and dips steeply 80^0 to the WNW, the other nodal plane strikes $N50^0E$ and dips shallowly 10^0 to the ESE. Any geologic model for these swarms should explain these anomalous mechanisms as well as the more numerous dominantly normal fault-plane solutions.

This abstract was written for the Fall 1994 meeting of the American Geophysical Union and is published in *EOS*, **75 no. 44**.

Non-Double-Couple Focal Mechanisms Observed in the Central Rio Grande Rift of New Mexico

R S Balch, A R Sanford and L H Jaksha (Geophysical Research Center, New Mexico Tech, Socorro, NM 87801); H E Hartse and L S House (Los Alamos National Laboratory, MS D-443, Los Alamos, NM 87545)

Microearthquake swarms have been recorded in the central Rio Grande rift (RGR) for more than 30 years. Since 1982 a telemetered network of short-period instruments has been operated continuously. For large earthquake swarms temporary instruments have been placed in the field following the main shocks, hence we have built relatively large databases of swarm events. We routinely combine reflected phases (P_zP, S_zP and S_zS) from the Socorro Magma Body (SMB), which underlies a large portion of the central RGR, with direct P and S phases to locate local earthquakes. Using P_zP, S_zP and S_zS phases in the hypocenter determination process greatly increases the precision of hypocenter parameters, particularly depth. Therefore, we have adequate high quality data for a study of the focal mechanisms of microearthquake swarms in the RGR. One microearthquake swarm that we have investigated occurred between February 25 and March 16, 1983 near San Acacia, New Mexico. The largest event was on March 2 and had a duration magnitude of 4.2. Arrays of three to five temporary stations were deployed at any of 12 sites near the epicentral region for 10 days following the main shock. Additional seismic data was recorded at up to 10 permanent stations. A total of 204 swarm earthquakes were located and 102 of these events had latitude, longitude and depth errors ≤ 0.5 km. The swarm was located at latitude 34^o $18'$ N, longitude 106^o $52'$ W, and events were evenly distributed between 3.3 and 6.3 km in depth, with an average depth of 4.9 km. The hypocentral volume roughly defines an ellipsoid with major axis striking ENE and plunging 45^o along strike. The major and minor axis were found to be 4.0 and 1.5 km in length, respectively. The epicentral region lies near the apex of a geodetically determined surface uplift believed to be the result of inflation of the SMB, and is geologically situated along the accommodation zone between two major basins in the central RGR. We use flat-layered velocity models, so the possibility of unmodeled velocity contrasts was a concern. Examination of the Bouguer gravity anomaly map in the San Acacia area clearly shows a saddle between the two basins, and validates the distribution of swarm-specific station corrections. An unusual observation about the swarm involves the focal mechanisms. A 30 event subset of the well-constrained hypocenter data set was selected for source analysis. Twenty of the events could be constrained as double-couple normal faults mainly striking NNW. The remaining 10 events do not fit any double-couple source (see Figure). The small area of the dilatational arrivals over the focal sphere may imply that these mechanisms involve an additional component to the standard double-couple without moment source, perhaps simultaneous opening of fractures.

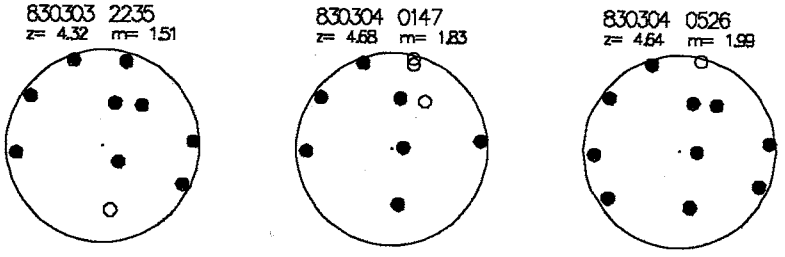

This abstract was written for the Spring 1995 meeting of the Seismological Society of America and is published in *Seis. Res. Letters*, **66 no. 2.**.

EXOTIC SOURCES OBSERVED IN THE CENTRAL RIO GRANDE RIFT

Balch, R.S., Sanford, A.R., and Jaksha, L.H., Geophysical Research Center, New Mexico Tech, Socorro, NM 87801, balch@griffy.nmt.edu; Hartse, H.E., and House, L.S., Los Alamos National Laboratory, MS D-443, Los Alamos, NM 87545.

Accurate hypocenter locations and source mechanisms are necessary for a study of the mechanisms of microearthquake swarms in continental rifts. The Socorro Magma Body (SMB) which underlies a large portion of the central Rio Grande rift (RGR) allows the use of reflected phases in all aspects of microearthquake analysis. The use of P_zP, S_zP and S_zS phases in the hypocenter determination process greatly increases the precision of hypocenter parameters, particularly depth. Amplitude ratios from reflected phases may be used to further constrain focal mechanisms by adding data from the lower focal sphere. A microearthquake swarm occurred between February 25 and March 16, 1983 near San Acacia, New Mexico. Arrays of three to five temporary stations were deployed at any of 12 sites near the epicentral region for 10 days following the M_d=4.2 main shock on March 2. Additional seismic data was recorded at up to 10 permanent stations. A total of 204 swarm earthquakes were located and 102 of these events had latitude, longitude and depth errors $\leq$ 0.5 km. The swarm was located at 34^o $18.5'$ N, 106^o $52'$ W, and events were evenly distributed between 3.3 and 6.3 km in depth. The hypocentral volume roughly defines an ellipsoid with major axis striking ENE and plunging 45^o along strike. The major and minor axis were found to be 4.0 and 1.5 km in length, respectively. The epicentral region lies near the apex of a geodetically determined surface uplift believed to be the result of inflation of the SMB, and is geologically situated along the transfer zone between two major basins in the central RGR. Examination of the Bouguer gravity anomaly map in the San Acacia area clearly shows a saddle between the two basins, and validates the distribution of swarm-specific station corrections. The most interesting observations about the swarm concerns the focal mechanisms. A 30 event subset of the well constrained hypocenter data set was selected for source analysis. Twenty of the events could be constrained as double-couple normal faults striking roughly NNW. The remaining 10 events do not fit any double-couple source. The small area of the dilatational arrivals over the focal sphere may imply that these mechanisms involve an additional component to the standard double-couple without moment source, perhaps simultaneous opening of fractures. The exotic sources occupy a small sub-volume of the swarm, and may be related to migration of over-pressured fluids.

This abstract was prepared for the 1996 Annual Meeting of the Seismological Society of America and was published in *Seism. Res. Letters*, **67 no. 2**.

A NEW MAP OF THE GEOGRAPHIC EXTENT OF THE SOCORRO MIDCRUSTAL MAGMA BODY

Balch, R.S., and Sanford, A. R. Geophysical Research Center, New Mexico Tech, Socorro, NM 87801, balch@griffy.nmt.edu; Hartse, H.E., Los Alamos National Laboratory, MS C-335, Los Alamos, NM 87545.

For 35 years clear, strong reflected phases (P_zP, S_zP and S_zS) from off the sill-like, midcrustal Socorro Magma Body (SMB) have been observed on microearthquake seismograms recorded in the central Rio Grande rift. In the 1970's the lateral extent of the magma body was estimated at 1700 km^2 by mapping reflection points for observed S_zS arrivals. We have remapped the magma body using reflection points associated with all three phases, COCORP reflection profiles [*Brown et al.*, 1980], and a 1975 refraction study [*Olsen et al.*, 1980]. Our microearthquake reflection data consists of 710 P_zP, 2186 S_zP, and 2622 S_zS reflections recorded between 1975 and 1995 by the New Mexico Tech seismic network.. The 5518 reflection point positions were calculated from 1200 hypocenters using a two-layer, one-dimensional velocity model with station corrections. These reflection points and the COCORP lines indicate that the SMB must cover an area of at least 3400 km^2. By comparing the distribution of observed reflection points with a map of the positions of all possible magma body reflections reflections, limits can be set for the northern and southern boundaries of the SMB. The ~80 km north-south extent of the magma body falls just inside the ~100 km north-south range of relatively high seismicity in the vicinity of Socorro. This area, which we have designated the Socorro Seismic Anomaly (SSA), covers about 5000 km^2 and has the same elliptical shape as the outline of the magma body based on observed reflection points. The close spatial relation between the SSA and the midcrustal magma body along their northern and southern boundaries suggests that the observed seismicity can be used to place limits on the eastern and western boundaries. Using the distribution of earthquakes within the SSA over the last 34 years, the maximum east-west extent of the SMB is ~60 km, our observed value from the map of reflection points is ~50 km. Two factors indicate that the upper surface of the magma body displays no regional dip or significant relief: Theoretical arrival times calculated by assuming a flat horizontal reflector match observed times to within assumed timing errors; and positive and negative arrival time residuals correspond to reflecting points which are evenly distributed across the magma body surface. Considering timing errors, maximum possible relief on the magma body surface is about 1.0 km.

This abstract was prepared for the Fall 1995 Meeting of the American Geophysical Union and was electronically submitted and lost on the internet. Though accepted for the meeting it was not published.

Subsurface Fault Delineation Using Focal Mechanisms from Three Earthquake Swarms in the Central Rio Grande Rift

R S Balch, A R Sanford and L H Jaksha (Geophysical Research Center, New Mexico Tech, Socorro, NM 87801); H E Hartse and L S House (Los Alamos National Laboratory, MS D-443, Los Alamos, NM 87545)

We have been investigating three spatially and temporally-related earthquake swarms that occurred along a 16 km linear trend in the central Rio Grande rift of New Mexico. The Arroyo del Coyote (ADC) swarm (16 August 1985 to 8 May 1986), which occurred near the center of the study area, had a M_d=4.0 main shock 12 hours into the sequence. The northern Puertecito de Bowling Green (PBG) swarm (17-20 September 1985) had three events with M_d=2.73, 2.52 and 2.57 on 19 September 1985. The southern Loma de las Cañas (LDC) swarm (16 April to 23 May 1986) had a main shock of M_d=3.1 on 28 April 1986. The swarms were recorded within a permanent, telemetered network of 11 stations, supplemented with three to six temporary stations. We used direct P and S phases for locating events, and, when observed, we included reflected phases P_zP, S_zP, and S_zS from the mid-crustal Socorro magma body in the location process. Including the reflected phases reduces error on focal depth estimates. A total of 840 events were recorded, and we computed hypocenters for 426 of these events. We calculated 309 locations with high-quality solutions (lat. lon. and depth errors $\leq$ 0.5 km). In cross-section, the swarms occupy a slab-like volume 2.5 km thick, dipping 10° north, and ranging in depth between 6.0 and 9.5 km.

We obtained fault mechanisms for 154 of the best located events. The central ADC swarm exhibited three styles of faulting. Thirty-one events have strike-slip solutions with an average T-axis orientation of 248 $\pm$10, 22 events have strike-slip solutions with an average T-axis orientation of 214 $\pm$ 9, and 7 events have normal fault mechanisms. For all three cases the T-axis plunge is nearly horizontal. Type 1 events were most common prior to and during the northern PBG swarm, while Type 2 events were more common from 27 August 1985 to the southern LDC swarm onset. The northern PBG swarm had focal mechanisms that are similar (T-axis orientation 237 $\pm$5) to the ADC Type 1 events, and the southern LDC swarm had mechanisms that are similar (T-axis orientation 220 $\pm$8) to the ADC Type 2 events. We believe the PBG events are aligned with the Type 1 ADC events and the LDC events are aligned with the Type 2 ADC events.

These swarms probably represent activity on a single left-lateral strike-slip fault that has a sharp bend at the location of the ADC swarm. The spatial separation of the Type 1 and 2 mechanisms narrowly constrain the location of the kink in the fault. Also, the strongest event of the three swarms (M_d=4.0) occurred near the kink, where higher stress accumulation would be expected, and the focal mechanisms closest to the main shock exhibit the greatest variability in faulting style. The proposed fault has no surface expression though its trend mimics structural grain in exposed rock 2 km to the east.

Appendix II - Moment Tensor for Tensile-Shear Cracks

For the tensile shear crack in Figure 4.1 a cartesian coordinate system was defined with x, y and z corresponding to north, east and downward vertical directions, respectively. $\vec{u}^P$, $\vec{u}^{SV}$ and $\vec{u}^{SH}$ are the respective displacement vectors for the P, SV and SH waves. With $\dot{M}$ the time derivative of the moment tensor, **M**, $\vec{u}^P$, $\vec{u}^{SV}$ and $\vec{u}^{SH}$ at a point $\vec{x}$ at time t from a point source ξ can be described as follows:

$$\vec{u}^P(\vec{x},t) = \Big(\frac{{}^t\vec{a}(\xi)\dot{M}(t-T^P)\gamma}{G^P}\Big)\vec{a}(\vec{x}) \tag{1}$$

$$\vec{u}^{SV}(\vec{x},t) = \Big(\frac{{}^t\vec{b}(\xi)\dot{\vec{M}}(t-T^S)\gamma}{G^S}\Big)\vec{b}(\vec{x}) \tag{2}$$

$$\vec{u}^{SH}(\vec{x},t) = \Big(\frac{{}^t\vec{c}(\xi)\dot{\vec{M}}(t-T^S)\gamma}{G^S}\Big)\vec{c}(\vec{x}) \tag{3}$$

$$G^P = 4\pi\rho^{1/2}(\xi)\rho^{1/2}(\vec{x})\alpha^{5/2}(\xi)\alpha^{1/2}(\vec{x})R^P(\vec{x},\xi) \tag{4}$$

$$G^P = 4\pi\rho^{1/2}(\xi)\rho^{1/2}(\vec{x})\beta^{5/2}(\xi)\beta^{1/2}(\vec{x})R^S(\vec{x},\xi) \tag{5}$$

Where ρ, α and β are the density and P and S wave velocities respectively [*Aki and Richards*, 1980]. T^P and T^S are ray travel times. R^P and R^S are the inverses of geometrical spreading factors for the P and the S waves. $\vec{a}$, $\vec{b}$ and $\vec{c}$ are unit vectors denoting direction of particle motion for the P, SV and SH waves. γ is the unit vector describing the direction in which a ray leaves the source. Each component of ($\vec{a}$, $\vec{b}$, $\vec{c}$) is expressed at the source by an azimuthal angle (ϕ) and an incident angle (i) (Figure A.1).

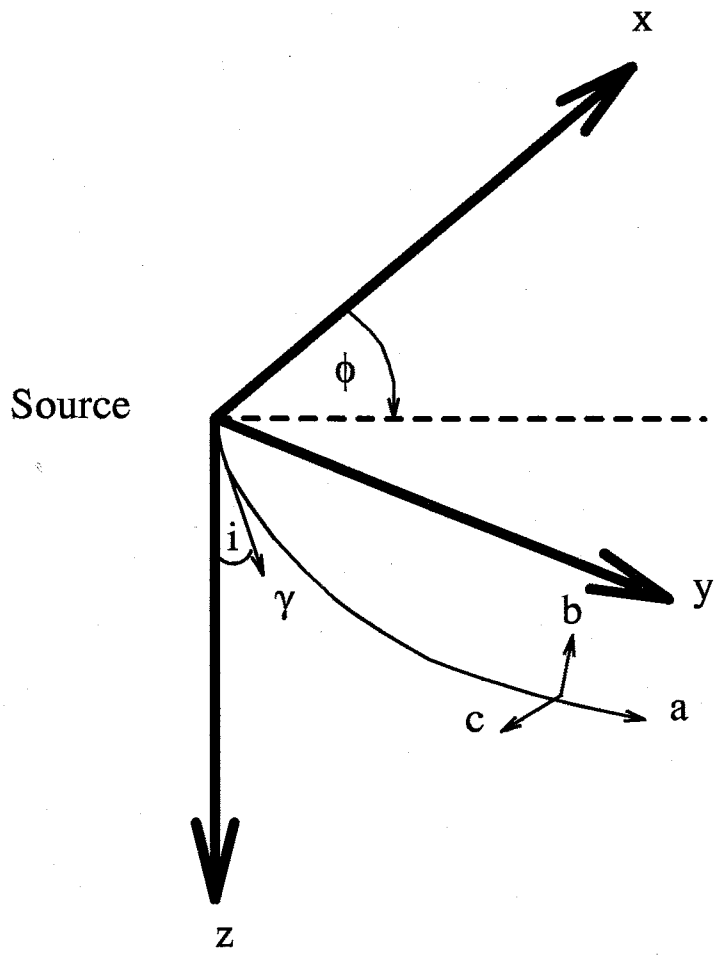

Figure A.1. Coordinate system used for tensile-shear crack moment tensor formulation [*Shimizu et al.*, 1987].

$$(a_1, a_2, a_3) = (\gamma_1, \gamma_2, \gamma_3)$$
$$= (sin(i)cos(\phi), sin(i)sin(\phi), cos(i)) \quad (6)$$

$$(b_1, b_2, b_3) = (cos(i)cos(\phi), cos(i)sin(\phi), -sin(i)) \quad (7)$$

$$(c_1, c_2, c_3) = (-sin(\phi), cos(\phi), 0) \quad (8)$$

The time derivatives of equations (1)-(3) yield theoretical expressions for the particle velocity of the P, SV and SH waves. In other words, these particle velocities can be expressed by the seismic moment acceleration $\ddot{M}$. What remains is to derive **M** for the case of a tensile-shear crack. Since seismic moments are scalar values, separate **M** values can be derived for both a shear and tensile source, then summed.

The moment tensor $\mathbf{M}_T$ for a tensile crack may be written in the following form, for a tensile crack on the y'-z' plane (Figure A.2) opening in the x' direction [*Burridge and Knoppoff*, 1964 and *Aki and Richards*, 1980]:

$$M = \begin{pmatrix} 3m_T & 0 & 0 \\ 0 & m_T & 0 \\ 0 & 0 & m_T \end{pmatrix} \quad (9)$$

Assuming $\lambda = \mu$. This tensile crack is equivalent to the superposition of three vector dipoles in the limit as the crack becomes a point source. This source supplies only compressional first motions.

If a shear were to occur during the tensile failure, it is reasonable to assume the shear tension axis (σ_1) would coincide with the greatest tension axis (x') of the tensile crack. σ_3 lies in the y'-z' plane (Figure A.3) at an angle θ from the z' axis. A moment tensor for this shear crack is as follows:

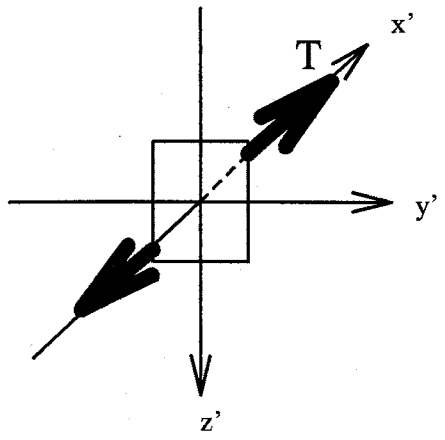

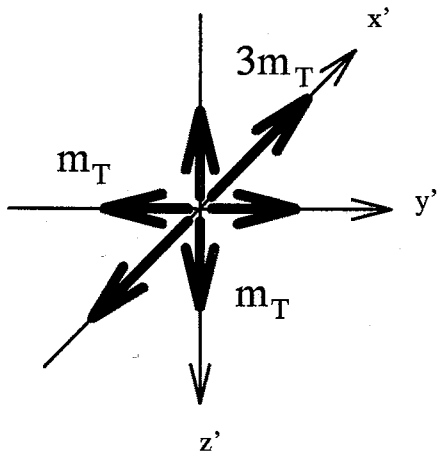

Figure A.2. A schematic tensile crack with dislocation occurring in the x′ direction. The lower picture represents the body force equivalent. $3m_T$ is the tensile seismic moment.

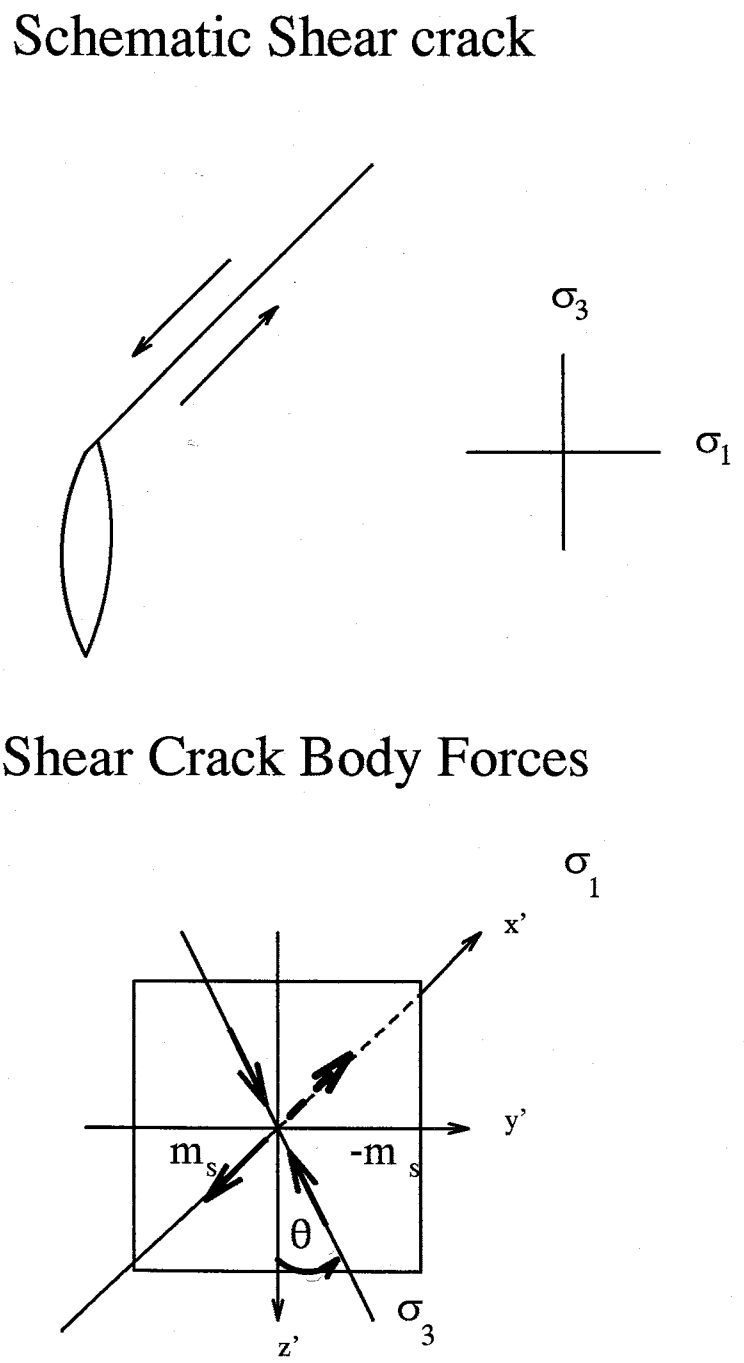

Figure A.3. Schematic shear crack associated with the tensile crack of Figure A.2. The shear crack shares the tension axis with the tensile crack. The lower figure presents the body force equivalents. m_S is the seismic moment of one of the double-couples.

$$M = \begin{pmatrix} m_s & 0 & 0 \\ 0 & -m_s sin^2\theta & -m_s sin\theta cos\theta \\ 0 & -m_s sin\theta cos\theta & -m_s cos^2\theta \end{pmatrix} \quad (10)$$

The moment tensor for the tensile-shear crack opening in the x$'$ is defined as $\mathbf{M} = \mathbf{M}_T + \mathbf{M}_S$.

For arbitrary orientation of the crack equations 6-8 are replaced with the following general forms:

$$(a_1, a_2, a_3) = (a_1' cos\delta + a_3' sin\delta, a_2', a_3' cos\delta - a_1' sin\delta) \quad (11)$$

$$(b_1, b_2, b_3) = (b_1' cos\delta + b_3' sin\delta, b_2', b_3' cos\delta - b_1' sin\delta) \quad (12)$$

$$(c_1, c_2, c_3) = (c_1' cos\delta, c_2', -c_3' sin\delta) \quad (13)$$

Here $(a_1', a_2', a_3'), (b_1', b_2', b_3'), (c_1', c_2', c_3')$ define the unit vectors obtained for changing the angles i and ϕ with i_S and ϕ_S - ϕ_N, respectively. ϕ_N, δ, ϕ_S and i_S are the azimuth of the normal to the crack (x$'$-direction) measured clockwise from north, the plunge angle of the normal measured downward from the horizontal, the azimuth of a seismic ray at the source (measured clockwise from north), and the incident angle measured downward from the vertical, respectively.

Shimizu et al. [1987] then state that the particle velocity amplitudes of the seismic body waves radiated from the tensile-shear source can be defined using the following five parameters: ϕ_N, δ, $\ddot{m}_T$, θ and $\ddot{m}_S$. The authors estimated these values by incrementing ϕ_N and δ every five degrees and using the following equations to compute $\ddot{m}_T$, $\ddot{m}_S$ and θ from observations of P and S wave particle velocity amplitudes ($\dot{u}_j^{PO}$ and $\dot{u}_j^{SVO}$) at each of j stations.

$$\dot{u}_j^{PO} = \dot{u}_j^P + \frac{\partial \dot{u}_j^P}{\partial \ddot{m}_T}\Delta\ddot{m}_T + \frac{\partial \dot{u}_j^P}{\partial \ddot{m}_S}\Delta\ddot{m}_S + \frac{\partial \dot{u}_j^P}{\partial \theta}\Delta\theta \tag{14}$$

$$|\dot{u}_j^{SVO}| = |\dot{u}_j^{SV}| + \frac{\partial |\dot{u}_j^{SV}|}{\partial \ddot{m}_T}\Delta\ddot{m}_T + \frac{\partial |\dot{u}_j^{SV}|}{\partial \ddot{m}_S}\Delta\ddot{m}_S + \frac{\partial |\dot{u}_j^{SV}|}{\partial \theta}\Delta\theta \tag{15}$$

From these two equations, they calculated increments for $\Delta\ddot{m}_T$, $\Delta\ddot{m}_S$ and $\Delta\theta$ using least squares approximations iteratively until the increments became small. This gave them the most probable values for each given set of ϕ_N and δ. The "best fit" solution was found by minimizing the sum of the squared amplitude residual as follows:

$$S.S. = \sum_{j=1}^{N} \left[(\dot{u}_j^{PO} - \dot{u}_j^P)^2 w_{Pj} + (|\dot{u}_j^{SVO}| - |\dot{u}_j^{SV}|)^2 w_S j \right] \tag{16}$$

N is the number of stations, w_P and w_S are the P and S weights.

The usefulness of this technique is in gaining information on the orientation of fractures for this type of non-double-couple (NDC) fault mechanism.

Appendix III - Digital Seismogram Correlations

In this appendix are plotted all of the events in the sub-types identified using cross-correlation for the May and July, 1983 Socorro Mountain swarms. All cross-correlations were computed using intrinsic functions of **SAC2000** (copyright 1987, Regents of the University of California). A simple script for computing the correlation coefficient between two events is listed below:

```
**********************************

1) read $1

2) cor

3) setbb cc1 &1,depmax

4) read p1

5) cor

6) setbb cc2 &1,depmax

7) eval as f to denom %cc1 * %cc2

8) eval as f to denom sqrt %denom

9) read $1 p1

10) cor

11) div %cc1 %denom

12) lh depmax (or depmin)

13) writebbf temp

**********************************
```

Line 1 reads in the master event and line 2 computes the auto and cross-correlations functions. Line 3 writes the cross-correlation functions to temporary storage (blackboard) and to the event header variable, depmax. Lines 3, 4 and 5 repeat the process of lines 1, 2 and 3 for the event to correlate the master with. Lines 7 to 11 use the intrinsic Evaluate function of **SAC2000** to compute the correlation coefficient between the two events, which is displayed to the screen using the Listhdr command in line 12 and written to a file in line 13. Depmax gives the positive coefficient, while depmin gives the negative coefficient. To correlate a master event with a number of different time-series the above macro can be incremented and looped.

Seismograms and cross-correlations for the Socorro Mountain sequence event sub-types care found in Figures A.4 to figure A.11.

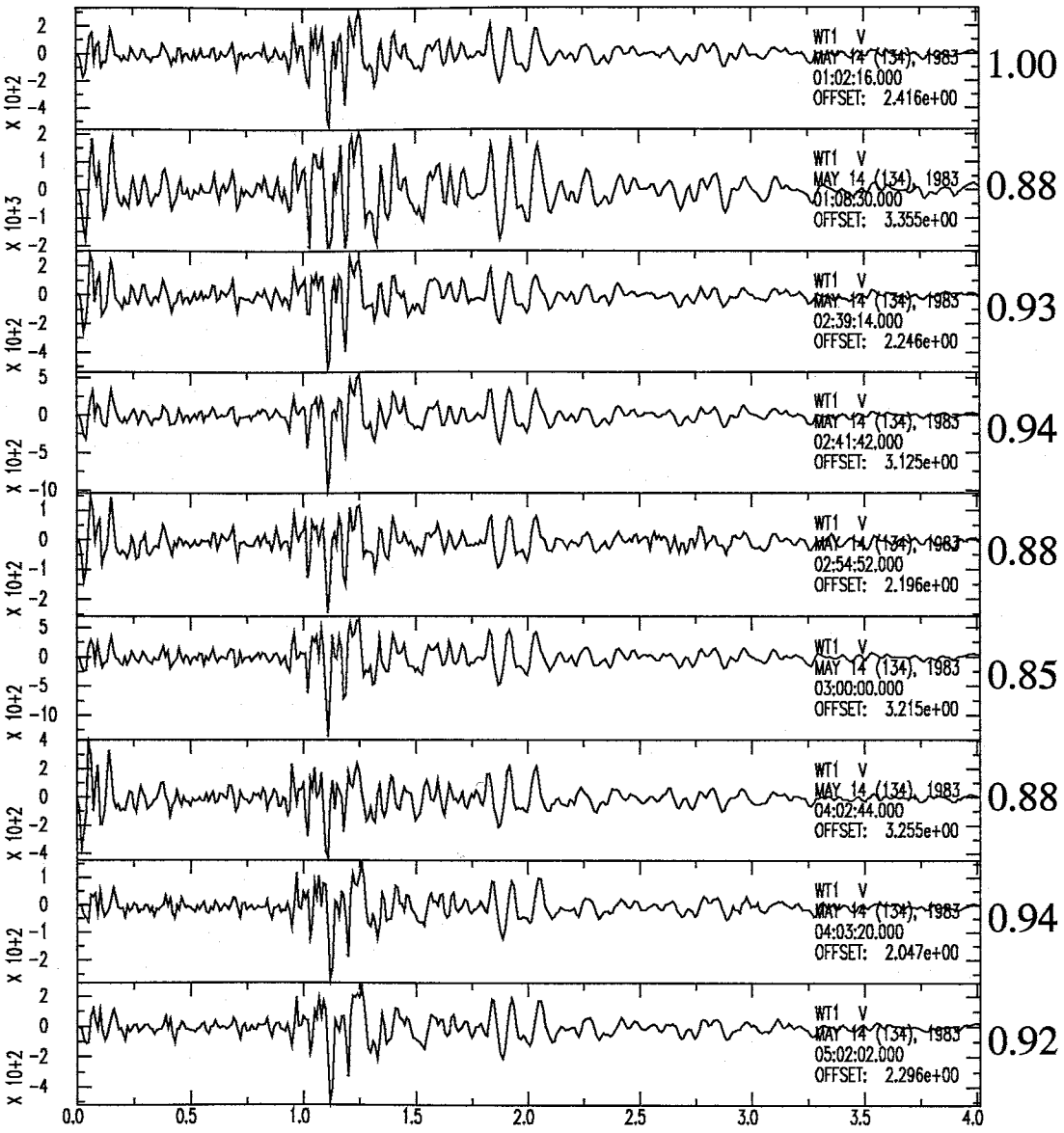

Figure A.4. Sub-type I seismograms and cross-correlation coefficients. Sub-type I events were limited to the May Socorro Mountain swarm and had an additional phase at two seconds (S-wave multiple?).

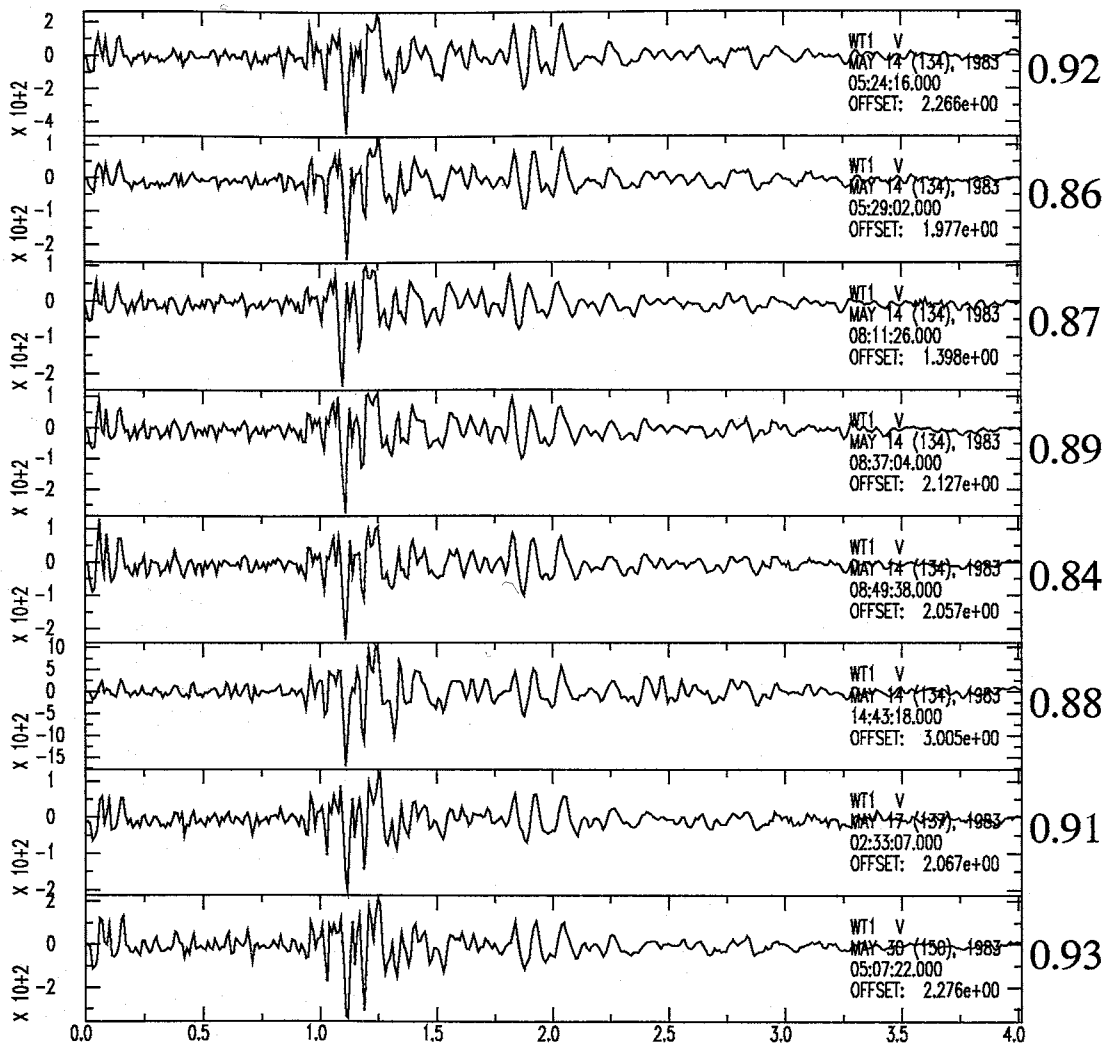

Figure A.4. Continued.

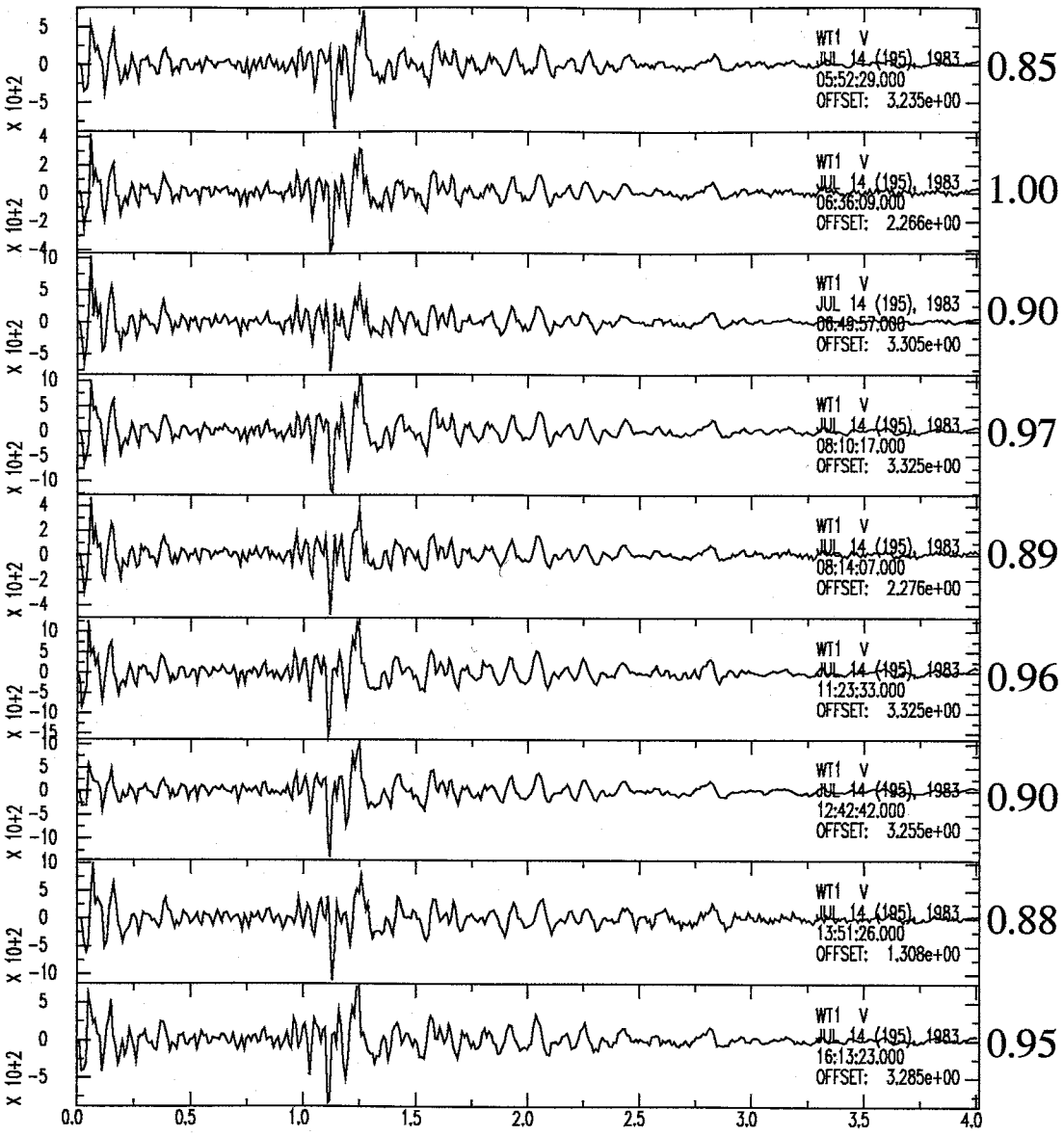

Figure A.5. Sub-type II events and cross-correlation coefficients. Sub-type II events were dominant overall.

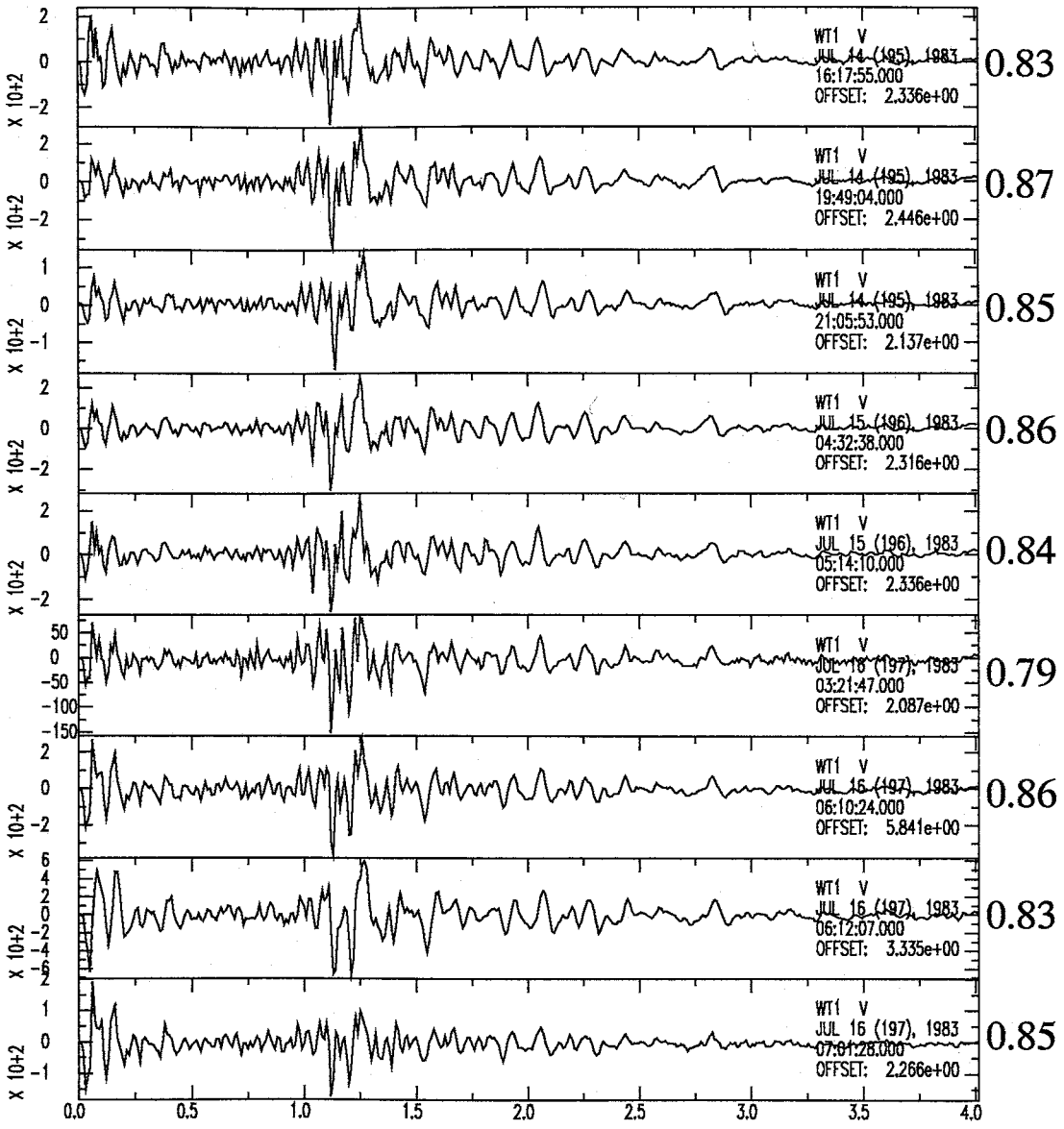

Figure A.5. Continued.

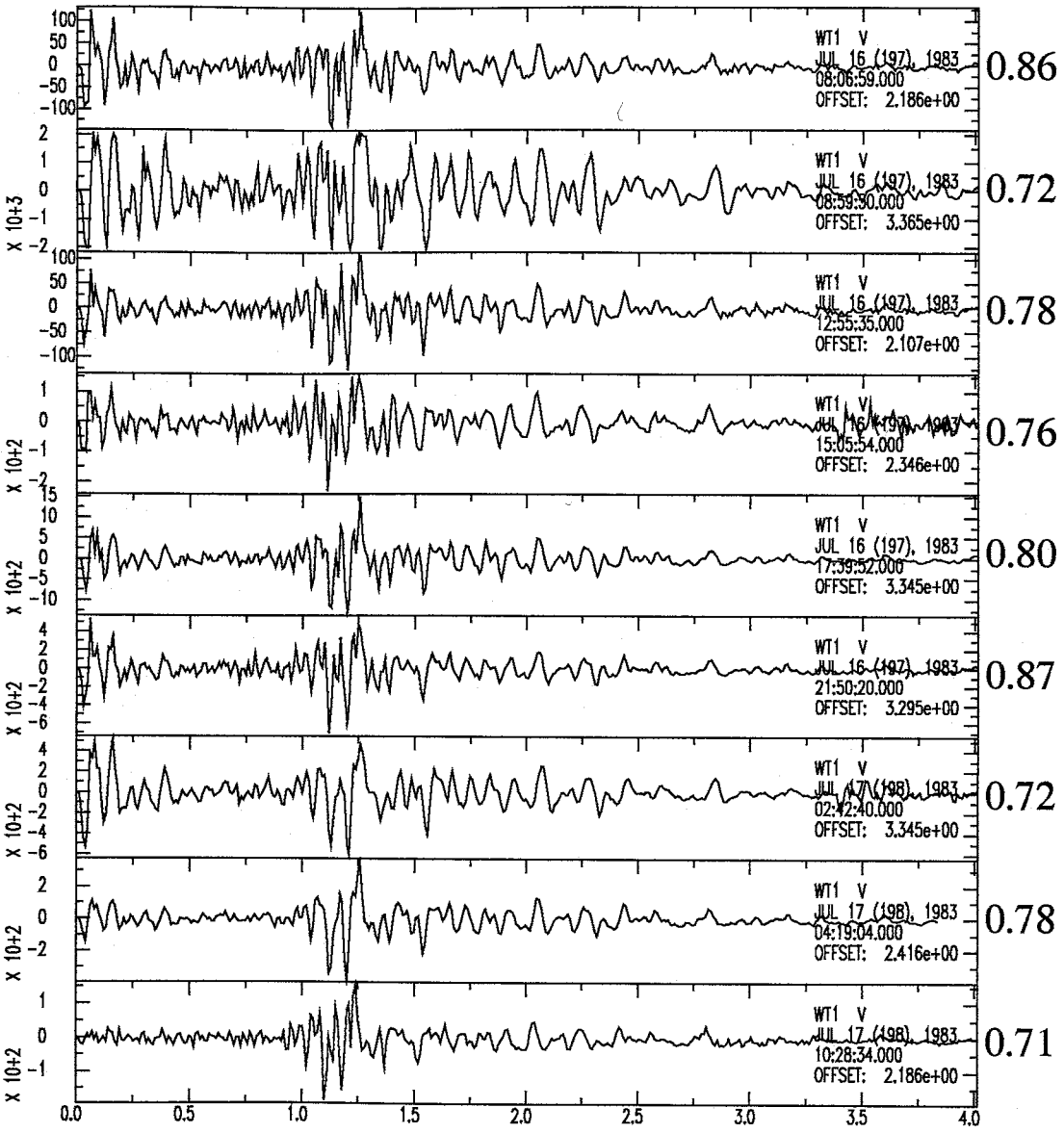

Figure A.5. Continued.

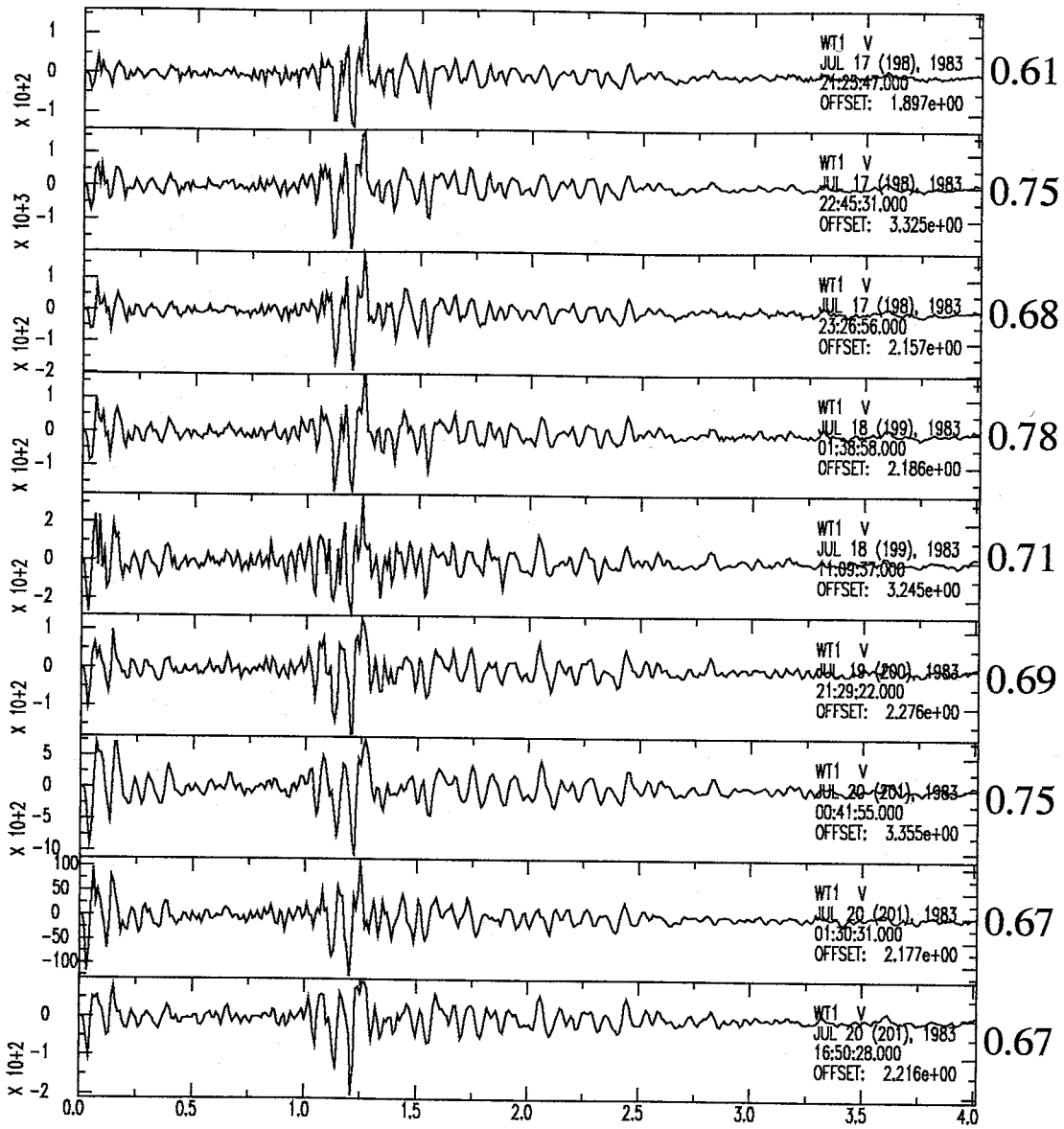

Figure A.5. Continued.

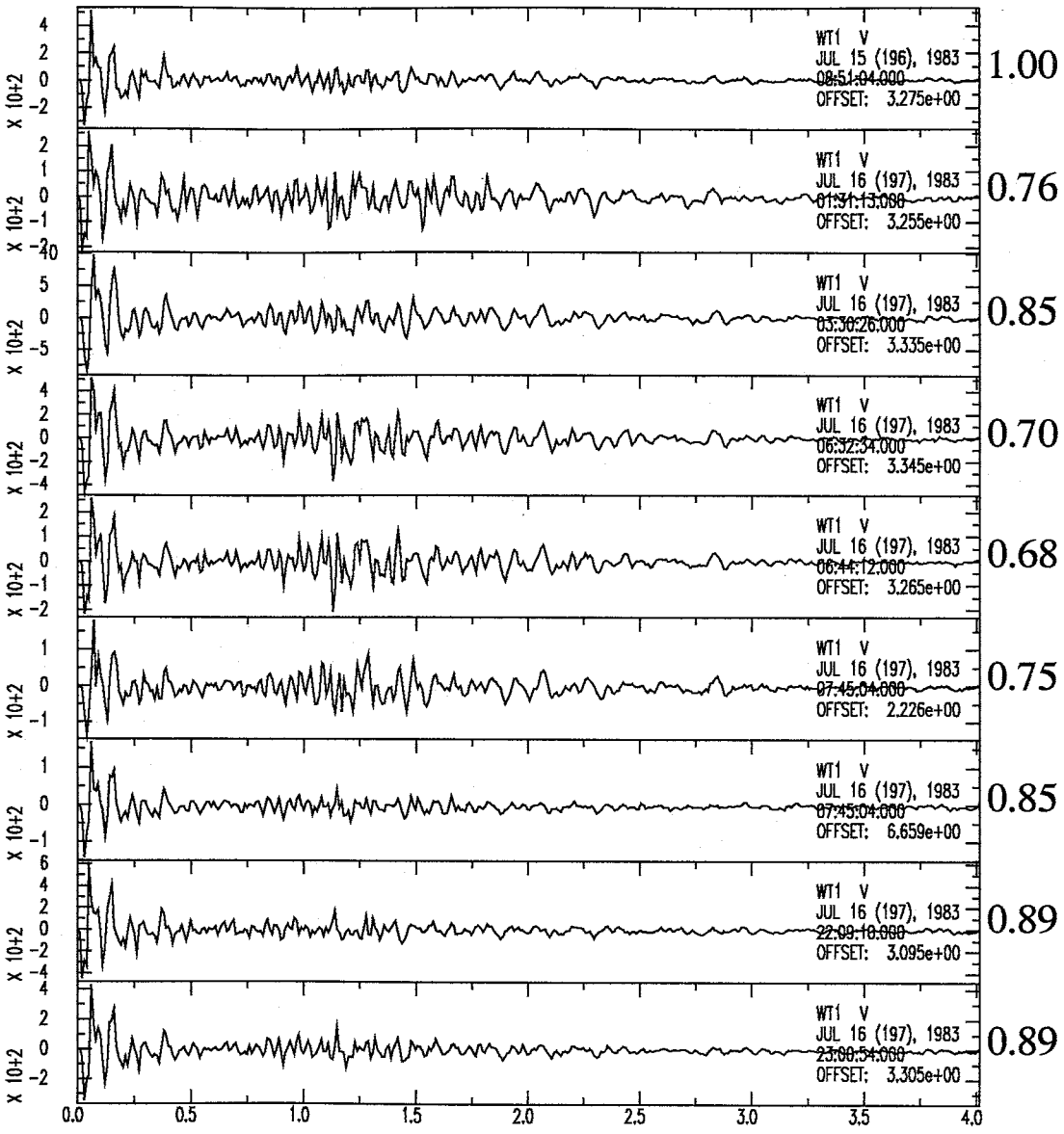

Figure A.6. Sub-type III events with cross-correlation coefficients.

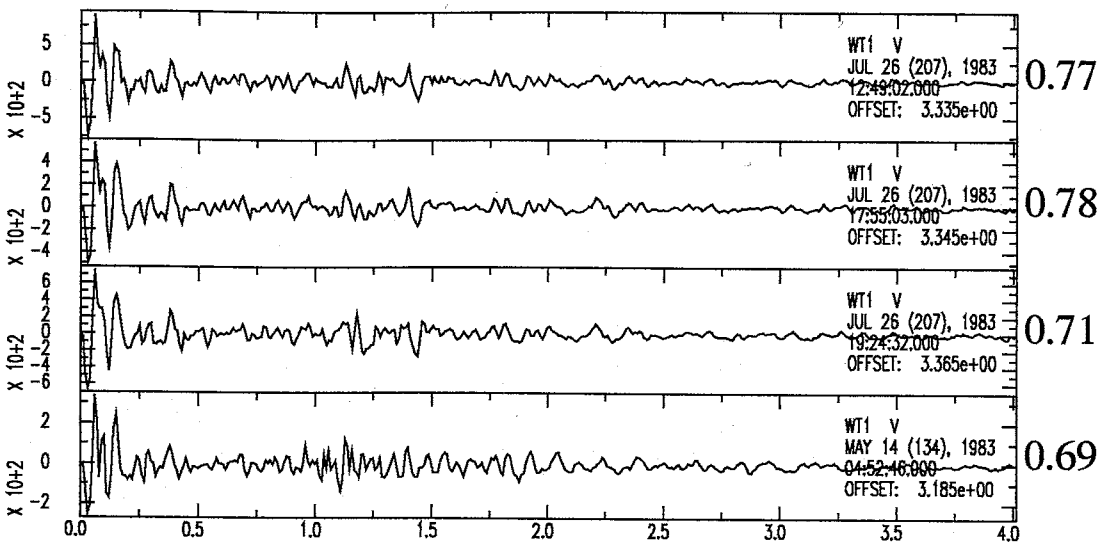

Figure A.6. Continued. Note that the last plotted event was from the May swarm.

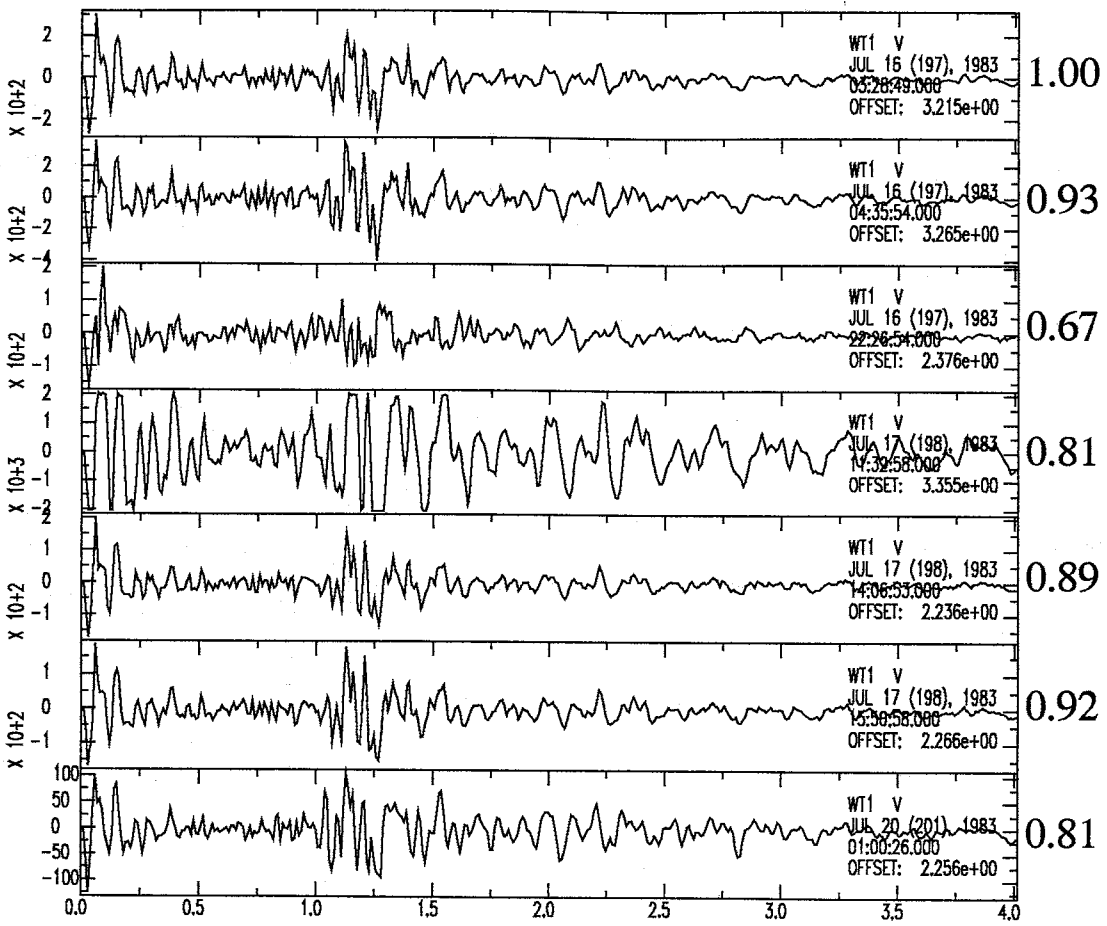

Figure A.7. Sub-type IV events with cross-corellation coefficients.

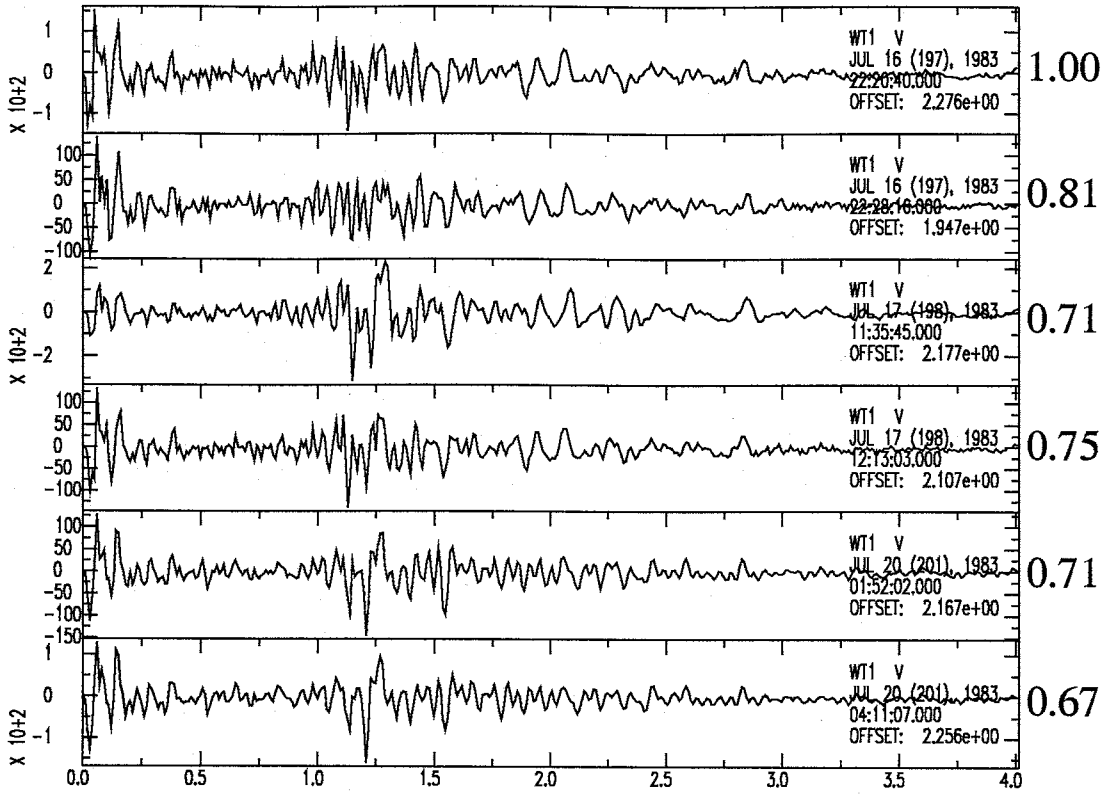

Figure A.8. Sub-type V events with cross-corellation coefficients.

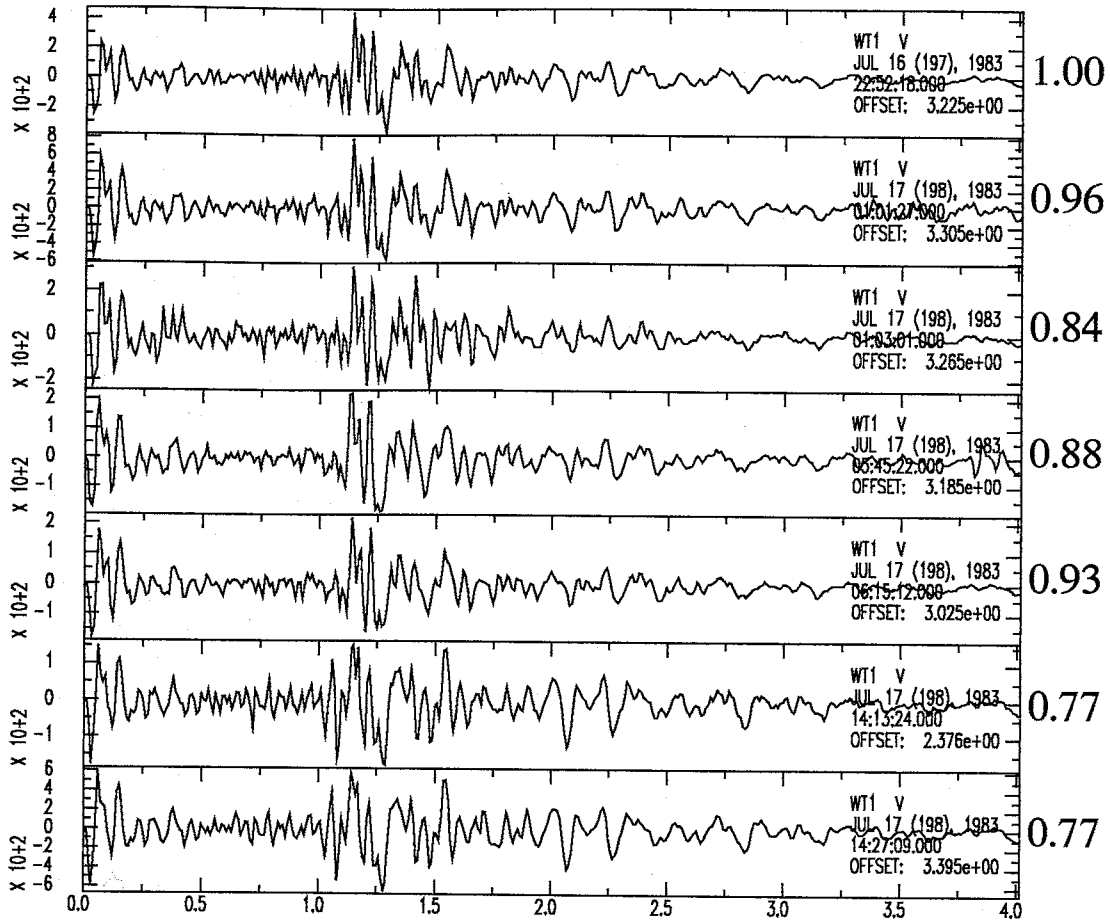

Figure A.9. Sub-type VI events with cross-corellation coefficients.

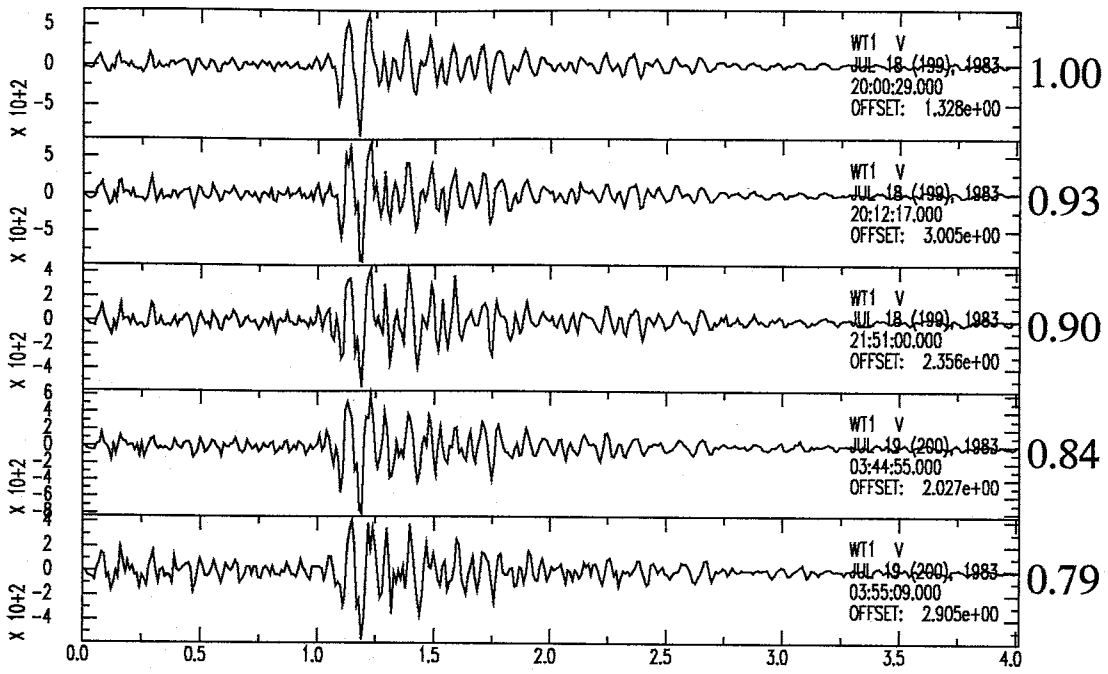

Figure A.10. Sub-type VII events with cross-corellation coefficients.

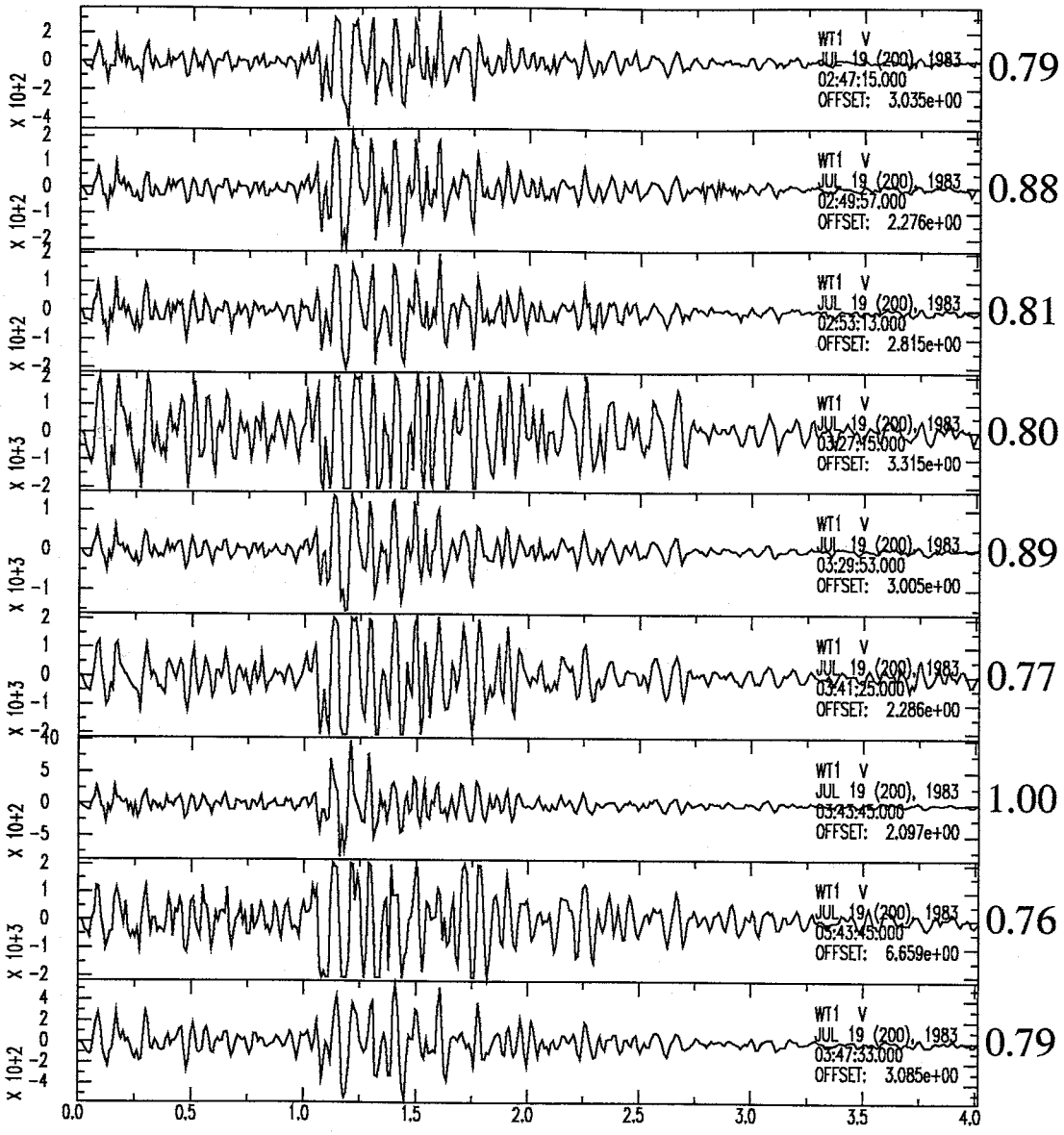

Figure A.11. Sub-type VIII events with cross-corellation coefficients.

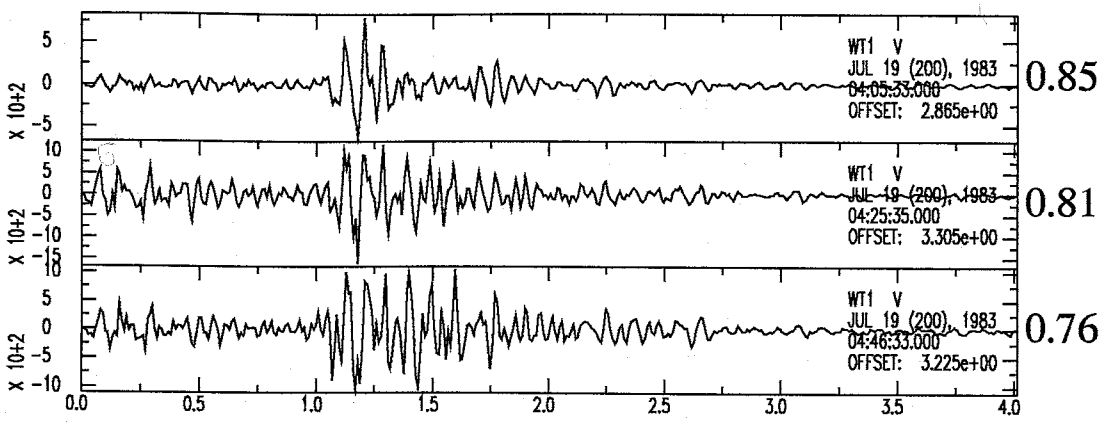

Figure A.11. Continued.

Appendix IV - Improvements Using Tailored Station Delays

For each of the studied swarms station corrections were independently computed using available good quality earthquakes and **SEISMOS**. Each data set was alternately inverted for station corrections (holding hypocenter locations constant) and locations (holding station corrections constant) until convergence. Station corrections (or delays) are commonly used to correct travel-times for near surface velocity variations from the accepted model due to site geology. For example, a station on low-velocity valley fill sediments would record arrival times later than predicted by the velocity model and a negative correction to the travel-time would be necessary to compensate. Plotted in Figures A.12 to A.16 are uncorrected and corrected epicenters for the five studied swarms. Tables A.1 and A.2 contain the computed swarm specific station corrections used in computing hypocenters for the five swarms in this study.

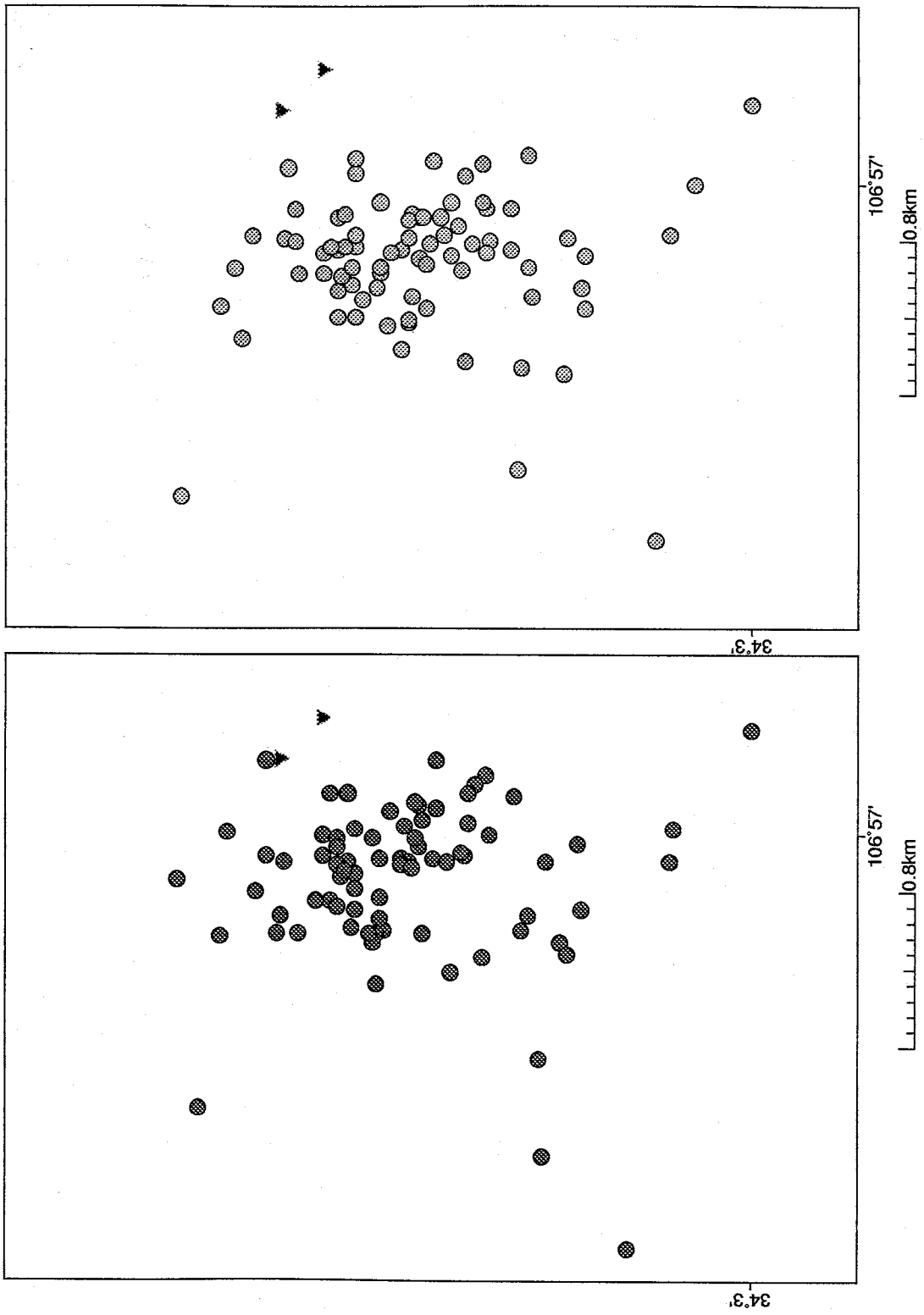

Figure A.12. Uncorrected (dark) and corrected (light) epicenters for the Socorro Mountain Sequence. Note the shift of the seismicity towards the southwest with the corrections. North is towards the left-hand margin.

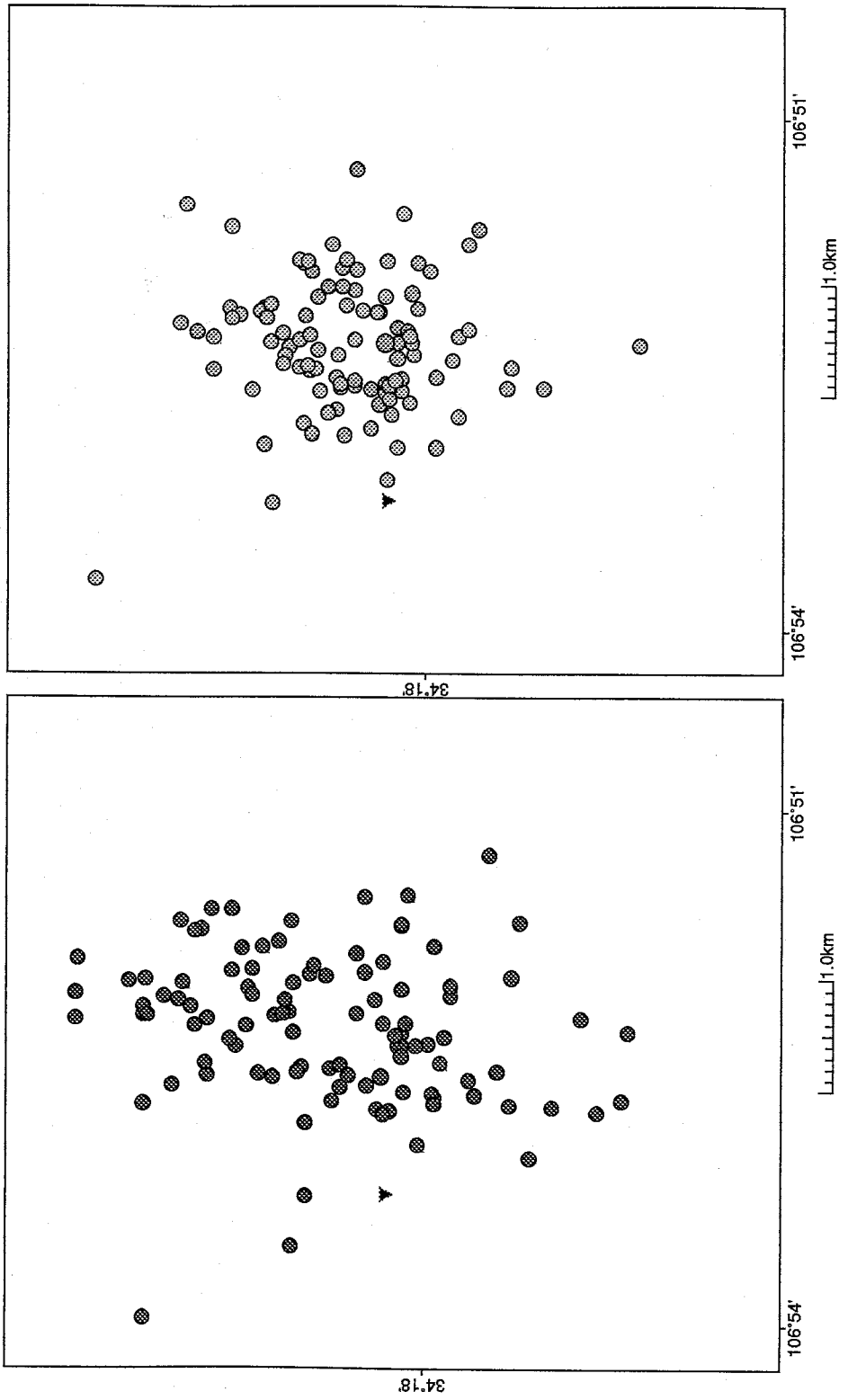

Figure A.13. Uncorrected (dark) and corrected (light) epicenters for the San Acacia swarm. Note the reduction in area occupied by the seismicity for the corrected solutions. North is towards the left-hand margin.

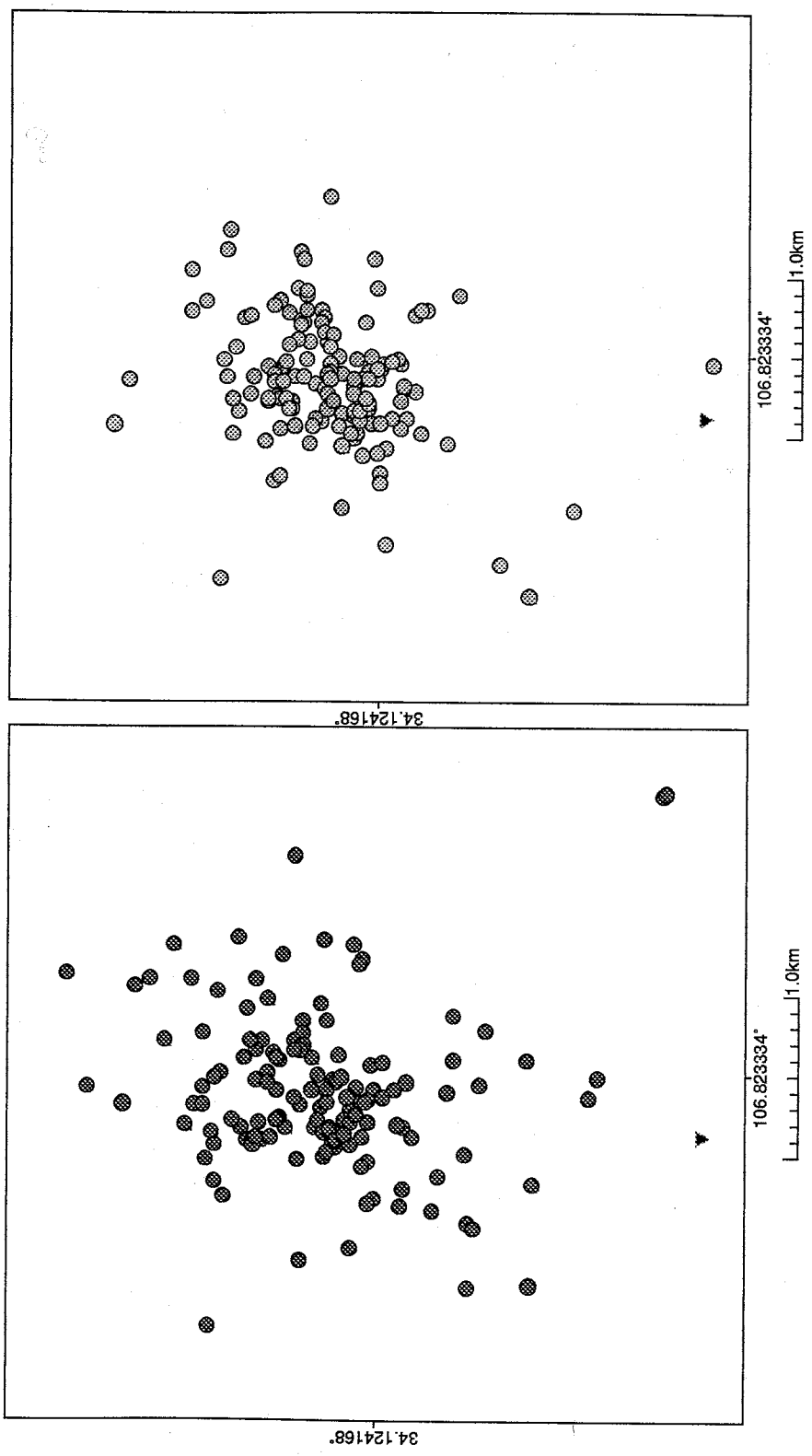

Figure A.14. Uncorrected (dark) and corrected (light) epicenters for the Arroyo del Coyote swarm. Note the reduction in area occupied by the seismicity for the corrected solutions. North is towards the left-hand margin.

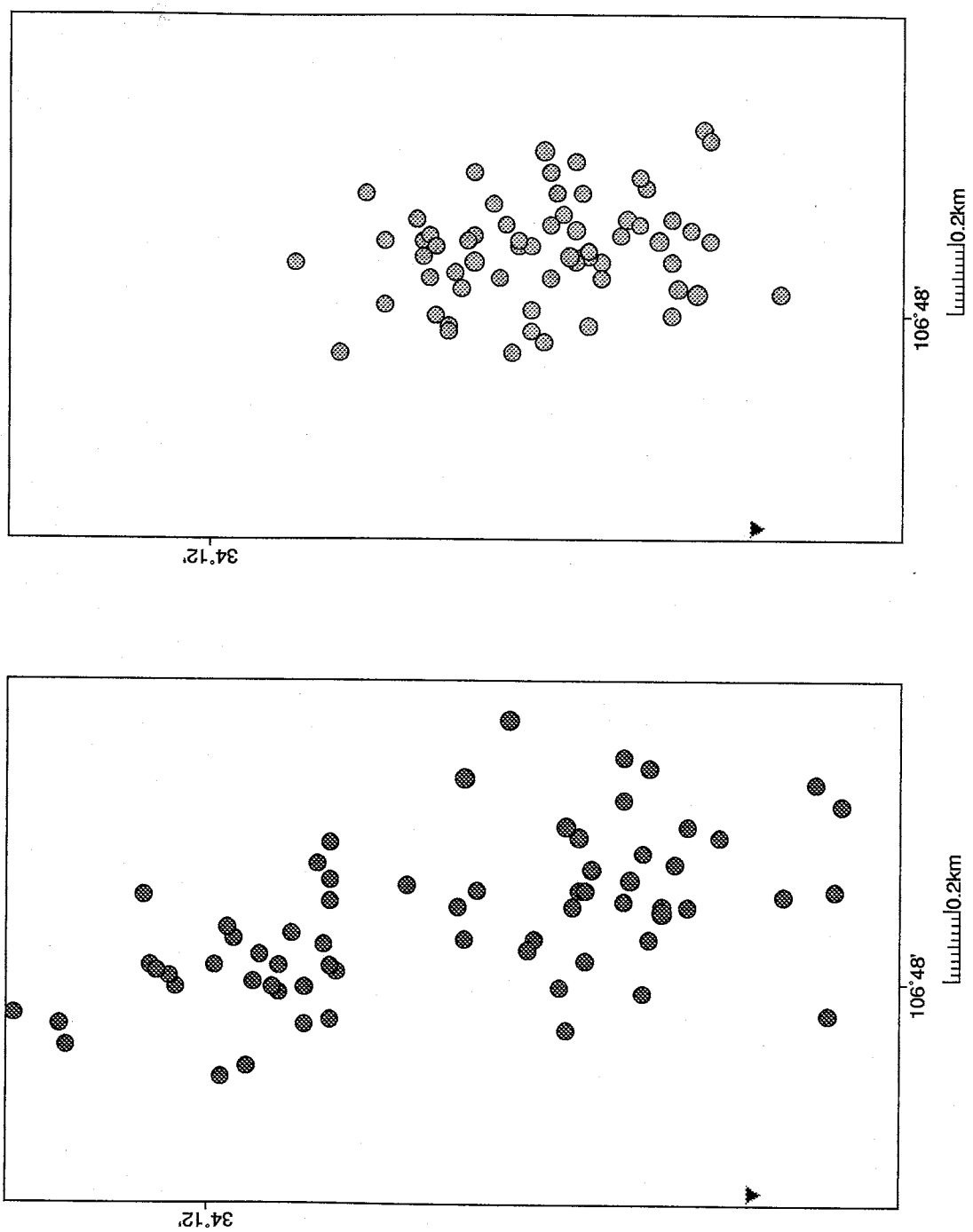

Figure A.15. Uncorrected (dark) and corrected (light) epicenters for the Puertecito de Bowling Green swarm. Note the reduction in area occupied by the seismicity for the corrected solutions. North is towards the left-hand margin.

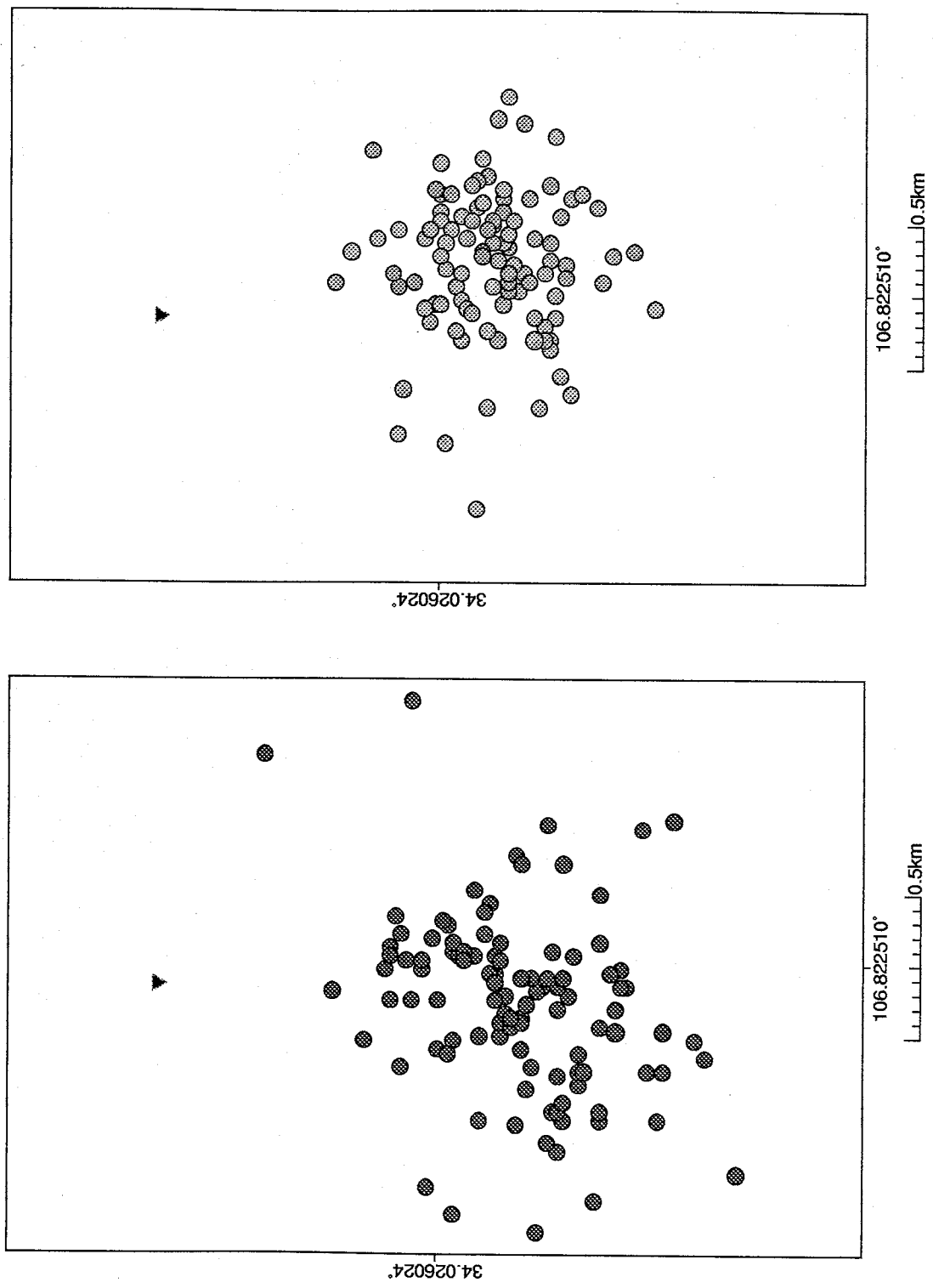

Figure A.16. Uncorrected (dark) and corrected (light) epicenters for the Loma de las Cañas swarm. Note the reduction in area occupied by the seismicity for the corrected solutions. North is towards the left-hand margin.

Station Corrections for the San Acacia Swarm				
Station	Latitude	Longitude	Elevation(m)	Correction(s)
BAR	34.1500	-106.6278	2121	0.018
BMT	34.2750	-107.2602	1987	0.041
CAR	33.9525	-106.7345	1658	0.111
LAZ	34.4020	-107.1393	1878	-0.103
LPM	34.3117	-106.6318	1737	-0.119
MLM	34.8142	-107.1450	2088	-0.031
SB	33.9752	-107.1807	3230	0.150
SMC	33.7787	-107.0193	1560	0.107
WTX	34.0722	-106.9458	1555	-0.080
ALQ	34.9417	-106.4583	1853	-0.052
ALA	34.2602	-106.9132	1417	0.103
SAH	34.2500	-106.9055	1415	0.245
RSD	34.3032	-106.8872	1481	-0.172
LJ1	34.3520	-106.8852	1489	0.122
SAD	34.2628	-106.8858	1445	-0.209
BB2	34.4070	-106.6837	1573	0.131
RS1	34.3022	-106.9218	1475	-0.072
BG2	34.2068	-106.8632	1469	-0.008
LJ2	34.3837	-106.8938	1518	0.584
RS2	34.3012	-106.9338	1494	-0.004
WM2	34.3422	-106.9212	1518	0.385

Station Corrections for the Socorro Mountain Sequence				
Station	Latitude	Longitude	Elevation(m)	Correction(s)
BAR	34.1500	-106.6278	2121	0.103
BMT	34.2750	-107.2602	1987	0.145
CAR	33.9525	-106.7345	1658	0.041
LAZ	34.4020	-107.1393	1878	0.032
LPM	34.3117	-106.6318	1737	-0.083
MLM	34.8142	-107.1450	2088	-0.023
POL	34.1783	-106.9692	1717	-0.024
SB	33.9752	-107.1807	3230	0.125
SMC	33.7787	-107.0193	1560	0.017
SNM	34.0702	-106.9418	1511	-0.034
WTX	34.0722	-106.9458	1555	-0.080

Table A.1. Computed station corrections for the San Acacia swarm (upper) and Socorro Mountain sequence (lower). The San Acacia corrections were computed relative to the 2-layer velocity model of *Hartse* [1991] and the Socorro Mountain corrections were computed relative to the single-layer velocity model of *Balch* [1992].

Station corrections for the Arroyo del Coyote Swarm				
Station	Latitude	Longitude	Elevation(m)	Correction(s)
BAR	34.1500	-106.6278	2121	0.015
CAR	33.9525	-106.7345	1658	0.020
LAZ	34.4020	-107.1393	1878	0.019
LEM	34.1655	-106.9742	1698	-0.064
LPM	34.3117	-106.6318	1737	-0.234
MAG	34.1625	-107.2320	1926	-0.043
MLM	34.8142	-107.1450	2088	-0.023
SB	33.9752	-107.1807	3230	0.117
SMC	33.7787	-107.0193	1560	0.110
WTX	34.0722	-106.9458	1555	-0.080
LQ1	34.1597	-106.8881	1408	0.079
LQ2	34.1411	-106.9069	1411	-0.146
LQ5	34.1467	-106.9047	1410	-0.125
JHLS	34.1454	-106.8444	1524	0.098
YRD	34.1617	-106.8024	1548	-0.009
SH	34.1596	-106.7803	1569	-0.083
LJGB	34.1092	-106.8719	1402	0.019
FTS	34.1858	-106.8066	1573	0.080
ODA	34.1058	-106.8274	1526	0.023

Station corrections for the Puertecito de Bowling Green swarm				
Station	Latitude	Longitude	Elevation(m)	Correction(s)
BAR	34.1500	-106.6278	2121	0.089
CAR	33.9525	-106.7345	1658	0.036
LAZ	34.4020	-107.1393	1878	0.018
LEM	34.1655	-106.9742	1698	-0.090
LPM	34.3117	-106.6318	1737	-0.237
MAG	34.1625	-107.2320	1926	-0.081
MLM	34.8142	-107.1450	2088	-0.145
SB	33.9752	-107.1807	3230	0.078
SMC	33.7787	-107.0193	1560	0.106
WTX	34.0722	-106.9458	1555	-0.080
FTS	34.1858	-106.8066	1573	0.030
ODA	34.1058	-106.8274	1526	-0.044

Table A.2. Computed station corrections for the East Rift sequence. Corrections for the Arroyo del Coyote and the Puertecito de Bowling Green swarms are in the upper and lower tables, respectively

Station corrections for the Loma de las Cañas swarm				
Station	Latitude	Longitude	Elevation(m)	Correction(s)
BAR	34.1500	-106.6278	2121	0.097
CAR	33.9525	-106.7345	1658	-0.031
LAZ	34.4020	-107.1393	1878	-0.060
LEM	34.1655	-106.9742	1698	-0.001
LPM	34.3117	-106.6318	1737	-0.172
MAG	34.1625	-107.2320	1926	-0.131
MLM	34.8142	-107.1450	2088	-0.048
SB	33.9752	-107.1807	3230	0.206
SMC	33.7787	-107.0193	1560	-0.076
WTX	34.0722	-106.9458	1555	-0.080
LC1	33.9877	-106.8448	1410	0.154
LC2	34.0307	-106.7861	1593	0.077
LC3	34.0349	-106.8233	1490	0.188

Table A.3. Computed station corrections for the East Rift sequence. Corrections for the Loma de las Cañas swarm.

Appendix V - Best Swarm Hypocenters

This appendix contains the event headers for the best swarm epicenters. The best events have latitude, longitude and depth errors less than 0.5 km at 1 std. The hypocenters for all focal mechanisms computed in this study are a subset of the best event headers. The header label at the top of each page describes the data in the column(s) directly beneath it as described below:

yymmdd - year, month and day
hhmm - hour and minute (GMT)
sec - origin time in seconds
latitude - north latitude in degrees and minutes
longitude - west longitude in degrees and minutes
depth - depth in km relative to station SNM (1.511 km above sea level)
mag - duration magnitude using M_d=2.79LOG(duration)-3.63
xerr - latitude error in km at 1 std
yerr - longitude error in km at 1 std
derr - depth error in km at 1 std
R - goodness of fit factor from *Jackson* [1972]

101 Best San Acacia Swarm Hypocenters

yymmdd	hhmm	sec	latitude	longitude	depth	mag	xerr	yerr	derr	R
830225	0912	24.55	34 17.58	-106 52.45	4.39	0.85	0.24	0.35	0.47	1.283
830226	1136	44.30	34 18.34	-106 51.88	4.72	1.13	0.24	0.29	0.48	0.758
830226	1203	32.11	34 18.31	-106 52.12	5.17	0.58	0.25	0.40	0.48	0.911
830226	1553	37.77	34 18.67	-106 52.33	4.18	1.08	0.22	0.30	0.44	1.121
830226	1608	24.64	34 18.14	-106 52.31	5.47	0.14	0.32	0.42	0.47	0.774
830226	2015	20.51	34 18.95	-106 52.14	5.30	0.49	0.27	0.40	0.50	0.728
830226	2223	23.23	34 18.21	-106 52.04	4.96	0.73	0.24	0.32	0.38	0.760
830228	0645	23.63	34 18.76	-106 52.30	4.93	0.25	0.39	0.46	0.42	0.799
830228	0721	35.46	34 18.14	-106 52.22	4.09	0.46	0.30	0.43	0.40	0.730
830303	0017	23.80	34 18.44	-106 52.70	4.71	0.64	0.35	0.44	0.50	0.829
830303	0304	59.52	34 18.70	-106 52.25	5.51	1.16	0.23	0.34	0.41	0.610
830303	0345	07.63	34 18.35	-106 52.00	5.46	0.48	0.23	0.43	0.47	0.680
830303	0408	01.94	34 18.41	-106 51.98	5.79	0.69	0.27	0.41	0.39	0.655
830303	0420	09.48	34 18.69	-106 52.38	4.99	0.47	0.25	0.47	0.49	0.710
830303	0423	21.82	34 18.71	-106 52.43	4.98	0.39	0.24	0.49	0.49	0.604
830303	0429	34.60	34 18.79	-106 52.90	4.74	1.28	0.24	0.34	0.48	1.393
830303	0501	59.80	34 19.12	-106 52.24	4.74	1.18	0.23	0.33	0.49	0.948
830303	0630	22.10	34 18.62	-106 52.29	4.27	0.03	0.25	0.48	0.49	0.927
830303	0631	59.34	34 18.57	-106 52.47	5.56	1.26	0.24	0.30	0.49	0.811
830303	0804	41.13	34 18.05	-106 51.84	5.36	0.43	0.26	0.42	0.35	0.611
830303	0805	12.09	34 18.60	-106 51.84	5.63	1.47	0.24	0.34	0.42	0.591
830303	0822	52.51	34 18.41	-106 51.87	5.67	0.45	0.26	0.41	0.40	0.575
830303	0854	43.48	34 18.62	-106 51.82	5.76	0.65	0.23	0.37	0.48	0.441
830303	0925	53.78	34 18.57	-106 52.26	5.58	0.42	0.25	0.40	0.33	0.847
830303	1021	21.71	34 18.06	-106 52.38	5.13	0.53	0.27	0.50	0.46	0.995
830303	1315	57.11	34 18.60	-106 52.78	3.40	0.57	0.23	0.42	0.41	0.720

yymmdd	hhmm	sec	latitude	longitude	depth	mag	xerr	yerr	derr	R
830303	1325	25.74	34 18.97	-106 52.10	5.16	0.14	0.28	0.45	0.40	0.546
830303	1346	10.85	34 19.04	-106 52.46	4.68	0.42	0.25	0.45	0.47	0.771
830303	1456	03.32	34 18.23	-106 52.13	5.07	0.49	0.32	0.46	0.33	0.463
830303	1607	15.01	34 18.19	-106 51.83	6.06	1.25	0.26	0.30	0.39	0.660
830303	1845	38.62	34 18.47	-106 51.73	5.82	0.17	0.27	0.38	0.39	0.599
830303	1903	36.81	34 18.05	-106 52.11	5.43	0.03	0.40	0.34	0.48	0.814
830303	1927	32.70	34 17.98	-106 51.89	5.90	-0.05	0.25	0.36	0.35	0.914
830303	2036	51.77	34 18.59	-106 52.15	5.15	0.41	0.24	0.34	0.41	0.736
830303	2054	26.18	34 17.87	-106 52.41	5.56	0.47	0.25	0.30	0.34	0.669
830303	2235	28.49	34 17.60	-106 52.57	4.32	1.51	0.23	0.24	0.37	1.046
830303	2332	35.65	34 18.07	-106 52.31	5.51	0.84	0.22	0.33	0.34	1.438
830304	0026	09.69	34 18.56	-106 51.89	5.44	0.51	0.20	0.25	0.38	0.744
830304	0110	29.62	34 18.44	-106 52.51	4.41	0.00	0.35	0.32	0.34	1.164
830304	0147	56.58	34 18.23	-106 52.67	4.68	1.84	0.24	0.23	0.40	1.105
830304	0149	24.52	34 18.20	-106 52.31	4.60	2.95	0.21	0.24	0.36	0.500
830304	0306	10.66	34 17.96	-106 52.51	4.16	0.20	0.31	0.30	0.40	0.864
830304	0326	49.56	34 18.79	-106 52.10	4.75	0.95	0.21	0.25	0.41	1.031
830304	0331	33.81	34 18.09	-106 52.24	5.36	0.43	0.23	0.25	0.38	0.889
830304	0408	44.49	34 18.39	-106 52.09	5.11	-0.26	0.29	0.27	0.47	1.104
830304	0526	10.76	34 18.14	-106 52.40	4.64	1.99	0.21	0.22	0.40	0.785
830304	0609	21.07	34 18.81	-106 52.12	5.21	0.47	0.24	0.40	0.49	0.448
830304	0612	29.80	34 19.20	-106 52.19	4.84	0.19	0.23	0.37	0.40	0.612
830304	0628	03.69	34 18.63	-106 52.45	3.34	0.06	0.36	0.38	0.40	1.090
830304	0847	18.34	34 18.91	-106 52.14	5.16	0.37	0.23	0.32	0.34	0.949
830304	0940	32.91	34 19.04	-106 52.27	5.38	0.71	0.22	0.32	0.40	0.457
830304	0946	16.77	34 19.61	-106 53.69	4.90	0.27	0.28	0.35	0.40	0.945
830304	0950	42.12	34 18.42	-106 52.57	4.38	0.65	0.21	0.36	0.39	0.742
830304	1036	20.49	34 18.43	-106 52.38	5.64	0.53	0.35	0.44	0.39	0.626
830304	1353	28.80	34 18.48	-106 52.72	5.53	1.11	0.20	0.29	0.34	0.966
830304	1521	28.04	34 18.75	-106 53.24	4.75	0.03	0.46	0.44	0.39	0.768
830304	1820	06.91	34 18.08	-106 52.27	4.57	1.31	0.21	0.26	0.39	0.779
830304	1825	14.67	34 18.19	-106 53.11	3.76	0.00	0.43	0.41	0.47	1.198
830304	1946	59.01	34 18.14	-106 52.92	3.64	-0.25	0.38	0.44	0.44	1.133
830304	2149	21.48	34 18.42	-106 52.55	3.90	1.01	0.21	0.25	0.40	0.704
830305	0016	26.51	34 18.40	-106 52.85	4.40	0.57	0.41	0.32	0.50	0.953
830305	0159	54.41	34 18.27	-106 52.81	4.39	0.36	0.37	0.49	0.45	0.661
830305	0220	01.19	34 18.27	-106 52.58	4.27	-0.12	0.26	0.35	0.29	0.959
830305	0502	50.07	34 18.56	-106 52.84	4.68	0.17	0.34	0.30	0.42	0.884
830305	1105	25.48	34 17.74	-106 51.64	5.40	1.07	0.26	0.40	0.49	0.605
830305	1220	21.31	34 18.21	-106 52.55	4.55	0.06	0.32	0.45	0.47	0.848
830305	2243	33.79	34 18.12	-106 52.59	5.67	0.40	0.21	0.43	0.47	0.844
830306	0011	21.86	34 18.39	-106 51.82	5.91	1.27	0.22	0.27	0.38	1.009
830306	0300	51.06	34 18.11	-106 51.55	5.65	0.51	0.22	0.25	0.34	0.765
830306	1002	50.37	34 18.13	-106 52.52	5.01	0.34	0.34	0.30	0.42	0.550
830306	1846	03.93	34 18.54	-106 52.46	4.65	0.40	0.31	0.44	0.44	0.705
830306	1900	17.11	34 18.85	-106 52.58	4.39	0.51	0.25	0.37	0.40	1.198
830306	2213	29.86	34 17.84	-106 52.27	4.37	1.41	0.27	0.32	0.39	0.653
830306	2326	23.18	34 18.24	-106 52.13	5.15	0.68	0.25	0.26	0.36	0.972
830307	1925	04.64	34 18.52	-106 52.59	5.16	0.60	0.25	0.37	0.48	0.795
830308	0606	45.01	34 18.21	-106 52.60	4.75	1.49	0.24	0.29	0.36	0.749
830308	0619	00.20	34 18.18	-106 52.56	4.62	2.33	0.23	0.25	0.35	1.329
830308	1352	34.99	34 18.53	-106 52.35	5.92	0.41	0.30	0.33	0.42	1.315

yymmdd	hhmm	sec	latitude		longitude		depth	mag	xerr	yerr	derr	R
830308	1604	43.20	34	18.95	-106	51.62	5.85	1.28	0.25	0.34	0.47	0.820
830309	0905	59.37	34	18.07	-106	52.02	4.17	1.93	0.25	0.25	0.49	1.194
830309	0949	43.54	34	18.08	-106	52.66	3.73	0.68	0.27	0.36	0.44	0.796
830309	1405	11.87	34	18.58	-106	52.44	4.63	0.59	0.25	0.41	0.49	0.889
830309	1910	20.04	34	17.84	-106	52.74	3.66	0.28	0.24	0.35	0.44	0.571
830309	2303	26.30	34	17.96	-106	52.92	4.39	1.36	0.23	0.28	0.38	0.764
830309	2312	18.05	34	18.35	-106	52.53	4.83	0.67	0.24	0.31	0.49	0.361
830309	2325	35.11	34	18.15	-106	52.53	4.41	1.62	0.25	0.24	0.38	0.998
830309	2359	00.68	34	18.18	-106	52.64	3.83	0.40	0.24	0.31	0.43	0.803
830310	0811	54.61	34	17.42	-106	52.57	3.69	0.82	0.23	0.27	0.48	0.706
830310	0845	04.61	34	18.35	-106	52.29	4.55	0.18	0.31	0.29	0.44	1.056
830310	0958	31.51	34	18.17	-106	52.73	4.33	0.38	0.30	0.41	0.40	0.733
830310	1019	25.96	34	18.34	-106	51.29	6.27	0.41	0.37	0.32	0.39	1.348
830310	1119	17.06	34	18.58	-106	51.83	6.03	0.27	0.27	0.33	0.37	0.464
830311	0755	58.93	34	19.17	-106	51.49	5.99	0.23	0.31	0.42	0.50	0.281
830311	0950	32.08	34	18.53	-106	52.04	5.19	0.68	0.24	0.34	0.42	0.773
830311	1017	01.52	34	17.79	-106	52.23	4.38	1.21	0.30	0.33	0.45	0.309
830311	1046	13.55	34	18.78	-106	52.16	4.99	0.87	0.25	0.31	0.45	0.568
830312	0413	53.42	34	16.96	-106	52.32	4.79	0.87	0.23	0.33	0.44	0.501
830312	1037	15.88	34	18.95	-106	52.16	5.40	0.53	0.21	0.50	0.43	0.641
830313	1955	10.02	34	18.48	-106	51.98	5.79	0.14	0.20	0.43	0.45	0.515
830313	2043	08.70	34	18.76	-106	52.08	5.92	0.69	0.23	0.47	0.48	0.719
830315	1018	09.90	34	17.79	-106	51.73	5.70	0.51	0.26	0.42	0.50	0.676

78 Best Socorro Mountain Swarm Hypocenters

yymmdd	hhmm	sec	latitude		longitude		depth	mag	xerr	yerr	derr	R
830510	0434	56.44	34	03.83	106	57.14	7.87	0.50	0.26	0.34	0.41	0.714
830510	0627	42.39	34	03.76	106	56.93	8.58	0.90	0.25	0.26	0.35	0.897
830510	0657	02.50	34	03.94	106	57.11	8.06	0.40	0.22	0.33	0.33	0.728
830510	0717	27.68	34	03.00	106	56.73	9.63	0.04	0.26	0.46	0.46	1.176
830510	0838	52.87	34	03.94	106	57.25	8.43	1.75	0.24	0.28	0.44	1.025
830510	0844	44.46	34	04.21	106	57.30	8.09	0.30	0.39	0.44	0.35	0.801
930510	1105	46.62	34	03.96	106	57.10	8.05	1.35	0.23	0.27	0.39	1.046
830510	1142	06.79	34	03.62	106	57.38	8.46	0.67	0.28	0.38	0.50	0.767
830510	1157	22.80	34	03.52	106	57.18	7.96	0.02	0.33	0.48	0.48	0.796
830510	1434	37.17	34	03.85	106	57.24	8.45	0.08	0.28	0.41	0.45	0.677
830510	1637	29.26	34	03.68	106	57.08	8.73	0.52	0.24	0.25	0.37	0.829
830511	0557	16.56	34	04.03	106	57.48	7.96	0.06	0.26	0.48	0.47	0.874
830511	0600	21.08	34	03.79	106	57.20	9.14	0.49	0.25	0.36	0.41	0.685
830511	0611	18.40	34	03.91	106	57.20	8.72	0.50	0.22	0.35	0.50	1.193
830511	0616	17.48	34	03.96	106	57.38	8.15	0.90	0.24	0.29	0.35	0.943
830511	1359	29.73	34	03.99	106	57.56	9.03	0.91	0.31	0.28	0.36	1.073
830511	1430	29.86	34	03.48	106	57.35	8.80	1.19	0.26	0.28	0.37	1.118
830511	1433	07.38	34	04.12	106	57.45	9.02	0.92	0.26	0.34	0.46	1.061
830511	1452	22.92	34	03.66	106	57.96	7.93	0.89	0.34	0.32	0.40	1.168
830511	1526	45.07	34	03.85	106	57.06	9.03	1.63	0.24	0.24	0.45	1.338
830511	1549	05.40	34	03.27	106	58.20	7.53	0.22	0.44	0.48	0.37	0.899
830511	1728	52.95	34	04.05	106	57.30	7.86	0.24	0.33	0.41	0.44	0.741
830511	1743	07.55	34	03.92	106	57.42	7.73	0.23	0.26	0.44	0.40	0.578
830513	0813	34.56	34	04.10	106	57.39	8.33	-0.39	0.28	0.45	0.42	0.720
830513	1613	48.88	34	03.74	106	57.19	7.24	-0.01	0.37	0.50	0.50	0.498
830514	0108	28.23	34	03.65	106	57.62	8.68	0.60	0.22	0.27	0.31	1.413

yymmdd	hhmm	sec	latitude	longitude	depth	mag	xerr	yerr	derr	R
830514	1443	19.75	34 03.97	106 57.47	8.81	-0.02	0.34	0.35	0.32	0.901
830714	0649	56.07	34 03.53	106 57.64	9.09	0.09	0.42	0.50	0.40	1.191
830714	0810	15.01	34 04.28	106 57.30	8.44	0.14	0.34	0.47	0.38	1.223
830714	1109	42.37	34 03.97	106 57.46	8.25	0.88	0.34	0.40	0.31	0.795
830714	1139	46.49	34 04.12	106 57.21	9.04	0.33	0.29	0.44	0.33	0.970
830714	1242	41.04	34 03.68	106 57.22	8.43	0.06	0.35	0.44	0.32	0.984
830714	1351	25.70	34 03.16	106 57.00	8.37	-0.22	0.36	0.50	0.37	1.301
830714	1613	20.68	34 04.06	106 57.35	8.10	-0.06	0.38	0.49	0.42	0.766
830714	1617	53.48	34 03.82	106 57.29	8.21	0.09	0.36	0.50	0.37	0.894
830714	1949	02.95	34 04.46	106 57.28	8.82	0.49	0.39	0.47	0.50	0.890
830715	0514	09.01	34 04.12	106 56.96	8.08	0.00	0.41	0.49	0.48	0.757
830715	0851	03.59	34 03.75	106 57.08	7.62	0.31	0.25	0.39	0.42	1.232
830716	0310	37.44	34 04.50	106 57.41	8.00	0.85	0.30	0.38	0.00	1.253
830716	0330	25.03	34 04.45	106 57.52	8.92	0.60	0.24	0.38	0.30	0.891
830716	0435	52.14	34 04.32	106 57.18	8.43	0.38	0.33	0.46	0.35	0.821
830716	0436	36.60	34 04.21	106 57.23	8.80	0.27	0.41	0.48	0.44	0.586
830716	0612	06.28	34 03.81	106 57.60	8.30	0.57	0.27	0.35	0.30	1.158
830716	0632	33.62	34 03.63	106 56.90	7.78	0.51	0.33	0.44	0.39	0.654
830716	0859	48.65	34 04.18	106 57.22	8.81	1.24	0.23	0.27	0.40	1.187
830716	1739	49.91	34 03.75	106 57.23	9.47	0.32	0.25	0.37	0.37	0.857
830716	2150	18.37	34 03.76	106 57.06	8.13	0.17	0.30	0.41	0.34	0.983
830716	2206	12.29	34 04.05	106 57.06	7.13	2.13	0.22	0.24	0.43	1.305
830716	2200	51.19	34 03.90	106 56.92	8.10	1.00	0.22	0.26	0.28	1.141
830717	0101	26.85	34 03.81	106 56.97	8.65	0.39	0.23	0.37	0.32	0.442
830717	0242	38.13	34 04.29	106 57.08	7.98	0.56	0.27	0.38	0.36	0.718
830717	1132	56.48	34 04.31	106 56.94	8.00	1.67	0.22	0.24	0.45	0.693
830717	1427	08.39	34 04.13	106 57.34	8.46	0.43	0.27	0.41	0.40	0.588
830717	2245	29.37	34 03.87	106 57.17	8.98	0.98	0.26	0.38	0.35	1.226
830718	1109	35.86	34 04.12	106 56.91	7.74	0.49	0.34	0.47	0.41	0.439
830718	1756	25.80	34 04.05	106 57.28	7.91	0.66	0.23	0.30	0.31	1.101
830719	0257	04.59	34 03.63	106 57.28	8.77	0.31	0.36	0.46	0.33	0.994
830719	0327	11.16	34 04.17	106 57.36	7.69	0.26	0.31	0.33	0.30	0.785
830719	0340	07.25	34 03.88	106 57.11	8.43	1.92	0.22	0.24	0.35	0.871
830719	0343	45.11	34 03.99	106 57.22	7.53	0.37	0.36	0.42	0.48	0.790
830719	0440	28.61	34 03.97	106 57.18	8.83	0.68	0.26	0.30	0.35	0.602
830719	0442	47.10	34 04.16	106 57.31	8.54	1.20	0.22	0.25	0.34	0.692
830719	0503	16.17	34 04.18	106 57.45	8.09	0.36	0.25	0.43	0.29	0.675
830719	0912	54.42	34 04.02	106 57.23	8.31	0.92	0.26	0.37	0.44	0.986
830719	1230	30.27	34 04.61	106 58.05	8.24	0.42	0.28	0.37	0.37	1.445
830719	1332	15.13	34 04.12	106 57.17	8.36	0.44	0.22	0.33	0.33	0.784
830719	1622	47.29	34 03.47	106 57.24	8.44	0.02	0.34	0.48	0.40	0.888
830719	2022	59.59	34 03.23	106 57.17	8.82	0.32	0.34	0.49	0.42	1.001
830720	0041	54.40	34 03.92	106 57.27	8.43	1.01	0.22	0.24	0.27	0.993
830720	0130	29.16	34 04.29	106 57.19	8.26	0.00	0.33	0.46	0.41	0.628
830720	0146	06.22	34 03.47	106 57.42	8.82	0.34	0.35	0.43	0.38	0.589
830720	0152	01.37	34 04.41	106 57.17	7.55	0.00	0.28	0.43	0.41	0.784
830720	0411	06.23	34 04.18	106 57.11	8.04	0.22	0.32	0.48	0.37	0.655
830720	1650	26.72	34 04.15	106 57.21	8.29	0.40	0.30	0.43	0.41	0.858
830720	1657	16.03	34 04.15	106 57.10	8.93	1.00	0.27	0.28	0.35	0.772
830720	1658	08.66	34 04.13	106 57.28	8.42	0.39	0.38	0.47	0.49	0.619
830720	1722	45.77	34 03.93	106 57.11	9.04	0.41	0.27	0.34	0.29	0.708
830720	1752	40.05	34 04.19	106 57.21	9.19	0.24	0.38	0.46	0.39	0.801

138 Best Arroyo del Coyote Swarm Hypocenters

yymmdd	hhmm	sec	latitude	longitude	depth	mag	xerr	yerr	derr	R
850816	0243	06.38	34 07.49	106 49.46	7.94	0.65	0.34	0.36	0.37	0.625
850816	1500	57.85	34 07.33	106 49.23	6.65	1.23	0.43	0.44	0.48	0.973
850816	1502	39.87	34 07.69	106 49.34	7.00	0.86	0.28	0.32	0.41	0.951
850816	1503	20.80	34 07.33	106 49.54	6.87	1.37	0.46	0.38	0.49	0.798
850816	1506	56.75	34 07.46	106 49.12	6.73	0.91	0.28	0.33	0.37	1.031
850816	1507	48.62	34 07.29	106 49.21	7.52	0.89	0.31	0.34	0.49	0.616
850816	1510	54.82	34 07.73	106 49.12	8.14	0.55	0.31	0.33	0.50	0.731
850816	1525	20.83	34 07.36	106 49.65	8.25	0.69	0.28	0.28	0.45	0.664
850816	1528	31.59	34 07.31	106 49.71	7.74	0.80	0.34	0.33	0.33	0.833
850816	1533	47.71	34 07.74	106 49.48	7.81	0.57	0.25	0.31	0.47	0.853
850816	1535	31.53	34 07.63	106 49.34	7.38	1.12	0.25	0.29	0.43	0.753
850816	1541	48.51	34 07.38	106 49.69	8.29	0.53	0.29	0.30	0.45	0.855
850816	1542	23.08	34 07.65	106 49.21	7.43	1.22	0.22	0.24	0.43	0.730
850816	1544	23.10	34 08.09	106 49.04	7.53	0.38	0.25	0.32	0.50	0.795
850816	1547	26.54	34 07.83	106 49.58	7.78	1.21	0.37	0.28	0.46	0.855
850816	1553	41.25	34 07.72	106 48.97	8.49	0.95	0.21	0.25	0.38	1.049
850816	1600	25.69	34 07.79	106 49.17	8.11	1.13	0.24	0.23	0.48	1.011
850816	1607	51.73	34 07.41	106 49.65	9.28	0.32	0.38	0.47	0.50	0.612
850816	1748	13.17	34 07.54	106 49.73	8.18	0.66	0.23	0.31	0.38	0.795
850816	2013	27.53	34 07.58	106 49.63	7.85	0.73	0.23	0.31	0.31	0.687
850816	2035	41.67	34 08.09	106 49.21	8.18	0.56	0.28	0.35	0.35	0.749
850816	2046	47.42	34 07.71	106 49.00	8.18	0.27	0.45	0.37	0.00	0.845
850816	2049	14.25	34 07.51	106 49.49	8.13	0.37	0.25	0.32	0.35	0.823
850816	2140	45.31	34 07.48	106 49.67	7.82	0.75	0.19	0.26	0.32	0.917
850816	2230	50.50	34 07.59	106 49.40	7.84	0.36	0.25	0.33	0.32	0.713
850816	2243	43.18	34 07.59	106 49.47	6.98	0.22	0.26	0.33	0.43	0.464
850817	0000	25.76	34 07.72	106 49.25	7.67	0.50	0.25	0.27	0.23	0.944
850817	0004	19.24	34 07.93	106 49.62	7.30	0.36	0.26	0.32	0.31	0.852
850817	0021	11.46	34 07.81	106 49.90	7.20	0.66	0.34	0.44	0.35	0.635
850817	0055	56.53	34 07.64	106 49.24	8.53	0.56	0.27	0.41	0.47	1.061
850817	0109	59.87	34 07.98	106 49.41	10.1	0.24	0.34	0.36	0.50	0.866
850817	0123	58.88	34 07.96	106 48.88	8.94	0.26	0.36	0.36	0.47	1.052
850817	0124	22.18	34 07.43	106 49.77	8.02	0.93	0.23	0.22	0.25	0.911
850817	0144	37.64	34 07.71	106 49.26	8.25	-0.01	0.41	0.44	0.40	0.881
850817	0246	16.55	34 07.37	106 49.53	7.82	0.17	0.27	0.27	0.27	0.840
850817	0250	16.36	34 07.65	106 49.66	7.50	0.78	0.20	0.24	0.20	0.821
850817	0448	27.75	34 07.76	106 49.22	8.96	0.13	0.34	0.37	0.33	0.794
850817	0514	46.57	34 07.45	106 49.45	9.02	1.98	0.24	0.22	0.42	1.145
850817	0542	58.15	34 07.81	106 49.19	8.15	0.41	0.34	0.46	0.40	0.404
850817	0624	12.82	34 07.70	106 49.15	7.82	0.29	0.40	0.46	0.35	0.826
850817	0645	36.08	34 07.54	106 49.64	7.82	0.35	0.23	0.26	0.26	0.846
850817	0650	56.60	34 07.73	106 49.33	7.75	0.25	0.30	0.35	0.34	0.951
850817	0725	23.24	34 07.78	106 49.44	7.86	0.26	0.32	0.39	0.41	1.051
850817	0725	34.89	34 07.76	106 49.35	7.78	-0.06	0.35	0.39	0.46	0.582
850817	0731	25.20	34 07.53	106 49.71	7.42	0.42	0.25	0.29	0.29	0.797
850817	0737	06.84	34 07.18	106 49.15	7.32	0.29	0.35	0.49	0.32	1.131
850817	1119	50.53	34 07.67	106 49.51	8.26	0.32	0.30	0.33	0.27	0.928
850817	1247	30.49	34 07.80	106 49.56	8.12	0.75	0.27	0.29	0.29	0.998
850817	1331	59.17	34 07.70	106 49.21	8.26	0.03	0.39	0.49	0.42	0.895
850817	1359	40.94	34 07.97	106 49.48	8.34	0.17	0.38	0.34	0.32	0.806
850817	1515	25.66	34 07.58	106 49.47	7.57	0.34	0.24	0.30	0.25	0.893

yymmdd	hhmm	sec	latitude		longitude		depth	mag	xerr	yerr	derr	R
850817	1624	36.79	34	07.65	106	49.26	7.18	0.08	0.31	0.41	0.45	0.911
850817	1657	22.36	34	07.64	106	49.30	6.79	0.23	0.38	0.38	0.50	0.785
850817	1753	36.07	34	07.95	106	49.71	7.85	0.17	0.28	0.32	0.31	1.021
850817	1804	24.71	34	07.45	106	49.87	8.18	0.73	0.22	0.27	0.30	0.753
850817	1806	20.86	34	07.54	106	49.52	7.30	0.56	0.21	0.25	0.32	0.704
850817	1949	24.64	34	07.79	106	49.57	7.65	0.76	0.20	0.23	0.27	1.000
850817	2122	42.19	34	07.75	106	49.58	7.42	0.27	0.23	0.28	0.31	0.759
850817	2134	10.94	34	07.83	106	49.44	7.11	1.62	0.21	0.20	0.33	0.986
850817	2137	36.39	34	07.81	106	49.43	7.57	0.21	0.25	0.31	0.31	0.849
850817	2144	16.77	34	07.53	106	49.41	8.37	0.64	0.22	0.29	0.32	0.764
850817	2317	03.95	34	07.97	106	48.96	8.66	0.50	0.26	0.33	0.28	0.919
850817	2357	35.03	34	07.94	106	49.36	7.93	0.12	0.42	0.39	0.38	0.846
850817	2358	59.84	34	07.95	106	49.57	7.68	0.37	0.34	0.30	0.28	0.802
850818	0028	02.03	34	07.88	106	49.48	7.69	0.82	0.19	0.21	0.25	0.756
850818	0124	15.06	34	07.91	106	49.24	7.71	0.22	0.45	0.39	0.40	0.588
850818	0302	57.16	34	07.89	106	49.23	8.57	0.19	0.43	0.46	0.44	0.475
850818	0354	01.67	34	07.79	106	49.69	7.60	0.35	0.27	0.31	0.24	1.061
850818	0357	11.52	34	07.83	106	49.57	7.32	0.82	0.21	0.26	0.25	0.797
850818	0531	03.60	34	07.51	106	49.80	8.46	0.81	0.25	0.31	0.27	0.684
850818	0624	29.72	34	07.59	106	49.68	7.69	0.35	0.23	0.36	0.25	0.822
850818	1029	08.62	34	07.77	106	49.57	7.89	0.79	0.20	0.21	0.26	0.868
850818	1303	41.20	34	07.99	106	50.30	7.44	0.47	0.28	0.32	0.29	1.271
850818	1447	04.97	34	07.62	106	49.43	8.17	1.40	0.19	0.24	0.26	0.911
850818	1450	02.53	34	07.81	106	49.47	8.25	0.00	0.38	0.35	0.27	0.650
850818	1548	15.65	34	07.54	106	49.55	7.91	2.00	0.22	0.20	0.30	0.704
850818	1654	44.02	34	07.79	106	49.88	7.80	0.84	0.22	0.22	0.27	0.860
850818	1934	17.88	34	07.62	106	48.75	7.80	0.02	0.46	0.36	0.45	0.850
850818	2214	27.50	34	07.70	106	49.13	8.07	0.32	0.30	0.30	0.27	0.787
850818	2255	04.76	34	07.75	106	49.61	8.08	0.26	0.28	0.29	0.28	0.867
850818	2305	49.18	34	07.72	106	49.27	8.36	0.23	0.28	0.31	0.30	0.787
850819	0129	52.77	34	07.44	106	49.43	8.56	-0.04	0.38	0.43	0.38	0.476
850819	0540	46.28	34	07.62	106	49.46	8.25	0.20	0.33	0.37	0.48	0.574
850819	1430	58.87	34	07.47	106	49.00	8.22	0.58	0.28	0.30	0.48	0.796
850819	1505	17.58	34	07.61	106	49.31	8.50	0.43	0.34	0.40	0.40	0.516
850820	0050	14.21	34	07.62	106	49.36	8.95	0.47	0.37	0.41	0.47	0.556
850820	0226	03.62	34	07.04	106	50.24	8.36	0.60	0.28	0.33	0.34	1.208
850820	0736	11.81	34	07.58	106	50.01	8.31	0.61	0.22	0.29	0.36	0.851
850820	1223	28.04	34	07.38	106	49.43	8.08	0.36	0.38	0.36	0.38	0.835
850820	1359	11.54	34	08.30	106	49.49	7.54	0.29	0.33	0.42	0.37	0.680
850821	2352	13.74	34	08.04	106	49.17	7.98	0.14	0.45	0.45	0.44	0.840
850822	1800	41.00	34	07.77	106	49.42	7.79	0.78	0.22	0.26	0.50	0.867
850823	0525	14.92	34	07.70	106	49.41	8.20	0.56	0.23	0.27	0.43	0.675
850823	0924	44.63	34	07.22	106	49.75	7.77	0.59	0.22	0.26	0.39	0.897
850823	2216	57.07	34	07.49	106	49.60	8.37	0.54	0.22	0.31	0.36	0.887
850826	0816	22.87	34	07.67	106	49.65	8.44	0.74	0.21	0.30	0.48	0.720
850827	0327	07.67	34	07.68	106	49.68	7.13	0.33	0.31	0.39	0.45	0.620
850827	1033	14.82	34	07.63	106	49.47	8.15	0.86	0.21	0.23	0.42	0.708
850830	0628	10.76	34	07.54	106	49.62	7.48	0.18	0.36	0.37	0.47	0.721
850831	0541	30.56	34	07.64	106	49.53	8.79	0.71	0.23	0.31	0.37	0.829
850831	0656	24.76	34	07.76	106	49.61	8.35	0.42	0.23	0.32	0.41	0.772
850901	1457	54.45	34	07.43	106	50.16	8.55	0.98	0.23	0.24	0.41	0.874
850905	1030	58.21	34	07.84	106	49.74	8.33	0.48	0.28	0.45	0.43	0.738

yymmdd	hhmm	sec	latitude		longitude		depth	mag	xerr	yerr	derr	R
850908	0152	59.31	34	07.69	106	49.75	8.60	0.16	0.27	0.41	0.48	0.508
850830	0628	10.74	34	07.52	106	49.66	7.78	0.18	0.36	0.38	0.43	0.822
850908	1922	17.91	34	07.49	106	49.61	8.32	0.74	0.22	0.27	0.35	0.658
850908	2217	45.88	34	07.81	106	49.50	8.90	0.10	0.27	0.43	0.43	0.861
850910	0824	31.65	34	07.52	106	49.62	8.90	0.57	0.23	0.30	0.42	0.856
850913	0545	19.01	34	07.45	106	49.67	7.52	1.75	0.22	0.22	0.46	0.778
850913	1311	22.66	34	07.54	106	49.49	8.33	0.71	0.27	0.33	0.42	0.838
850918	0039	34.35	34	07.45	106	49.91	8.68	1.18	0.22	0.28	0.36	0.880
850920	1927	02.82	34	07.71	106	49.48	7.64	1.11	0.22	0.24	0.31	0.870
850920	2013	39.68	34	07.78	106	49.50	7.45	0.81	0.23	0.31	0.28	0.699
850920	2014	46.97	34	07.46	106	49.49	8.13	0.25	0.39	0.37	0.44	0.716
850920	2200	06.91	34	07.63	106	49.55	7.37	0.98	0.26	0.27	0.29	0.775
850921	0708	50.54	34	07.39	106	49.41	8.32	0.74	0.25	0.27	0.31	0.846
850921	0709	18.80	34	07.48	106	49.40	7.82	1.34	0.20	0.25	0.33	0.901
850921	0711	47.56	34	07.50	106	49.26	8.39	0.81	0.26	0.30	0.30	0.796
850921	0732	31.93	34	07.38	106	49.58	8.06	1.01	0.25	0.30	0.31	0.644
850921	0804	00.41	34	07.63	106	49.61	7.87	2.08	0.20	0.19	0.35	0.721
850921	1906	25.46	34	07.89	106	49.55	8.68	0.29	0.35	0.43	0.44	0.777
850928	0926	41.51	34	07.41	106	49.42	8.69	1.02	0.24	0.34	0.44	0.795
850929	0354	49.27	34	07.58	106	49.76	8.44	1.93	0.22	0.24	0.50	0.644
851017	0431	20.28	34	07.46	106	49.45	8.03	0.90	0.24	0.35	0.43	0.567
851017	1322	39.01	34	07.49	106	49.59	8.70	1.57	0.22	0.22	0.43	0.885
851028	0829	38.90	34	07.74	106	49.68	7.77	1.44	0.20	0.20	0.37	0.914
851124	0316	31.70	34	07.55	106	49.71	8.48	0.88	0.24	0.46	0.37	0.608
851225	0738	14.53	34	06.32	106	49.43	6.13	1.14	0.25	0.36	0.48	0.528
860106	0705	38.34	34	07.50	106	49.57	8.21	1.01	0.24	0.38	0.47	0.641
860114	0004	29.81	34	07.62	106	49.49	7.72	1.93	0.22	0.21	0.39	0.624
860205	0130	54.75	34	07.49	106	49.49	7.98	1.08	0.22	0.29	0.36	0.659
860213	0243	18.66	34	07.37	106	49.52	9.15	1.62	0.22	0.25	0.35	0.610
860329	0853	27.89	34	07.61	106	49.58	8.53	0.78	0.26	0.34	0.42	0.532
860404	1733	20.85	34	08.36	106	49.67	7.12	2.10	0.21	0.21	0.42	0.861
860429	1209	03.98	34	06.94	106	50.37	7.63	2.08	0.23	0.21	0.45	0.593
840429	1754	31.80	34	07.46	106	49.79	8.60	0.98	0.30	0.29	0.38	0.819
850816	1500	57.84	34	07.31	106	49.21	6.80	1.23	0.43	0.44	0.47	0.940
860508	1859	50.25	34	06.79	106	50.02	9.00	0.85	0.25	0.35	0.42	1.261

65 Best Puertecito de Bowling Green Swarm Hypocenters

yymmdd	hhmm	sec	latitude		longitude		depth	mag	xerr	yerr	derr	R
850917	1029	19.19	34	11.46	106	47.77	9.29	0.59	0.24	0.32	0.37	0.967
850917	1032	40.40	34	11.32	106	47.76	9.31	1.33	0.22	0.22	0.43	0.988
850917	1033	32.55	34	11.50	106	48.03	9.31	0.53	0.22	0.31	0.38	0.685
850917	1036	22.05	34	11.59	106	47.85	9.24	0.76	0.22	0.29	0.35	0.835
850917	1038	11.94	34	11.66	106	47.93	9.19	0.55	0.31	0.38	0.44	0.785
850917	1039	10.51	34	11.55	106	47.93	9.62	0.48	0.26	0.35	0.45	0.816
850917	1041	25.89	34	11.52	106	47.87	9.53	1.03	0.24	0.28	0.36	0.818
850917	1105	48.42	34	11.43	106	47.84	9.06	1.90	0.23	0.21	0.44	0.768
850917	1106	25.24	34	11.76	106	47.77	9.37	0.62	0.28	0.41	0.47	0.733
850917	1107	33.43	34	11.60	106	47.86	9.24	0.42	0.30	0.39	0.49	0.732
850917	1142	08.33	34	11.45	106	47.81	9.59	1.09	0.22	0.27	0.42	0.675
850917	1950	50.85	34	11.68	106	47.82	9.85	0.99	0.22	0.31	0.39	1.012
850917	1953	33.15	34	11.42	106	47.89	9.96	0.32	0.27	0.35	0.49	0.805
850917	2134	42.96	34	11.73	106	47.98	10.0	0.66	0.28	0.35	0.44	0.731

yymmdd	hhmm	sec	latitude		longitude		depth	mag	xerr	yerr	derr	R
850917	2206	07.18	34	11.54	106	47.83	9.64	0.31	0.30	0.47	0.44	0.617
850918	1114	55.48	34	11.39	106	47.90	8.75	1.41	0.21	0.20	0.33	0.674
850918	1137	23.00	34	11.53	106	48.07	9.21	0.68	0.24	0.35	0.38	0.972
850918	1701	16.66	34	11.25	106	47.84	9.57	1.18	0.23	0.23	0.32	0.936
850918	1711	27.56	34	11.67	106	47.86	9.83	0.22	0.28	0.43	0.46	0.592
850918	1714	55.89	34	11.39	106	47.93	9.64	0.96	0.22	0.30	0.36	1.036
850918	1716	44.31	34	11.73	106	47.86	9.57	0.36	0.27	0.38	0.41	0.894
850918	1733	31.58	34	11.59	106	47.73	10.2	0.71	0.22	0.31	0.44	0.864
850918	1802	07.30	34	11.28	106	47.90	9.47	1.42	0.22	0.20	0.33	0.609
850918	1803	40.63	34	11.56	106	47.79	10.0	0.67	0.21	0.28	0.39	0.852
850918	1820	42.08	34	11.80	106	48.07	9.47	0.56	0.22	0.30	0.43	0.786
850918	1822	14.46	34	11.41	106	47.89	9.65	1.54	0.22	0.20	0.37	0.927
850918	1823	03.31	34	11.48	106	48.05	9.30	1.38	0.22	0.22	0.36	0.810
850918	1824	05.74	34	11.66	106	47.85	9.69	0.12	0.28	0.41	0.47	0.798
850918	1830	59.04	34	11.67	106	47.89	10.5	1.02	0.22	0.26	0.36	0.928
850918	1841	35.99	34	11.65	106	48.00	9.40	0.29	0.30	0.45	0.50	0.857
850918	1909	23.06	34	11.47	106	47.83	9.09	0.86	0.25	0.30	0.34	0.961
850918	1916	15.15	34	11.36	106	47.85	9.65	1.04	0.23	0.26	0.36	0.828
850918	1919	31.09	34	11.35	106	47.82	9.25	2.28	0.22	0.19	0.37	0.895
850918	1920	51.07	34	11.65	106	47.87	9.47	0.64	0.27	0.38	0.40	0.944
850918	1921	08.77	34	11.41	106	47.88	9.50	0.84	0.21	0.25	0.39	0.638
850918	1923	09.00	34	11.41	106	48.02	9.68	1.84	0.22	0.19	0.40	0.861
850918	1926	03.44	34	11.61	106	47.95	9.24	1.18	0.23	0.30	0.38	0.976
850918	1938	00.42	34	11.27	106	47.95	9.08	2.21	0.22	0.20	0.38	0.871
850918	1939	29.04	34	11.28	106	48.00	9.03	1.47	0.25	0.21	0.34	0.995
850918	1940	29.25	34	11.43	106	47.90	9.53	0.51	0.22	0.31	0.48	0.882
850918	1950	17.82	34	11.47	106	47.93	9.75	1.11	0.21	0.24	0.44	0.847
850918	2000	19.69	34	11.50	106	47.87	9.68	0.70	0.21	0.30	0.35	0.652
850918	2023	23.92	34	11.42	106	47.77	9.81	1.32	0.23	0.22	0.39	0.855
850918	2119	19.93	34	11.30	106	47.86	9.00	2.39	0.22	0.20	0.44	0.916
850918	2125	52.13	34	11.28	106	47.82	9.62	1.24	0.22	0.24	0.33	0.763
850918	2135	02.32	34	11.62	106	47.92	10.2	0.72	0.28	0.34	0.46	0.653
850918	2140	06.67	34	11.52	106	47.86	9.50	1.30	0.21	0.24	0.38	0.985
850919	0224	05.43	34	11.24	106	47.96	8.73	2.73	0.22	0.20	0.47	0.932
850919	0227	26.05	34	11.23	106	47.65	10.4	1.51	0.22	0.26	0.41	1.075
850919	0228	13.05	34	11.44	106	47.89	9.47	2.45	0.26	0.21	0.44	0.828
850919	0231	08.57	34	11.48	106	47.69	10.0	2.52	0.27	0.20	0.41	0.761
850919	0234	05.08	34	11.47	106	47.83	9.29	0.99	0.23	0.33	0.40	0.727
850919	0257	19.16	34	11.22	106	47.67	9.95	1.15	0.22	0.24	0.42	0.866
850919	0303	24.75	34	11.63	106	48.02	9.28	1.35	0.22	0.24	0.41	0.591
850919	0406	56.86	34	11.33	106	47.83	9.38	0.51	0.25	0.33	0.43	0.556
850919	0630	37.41	34	11.43	106	47.71	9.44	1.60	0.25	0.21	0.33	0.793
850919	0938	41.68	34	11.59	106	47.90	9.15	2.57	0.28	0.19	0.42	0.851
850919	0944	39.12	34	11.47	106	47.73	9.65	1.48	0.26	0.22	0.33	0.741
850919	0945	53.73	34	11.63	106	48.03	9.59	0.71	0.33	0.40	0.39	0.880
850919	1005	03.74	34	11.50	106	47.99	9.63	1.42	0.26	0.23	0.32	0.776
850920	1426	50.93	34	11.22	106	47.86	9.09	0.98	0.22	0.29	0.31	0.770
850920	1437	34.10	34	11.11	106	47.96	9.22	1.53	0.26	0.22	0.38	0.856
850920	1616	33.85	34	11.41	106	47.88	8.90	0.42	0.22	0.33	0.48	0.817
850920	1620	28.20	34	11.33	106	47.74	9.16	0.83	0.23	0.30	0.34	0.671
850920	1639	38.95	34	11.87	106	47.90	9.07	0.32	0.27	0.44	0.48	0.621

106 Best Loma de las Cañas Swarm Hypocenters

yymmdd	hhmm	sec	latitude	longitude	depth	mag	xerr	yerr	derr	R
860416	1136	10.30	34 01.45	106 49.27	6.20	0.80	0.23	0.24	0.38	1.108
860416	1519	43.96	34 01.23	106 49.26	6.09	0.50	0.30	0.34	0.41	0.769
850418	1521	54.23	34 01.32	106 49.31	6.61	0.45	0.25	0.30	0.43	1.011
860419	1344	31.43	34 01.56	106 49.16	6.27	0.98	0.25	0.31	0.41	0.905
860426	1054	13.01	34 01.40	106 48.96	5.14	0.84	0.22	0.23	0.36	0.953
860426	2258	57.57	34 01.15	106 49.38	6.75	0.29	0.31	0.29	0.47	0.920
860427	1118	54.51	34 01.33	106 49.17	7.07	0.44	0.26	0.27	0.44	0.718
860427	1645	45.05	34 01.43	106 49.24	6.29	0.34	0.31	0.40	0.45	0.847
860427	1918	23.45	34 01.56	106 49.18	5.97	0.74	0.23	0.24	0.36	1.007
860427	1025	36.97	34 01.38	106 49.22	6.62	0.28	0.32	0.45	0.46	0.901
860427	1141	43.04	34 01.47	106 49.08	6.22	0.60	0.23	0.24	0.41	0.983
860427	1814	31.18	34 01.49	106 49.09	6.12	0.67	0.23	0.23	0.31	0.833
860427	1815	00.93	34 01.54	106 49.20	6.39	0.62	0.23	0.24	0.35	0.843
860427	2217	36.51	34 01.50	106 49.10	6.66	0.46	0.26	0.29	0.40	0.635
860427	2346	55.30	34 01.56	106 49.12	6.20	0.50	0.29	0.40	0.50	0.959
860427	2358	19.50	34 01.55	106 49.23	5.86	1.81	0.31	0.25	0.40	0.876
860428	1042	18.29	34 01.31	106 49.13	6.40	0.34	0.29	0.39	0.44	0.947
860428	1044	36.57	34 01.29	106 49.12	6.21	0.59	0.25	0.27	0.34	0.749
860428	1110	30.15	34 01.44	106 49.13	6.43	0.11	0.34	0.35	0.44	0.824
860428	1159	09.99	34 01.34	106 49.40	6.68	-0.02	0.47	0.50	0.49	1.061
860428	1318	37.19	34 01.44	106 49.23	6.29	1.10	0.22	0.23	0.34	0.992
860428	1315	04.63	34 01.44	106 49.37	6.64	1.77	0.23	0.22	0.43	0.873
860428	1315	58.07	34 01.47	106 49.20	6.97	0.54	0.24	0.25	0.40	0.923
860428	1324	02.87	34 01.35	106 49.27	6.07	0.39	0.29	0.34	0.42	0.998
860428	1325	55.14	34 01.32	106 49.28	6.50	1.03	0.25	0.33	0.39	0.974
860428	1350	03.64	34 01.34	106 49.35	6.71	1.22	0.24	0.23	0.39	0.851
860428	1359	58.06	34 01.56	106 49.05	5.99	1.39	0.27	0.28	0.39	0.938
860428	14 1	28.66	34 01.49	106 49.15	6.31	0.49	0.29	0.35	0.35	0.927
860428	1537	33.43	34 01.53	106 49.33	6.34	0.61	0.23	0.24	0.35	1.002
860428	1542	04.30	34 01.45	106 49.45	6.38	1.79	0.25	0.23	0.41	0.944
860428	1547	57.50	34 01.52	106 49.17	6.28	1.20	0.22	0.24	0.35	0.908
860428	1648	27.31	34 01.54	106 49.12	6.05	1.06	0.22	0.28	0.31	0.970
860428	17 8	56.27	34 01.31	106 49.57	5.95	0.38	0.35	0.36	0.42	0.809
860428	1720	22.81	34 01.63	106 49.56	6.11	1.69	0.23	0.23	0.39	0.832
860428	1759	13.66	34 01.36	106 49.42	6.38	1.25	0.22	0.25	0.30	1.181
860428	1853	18.15	34 01.37	106 49.60	6.46	0.37	0.43	0.37	0.46	0.859
860428	1944	57.24	34 01.55	106 49.29	6.90	0.33	0.27	0.35	0.42	0.800
860428	1013	58.33	34 01.46	106 49.23	6.43	0.91	0.22	0.29	0.33	0.869
860428	1119	56.23	34 01.35	106 49.45	6.63	0.63	0.25	0.26	0.34	1.083
860428	1151	37.81	34 01.46	106 49.33	6.26	1.55	0.24	0.24	0.42	1.019
860428	1236	57.01	34 01.43	106 49.33	6.65	0.41	0.25	0.28	0.42	0.988
860428	1259	43.28	34 01.59	106 49.22	5.78	0.51	0.27	0.33	0.42	0.658
860428	1318	34.67	34 01.52	106 49.36	5.87	0.33	0.43	0.38	0.49	0.701
860428	1510	50.33	34 01.26	106 49.15	6.47	0.45	0.26	0.25	0.45	0.978
860428	1537	57.42	34 01.25	106 49.32	6.36	0.68	0.23	0.24	0.46	0.929
860428	1656	06.78	34 01.38	106 49.40	6.25	0.44	0.29	0.30	0.41	0.872
860428	1911	24.80	34 01.32	106 49.31	5.70	0.19	0.49	0.40	0.44	0.770
860429	1047	19.62	34 01.53	106 49.43	6.27	0.48	0.37	0.41	0.38	0.666
860429	1248	48.50	34 01.50	106 49.39	5.63	0.64	0.28	0.32	0.40	0.621
860429	1252	59.73	34 01.52	106 49.45	6.07	0.54	0.37	0.32	0.44	0.636
860429	1332	24.47	34 01.64	106 49.20	6.25	0.82	0.26	0.33	0.36	0.821

yymmdd	hhmm	sec	latitude		longitude		depth	mag	xerr	yerr	derr	R
860429	1530	22.98	34	01.44	106	49.16	5.63	1.04	0.22	0.32	0.40	1.127
860429	1620	53.56	34	01.47	106	49.60	6.69	0.55	0.26	0.32	0.46	0.813
860429	1830	31.27	34	01.73	106	49.25	6.06	2.12	0.22	0.30	0.40	0.792
860429	1831	33.02	34	01.68	106	49.22	6.16	0.83	0.23	0.33	0.41	0.884
860429	1835	13.54	34	01.40	106	49.30	6.14	1.46	0.22	0.24	0.37	0.816
860429	1022	09.86	34	01.35	106	49.47	6.12	0.39	0.43	0.35	0.45	0.922
860429	1520	18.24	34	01.51	106	49.22	5.98	1.25	0.23	0.22	0.32	0.808
860429	1532	49.65	34	01.57	106	49.37	6.26	0.26	0.31	0.31	0.46	1.064
860429	1613	54.17	34	01.53	106	49.43	6.59	0.69	0.33	0.31	0.46	0.814
860429	1642	51.05	34	01.64	106	49.66	6.18	0.38	0.28	0.29	0.35	1.267
860430	1017	39.58	34	01.41	106	49.34	6.25	0.55	0.26	0.23	0.27	0.940
860430	1011	26.09	34	01.43	106	48.90	5.89	0.18	0.41	0.34	0.43	0.793
860430	1128	29.65	34	01.48	106	49.14	5.93	0.87	0.20	0.21	0.23	1.107
860430	0131	52.38	34	01.46	106	49.19	6.47	0.38	0.29	0.35	0.34	0.727
860430	1319	56.75	34	01.39	106	49.32	5.46	0.06	0.34	0.46	0.45	0.534
860430	0407	44.56	34	01.58	106	49.20	5.91	1.15	0.21	0.21	0.24	0.958
860430	0447	34.55	34	01.64	106	49.33	6.47	0.19	0.44	0.43	0.40	0.613
860430	0539	53.04	34	01.46	106	49.18	5.94	1.09	0.22	0.22	0.27	0.938
860430	0641	49.04	34	01.43	106	49.21	6.44	0.98	0.24	0.24	0.31	0.896
860430	1031	21.03	34	01.52	106	49.30	5.74	0.09	0.27	0.34	0.40	0.745
860430	1612	19.09	34	01.57	106	49.11	5.82	1.35	0.21	0.20	0.28	0.931
860430	1615	28.02	34	01.56	106	49.37	6.36	1.18	0.24	0.22	0.25	1.134
860430	1731	07.10	34	01.50	106	49.18	5.97	0.24	0.45	0.40	0.46	0.484
860430	1806	54.07	34	01.58	106	49.41	6.61	0.53	0.36	0.35	0.34	0.878
8605	1	0353	29.45	34	01.56	106	49.26	6.48	0.39	0.33	0.31	0.32	0.757
8605	1	0932	07.57	34	01.61	106	49.32	5.87	0.56	0.29	0.26	0.28	1.012
8605	1	1143	37.07	34	01.65	106	49.30	6.16	0.41	0.36	0.37	0.43	0.955
8605	1	1336	56.90	34	01.19	106	49.25	5.89	0.36	0.36	0.34	0.32	0.960
8605	1	1628	33.12	34	01.45	106	48.95	6.35	1.92	0.22	0.23	0.30	0.832
8605	1	19	6	59.60	34	01.34	106	48.99	6.55	0.49	0.36	0.33	0.38	0.694
8605	1	2130	25.79	34	01.51	106	49.38	6.39	0.49	0.33	0.35	0.36	1.080
8605	2	1232	56.73	34	01.59	106	49.38	6.26	0.31	0.30	0.35	0.33	0.747
8605	2	1348	51.51	34	01.36	106	49.30	6.06	0.34	0.31	0.36	0.37	0.760
8605	2	1412	19.46	34	01.42	106	49.18	6.14	0.35	0.26	0.31	0.34	0.971
8605	2	1245	21.06	34	01.55	106	49.68	5.78	0.27	0.43	0.39	0.36	1.007
8605	3	0646	30.53	34	01.49	106	49.83	5.85	0.47	0.31	0.31	0.45	0.933
8605	4	0749	14.94	34	01.43	106	49.34	6.30	0.91	0.23	0.25	0.48	1.121
8605	4	1810	16.09	34	01.35	106	49.10	6.57	1.75	0.22	0.24	0.37	0.923
8605	4	1950	03.96	34	01.48	106	49.25	6.09	0.58	0.26	0.24	0.36	0.983
8605	4	2230	39.62	34	01.42	106	49.28	7.06	1.49	0.22	0.23	0.34	1.210
8605	5	1442	16.73	34	01.36	106	49.45	5.16	0.50	0.34	0.30	0.41	0.979
8605	5	1447	01.44	34	01.33	106	49.53	6.28	0.57	0.26	0.26	0.37	1.021
860510	0648	14.36	34	01.48	106	49.26	6.25	1.84	0.26	0.39	0.38	0.981
860510	0648	46.46	34	01.44	106	49.11	6.51	1.07	0.30	0.41	0.44	0.671
860511	1503	57.63	34	01.38	106	49.45	5.39	2.44	0.22	0.22	0.43	0.974
860511	1743	33.46	34	01.69	106	49.02	6.07	0.75	0.32	0.41	0.46	0.936
860511	1801	16.42	34	01.50	106	49.39	6.39	1.14	0.22	0.24	0.31	1.336
860511	2105	29.48	34	01.48	106	49.04	5.86	0.56	0.24	0.30	0.38	0.849
860511	2107	08.69	34	01.47	106	49.20	6.06	1.03	0.23	0.25	0.40	1.140
860512	0551	30.41	34	01.39	106	49.13	6.36	0.57	0.28	0.38	0.47	0.854
860513	1728	02.99	34	01.47	106	49.43	6.19	1.74	0.24	0.24	0.37	0.941
860514	0645	44.93	34	01.35	106	49.23	6.23	0.97	0.22	0.23	0.38	0.812

yymmdd	hhmm	sec	latitude		longitude		depth	mag	xerr	yerr	derr	R
860514	1244	17.56	34	01.43	106	49.32	6.87	1.28	0.21	0.23	0.38	0.952
860515	1316	21.34	34	01.43	106	49.30	6.28	1.74	0.23	0.24	0.47	1.013
860523	1801	34.49	34	01.76	106	49.32	6.48	1.29	0.21	0.24	0.43	0.945

Appendix VI - General Data Set

This appendix contains the event headers for the 1181 epicenters of the general data set. The events have latitude, longitude and depth errors less than 1.0 km at 1 std, with average errors of 0.31 km, 0.37 km and 0.46 km, respectively. The header label at the top of each page describes the data in the column(s) directly beneath it as described below:

yymmdd - year, month and day
hhmm - hour and minute (GMT)
sec - origin time in seconds
latitude - north latitude in degrees and minutes
longitude - west longitude in degrees and minutes
depth - depth in km relative to station SNM (1.511 km above sea level)
mag - duration magnitude using M_d=2.79LOG(duration)-3.63
xerr - latitude error in km at 1 std
yerr - longitude error in km at 1 std
derr - depth error in km at 1 std
R - goodness of fit factor from *Jackson* [1972]

1181 General Data Set Hypocenters

yymmdd	hhmm	sec	latitude	longitude	depth	mag	xerr	yerr	derr	R
850816	0243	06.38	34 07.49	106 49.46	7.94	0.65	0.34	0.36	0.37	0.625
850816	1500	57.85	34 07.33	106 49.23	6.65	1.23	0.43	0.44	0.48	0.973
850816	1502	39.87	34 07.69	106 49.34	7.00	0.86	0.28	0.32	0.41	0.951
850816	1503	20.80	34 07.33	106 49.54	6.87	1.37	0.46	0.38	0.49	0.798
850816	1505	30.03	34 06.68	106 48.16	7.86	0.42	0.65	0.83	0.76	0.670
850816	1505	50.27	34 06.96	106 49.11	6.56	0.86	0.70	0.49	0.64	0.590
850816	1506	56.75	34 07.46	106 49.12	6.73	0.91	0.28	0.33	0.37	1.031
850816	1507	48.62	34 07.29	106 49.21	7.52	0.89	0.31	0.34	0.49	0.616
850816	1510	01.29	34 07.52	106 49.32	8.61	0.23	0.55	0.63	0.71	0.593
850816	1510	54.82	34 07.73	106 49.12	8.14	0.55	0.31	0.33	0.50	0.731
850816	1512	40.10	34 07.41	106 49.54	8.03	0.20	0.34	0.35	0.58	0.601
850816	1525	20.83	34 07.36	106 49.65	8.25	0.69	0.28	0.28	0.45	0.664
850816	1528	31.59	34 07.31	106 49.71	7.74	0.80	0.34	0.33	0.33	0.833
850816	1531	06.52	34 07.59	106 49.44	7.87	0.50	0.30	0.35	0.62	0.751
850816	1533	47.71	34 07.74	106 49.48	7.81	0.57	0.25	0.31	0.47	0.853
850816	1535	31.53	34 07.63	106 49.34	7.38	1.12	0.25	0.29	0.43	0.753
850816	1541	48.51	34 07.38	106 49.69	8.29	0.53	0.29	0.30	0.45	0.855
850816	1542	23.08	34 07.65	106 49.21	7.43	1.22	0.22	0.24	0.43	0.730
850816	1544	23.10	34 08.09	106 49.04	7.53	0.38	0.25	0.32	0.50	0.795
850816	1547	26.54	34 07.83	106 49.58	7.78	1.21	0.37	0.28	0.46	0.855
850816	1553	41.25	34 07.72	106 48.97	8.49	0.95	0.21	0.25	0.38	1.049
850816	1554	40.66	34 07.14	106 49.81	8.86	0.20	0.38	0.42	0.61	1.034
850816	1555	18.15	34 07.76	106 49.26	8.70	0.29	0.25	0.32	0.65	0.573
850816	1600	25.69	34 07.79	106 49.17	8.11	1.13	0.24	0.23	0.48	1.011
850816	1607	51.73	34 07.41	106 49.65	9.28	0.32	0.38	0.47	0.50	0.612
850816	1614	50.29	34 07.87	106 49.35	9.16	0.18	0.45	0.42	0.66	0.768

yymmdd	hhmm	sec	latitude		longitude		depth	mag	xerr	yerr	derr	R
850816	1628	51.82	34	07.85	106	49.05	8.48	0.28	0.47	0.61	0.50	0.503
850816	1725	00.83	34	07.60	106	48.99	5.24	0.14	0.34	0.41	0.93	1.014
850816	1748	13.17	34	07.54	106	49.73	8.18	0.66	0.23	0.31	0.38	0.795
850816	1803	07.36	34	07.90	106	49.51	8.56	0.39	0.34	0.58	0.48	0.692
850816	1803	43.56	34	07.91	106	49.63	7.39	0.25	0.28	0.79	0.47	0.823
850816	1805	18.81	34	07.88	106	49.50	8.18	0.46	0.39	0.61	0.44	1.074
850816	1902	54.50	34	07.74	106	49.57	8.31	0.18	0.29	0.74	0.40	0.574
850816	1949	31.43	34	07.78	106	49.43	6.68	0.34	0.35	0.65	0.40	1.292
850816	2013	27.53	34	07.58	106	49.63	7.85	0.73	0.23	0.31	0.31	0.687
850816	2029	41.10	34	07.01	106	49.14	7.09	0.17	0.50	0.66	0.63	1.019
850816	2035	41.67	34	08.09	106	49.21	8.18	0.56	0.28	0.35	0.35	0.749
850816	2046	47.42	34	07.71	106	49.00	8.18	0.27	0.45	0.37	0.00	0.845
850816	2049	14.25	34	07.51	106	49.49	8.13	0.37	0.25	0.32	0.35	0.823
850816	2140	45.31	34	07.48	106	49.67	7.82	0.75	0.19	0.26	0.32	0.917
850816	2148	57.92	34	08.02	106	49.14	8.94	0.42	0.38	0.53	0.30	0.764
850816	2157	10.39	34	07.59	106	49.39	6.58	0.54	0.55	0.52	0.68	0.620
850816	2207	39.52	34	08.37	106	48.97	6.66	-0.03	0.47	0.74	0.43	1.106
850816	2211	43.71	34	08.08	106	49.36	8.27	0.14	0.51	0.42	0.60	0.941
850816	2230	50.50	34	07.59	106	49.40	7.84	0.36	0.25	0.33	0.32	0.713
850816	2243	43.18	34	07.59	106	49.47	6.98	0.22	0.26	0.33	0.43	0.464
850816	2318	43.13	34	07.87	106	49.35	8.44	0.11	0.38	0.67	0.61	0.341
850817	0000	25.76	34	07.72	106	49.25	7.67	0.50	0.25	0.27	0.23	0.944
850817	0004	19.24	34	07.93	106	49.62	7.30	0.36	0.26	0.32	0.31	0.852
850817	0021	11.46	34	07.81	106	49.90	7.20	0.66	0.34	0.44	0.35	0.635
850817	0055	56.53	34	07.64	106	49.24	8.53	0.56	0.27	0.41	0.47	1.061
850817	0109	59.87	34	07.98	106	49.41	10.1	0.24	0.34	0.36	0.50	0.866
850817	0123	58.88	34	07.96	106	48.88	8.94	0.26	0.36	0.36	0.47	1.052
850817	0124	22.18	34	07.43	106	49.77	8.02	0.93	0.23	0.22	0.25	0.911
850817	0144	37.64	34	07.71	106	49.26	8.25	-0.01	0.41	0.44	0.40	0.881
850817	0200	38.18	34	08.10	106	49.29	7.80	-0.17	0.44	0.60	0.55	0.817
850817	0246	16.55	34	07.37	106	49.53	7.82	0.17	0.27	0.27	0.27	0.840
850817	0250	16.36	34	07.65	106	49.66	7.50	0.78	0.20	0.24	0.20	0.821
850817	0319	44.44	34	07.69	106	48.60	5.50	-0.11	0.54	0.59	0.48	0.776
850817	0405	43.83	34	08.04	106	49.12	8.20	0.12	0.51	0.38	0.37	0.873
850817	0448	27.75	34	07.76	106	49.22	8.96	0.13	0.34	0.37	0.33	0.794
850817	0453	17.55	34	08.28	106	49.06	9.12	-0.06	0.46	0.70	0.44	0.869
850817	0514	46.57	34	07.45	106	49.45	9.02	1.98	0.24	0.22	0.42	1.145
850817	0542	58.15	34	07.81	106	49.19	8.15	0.41	0.34	0.46	0.40	0.404
850817	0624	12.82	34	07.70	106	49.15	7.82	0.29	0.40	0.46	0.35	0.826
850817	0645	36.08	34	07.54	106	49.64	7.82	0.35	0.23	0.26	0.26	0.846
850817	0650	56.60	34	07.73	106	49.33	7.75	0.25	0.30	0.35	0.34	0.951
850817	0725	23.24	34	07.78	106	49.44	7.86	0.26	0.32	0.39	0.41	1.051
850817	0725	34.89	34	07.76	106	49.35	7.78	-0.06	0.35	0.39	0.46	0.582
850817	0731	25.20	34	07.53	106	49.71	7.42	0.42	0.25	0.29	0.29	0.797
850817	0737	06.84	34	07.18	106	49.15	7.32	0.29	0.35	0.49	0.32	1.131
850817	0902	18.43	34	08.46	106	49.54	8.08	-0.05	0.32	0.55	0.31	0.771
850817	1119	50.53	34	07.67	106	49.51	8.26	0.32	0.30	0.33	0.27	0.928
850817	1247	30.49	34	07.80	106	49.56	8.12	0.75	0.27	0.29	0.29	0.998
850817	1331	59.17	34	07.70	106	49.21	8.26	0.03	0.39	0.49	0.42	0.895
850817	1347	24.33	34	07.92	106	49.19	9.16	0.09	0.55	0.62	0.34	0.774
850817	1359	40.94	34	07.97	106	49.48	8.34	0.17	0.38	0.34	0.32	0.806
850817	1515	25.66	34	07.58	106	49.47	7.57	0.34	0.24	0.30	0.25	0.893

yymmdd	hhmm	sec	latitude	longitude	depth	mag	xerr	yerr	derr	R
850817	1624	36.79	34 07.65	106 49.26	7.18	0.08	0.31	0.41	0.45	0.911
850817	1657	22.36	34 07.64	106 49.30	6.79	0.23	0.38	0.38	0.50	0.785
850817	1752	18.12	34 07.68	106 49.51	8.46	-0.27	0.61	0.58	0.88	0.516
850817	1753	36.07	34 07.95	106 49.71	7.85	0.17	0.28	0.32	0.31	1.021
850817	1804	24.71	34 07.45	106 49.87	8.18	0.73	0.22	0.27	0.30	0.753
850817	1806	20.86	34 07.54	106 49.52	7.30	0.56	0.21	0.25	0.32	0.704
850817	1949	24.64	34 07.79	106 49.57	7.65	0.76	0.20	0.23	0.27	1.000
850817	2122	42.19	34 07.75	106 49.58	7.42	0.27	0.23	0.28	0.31	0.759
850817	2134	10.94	34 07.83	106 49.44	7.11	1.62	0.21	0.20	0.33	0.986
850817	2137	36.39	34 07.81	106 49.43	7.57	0.21	0.25	0.31	0.31	0.849
850817	2144	16.77	34 07.53	106 49.41	8.37	0.64	0.22	0.29	0.32	0.764
850817	2144	32.55	34 07.92	106 48.90	8.69	0.34	0.49	0.66	0.46	0.803
850817	2317	03.95	34 07.97	106 48.96	8.66	0.50	0.26	0.33	0.28	0.919
850817	2330	04.08	34 07.60	106 48.99	7.18	0.32	0.40	0.36	0.58	0.902
850817	2357	35.03	34 07.94	106 49.36	7.93	0.12	0.42	0.39	0.38	0.846
850817	2358	59.84	34 07.95	106 49.57	7.68	0.37	0.34	0.30	0.28	0.802
850818	0028	02.03	34 07.88	106 49.48	7.69	0.82	0.19	0.21	0.25	0.756
850818	0124	15.06	34 07.91	106 49.24	7.71	0.22	0.45	0.39	0.40	0.588
850818	0302	57.16	34 07.89	106 49.23	8.57	0.19	0.43	0.46	0.44	0.475
850818	0339	06.20	34 07.88	106 49.58	7.76	0.29	0.31	0.54	0.38	0.917
850818	0354	01.67	34 07.79	106 49.69	7.60	0.35	0.27	0.31	0.24	1.061
850818	0357	11.52	34 07.83	106 49.57	7.32	0.82	0.21	0.26	0.25	0.797
850818	0443	43.56	34 07.53	106 49.07	7.05	0.19	0.39	0.42	0.51	0.709
850818	0531	03.60	34 07.51	106 49.80	8.46	0.81	0.25	0.31	0.27	0.684
850818	0624	29.72	34 07.59	106 49.68	7.69	0.35	0.23	0.36	0.25	0.822
850818	1029	08.62	34 07.77	106 49.57	7.89	0.79	0.20	0.21	0.26	0.868
850818	1106	51.40	34 08.51	106 49.03	9.12	0.34	0.51	0.56	0.43	0.630
850818	1217	58.32	34 08.01	106 49.18	8.50	0.27	0.40	0.50	0.64	0.668
850818	1303	41.20	34 07.99	106 50.30	7.44	0.47	0.28	0.32	0.29	1.271
850818	1447	04.97	34 07.62	106 49.43	8.17	1.40	0.19	0.24	0.26	0.911
850818	1450	02.53	34 07.81	106 49.47	8.25	0.00	0.38	0.35	0.27	0.650
850818	1548	15.65	34 07.54	106 49.55	7.91	2.00	0.22	0.20	0.30	0.704
850818	1654	44.02	34 07.79	106 49.88	7.80	0.84	0.22	0.22	0.27	0.860
850818	1934	17.88	34 07.62	106 48.75	7.80	0.02	0.46	0.36	0.45	0.850
850818	2214	27.50	34 07.70	106 49.13	8.07	0.32	0.30	0.30	0.27	0.787
850818	2255	04.76	34 07.75	106 49.61	8.08	0.26	0.28	0.29	0.28	0.867
850818	2305	49.18	34 07.72	106 49.27	8.36	0.23	0.28	0.31	0.30	0.787
850819	0129	52.77	34 07.44	106 49.43	8.56	-0.04	0.38	0.43	0.38	0.476
850819	0540	46.28	34 07.62	106 49.46	8.25	0.20	0.33	0.37	0.48	0.574
850819	1430	58.87	34 07.47	106 49.00	8.22	0.58	0.28	0.30	0.48	0.796
850819	1505	17.58	34 07.61	106 49.31	8.50	0.43	0.34	0.40	0.40	0.516
850819	1935	33.95	34 07.50	106 49.49	8.10	2.24	0.23	0.20	0.58	0.558
850820	0050	14.21	34 07.62	106 49.36	8.95	0.47	0.37	0.41	0.47	0.556
850820	0226	03.62	34 07.04	106 50.24	8.36	0.60	0.28	0.33	0.34	1.208
850820	0736	11.81	34 07.58	106 50.01	8.31	0.61	0.22	0.29	0.36	0.851
850820	1223	28.04	34 07.38	106 49.43	8.08	0.36	0.38	0.36	0.38	0.835
850820	1359	11.54	34 08.30	106 49.49	7.54	0.29	0.33	0.42	0.37	0.680
850821	0447	43.59	34 08.00	106 49.64	8.33	0.17	0.50	0.70	0.36	0.453
850821	1951	40.53	34 07.79	106 50.02	8.24	0.31	0.35	0.36	0.52	0.690
850821	2352	13.74	34 08.04	106 49.17	7.98	0.14	0.45	0.45	0.44	0.840
850822	18	0 41.00	34 07.77	106 49.42	7.79	0.78	0.22	0.26	0.50	0.867
850823	0525	14.92	34 07.70	106 49.41	8.20	0.56	0.23	0.27	0.43	0.675

yymmdd	hhmm	sec	latitude		longitude		depth	mag	xerr	yerr	derr	R
850823	0924	44.63	34	07.22	106	49.75	7.77	0.59	0.22	0.26	0.39	0.897
850823	2216	57.07	34	07.49	106	49.60	8.37	0.54	0.22	0.31	0.36	0.887
850826	0739	59.91	34	07.47	106	49.35	9.13	1.44	0.22	0.22	0.52	0.795
850826	0816	22.87	34	07.67	106	49.65	8.44	0.74	0.21	0.30	0.48	0.720
850827	0327	07.67	34	07.68	106	49.68	7.13	0.33	0.31	0.39	0.45	0.620
850827	1033	14.82	34	07.63	106	49.47	8.15	0.86	0.21	0.23	0.42	0.708
850830	0628	10.76	34	07.54	106	49.62	7.48	0.18	0.36	0.37	0.47	0.721
850831	0541	30.56	34	07.64	106	49.53	8.79	0.71	0.23	0.31	0.37	0.829
850831	0656	24.76	34	07.76	106	49.61	8.35	0.42	0.23	0.32	0.41	0.772
850831	2247	43.35	34	07.60	106	49.52	8.61	2.20	0.23	0.22	0.59	0.899
850901	1457	54.45	34	07.43	106	50.16	8.55	0.98	0.23	0.24	0.41	0.874
850905	1030	58.21	34	07.84	106	49.74	8.33	0.48	0.28	0.45	0.43	0.738
850908	0152	59.31	34	07.69	106	49.75	8.60	0.16	0.27	0.41	0.48	0.508
850830	0628	10.74	34	07.52	106	49.66	7.78	0.18	0.36	0.38	0.43	0.822
850908	1123	13.95	34	07.72	106	49.51	7.91	0.07	0.30	0.44	0.56	0.793
850908	1922	17.91	34	07.49	106	49.61	8.32	0.74	0.22	0.27	0.35	0.658
850908	2217	45.88	34	07.81	106	49.50	8.90	0.10	0.27	0.43	0.43	0.861
850910	0824	31.65	34	07.52	106	49.62	8.90	0.57	0.23	0.30	0.42	0.856
850913	0545	19.01	34	07.45	106	49.67	7.52	1.75	0.22	0.22	0.46	0.778
850913	1311	22.66	34	07.54	106	49.49	8.33	0.71	0.27	0.33	0.42	0.838
850918	0039	34.35	34	07.45	106	49.91	8.68	1.18	0.22	0.28	0.36	0.880
850920	1927	02.82	34	07.71	106	49.48	7.64	1.11	0.22	0.24	0.31	0.870
850920	2013	39.68	34	07.78	106	49.50	7.45	0.81	0.23	0.31	0.28	0.699
850920	2014	46.97	34	07.46	106	49.49	8.13	0.25	0.39	0.37	0.44	0.716
850920	2132	32.04	34	08.01	106	49.71	7.94	0.27	0.45	0.51	0.47	0.752
850920	2200	06.91	34	07.63	106	49.55	7.37	0.98	0.26	0.27	0.29	0.775
850921	0708	50.54	34	07.39	106	49.41	8.32	0.74	0.25	0.27	0.31	0.846
850921	0709	18.80	34	07.48	106	49.40	7.82	1.34	0.20	0.25	0.33	0.901
850921	0711	47.56	34	07.50	106	49.26	8.39	0.81	0.26	0.30	0.30	0.796
850921	0732	31.93	34	07.38	106	49.58	8.06	1.01	0.25	0.30	0.31	0.644
850921	0804	00.41	34	07.63	106	49.61	7.87	2.08	0.20	0.19	0.35	0.721
850921	1906	25.46	34	07.89	106	49.55	8.68	0.29	0.35	0.43	0.44	0.777
850928	0926	41.51	34	07.41	106	49.42	8.69	1.02	0.24	0.34	0.44	0.795
850929	0354	49.27	34	07.58	106	49.76	8.44	1.93	0.22	0.24	0.50	0.644
851015	0158	17.41	34	07.90	106	49.43	8.96	0.15	0.33	0.67	0.39	0.392
851017	0431	20.28	34	07.46	106	49.45	8.03	0.90	0.24	0.35	0.43	0.567
851017	1322	39.01	34	07.49	106	49.59	8.70	1.57	0.22	0.22	0.43	0.885
851017	1421	32.89	34	07.47	106	49.79	8.36	0.82	0.24	0.39	0.63	0.673
851028	0829	38.90	34	07.74	106	49.68	7.77	1.44	0.20	0.20	0.37	0.914
851124	0316	31.70	34	07.55	106	49.71	8.48	0.88	0.24	0.46	0.37	0.608
851225	0738	14.53	34	06.32	106	49.43	6.13	1.14	0.25	0.36	0.48	0.528
860106	0705	38.34	34	07.50	106	49.57	8.21	1.01	0.24	0.38	0.47	0.641
860114	0004	29.81	34	07.62	106	49.49	7.72	1.93	0.22	0.21	0.39	0.624
860205	0130	54.75	34	07.49	106	49.49	7.98	1.08	0.22	0.29	0.36	0.659
860213	0243	18.66	34	07.37	106	49.52	9.15	1.62	0.22	0.25	0.35	0.610
860329	0853	27.89	34	07.61	106	49.58	8.53	0.78	0.26	0.34	0.42	0.532
860404	1733	20.85	34	08.36	106	49.67	7.12	2.10	0.21	0.21	0.42	0.861
860429	1209	03.98	34	06.94	106	50.37	7.63	2.08	0.23	0.21	0.45	0.593
860429	1754	31.80	34	07.46	106	49.79	8.60	0.98	0.30	0.29	0.38	0.819
860501	1600	57.84	34	07.31	106	49.21	6.80	1.23	0.43	0.44	0.47	0.940
860508	1859	50.25	34	06.79	106	50.02	9.00	0.85	0.25	0.35	0.42	1.261
820919	2225	35.85	34	02.04	107	03.59	9.27	0.43	0.39	0.49	0.44	0.805

yymmdd	hhmm	sec	latitude	longitude	depth	mag	xerr	yerr	derr	R
830304	1820	06.91	34 18.19	106 52.68	4.63	1.21	0.25	0.41	0.47	0.493
830428	0210	21.65	34 06.88	106 51.92	4.37	0.57	0.30	0.33	0.53	0.670
840227	0102	06.93	34 01.77	106 59.68	6.54	-0.07	0.38	0.51	0.37	0.689
840716	1612	15.60	34 04.49	106 50.61	6.55	0.04	0.29	0.31	0.57	0.730
840722	1655	38.07	34 04.50	106 50.62	7.97	-0.20	0.23	0.32	0.53	0.685
840902	2157	39.89	33 56.73	106 59.28	5.78	0.01	0.31	0.40	0.68	0.572
840910	0630	03.89	33 56.65	106 59.18	5.41	-0.08	0.38	0.25	0.63	0.747
840922	0515	16.64	34 10.51	106 52.07	7.00	0.02	0.33	0.57	0.41	0.524
841007	1148	43.33	34 11.13	106 52.39	6.25	0.77	0.28	0.32	0.54	0.523
841007	1349	05.76	34 00.18	106 57.81	9.72	-0.17	0.27	0.35	0.42	0.575
841013	2055	00.56	34 11.23	106 52.33	6.37	0.05	0.25	0.44	0.63	0.748
841029	0908	25.26	34 07.93	106 52.21	6.61	0.25	0.30	0.34	0.56	0.755
850301	2206	07.60	34 06.09	106 59.36	10.4	0.22	0.25	0.49	0.44	0.643
850321	0917	51.31	34 26.32	106 54.82	5.52	0.07	0.38	0.64	0.59	0.904
850324	1105	47.11	34 18.35	107 01.50	5.78	0.32	0.36	0.49	0.47	0.564
850329	0913	06.40	34 18.55	107 01.46	5.68	0.33	0.31	0.46	0.69	0.571
850407	0028	44.69	34 14.19	106 51.82	4.76	1.02	0.28	0.33	0.62	0.399
850501	1219	26.11	34 04.33	106 55.06	2.59	0.52	0.27	0.31	0.61	0.616
850708	0434	18.60	34 05.56	106 58.16	3.07	0.35	0.56	0.55	0.46	0.937
850817	18 4	24.80	34 07.46	106 49.68	7.61	0.14	0.29	0.34	0.47	0.710
850817	1949	24.71	34 07.83	106 49.32	8.24	0.13	0.26	0.51	0.54	0.597
850819	2223	50.83	33 56.55	106 59.72	4.92	0.41	0.35	0.42	0.80	0.580
851013	1223	34.14	34 22.74	107 03.22	9.04	0.03	0.44	0.45	0.63	0.549
851014	0421	28.39	34 04.88	106 55.87	3.68	0.09	0.48	0.54	0.40	0.576
851018	0616	05.67	34 18.59	106 51.68	5.28	-0.35	0.31	0.50	0.36	0.662
851103	0240	24.12	34 05.40	106 51.23	6.23	0.34	0.34	0.54	0.54	0.617
860219	0732	51.48	33 59.60	106 58.81	9.84	-0.24	0.41	0.44	0.48	0.537
860220	1444	41.88	34 01.73	106 59.05	7.51	-0.08	0.36	0.55	0.45	0.959
860222	1158	06.86	34 02.02	107 04.02	8.24	0.87	0.29	0.29	0.40	0.506
860310	0458	30.66	34 17.25	106 55.30	6.61	-0.53	0.27	0.40	0.45	0.489
860325	0902	09.70	34 02.47	107 03.74	8.84	-0.23	0.40	0.48	0.34	0.850
860405	1452	20.91	34 19.39	107 00.80	6.22	1.13	0.32	0.59	0.54	0.514
860531	0031	08.19	34 01.16	107 03.42	8.25	-0.03	0.26	0.40	0.36	0.514
860808	0708	00.40	33 59.56	106 59.70	4.38	0.15	0.28	0.23	0.51	0.697
860831	0101	10.82	34 12.92	106 53.01	7.43	0.31	0.29	0.30	0.45	0.538
861103	1236	57.11	34 00.02	106 58.00	9.82	-0.10	0.31	0.37	0.34	0.598
861106	1857	59.91	34 00.17	106 58.11	10.0	0.16	0.30	0.27	0.43	0.643
870822	1049	44.20	34 09.51	106 44.15	7.76	0.62	0.25	0.25	0.53	0.731
871103	0211	15.25	33 59.40	106 58.86	8.18	0.55	0.24	0.23	0.42	0.876
871124	0352	01.87	33 58.43	106 59.13	5.36	0.12	0.23	0.29	0.36	0.782
871218	0125	45.02	34 08.18	106 54.97	4.92	0.22	0.32	0.33	0.61	0.695
871227	2211	55.84	34 23.58	107 03.51	3.31	0.70	0.25	0.39	0.57	0.794
880121	1519	26.98	34 18.57	106 52.98	6.09	-0.31	0.35	0.42	0.49	0.602
880125	0318	49.65	33 57.12	107 02.86	5.97	0.05	0.29	0.24	0.58	0.672
880127	1359	26.03	34 03.15	107 02.95	8.49	-0.22	0.24	0.28	0.31	0.641
880128	1749	54.95	34 01.09	107 02.84	8.40	0.81	0.25	0.24	0.36	0.826
880204	2354	26.45	34 02.58	106 53.57	9.03	-0.10	0.28	0.44	0.43	0.424
880301	0759	16.82	34 01.80	106 59.25	8.55	0.04	0.35	0.43	0.33	0.745
880306	0419	16.96	34 01.62	106 59.24	9.15	0.19	0.24	0.34	0.38	0.750
880317	0815	54.01	34 03.19	107 03.85	7.55	0.28	0.34	0.47	0.44	0.776
880416	2123	54.49	34 00.79	106 48.52	6.64	0.33	0.30	0.41	0.59	0.632
880424	0918	39.82	34 01.70	107 02.43	9.40	0.24	0.30	0.35	0.32	0.590

yymmdd	hhmm	sec	latitude		longitude		depth	mag	xerr	yerr	derr	R
880428	1613	18.16	33	58.61	106	54.82	5.65	0.48	0.31	0.29	0.78	0.524
880503	2134	03.85	34	07.42	106	49.44	8.36	0.10	0.30	0.36	0.52	0.589
880516	1521	07.25	34	02.03	107	01.49	9.65	0.28	0.25	0.27	0.32	1.539
880618	1658	13.13	34	18.82	106	54.86	5.51	0.28	0.31	0.44	0.67	0.564
880722	0811	00.13	34	17.72	106	40.88	7.72	0.51	0.49	0.54	0.66	0.617
880818	1623	04.19	33	55.04	106	57.04	4.58	0.67	0.33	0.38	0.76	0.737
880930	1428	27.19	34	08.15	106	54.52	3.01	0.39	0.31	0.32	0.75	0.609
881003	0103	10.45	34	05.31	107	02.34	8.12	0.54	0.38	0.47	0.61	0.633
881027	0426	49.45	34	07.71	106	55.35	2.67	0.04	0.34	0.46	0.58	0.780
890927	2343	08.32	34	00.98	107	01.82	9.55	0.31	0.26	0.42	0.63	0.559
891027	0650	51.26	33	59.98	106	58.23	9.85	0.68	0.25	0.29	0.43	0.879
900419	2215	28.58	34	23.22	106	47.73	5.57	1.59	0.31	0.39	0.74	0.578
900505	2055	55.44	34	27.09	106	53.14	4.98	0.45	0.28	0.67	0.63	0.698
900506	0711	59.47	34	26.98	106	52.96	5.56	0.44	0.27	0.44	0.53	0.854
900603	0008	08.26	34	26.72	106	53.12	4.97	-0.06	0.25	0.40	0.43	0.994
900603	1114	14.03	34	26.77	106	53.48	4.28	0.16	0.25	0.38	0.36	1.017
900613	1236	06.82	34	27.23	106	52.59	7.14	0.33	0.28	0.53	0.61	0.884
900621	1554	46.26	34	27.25	106	52.73	6.86	0.65	0.26	0.44	0.48	1.022
900901	0841	23.91	34	18.53	107	07.13	9.12	0.33	0.37	0.35	0.38	0.711
900901	1047	32.89	34	18.29	107	07.22	9.41	0.98	0.28	0.29	0.36	0.749
860416	0129	41.19	34	00.98	106	49.81	5.61	0.36	0.35	0.39	0.78	1.075
860416	0136	10.25	34	01.12	106	49.55	6.39	0.80	0.23	0.25	0.38	1.305
860416	1509	43.92	34	00.91	106	49.55	6.12	0.50	0.30	0.35	0.41	0.899
850418	0521	54.19	34	00.99	106	49.51	6.78	0.45	0.25	0.31	0.42	1.099
860419	0344	31.40	34	01.21	106	49.36	6.50	0.98	0.25	0.31	0.41	1.070
860426	1054	12.97	34	01.07	106	49.22	5.20	0.84	0.23	0.23	0.36	1.043
860426	2258	57.53	34	00.72	106	49.62	7.01	0.29	0.31	0.29	0.47	1.071
860427	0118	54.47	34	00.89	106	49.37	7.21	0.44	0.26	0.28	0.44	0.818
860427	0645	45.02	34	01.15	106	49.45	6.39	0.34	0.32	0.41	0.45	1.112
860427	0918	23.41	34	01.20	106	49.40	6.09	0.74	0.24	0.24	0.36	1.248
860427	1025	36.95	34	01.10	106	49.40	6.68	0.28	0.33	0.46	0.46	1.052
860427	1141	42.99	34	01.13	106	49.33	6.43	0.60	0.23	0.24	0.41	1.250
860427	1814	31.14	34	01.15	106	49.35	6.21	0.67	0.23	0.23	0.31	0.970
860427	1815	00.89	34	01.19	106	49.45	6.56	0.62	0.23	0.24	0.34	1.085
860427	2217	36.46	34	01.09	106	49.34	6.86	0.46	0.26	0.29	0.40	0.809
860427	2346	55.29	34	01.26	106	49.26	6.28	0.50	0.30	0.41	0.50	1.074
860427	2358	19.48	34	01.27	106	49.35	5.69	1.81	0.31	0.25	0.40	1.187
860428	0042	18.28	34	01.03	106	49.27	6.41	0.34	0.30	0.40	0.45	1.022
860428	0044	36.53	34	00.91	106	49.36	6.30	0.59	0.25	0.27	0.34	0.819
860428	0100	30.12	34	01.11	106	49.35	6.42	0.11	0.35	0.36	0.44	0.900
860428	0106	08.64	34	01.27	106	49.21	6.07	0.08	0.37	0.38	0.55	0.828
860428	0159	09.97	34	01.10	106	49.59	6.60	-0.02	0.48	0.51	0.49	1.310
860428	0308	37.14	34	01.12	106	49.50	6.37	1.10	0.22	0.23	0.34	1.179
860428	0315	04.59	34	01.08	106	49.61	6.69	1.77	0.23	0.22	0.43	1.307
860428	0315	58.02	34	01.12	106	49.45	7.18	0.54	0.24	0.25	0.39	1.180
860428	0324	02.84	34	01.02	106	49.50	6.10	0.39	0.29	0.34	0.42	1.180
860428	0325	55.11	34	00.99	106	49.49	6.67	1.03	0.25	0.34	0.39	1.076
860428	0350	03.59	34	00.98	106	49.60	6.90	1.22	0.24	0.24	0.38	1.103
860428	0359	58.02	34	01.21	106	49.33	5.93	1.39	0.27	0.28	0.39	1.089
860428	0401	28.63	34	01.21	106	49.40	6.36	0.49	0.29	0.36	0.34	1.055
860428	0537	33.38	34	01.20	106	49.58	6.38	0.61	0.23	0.24	0.35	1.221
860428	0542	04.26	34	01.06	106	49.74	6.55	1.79	0.25	0.23	0.41	1.262

yymmdd	hhmm	sec	latitude	longitude	depth	mag	xerr	yerr	derr	R
860428	0547	57.45	34 01.17	106 49.44	6.45	1.20	0.22	0.24	0.35	1.219
860428	0633	14.10	34 01.41	106 49.26	6.28	0.17	0.37	0.52	0.43	1.226
860428	0648	27.27	34 01.24	106 49.39	6.10	1.06	0.22	0.28	0.31	1.168
860428	0708	56.25	34 01.00	106 49.75	5.91	0.38	0.35	0.37	0.42	1.043
860428	0720	22.77	34 01.26	106 49.83	6.26	1.69	0.23	0.23	0.39	1.032
860428	0759	13.61	34 01.02	106 49.70	6.43	1.25	0.22	0.25	0.30	1.331
860428	0830	36.61	34 01.27	106 49.38	5.89	0.08	0.52	0.61	0.57	0.685
860428	0848	05.21	34 01.04	106 49.70	6.10	0.30	0.50	0.70	0.49	1.127
860428	0853	18.09	34 01.08	106 49.96	6.39	0.37	0.43	0.38	0.46	0.959
860428	0944	57.22	34 01.20	106 49.47	6.97	0.33	0.28	0.35	0.42	1.085
860428	1013	58.29	34 01.11	106 49.48	6.54	0.91	0.22	0.29	0.33	1.057
860428	1109	56.19	34 01.00	106 49.72	6.70	0.63	0.25	0.27	0.34	1.228
860428	1118	34.33	34 01.14	106 49.32	6.51	0.12	0.33	0.46	0.55	0.859
860428	1151	37.76	34 01.12	106 49.65	6.28	1.55	0.24	0.25	0.42	1.268
860428	1236	56.97	34 01.02	106 49.56	6.84	0.41	0.25	0.28	0.42	1.176
860428	1259	43.26	34 01.23	106 49.41	5.81	0.51	0.27	0.33	0.42	0.762
860428	1259	49.48	34 01.11	106 49.28	6.96	3.09	0.26	0.26	0.58	0.925
860428	1302	35.41	34 01.28	106 50.29	5.89	0.27	0.56	0.41	0.51	0.699
860428	1318	34.59	34 01.24	106 49.85	5.80	0.33	0.42	0.39	0.49	0.769
860428	1332	34.79	34 01.24	106 49.97	5.78	1.07	0.27	0.26	0.54	1.038
860428	1341	11.09	34 00.84	106 49.91	6.15	0.27	0.55	0.46	0.54	0.713
860428	1510	50.28	34 00.94	106 49.42	6.63	0.45	0.26	0.26	0.46	1.212
860428	1537	57.38	34 00.96	106 49.54	6.47	0.68	0.23	0.24	0.46	1.041
860428	1656	06.75	34 01.06	106 49.63	6.26	0.44	0.29	0.30	0.41	1.067
860428	1901	24.77	34 01.03	106 49.55	5.69	0.19	0.50	0.41	0.44	0.732
860429	0047	19.60	34 01.24	106 49.63	6.29	0.48	0.38	0.42	0.38	0.947
860429	0114	35.43	34 01.45	106 49.64	6.36	0.06	0.47	0.54	0.52	0.914
860429	0248	48.48	34 01.19	106 49.61	5.68	0.64	0.28	0.32	0.40	0.778
860429	0252	59.69	34 01.21	106 49.78	6.00	0.54	0.37	0.33	0.44	0.826
860429	0321	12.36	34 01.21	106 49.65	6.20	0.26	0.42	0.47	0.55	1.038
860429	0332	24.44	34 01.42	106 49.38	6.33	0.82	0.26	0.34	0.36	0.928
860429	0507	34.78	34 01.08	106 49.77	6.38	0.43	0.34	0.34	0.58	1.107
860429	0530	22.95	34 01.19	106 49.39	5.79	1.04	0.22	0.32	0.40	1.192
860429	0620	53.51	34 01.16	106 49.88	6.82	0.55	0.27	0.33	0.46	0.955
860429	0625	47.42	34 01.25	106 49.67	6.78	0.65	0.33	0.35	0.69	0.659
860429	0649	39.98	34 01.22	106 49.30	7.46	0.89	0.24	0.32	0.53	0.894
860429	0652	00.01	34 01.31	106 49.89	6.00	0.49	0.42	0.33	0.52	1.057
860429	0730	26.00	34 00.97	106 50.15	5.74	0.31	0.62	0.52	0.52	0.607
860429	0747	02.75	34 01.20	106 49.58	5.92	0.46	0.38	0.41	0.51	1.013
860429	0828	23.07	34 01.50	106 49.32	6.28	0.67	0.34	0.43	0.52	1.160
860429	0830	31.26	34 01.46	106 49.48	6.09	2.12	0.22	0.30	0.40	1.159
860429	0831	32.98	34 01.43	106 49.49	6.26	0.83	0.23	0.34	0.41	1.145
860429	0835	13.49	34 01.07	106 49.57	6.25	1.46	0.22	0.24	0.37	1.039
860429	1022	09.81	34 01.08	106 49.79	6.11	0.39	0.44	0.36	0.45	1.034
860429	1229	18.50	34 01.33	106 50.13	5.66	0.28	0.53	0.37	0.56	0.794
860429	1520	18.20	34 01.22	106 49.51	5.92	1.25	0.23	0.22	0.32	0.959
860429	1532	49.61	34 01.24	106 49.62	6.36	0.26	0.31	0.32	0.46	1.113
860429	1603	54.11	34 01.22	106 49.72	6.73	0.69	0.33	0.32	0.46	0.950
860429	1642	51.02	34 01.31	106 49.93	6.20	0.38	0.28	0.30	0.35	1.525
860429	2154	44.89	34 01.41	106 48.75	6.70	0.41	0.42	0.46	0.58	1.067
860430	0007	39.58	34 01.16	106 49.47	6.62	0.55	0.27	0.23	0.27	1.321
860430	0011	26.08	34 01.20	106 48.99	6.09	0.18	0.42	0.35	0.43	1.039

yymmdd	hhmm	sec	latitude	longitude	depth	mag	xerr	yerr	derr	R
860430	0128	29.64	34 01.32	106 49.35	6.20	0.87	0.20	0.21	0.22	1.325
860430	0131	52.38	34 01.28	106 49.33	6.64	0.38	0.29	0.36	0.34	0.877
860430	1319	56.74	34 01.07	106 49.53	5.59	0.06	0.34	0.47	0.45	0.764
860430	0407	44.56	34 01.40	106 49.43	6.26	1.15	0.21	0.21	0.23	1.230
860430	0447	34.54	34 01.39	106 49.52	6.63	0.19	0.45	0.44	0.40	0.849
860430	0539	53.03	34 01.23	106 49.38	6.49	1.09	0.22	0.22	0.27	1.092
860430	0612	59.72	34 00.67	106 49.38	5.95	0.06	0.80	0.95	0.93	0.338
860430	0641	49.02	34 01.23	106 49.45	6.91	0.98	0.24	0.25	0.31	1.272
860430	0642	03.96	34 00.82	106 49.37	6.47	0.17	0.39	0.50	0.56	0.737
860430	0758	55.86	34 00.82	106 49.51	5.59	0.12	0.85	0.43	0.60	0.740
860430	1031	21.01	34 01.28	106 49.46	6.21	0.09	0.28	0.35	0.40	0.965
860430	1203	51.15	34 01.17	106 49.44	6.10	1.61	0.30	0.69	0.44	0.846
860430	1414	44.20	34 01.27	106 49.26	6.00	0.27	0.52	0.59	0.47	0.623
860430	1612	19.10	34 01.39	106 49.25	6.21	1.35	0.21	0.20	0.28	1.303
860430	1615	28.04	34 01.41	106 49.70	6.49	1.18	0.23	0.22	0.25	1.401
860430	1731	07.09	34 01.21	106 49.31	6.02	0.24	0.46	0.41	0.46	0.664
860430	1806	54.06	34 01.42	106 49.62	6.78	0.53	0.36	0.36	0.34	0.989
860501	0353	29.45	34 01.37	106 49.39	6.82	0.39	0.33	0.32	0.32	0.939
860501	0610	04.48	34 01.20	106 48.67	6.06	0.14	0.60	0.39	0.51	0.488
860501	0635	10.77	34 00.95	106 49.24	6.15	0.06	0.78	0.68	0.61	0.310
860501	0932	07.55	34 01.27	106 49.42	6.53	0.56	0.29	0.26	0.28	1.378
860501	1143	37.10	34 01.61	106 49.25	6.41	0.41	0.36	0.37	0.43	1.402
860501	1336	56.97	34 01.05	106 48.96	6.14	0.36	0.36	0.34	0.32	1.181
860501	1605	39.03	34 01.28	106 48.73	5.87	0.13	0.70	0.48	0.50	0.691
860501	1628	33.09	34 01.03	106 49.11	6.95	1.92	0.22	0.23	0.30	1.023
860501	1906	59.56	34 00.93	106 49.08	7.22	0.49	0.36	0.34	0.39	0.896
860501	1918	14.96	34 01.11	106 48.84	6.94	0.13	0.54	0.39	0.35	0.566
860501	1939	47.26	34 01.17	106 48.76	6.37	0.42	0.54	0.41	0.42	0.595
860501	2130	25.79	34 01.23	106 49.43	6.59	0.49	0.34	0.36	0.36	0.923
860502	0232	56.71	34 01.14	106 49.59	6.53	0.31	0.31	0.36	0.33	0.852
860502	0348	51.49	34 00.97	106 49.43	6.47	0.34	0.32	0.37	0.38	0.942
860502	0412	19.44	34 01.05	106 49.33	6.40	0.35	0.26	0.32	0.34	1.062
860502	1245	21.01	34 01.13	106 50.00	6.05	0.27	0.43	0.39	0.37	1.049
860502	2144	02.47	34 00.84	106 49.39	8.04	0.45	0.55	0.44	0.45	1.580
860503	0646	30.49	34 01.17	106 50.07	5.98	0.47	0.31	0.32	0.45	1.092
860504	0749	14.89	34 01.05	106 49.59	6.67	0.91	0.24	0.25	0.47	1.361
860504	1810	16.05	34 01.00	106 49.37	6.70	1.75	0.22	0.24	0.37	1.078
860504	1950	03.91	34 01.15	106 49.58	6.20	0.58	0.26	0.24	0.36	1.205
860504	2230	39.59	34 01.13	106 49.51	6.88	1.49	0.22	0.23	0.34	1.213
860505	1442	16.68	34 01.02	106 49.76	5.23	0.50	0.34	0.30	0.41	1.086
860505	1447	01.39	34 00.96	106 49.79	6.34	0.57	0.27	0.26	0.37	1.067
860510	0648	14.32	34 01.20	106 49.52	6.41	1.84	0.26	0.41	0.37	1.202
860510	0648	46.44	34 01.17	106 49.30	6.52	1.07	0.31	0.43	0.44	0.778
860511	1503	57.62	34 01.09	106 49.60	5.30	2.44	0.22	0.22	0.43	1.141
860511	1743	33.44	34 01.44	106 49.16	6.16	0.75	0.33	0.42	0.46	1.095
860511	1801	16.39	34 01.23	106 49.66	6.27	1.14	0.22	0.24	0.31	1.537
860511	2105	29.45	34 01.16	106 49.24	5.91	0.56	0.25	0.31	0.38	1.033
860511	2107	08.66	34 01.11	106 49.38	6.09	1.03	0.24	0.26	0.40	1.267
860511	2202	27.36	34 01.12	106 49.46	6.89	0.42	0.40	0.42	0.55	0.842
860512	0551	30.39	34 01.07	106 49.29	6.42	0.57	0.29	0.39	0.47	1.020
860513	1728	02.96	34 01.16	106 49.64	6.07	1.74	0.24	0.24	0.37	1.078
860514	0621	32.72	34 01.07	106 50.22	6.23	0.38	0.53	0.42	0.51	1.116

yymmdd	hhmm	sec	latitude		longitude		depth	mag	xerr	yerr	derr	R
860514	0645	44.89	34	01.02	106	49.47	6.32	0.97	0.22	0.23	0.38	0.965
860514	1244	17.51	34	01.09	106	49.58	7.04	1.28	0.21	0.23	0.38	1.104
860515	1316	21.30	34	01.13	106	49.52	6.45	1.74	0.23	0.24	0.47	1.160
860523	1801	34.44	34	01.44	106	49.53	6.76	1.29	0.21	0.24	0.43	1.042
750603	1510	15.65	34	01.46	107	02.04	9.01	-0.03	0.39	0.37	0.23	1.136
750616	2343	21.11	34	01.59	107	02.14	8.40	-0.22	0.35	0.34	0.27	1.069
750805	1419	22.51	34	01.41	107	02.77	8.83	-0.27	0.38	0.38	0.24	0.730
750813	0338	51.27	34	04.53	106	55.53	7.20	0.83	0.26	0.33	0.24	0.602
750813	0739	18.61	34	04.39	106	55.66	7.39	0.04	0.27	0.29	0.32	0.660
750813	1122	26.79	34	00.64	106	58.63	9.82	-0.12	0.32	0.38	0.31	0.535
750819	0811	46.87	34	03.08	106	58.04	9.11	-0.28	0.38	0.34	0.29	0.443
750819	1000	07.27	33	59.22	107	00.50	10.1	0.25	0.35	0.40	0.38	0.335
750820	1220	52.28	34	04.46	106	54.85	7.37	-0.07	0.31	0.35	0.30	0.950
750820	0344	48.84	34	01.43	107	02.56	8.20	0.77	0.40	0.34	0.27	0.362
750821	1918	42.16	34	02.94	106	57.92	9.56	0.27	0.34	0.32	0.27	0.883
751104	1630	11.94	34	02.34	107	03.86	8.00	-0.11	0.45	0.35	0.24	0.632
760123	0253	33.10	34	01.88	107	02.08	8.44	0.36	0.35	0.50	0.27	0.550
760129	1506	40.18	33	59.11	106	58.99	7.39	0.94	0.28	0.34	0.34	0.603
760217	0617	49.28	34	01.84	107	03.72	8.48	-0.76	0.50	0.65	0.33	0.386
760218	0544	56.15	34	01.10	107	03.26	8.57	-0.55	0.43	0.45	0.25	0.624
760218	2325	35.36	34	02.12	107	04.40	8.83	-0.32	0.50	0.34	0.26	0.745
760219	0008	36.99	34	01.22	107	03.46	8.58	0.15	0.40	0.33	0.20	0.734
760220	1251	45.42	34	01.19	107	02.93	8.92	-0.44	0.39	0.51	0.23	0.550
760413	0945	40.91	34	04.10	107	00.92	6.99	-0.36	0.43	0.29	0.28	0.773
760413	1141	25.65	34	02.07	107	03.71	8.31	-0.66	0.44	0.42	0.25	0.580
760414	0150	28.86	33	58.80	107	00.66	10.1	-0.62	0.50	0.46	0.24	0.656
760415	1155	20.18	34	03.99	107	01.34	6.44	-0.62	0.41	0.28	0.30	0.694
760416	1407	33.51	34	04.02	106	59.46	6.55	0.83	0.45	0.27	0.22	0.766
760608	0750	39.87	34	02.98	106	59.72	9.43	-0.82	0.53	0.33	0.25	0.558
760630	0844	01.76	34	00.61	107	02.12	9.08	-0.45	0.32	0.45	0.34	1.003
760715	1058	34.36	34	01.17	107	04.07	9.10	-0.42	0.24	0.40	0.21	0.945
760810	1228	42.03	34	03.50	106	59.93	9.16	0.20	0.31	0.44	0.24	0.909
760812	0456	05.46	34	03.28	107	00.18	8.50	0.73	0.30	0.34	0.33	0.944
760824	0131	13.88	34	03.04	107	01.32	6.16	-0.37	0.26	0.31	0.31	1.154
760827	0815	28.38	34	00.91	107	03.66	9.02	-0.15	0.33	0.50	0.29	0.476
760903	1324	58.45	34	00.37	106	58.72	10.5	-0.47	0.38	0.35	0.28	1.067
761007	2237	37.83	34	02.14	107	02.12	8.99	0.31	0.27	0.42	0.21	0.286
770121	1642	28.69	34	00.58	107	03.43	8.48	-0.44	0.32	0.38	0.25	1.142
770209	1059	58.90	34	01.18	106	59.96	6.91	0.29	0.33	0.29	0.30	0.531
770216	1444	49.60	34	00.89	107	03.20	8.77	-0.31	0.37	0.34	0.21	0.596
770308	0430	41.87	34	00.48	107	03.61	8.71	-0.23	0.31	0.48	0.31	0.425
770427	0804	40.36	34	01.58	107	01.74	4.28	-0.12	0.25	0.36	0.36	0.798
770427	1215	56.43	34	01.18	107	03.45	8.36	0.07	0.28	0.34	0.25	0.781
770428	1059	10.67	34	02.82	107	03.11	7.97	0.27	0.27	0.40	0.17	0.539
770602	0650	24.44	34	00.52	107	03.85	8.31	0.45	0.27	0.42	0.30	0.541
770603	2045	03.22	34	14.10	106	54.03	6.57	0.78	0.41	0.29	0.37	0.840
770714	1000	32.79	34	09.91	106	52.22	6.27	0.41	0.27	0.25	0.29	0.800
770714	1131	51.12	34	09.85	106	52.76	6.46	0.56	0.28	0.34	0.51	0.799
770715	1226	25.98	34	00.89	107	03.80	7.80	0.62	0.26	0.31	0.25	0.818
770727	1808	20.15	34	10.09	106	54.97	7.07	0.90	0.28	0.35	0.35	1.020
770817	0603	19.97	34	10.46	106	52.53	6.60	0.58	0.34	0.26	0.30	1.304
770817	1537	22.00	34	16.03	106	55.39	5.77	0.81	0.28	0.30	0.38	0.864

yymmdd	hhmm	sec	latitude	longitude	depth	mag	xerr	yerr	derr	R
770818	0811	19.54	34 20.63	106 53.19	7.68	0.56	0.41	0.30	0.39	1.326
770818	0930	13.52	34 09.83	106 52.24	5.40	-0.09	0.27	0.38	0.37	0.569
770818	1038	14.96	34 01.63	107 03.67	8.20	1.05	0.27	0.43	0.31	0.719
770819	0351	00.36	34 01.37	107 03.65	7.69	0.28	0.25	0.34	0.30	0.985
770819	0928	23.03	34 01.41	107 03.92	8.79	0.23	0.29	0.44	0.35	0.936
770824	1122	35.93	34 00.83	107 03.44	8.66	0.17	0.29	0.30	0.24	0.928
770825	0452	33.05	33 58.08	106 57.47	6.87	0.35	0.49	0.55	0.45	0.607
770825	0626	27.18	34 01.01	107 03.60	8.27	0.29	0.27	0.27	0.22	1.025
770901	0314	33.42	34 10.61	106 52.71	5.73	0.04	0.38	0.57	0.32	0.709
770902	0741	11.90	33 59.30	106 59.70	5.04	-0.13	0.35	0.35	0.30	0.671
770914	1741	16.32	34 20.72	106 52.98	5.24	0.95	0.23	0.28	0.52	1.074
770915	0053	35.46	34 02.25	107 03.39	8.20	0.53	0.29	0.40	0.22	1.322
770915	0101	34.30	34 15.73	106 55.20	6.10	0.50	0.22	0.25	0.30	0.698
770915	0645	16.83	34 20.95	106 52.82	5.09	0.53	0.24	0.27	0.44	1.092
770915	1143	34.25	34 18.97	106 55.19	6.30	0.32	0.27	0.24	0.32	1.082
770916	0804	08.25	34 04.04	106 59.51	5.80	-0.30	0.33	0.63	0.44	0.691
770920	0819	23.24	34 09.69	106 52.41	5.94	0.40	0.22	0.31	0.37	0.692
770921	0609	08.62	34 10.02	106 52.15	5.51	-0.13	0.23	0.34	0.30	0.817
770921	1921	54.97	34 24.62	107 00.12	4.36	0.52	0.49	0.42	0.42	1.032
770922	0520	27.85	34 20.45	106 52.94	6.89	1.19	0.25	0.29	0.34	0.800
770922	0822	18.23	34 09.77	106 52.06	5.61	-0.13	0.28	0.38	0.32	0.799
770922	1919	16.77	34 20.42	106 53.12	7.86	0.95	0.25	0.27	0.35	1.315
771018	0816	32.82	34 01.57	107 03.54	8.75	0.76	0.29	0.45	0.27	0.910
771115	1902	41.67	34 08.80	106 53.29	6.28	0.52	0.31	0.35	0.26	1.080
771215	1715	40.62	34 19.45	107 03.51	8.04	0.62	0.52	0.24	0.30	0.839
771221	0259	38.84	34 16.01	106 51.94	6.45	-0.41	0.25	0.30	0.37	1.312
780105	1203	23.30	34 16.62	106 53.65	6.35	0.26	0.22	0.25	0.27	1.173
780105	1327	47.38	34 13.60	106 55.54	7.01	0.21	0.30	0.52	0.26	1.021
780106	0149	02.79	34 13.05	106 59.54	4.91	0.31	0.45	0.28	0.22	0.412
780117	0505	01.34	34 19.10	106 44.24	8.06	0.25	0.27	0.35	0.24	1.018
780117	2314	21.30	34 21.05	106 52.70	6.73	0.05	0.37	0.52	0.39	0.816
780118	1224	32.79	34 09.98	106 51.89	5.69	0.87	0.29	0.52	0.23	1.316
820923	2332	31.03	33 54.74	106 38.74	4.07	1.85	0.44	0.45	0.59	0.784
950311	0744	57.07	33 52.54	106 34.09	4.87	1.40	0.63	0.49	0.69	1.027
830429	1734	27.55	34 20.85	106 41.72	8.25	1.30	0.29	0.28	0.95	1.491
830727	0925	49.45	34 04.06	106 57.68	8.09	1.39	0.63	0.51	0.35	0.854
840505	0832	34.25	34 12.48	106 42.53	10.1	1.70	0.36	0.31	0.80	0.721
900901	1047	32.94	34 18.20	107 07.28	8.98	1.42	0.46	0.37	0.53	0.685
901130	1819	53.50	34 02.64	107 02.86	9.26	1.50	0.31	0.28	0.81	0.853
901215	1217	35.32	34 05.13	106 55.09	4.29	1.78	0.25	0.24	0.53	0.667
930118	1837	32.27	34 26.27	106 59.86	3.41	1.17	0.46	0.87	0.77	0.517
930122	0516	38.25	34 04.97	106 38.52	6.97	1.12	0.89	0.50	0.89	0.531
940312	1753	28.43	34 21.91	106 43.99	7.59	1.11	0.50	0.72	0.86	0.750
940315	1215	41.91	34 21.72	106 43.24	9.85	0.96	0.54	0.72	0.83	0.950
940317	0742	43.01	34 01.20	106 57.76	8.99	0.83	0.38	0.40	0.50	0.952
940919	2317	49.40	33 57.02	106 58.25	7.79	0.45	0.34	0.35	0.71	1.494
941029	0231	32.23	34 04.31	106 55.33	5.07	1.03	0.33	0.44	0.82	0.800
941113	1519	43.83	34 09.90	106 56.97	2.86	0.90	0.49	0.49	0.79	0.620
941126	0852	21.91	34 11.88	106 54.99	6.36	1.02	0.35	0.41	0.76	0.594
941128	1217	41.39	34 18.09	106 36.81	4.38	-0.41	0.98	0.62	0.70	0.658
941207	0709	27.72	34 08.68	106 53.43	4.18	0.66	0.40	0.44	0.69	0.802
941230	0019	10.37	34 15.01	106 55.00	6.18	1.30	0.46	0.56	0.87	0.486

yymmdd	hhmm	sec	latitude	longitude	depth	mag	xerr	yerr	derr	R
950312	1924	15.02	34 00.33	107 00.17	1.47	1.89	0.27	0.23	0.55	1.026
950406	1655	22.29	34 18.29	107 00.88	7.09	0.80	0.21	0.27	0.29	0.734
821007	1616	40.26	34 18.72	106 48.72	5.86	0.35	0.28	0.44	0.56	0.812
821026	0104	33.88	34 18.23	106 48.91	7.61	0.73	0.28	0.37	0.62	1.260
821103	0922	27.47	34 18.78	106 48.77	5.32	1.27	0.34	0.48	0.61	0.994
830728	1358	47.66	33 53.31	106 47.30	8.98	2.03	0.34	0.42	0.79	1.035
840503	1802	23.55	34 12.34	106 42.02	7.78	1.14	0.34	0.27	0.94	0.796
861008	0936	58.79	34 08.86	106 44.33	8.23	1.42	0.28	0.21	0.75	0.955
861014	1541	55.63	34 09.02	106 44.45	5.52	1.03	0.26	0.27	0.75	1.005
870501	0412	27.62	33 57.60	106 46.90	2.62	2.11	0.28	0.29	0.98	1.097
950910	1348	15.46	34 06.89	106 49.70	5.60	1.12	0.19	0.23	0.28	0.859
950910	1602	17.05	34 06.99	106 49.72	5.17	1.13	0.16	0.25	0.28	1.078
950910	1902	29.69	34 06.94	106 49.61	5.54	1.09	0.19	0.25	0.27	1.021
950910	2104	49.36	34 07.26	106 49.75	5.47	0.39	0.25	0.53	0.36	0.857
950911	0637	00.74	34 07.10	106 49.61	5.17	0.98	0.19	0.23	0.30	1.234
950911	0759	40.31	34 06.84	106 49.63	4.90	1.01	0.19	0.23	0.31	1.168
950911	0900	58.75	34 06.99	106 49.66	5.81	1.08	0.18	0.25	0.28	1.268
950911	1213	14.67	34 06.65	106 49.60	5.28	1.50	0.19	0.22	0.32	1.004
950911	2122	32.45	34 06.89	106 49.57	5.54	0.92	0.21	0.24	0.32	0.981
950917	1740	17.42	34 06.76	106 49.67	5.34	1.95	0.20	0.22	0.40	0.802
950917	1750	19.45	34 06.89	106 49.68	5.67	1.03	0.20	0.28	0.29	0.897
950918	0310	48.89	34 07.09	106 49.63	5.47	1.18	0.18	0.23	0.28	1.228
950918	0820	55.51	34 06.90	106 49.63	5.08	1.93	0.18	0.22	0.34	1.325
950919	1527	03.49	34 06.87	106 49.59	5.68	1.57	0.20	0.23	0.30	1.053
950920	0909	36.16	34 06.95	106 49.69	5.89	0.84	0.19	0.26	0.29	0.869
950928	2017	04.84	34 06.74	106 49.61	5.72	1.54	0.19	0.22	0.31	0.741
950928	2142	29.66	34 06.79	106 49.62	5.90	1.36	0.19	0.23	0.31	0.801
950904	1759	14.13	34 01.35	106 51.94	4.34	1.40	0.25	0.25	0.58	1.024
950904	1849	52.10	34 06.04	106 48.29	5.54	2.41	0.23	0.25	0.53	0.627
950914	1607	30.02	34 06.05	106 48.24	4.91	1.14	0.19	0.21	0.32	1.033
950922	1037	57.84	34 18.26	106 55.44	6.35	0.84	0.23	0.29	0.41	1.328
950922	2245	56.25	34 21.30	106 42.58	8.71	1.35	0.33	0.43	0.37	0.914
950924	1603	51.57	34 02.00	107 01.73	7.56	1.37	0.20	0.26	0.26	1.415
950924	1606	44.74	34 02.07	107 01.97	9.22	0.16	0.30	0.36	0.29	0.890
950924	1610	25.43	34 01.94	107 01.91	8.89	0.33	0.29	0.35	0.28	0.887
950924	1758	40.95	34 01.78	107 01.69	7.81	1.57	0.21	0.21	0.28	1.225
950924	1810	55.02	34 01.71	107 01.70	8.80	0.59	0.28	0.26	0.29	0.750
950925	0445	57.79	34 01.76	107 01.67	8.54	1.49	0.21	0.22	0.28	1.192
900901	0841	24.01	34 18.23	107 06.73	8.25	0.65	0.28	0.30	0.28	1.450
900901	0843	58.72	34 17.96	107 06.97	8.01	1.20	0.26	0.22	0.38	1.373
900901	0921	02.85	34 18.42	107 07.00	8.79	0.90	0.27	0.24	0.28	1.183
900901	0924	29.32	34 18.42	107 06.69	7.53	0.41	0.31	0.44	0.36	1.164
900901	1047	32.93	34 18.38	107 07.21	8.40	1.33	0.25	0.22	0.32	1.282
900901	2020	26.74	34 18.04	107 06.82	9.44	0.63	0.29	0.33	0.34	1.103
900901	2111	57.38	34 18.26	107 06.91	8.93	0.75	0.26	0.29	0.36	1.025
900901	2131	06.67	34 18.26	107 07.16	9.18	2.06	0.33	0.25	0.49	0.935
900901	2214	20.34	34 18.25	107 07.01	8.96	0.68	0.26	0.27	0.32	0.904
900901	2219	24.97	34 18.04	107 06.81	8.53	0.48	0.32	0.39	0.35	1.081
900902	0115	30.63	34 18.32	107 07.04	8.72	0.91	0.26	0.27	0.32	1.079
900904	0533	35.77	34 18.27	107 07.04	9.60	0.88	0.28	0.29	0.31	1.314
900904	1440	40.15	34 18.39	107 07.36	9.31	2.19	0.31	0.26	0.49	1.349
900904	1722	45.81	34 18.69	107 06.93	9.50	0.72	0.26	0.31	0.32	1.541

yymmdd	hhmm	sec	latitude	longitude	depth	mag	xerr	yerr	derr	R
900904	1723	42.77	34 18.62	107 06.88	8.68	0.41	0.31	0.35	0.39	1.156
900904	1820	09.66	34 17.99	107 07.21	8.72	0.65	0.28	0.34	0.40	1.194
951014	0423	03.70	34 26.86	107 01.08	4.93	1.43	0.24	0.46	0.48	0.924
950828	1556	55.66	34 12.32	106 56.42	3.61	1.52	0.22	0.28	0.35	1.417
950911	0216	06.20	34 12.31	106 56.25	2.73	2.47	0.21	0.23	0.72	0.945
950911	0218	02.50	34 12.31	106 56.15	2.54	2.11	0.21	0.23	0.70	1.331
950911	1141	15.85	34 12.25	106 56.13	2.10	2.38	0.21	0.23	0.81	0.862
951012	1612	24.60	34 12.16	106 56.73	4.43	1.44	0.20	0.22	0.25	1.541
850917	1029	19.20	34 11.49	106 47.93	9.34	0.59	0.24	0.32	0.37	0.972
850917	1031	28.75	34 11.78	106 47.74	10.1	0.19	0.33	0.79	0.61	0.661
850917	1032	40.40	34 11.37	106 47.89	9.37	1.33	0.22	0.22	0.43	1.056
850917	1033	32.55	34 11.56	106 48.18	9.33	0.53	0.22	0.31	0.38	0.677
850917	1033	41.58	34 12.07	106 47.91	9.33	0.49	0.49	0.70	0.71	0.893
850917	1034	57.16	34 11.43	106 47.84	9.41	-0.17	0.52	0.79	0.77	0.732
850917	1036	22.06	34 11.64	106 47.99	9.26	0.76	0.22	0.29	0.35	0.805
850917	1038	02.09	34 11.60	106 48.11	9.69	0.06	0.25	0.37	0.51	0.750
850917	1038	11.95	34 11.67	106 48.09	9.23	0.55	0.31	0.38	0.44	0.785
850917	1039	10.52	34 11.56	106 48.09	9.68	0.48	0.26	0.35	0.45	0.826
850917	1039	58.52	34 11.30	106 47.93	10.2	0.00	0.32	0.75	0.60	0.862
850917	1041	25.90	34 11.53	106 48.03	9.60	1.03	0.24	0.28	0.36	0.838
850917	1105	48.42	34 11.48	106 47.98	9.07	1.90	0.23	0.21	0.44	0.807
850917	1106	25.27	34 11.73	106 47.95	9.43	0.62	0.28	0.41	0.47	0.754
850917	1107	33.45	34 11.61	106 48.02	9.27	0.42	0.30	0.39	0.48	0.749
850917	1129	31.27	34 11.50	106 47.83	10.3	0.13	0.29	0.47	0.55	0.519
850917	1131	27.21	34 11.71	106 47.94	9.33	0.24	0.30	0.46	0.50	0.710
850917	1142	08.34	34 11.49	106 47.95	9.59	1.09	0.22	0.27	0.42	0.674
850917	1950	50.86	34 11.73	106 47.96	9.87	0.99	0.22	0.31	0.39	0.940
850917	1953	33.15	34 11.49	106 48.04	10.0	0.32	0.27	0.36	0.48	0.747
850917	1954	20.86	34 12.02	106 48.02	9.69	0.14	0.30	0.71	0.51	0.514
850917	2134	42.96	34 11.80	106 48.13	10.1	0.66	0.28	0.35	0.44	0.709
850917	2206	07.20	34 11.53	106 48.03	9.66	0.31	0.30	0.47	0.44	0.621
850917	2206	38.59	34 11.53	106 47.57	8.83	0.38	0.26	0.34	0.71	1.351
850917	2206	43.20	34 12.00	106 48.47	7.00	0.56	0.40	0.50	0.00	1.111
850918	1114	55.48	34 11.43	106 48.04	8.82	1.41	0.21	0.20	0.32	0.665
850918	1137	23.00	34 11.55	106 48.23	9.30	0.68	0.24	0.35	0.38	0.955
850918	1148	19.79	34 11.54	106 48.00	10.0	0.32	0.30	0.47	0.59	0.523
850918	1603	37.32	34 11.68	106 47.99	10.2	0.25	0.29	0.54	0.59	0.572
850918	1701	16.67	34 11.26	106 48.02	9.60	1.18	0.23	0.23	0.32	0.927
850918	1702	07.39	34 11.44	106 47.96	10.2	0.22	0.28	0.42	0.55	0.650
850918	1711	27.57	34 11.69	106 48.03	9.91	0.22	0.28	0.43	0.46	0.590
850918	1714	55.89	34 11.44	106 48.07	9.67	0.96	0.22	0.30	0.36	1.052
850918	1716	44.32	34 11.75	106 48.03	9.61	0.36	0.27	0.38	0.41	0.846
850918	1721	13.65	34 11.78	106 48.16	10.2	0.25	0.30	0.54	0.59	0.522
850918	1733	31.58	34 11.65	106 47.88	10.2	0.71	0.22	0.31	0.44	0.821
850918	1802	07.30	34 11.32	106 48.05	9.52	1.42	0.22	0.20	0.33	0.636
850918	1803	40.64	34 11.59	106 47.92	10.1	0.67	0.21	0.28	0.39	0.856
850918	1820	42.08	34 11.85	106 48.22	9.48	0.56	0.22	0.31	0.43	0.790
850918	1822	14.46	34 11.46	106 48.04	9.71	1.54	0.22	0.20	0.36	0.954
850918	1823	03.30	34 11.54	106 48.21	9.35	1.38	0.22	0.22	0.36	0.814
850918	1824	05.75	34 11.68	106 48.02	9.71	0.12	0.28	0.41	0.47	0.807
850918	1829	21.61	34 11.84	106 47.93	9.96	0.02	0.29	0.53	0.67	0.557
850918	1830	59.04	34 11.71	106 48.05	10.5	1.02	0.22	0.26	0.36	0.865

yymmdd	hhmm	sec	latitude		longitude		depth	mag	xerr	yerr	derr	R
850918	1841	35.99	34	11.66	106	48.18	9.51	0.29	0.30	0.45	0.50	0.805
850918	1909	23.07	34	11.52	106	47.98	9.11	0.86	0.25	0.30	0.34	0.939
850918	1916	15.15	34	11.40	106	48.01	9.66	1.04	0.23	0.26	0.36	0.837
850918	1919	31.09	34	11.41	106	47.97	9.31	2.28	0.22	0.19	0.37	0.842
850918	1920	51.09	34	11.65	106	48.04	9.51	0.64	0.27	0.39	0.39	0.923
850918	1921	08.78	34	11.45	106	48.03	9.52	0.84	0.21	0.25	0.39	0.723
850918	1921	20.07	34	11.56	106	48.03	10.3	0.69	0.42	0.63	0.86	0.467
850918	1921	26.20	34	11.86	106	47.93	9.34	0.47	0.45	0.63	0.67	0.884
850918	1923	09.00	34	11.47	106	48.16	9.75	1.84	0.22	0.19	0.39	0.929
850918	1926	03.44	34	11.66	106	48.09	9.25	1.18	0.23	0.30	0.38	0.990
850918	1938	00.42	34	11.31	106	48.10	9.12	2.21	0.22	0.20	0.38	0.907
850918	1939	29.04	34	11.32	106	48.10	9.08	1.47	0.25	0.21	0.34	0.972
850918	1939	53.57	34	11.76	106	48.19	9.82	0.65	0.37	0.46	0.65	0.475
850918	1940	29.25	34	11.48	106	48.05	9.57	0.51	0.22	0.31	0.47	0.905
850918	1941	48.32	34	11.54	106	48.31	8.91	0.19	0.38	0.50	0.53	0.771
850918	1950	17.83	34	11.51	106	48.07	9.75	1.11	0.21	0.24	0.44	0.835
850918	2000	19.69	34	11.55	106	48.01	9.69	0.70	0.21	0.30	0.35	0.689
850918	2003	21.35	34	11.96	106	48.10	10.2	-0.09	0.43	0.88	0.71	0.295
850918	2023	23.93	34	11.45	106	47.92	9.83	1.32	0.23	0.22	0.38	0.910
850918	2119	19.93	34	11.37	106	48.00	9.07	2.39	0.22	0.20	0.44	0.930
850918	2125	52.14	34	11.33	106	47.96	9.63	1.24	0.21	0.24	0.33	0.768
850918	2135	02.32	34	11.67	106	48.07	10.2	0.72	0.27	0.34	0.46	0.626
850918	2140	06.67	34	11.56	106	48.00	9.53	1.30	0.21	0.24	0.38	0.951
850918	2140	22.65	34	11.88	106	48.26	8.66	0.58	0.32	0.52	0.57	0.958
850919	0224	05.43	34	11.29	106	48.11	8.82	2.73	0.22	0.20	0.47	0.908
850919	0227	26.06	34	11.29	106	47.80	10.5	1.51	0.22	0.26	0.41	1.075
850919	0228	13.04	34	11.49	106	47.99	9.54	2.45	0.26	0.21	0.43	0.914
850919	0231	08.56	34	11.53	106	47.80	10.1	2.52	0.27	0.20	0.41	0.826
850919	0234	05.08	34	11.51	106	47.96	9.31	0.99	0.23	0.33	0.40	0.768
850919	0235	02.88	34	11.36	106	48.41	9.06	0.17	0.46	0.81	0.64	0.521
850919	0257	19.16	34	11.27	106	47.80	9.95	1.15	0.22	0.24	0.42	0.934
850919	0303	24.76	34	11.68	106	48.17	9.27	1.35	0.22	0.24	0.40	0.567
850919	0406	56.87	34	11.31	106	48.02	9.30	0.51	0.24	0.33	0.42	0.653
850919	0407	01.99	34	11.69	106	48.06	9.62	0.93	0.46	0.47	0.52	0.694
850919	0426	08.36	34	11.68	106	48.25	9.50	0.24	0.41	0.61	0.65	0.800
850919	0611	47.70	34	11.85	106	48.11	9.85	0.49	0.39	0.58	0.51	0.583
850919	0630	37.41	34	11.45	106	47.80	9.37	1.60	0.25	0.21	0.33	0.850
850919	0938	41.67	34	11.61	106	47.97	9.10	2.57	0.27	0.19	0.42	0.915
850919	0944	39.11	34	11.48	106	47.79	9.58	1.48	0.26	0.22	0.33	0.841
850919	0944	57.68	34	10.92	106	47.54	9.02	0.68	0.58	0.64	0.51	0.977
850919	0945	53.73	34	11.64	106	48.13	9.60	0.71	0.33	0.40	0.38	0.831
850919	1005	03.73	34	11.52	106	48.06	9.57	1.42	0.26	0.23	0.32	0.776
850919	1007	44.87	34	10.92	106	48.66	9.82	0.27	0.40	0.46	0.54	0.731
850919	1010	41.89	34	11.63	106	48.06	9.67	0.38	0.39	0.47	0.52	0.450
850920	1426	50.93	34	11.24	106	48.03	8.94	0.98	0.22	0.29	0.31	0.797
850920	1437	34.10	34	11.12	106	48.06	9.00	1.53	0.25	0.22	0.38	0.885
850920	1616	33.86	34	11.46	106	48.05	8.79	0.42	0.22	0.33	0.48	0.751
850920	1620	28.20	34	11.36	106	47.92	8.98	0.83	0.23	0.30	0.34	0.705
850920	1639	38.96	34	11.87	106	48.09	8.95	0.32	0.26	0.44	0.48	0.571
900222	0031	54.02	33	57.08	106	34.17	4.86	1.10	0.29	0.30	0.32	0.915
900222	0233	31.63	33	57.24	106	34.87	4.36	-0.29	0.55	0.56	0.58	0.722
900222	0616	16.15	33	57.64	106	35.28	3.47	-0.06	0.38	0.28	0.60	0.760

yymmdd	hhmm	sec	latitude		longitude		depth	mag	xerr	yerr	derr	R
900222	0625	52.63	33	57.76	106	35.08	4.12	-0.31	0.47	0.30	0.58	0.753
900222	0652	52.99	33	57.65	106	35.01	2.86	0.56	0.41	0.22	0.77	0.934
900222	0755	49.72	33	57.84	106	35.32	3.40	-0.29	0.46	0.26	0.63	0.635
900222	1351	57.02	33	57.77	106	35.75	3.21	0.38	0.33	0.23	0.53	0.889
900222	1532	43.80	33	57.40	106	34.36	7.18	2.22	0.56	0.34	0.76	0.863
900223	0009	23.26	33	57.50	106	34.81	5.32	0.67	0.37	0.30	0.52	0.932
900923	0059	57.79	33	57.62	106	34.92	4.84	0.48	0.33	0.28	0.46	0.837
900223	0308	10.09	33	57.60	106	34.81	4.31	0.67	0.32	0.27	0.46	0.945
900223	0312	10.61	33	57.43	106	35.22	5.34	0.40	0.35	0.30	0.52	0.662
900223	0322	25.32	33	56.73	106	34.00	4.58	0.56	0.41	0.38	0.50	1.162
900223	0354	20.67	33	56.71	106	34.28	5.43	0.37	0.46	0.33	0.48	1.452
900223	0358	17.65	33	57.38	106	34.40	5.62	0.70	0.41	0.31	0.49	0.790
900223	0405	58.13	33	57.43	106	35.43	2.97	2.01	0.27	0.29	0.55	1.136
900223	0651	43.49	33	57.56	106	34.86	5.62	0.43	0.37	0.30	0.48	0.925
900223	0915	13.73	33	57.24	106	34.76	4.11	0.28	0.37	0.37	0.65	0.880
900227	2309	57.62	33	57.75	106	35.02	5.93	0.58	0.33	0.31	0.57	0.924
900227	2339	29.96	33	57.58	106	35.25	4.79	1.11	0.24	0.30	0.42	1.222
900228	0025	07.37	33	58.64	106	34.19	4.52	0.06	0.32	0.34	0.44	1.465
900228	0026	33.10	33	58.78	106	33.40	2.73	0.15	0.24	0.29	0.65	1.213
900228	0213	35.44	33	57.99	106	34.62	5.52	0.67	0.34	0.35	0.57	1.422
900228	0312	21.66	33	58.03	106	35.56	4.30	0.74	0.31	0.28	0.66	1.039
900228	0408	06.14	33	57.80	106	35.09	4.22	0.10	0.30	0.32	0.45	0.938
900228	0433	51.14	33	58.21	106	34.31	3.80	0.21	0.34	0.33	0.48	1.028
900228	0559	53.77	33	57.81	106	34.60	4.53	0.05	0.31	0.34	0.41	1.027
900228	0709	19.33	33	57.98	106	35.55	2.52	-0.06	0.52	0.28	0.79	0.728
900228	0715	11.70	33	58.08	106	34.99	3.73	0.07	0.33	0.30	0.52	0.853
900228	0735	45.38	33	57.36	106	34.59	4.14	0.01	0.36	0.30	0.38	0.778
900228	0856	19.95	33	57.36	106	34.60	3.87	0.86	0.23	0.26	0.36	1.038
900228	0914	52.01	33	57.67	106	34.67	5.03	0.34	0.39	0.56	0.73	0.896
900228	0930	09.78	33	57.89	106	34.82	2.45	0.25	0.33	0.22	0.45	0.885
900228	1018	00.61	33	57.44	106	34.80	4.17	0.87	0.30	0.27	0.38	0.944
900228	1029	52.41	33	57.48	106	34.55	4.01	0.59	0.29	0.33	0.52	1.133
900228	1446	36.66	33	56.97	106	35.04	3.26	0.33	0.29	0.35	0.64	1.131
900228	1623	23.98	33	56.99	106	34.97	3.05	0.59	0.28	0.32	0.60	1.501
900228	1648	56.81	33	56.79	106	35.17	2.23	0.32	0.31	0.31	0.75	1.379
900228	1716	32.38	33	57.01	106	35.13	2.92	1.03	0.28	0.33	0.64	1.502
900228	1841	43.94	33	56.69	106	34.82	2.80	0.56	0.28	0.33	0.59	1.418
900228	2328	33.79	33	57.71	106	35.29	4.64	0.56	0.22	0.22	0.36	1.143
900301	0045	11.70	33	57.74	106	34.99	5.19	1.01	0.23	0.25	0.43	1.309
900301	0054	46.18	33	58.03	106	35.03	4.21	0.21	0.23	0.23	0.47	1.248
900301	0131	01.48	33	57.30	106	34.82	4.84	0.63	0.30	0.34	0.47	1.009
900301	0141	21.76	33	57.65	106	34.58	4.72	0.49	0.23	0.25	0.44	1.259
900301	0420	03.71	33	57.63	106	34.55	4.99	1.00	0.25	0.29	0.43	1.323
900301	0601	56.07	33	57.52	106	34.49	4.12	0.23	0.25	0.25	0.44	1.121
900301	0616	56.61	33	57.60	106	34.47	4.14	0.39	0.24	0.23	0.43	1.071
900301	0727	14.07	33	57.61	106	34.61	4.04	0.31	0.23	0.22	0.43	1.366
900301	0929	36.64	33	58.19	106	34.70	2.83	-0.18	0.23	0.29	0.54	1.193
900301	1424	29.12	33	57.88	106	34.44	4.07	0.40	0.24	0.28	0.46	1.390
900301	1517	42.73	33	57.88	106	35.06	4.22	0.24	0.23	0.27	0.48	1.373
900301	1652	52.72	33	57.77	106	35.05	4.04	0.44	0.29	0.25	0.62	1.007
900301	1657	25.34	33	57.78	106	35.17	3.51	0.44	0.28	0.24	0.66	1.200
900301	1853	51.96	33	57.68	106	35.27	4.17	0.30	0.32	0.24	0.68	0.990

yymmdd	hhmm	sec	latitude		longitude		depth	mag	xerr	yerr	derr	R
900301	1945	43.92	33	57.58	106	34.62	5.56	0.12	0.33	0.29	0.61	1.108
900301	1946	52.21	33	57.66	106	34.73	4.53	0.50	0.30	0.26	0.60	1.046
900301	2044	50.92	33	58.00	106	34.98	3.75	-0.08	0.34	0.25	0.64	1.053
900302	1528	23.10	33	57.65	106	35.16	5.45	0.45	0.50	0.29	0.65	1.086
900303	0004	15.42	33	57.71	106	35.02	4.37	0.52	0.45	0.26	0.57	1.151
900303	0241	43.01	33	57.71	106	34.03	3.75	0.95	0.45	0.29	0.45	1.342
900303	0348	31.97	33	57.41	106	34.69	5.95	0.61	0.38	0.26	0.48	1.364
900303	0840	03.18	33	57.75	106	34.26	5.29	0.09	0.44	0.28	0.43	1.408
900303	0903	11.23	33	57.66	106	34.66	4.74	0.46	0.38	0.25	0.40	1.156
900303	0904	48.90	33	57.73	106	34.61	4.19	0.24	0.35	0.23	0.42	1.103
900303	1646	41.92	33	57.74	106	35.31	4.85	0.37	0.37	0.25	0.41	1.125
900303	1723	20.11	33	57.56	106	34.99	5.32	0.30	0.46	0.25	0.43	1.160
900303	2051	01.31	33	57.60	106	34.95	6.43	0.39	0.49	0.31	0.58	1.443
900303	2154	20.27	33	57.88	106	35.52	4.44	0.35	0.39	0.24	0.42	1.364
900304	03 9	48.28	33	57.77	106	35.67	6.21	0.23	0.50	0.28	0.51	1.126
900304	0948	21.39	33	58.21	106	35.87	4.81	0.36	0.55	0.30	0.58	0.759
830225	0257	54.69	34	18.37	106	52.49	3.92	2.60	0.26	0.20	0.96	0.781
830225	0351	27.72	34	18.57	106	52.31	5.40	0.20	0.41	0.63	0.61	0.668
830225	0849	55.31	34	18.29	106	53.05	5.10	1.82	0.26	0.20	0.82	1.435
830225	0912	24.53	34	17.69	106	52.86	4.29	0.85	0.23	0.34	0.47	1.119
830226	1115	41.43	34	18.14	106	52.74	7.00	3.00	0.23	0.21	0.00	1.517
830226	1118	20.32	34	18.32	106	52.38	3.38	0.86	0.26	0.43	0.55	1.130
830226	1118	46.19	34	18.56	106	52.35	6.13	0.19	0.26	0.52	0.44	0.859
830226	1136	44.31	34	18.29	106	52.32	4.65	1.13	0.23	0.28	0.48	0.916
830226	1203	32.09	34	18.43	106	52.55	4.95	0.58	0.25	0.40	0.48	0.954
830226	1553	37.78	34	18.68	106	52.74	3.90	1.08	0.22	0.29	0.44	1.301
830226	1608	24.62	34	18.23	106	52.72	5.39	0.14	0.32	0.42	0.47	0.812
830226	1719	43.30	34	18.47	106	52.64	7.00	1.09	0.24	0.32	0.00	1.187
830226	1739	32.92	34	18.65	106	52.58	4.98	0.67	0.26	0.39	0.59	1.109
830226	1900	42.68	34	18.45	106	52.94	3.47	1.13	0.23	0.27	0.53	1.089
830226	2015	20.50	34	19.02	106	52.54	5.33	0.49	0.27	0.41	0.49	0.722
830226	2223	23.23	34	18.21	106	52.46	4.84	0.73	0.23	0.29	0.38	0.739
830228	0645	23.62	34	18.86	106	52.69	4.70	0.25	0.39	0.46	0.43	0.879
830228	0721	35.44	34	18.25	106	52.64	4.04	0.46	0.30	0.43	0.40	0.817
830228	1204	40.09	34	18.35	106	52.65	4.83	0.62	0.25	0.33	0.51	0.615
830228	1349	13.29	34	18.19	106	52.82	4.65	1.45	0.22	0.23	0.72	0.726
830228	2312	42.13	34	18.31	106	52.45	4.80	2.14	0.22	0.20	0.66	1.101
830302	1805	46.32	34	18.51	106	52.67	4.51	1.61	0.22	0.22	0.57	0.671
830302	1814	33.46	34	18.49	106	52.87	4.27	1.44	0.23	0.24	0.75	0.737
830302	2322	19.58	34	18.07	106	52.80	7.00	4.20	0.26	0.20	0.00	2.093
830302	2334	16.15	34	18.86	106	52.66	5.91	0.49	0.54	0.79	0.71	0.584
830302	2344	09.45	34	17.62	106	52.78	5.17	0.74	0.26	0.30	0.76	1.549
830302	2347	16.93	34	18.93	106	52.32	0.80	0.67	0.30	0.41	1.29	0.737
830302	2347	33.17	34	18.96	106	52.25	4.80	1.10	0.67	0.66	0.94	0.857
830302	2348	15.91	34	18.54	106	52.42	5.05	1.52	0.23	0.26	1.03	1.007
830302	2349	45.56	34	18.52	106	52.46	7.00	0.97	0.34	0.32	0.00	1.228
830302	2350	36.23	34	18.68	106	52.04	7.00	2.69	0.25	0.18	0.00	2.272
830302	2353	41.70	34	19.14	106	51.99	7.00	0.93	0.39	0.47	0.00	0.780
830302	2356	28.14	34	18.66	106	52.73	6.44	0.30	0.27	0.47	0.60	0.415
830302	2357	20.78	34	18.55	106	52.46	2.79	0.87	0.34	0.38	0.61	0.905
830303	0014	22.77	34	17.49	106	52.73	4.26	0.87	0.35	0.56	0.44	0.975
830303	0017	23.77	34	18.57	106	53.08	4.77	0.64	0.35	0.44	0.50	0.834

yymmdd	hhmm	sec	latitude		longitude		depth	mag	xerr	yerr	derr	R
830303	0024	31.49	34	18.88	106	52.36	5.70	0.77	0.27	0.44	0.69	1.097
830303	0027	47.70	34	18.39	106	52.91	5.70	0.29	0.31	0.45	0.00	0.841
830303	0029	26.96	34	18.38	106	52.73	7.00	0.36	0.38	0.63	0.00	0.698
830303	0032	39.24	34	18.76	106	52.79	5.42	1.81	0.22	0.22	0.93	1.129
830303	0047	50.60	34	18.60	106	52.08	5.97	0.97	0.33	0.50	0.75	0.840
830303	0056	22.91	34	17.80	106	52.72	4.51	0.49	0.28	0.63	0.71	0.498
830303	0059	44.61	34	18.65	106	52.44	5.50	0.45	0.26	0.47	0.58	1.393
830303	0118	38.65	34	18.39	106	52.48	5.53	0.81	0.25	0.38	0.61	0.423
830303	0141	54.83	34	18.64	106	52.95	4.78	0.53	0.25	0.39	0.53	0.516
830303	0146	11.18	34	18.68	106	52.92	4.57	0.49	0.28	0.48	0.53	0.867
830303	0206	28.01	34	18.50	106	52.56	6.55	2.09	0.22	0.21	0.62	0.927
830303	0214	01.31	34	19.53	106	52.33	4.23	0.58	0.39	0.63	0.63	0.882
830303	0215	53.13	34	18.66	106	52.74	5.61	0.78	0.25	0.42	0.51	0.847
830303	0222	15.65	34	18.66	106	52.24	5.35	0.79	0.28	0.41	0.73	0.849
830303	0233	13.46	34	18.94	106	52.41	4.96	0.32	0.26	0.54	0.50	0.760
830303	0244	24.36	34	18.27	106	52.71	4.80	0.12	0.74	0.58	0.55	0.994
830303	0304	59.52	34	18.85	106	52.60	5.75	1.16	0.23	0.32	0.41	0.750
830303	0345	07.60	34	18.62	106	52.28	6.09	0.48	0.24	0.44	0.45	0.584
830303	0408	01.95	34	18.54	106	52.39	6.09	0.69	0.27	0.38	0.39	0.634
830303	0420	09.46	34	18.94	106	52.68	5.45	0.47	0.26	0.48	0.49	1.017
830303	0423	21.80	34	18.88	106	52.79	5.04	0.39	0.24	0.49	0.49	0.578
830303	0426	33.50	34	17.86	106	51.88	4.23	0.25	0.26	0.62	0.69	0.697
830303	0429	34.61	34	18.81	106	53.32	4.89	1.28	0.24	0.30	0.47	1.769
830303	0430	16.08	34	18.84	106	52.30	4.94	0.54	0.39	0.63	0.43	0.822
830303	0439	57.46	34	18.67	106	52.69	5.03	0.45	0.36	0.52	0.46	0.961
830303	0451	53.88	34	18.69	106	51.94	6.84	0.57	0.30	0.43	0.58	0.666
830303	0501	59.78	34	19.29	106	52.59	4.95	1.18	0.23	0.31	0.48	0.909
830303	0508	32.53	34	19.19	106	52.58	5.60	0.85	0.24	0.39	0.51	0.577
830303	0539	50.38	34	18.07	106	52.63	6.36	0.50	0.26	0.46	0.52	0.671
830303	0615	54.09	34	18.53	106	52.07	6.44	0.08	0.33	0.55	0.42	1.145
830303	0617	10.77	34	18.76	106	52.13	4.87	-0.09	0.40	0.52	0.43	0.843
830303	0630	22.09	34	18.60	106	52.67	4.39	0.03	0.25	0.48	0.48	1.023
830303	0636	47.45	34	18.58	106	52.89	5.04	0.00	0.40	0.57	0.36	0.475
830303	0804	41.13	34	18.28	106	52.21	5.85	0.43	0.26	0.40	0.34	0.878
830303	0805	12.08	34	18.69	106	52.18	6.22	1.47	0.22	0.25	0.41	0.852
830303	0822	52.51	34	18.60	106	52.17	6.13	0.45	0.26	0.41	0.39	0.704
830303	0835	55.54	34	18.32	106	52.17	5.20	1.39	0.25	0.36	0.64	0.984
830303	0854	43.45	34	18.85	106	52.15	6.27	0.65	0.23	0.38	0.48	0.632
830303	0910	12.56	34	18.51	106	52.54	5.93	0.94	0.25	0.36	0.59	0.793
830303	0923	49.01	34	19.22	106	52.86	4.63	1.32	0.23	0.27	0.47	1.565
830303	0925	53.78	34	18.82	106	52.56	5.95	0.42	0.25	0.41	0.33	1.099
830303	0939	14.95	34	18.85	106	52.49	4.84	0.22	0.30	0.63	0.52	0.457
830303	1021	21.71	34	18.26	106	52.64	5.50	0.53	0.28	0.50	0.46	0.927
830303	1119	12.85	34	18.12	106	52.36	5.87	1.79	0.24	0.22	0.51	1.131
830303	1133	51.69	34	18.38	106	51.99	5.71	0.71	0.29	0.43	0.36	0.900
830303	1154	18.08	34	18.54	106	52.81	4.98	0.57	0.31	0.53	0.58	0.897
830303	1250	50.68	34	18.31	106	53.03	5.00	0.32	0.31	0.68	0.35	1.078
830303	1315	57.09	34	18.81	106	53.11	4.09	0.57	0.24	0.43	0.41	0.909
830303	1320	12.81	34	18.66	106	53.03	4.14	0.09	0.31	0.57	0.35	0.973
830303	1321	55.46	34	18.98	106	52.66	4.40	0.11	0.37	0.53	0.42	0.985
830303	1325	25.74	34	19.26	106	52.52	5.36	0.14	0.28	0.46	0.40	0.597
830303	1346	10.83	34	19.29	106	52.80	4.87	0.42	0.25	0.45	0.47	1.106

yymmdd	hhmm	sec	latitude	longitude	depth	mag	xerr	yerr	derr	R
830303	1421	42.62	34 18.84	106 52.10	5.61	0.17	0.30	0.53	0.47	0.642
830303	1444	43.94	34 19.18	106 52.23	7.38	0.82	0.28	0.42	0.52	0.650
830303	1456	03.35	34 18.43	106 52.49	5.51	0.49	0.33	0.47	0.33	0.455
830303	1457	07.56	34 18.90	106 52.42	5.59	0.24	0.44	0.76	0.44	1.012
830303	1607	14.99	34 18.34	106 52.10	6.65	1.25	0.26	0.28	0.37	0.733
830303	1733	43.22	34 18.83	106 52.12	6.49	0.57	0.25	0.36	0.54	0.622
830303	1740	11.67	34 18.42	106 52.31	6.06	2.03	0.23	0.24	0.48	0.859
830303	1845	38.60	34 18.70	106 51.95	6.36	0.17	0.28	0.39	0.38	1.122
830303	1903	36.85	34 18.22	106 52.08	5.62	0.03	0.40	0.34	0.47	1.063
830303	1927	32.70	34 18.11	106 52.19	6.37	-0.05	0.25	0.36	0.34	1.072
830303	2036	51.75	34 18.83	106 52.47	5.84	0.41	0.25	0.35	0.40	1.090
830303	2054	26.18	34 18.07	106 52.76	6.10	0.47	0.25	0.31	0.34	0.875
830303	2235	28.49	34 17.69	106 52.85	4.62	1.51	0.23	0.23	0.36	1.390
830303	2332	35.63	34 18.22	106 52.64	6.03	0.84	0.22	0.34	0.33	1.669
830304	0000	22.30	34 18.50	106 52.77	3.78	2.03	0.21	0.22	0.41	1.121
830304	0026	09.68	34 18.72	106 52.20	5.86	0.51	0.20	0.25	0.37	0.890
830304	0110	29.70	34 18.48	106 52.46	4.37	0.00	0.34	0.32	0.34	1.194
830304	0116	42.10	34 17.85	106 52.36	3.71	0.00	0.61	0.30	0.91	1.436
830304	0147	56.58	34 18.34	106 52.95	5.18	1.84	0.24	0.21	0.38	1.163
830304	0149	24.51	34 18.34	106 52.63	5.16	1.76	0.21	0.23	0.34	0.744
830304	3206	10.70	34 18.02	106 52.63	4.30	0.20	0.32	0.30	0.40	0.901
830304	0326	49.53	34 18.96	106 52.41	5.38	0.95	0.21	0.26	0.39	1.286
830304	0331	33.81	34 18.25	106 52.52	5.67	0.43	0.23	0.25	0.37	1.035
830304	0408	44.52	34 18.49	106 52.24	5.39	-0.26	0.30	0.28	0.46	0.917
830304	0526	10.75	34 18.20	106 52.74	5.21	1.99	0.21	0.20	0.37	0.929
830304	0609	21.05	34 19.05	106 52.42	5.58	0.47	0.24	0.40	0.48	0.696
830304	0612	29.78	34 19.33	106 52.52	5.01	0.19	0.23	0.37	0.40	0.722
830304	0628	03.77	34 18.60	106 52.41	3.32	0.06	0.36	0.37	0.41	1.155
830304	0847	18.33	34 19.04	106 52.46	5.47	0.37	0.24	0.32	0.34	1.128
830304	0905	16.27	34 17.29	106 50.88	4.70	0.47	0.32	0.34	0.56	2.470
830304	0940	32.88	34 19.20	106 52.54	5.99	0.71	0.23	0.33	0.40	0.512
830304	0946	16.76	34 19.84	106 54.06	4.96	0.27	0.28	0.36	0.41	1.051
830304	0950	42.10	34 18.53	106 52.93	4.91	0.65	0.21	0.37	0.38	0.975
830304	1036	20.52	34 18.46	106 52.47	5.80	0.53	0.35	0.44	0.39	0.824
830304	1154	35.79	34 18.50	106 53.59	4.18	0.28	0.43	0.39	0.41	1.593
830304	1340	24.61	34 18.65	106 52.69	3.42	0.22	0.53	0.62	0.65	1.284
830304	1353	28.79	34 18.59	106 53.06	6.00	1.11	0.20	0.28	0.33	0.942
830304	1502	31.32	34 18.94	106 52.85	6.00	0.06	0.39	0.61	0.43	0.882
830304	1521	28.06	34 18.78	106 53.42	4.94	0.03	0.47	0.45	0.39	0.585
830304	1756	20.17	34 17.92	106 52.51	4.93	0.12	0.38	0.38	0.77	1.314
830304	1820	06.90	34 18.24	106 52.59	5.20	1.31	0.21	0.25	0.37	0.875
830304	1825	14.71	34 18.21	106 53.28	3.88	0.00	0.44	0.42	0.46	1.537
830304	1946	59.06	34 18.30	106 53.11	3.79	-0.25	0.39	0.44	0.43	1.099
830304	2030	33.10	34 18.78	106 52.16	4.97	-0.19	0.64	0.64	0.64	0.878
830304	2149	21.46	34 18.60	106 52.88	4.59	1.01	0.21	0.25	0.39	0.857
830305	0016	26.58	34 18.46	106 52.81	4.35	0.57	0.40	0.32	0.50	0.948
830305	0022	54.19	34 18.00	106 52.10	3.67	-0.13	0.47	0.53	0.87	0.409
830305	0159	54.44	34 18.47	106 53.03	4.79	0.36	0.38	0.50	0.46	0.564
830305	0220	01.22	34 18.54	106 52.88	4.47	-0.12	0.27	0.36	0.29	0.938
830305	0502	50.12	34 18.67	106 52.89	4.72	0.17	0.35	0.30	0.42	0.987
830305	1105	25.51	34 17.58	106 52.00	5.55	1.07	0.27	0.33	0.45	0.765
830305	1220	21.31	34 18.12	106 52.82	4.90	0.06	0.32	0.46	0.46	0.763

yymmdd	hhmm	sec	latitude		longitude		depth	mag	xerr	yerr	derr	R
830305	1229	08.46	34	18.49	106	53.03	4.29	-0.20	0.29	0.79	0.50	0.486
830305	1359	19.83	34	18.52	106	52.84	4.91	0.17	0.55	0.53	0.54	0.531
830305	2243	33.76	34	17.97	106	53.00	5.58	0.40	0.21	0.43	0.47	0.691
830305	2244	34.33	34	18.54	106	52.76	5.70	0.09	0.35	0.43	0.52	0.589
830306	0011	21.85	34	18.51	106	52.16	6.31	1.27	0.21	0.23	0.35	1.212
830306	0300	51.06	34	18.23	106	51.82	5.94	0.51	0.22	0.22	0.32	0.926
830306	1002	50.40	34	18.20	106	52.64	5.24	0.34	0.34	0.29	0.40	0.669
830306	1846	03.91	34	18.60	106	52.77	5.16	0.40	0.31	0.45	0.43	0.715
830306	1900	17.10	34	18.93	106	52.93	4.78	0.51	0.25	0.34	0.38	1.094
830306	2213	29.88	34	17.86	106	52.59	4.68	1.41	0.26	0.29	0.38	0.830
830306	2326	23.22	34	18.13	106	52.55	5.26	0.68	0.24	0.21	0.33	0.960
830307	0916	28.60	34	18.90	106	52.51	5.10	0.09	0.30	0.41	0.39	1.811
830307	1451	10.28	34	18.93	106	53.22	5.31	0.05	0.32	0.51	0.53	1.174
830307	1607	23.83	34	17.38	106	52.54	3.66	0.38	0.31	0.44	0.62	1.500
830307	1905	24.90	34	20.48	106	52.67	7.49	0.27	0.48	0.69	0.64	2.159
830307	1925	04.62	34	18.62	106	52.96	5.56	0.60	0.25	0.38	0.46	1.028
830307	2011	44.59	34	19.48	106	51.40	8.86	0.54	0.34	0.49	0.47	2.445
830307	2217	50.34	34	18.03	106	52.83	4.79	-0.01	0.35	0.72	0.46	0.604
830308	0606	45.03	34	18.15	106	53.05	4.98	1.49	0.22	0.23	0.33	0.912
830308	0619	00.22	34	18.16	106	52.94	4.75	2.33	0.21	0.20	0.32	1.173
830308	0642	06.03	34	18.60	106	52.03	5.89	0.56	0.28	0.35	0.39	1.893
830308	0742	26.26	34	17.85	106	52.07	7.86	0.51	0.32	0.39	0.50	2.034
830308	0827	29.35	34	17.40	106	52.17	5.46	1.85	0.24	0.26	0.50	0.986
830308	0913	18.71	34	18.76	106	52.40	10.8	0.59	0.29	0.58	0.63	2.195
830308	1243	46.73	34	18.86	106	51.53	6.60	0.16	0.38	0.42	0.39	2.152
830308	1352	34.98	34	18.63	106	52.69	6.28	0.41	0.30	0.34	0.41	1.604
830308	1604	43.24	34	18.85	106	52.03	6.09	1.28	0.25	0.24	0.41	0.916
830309	0905	59.35	34	18.17	106	52.32	4.81	1.93	0.25	0.20	0.45	1.045
830309	0949	43.52	34	18.05	106	53.03	4.34	0.68	0.27	0.35	0.43	0.640
830309	1405	11.86	34	18.67	106	52.84	4.73	0.59	0.25	0.41	0.49	0.879
830309	1425	08.52	34	17.90	106	53.11	6.14	0.79	0.33	0.36	0.70	0.932
830309	1503	25.17	34	18.19	106	52.80	5.33	1.19	0.28	0.24	0.53	0.647
830309	1745	47.89	34	18.78	106	52.16	5.22	0.36	0.39	0.68	0.64	1.207
830309	1910	20.03	34	17.84	106	53.08	4.23	0.28	0.24	0.36	0.43	0.822
830309	2303	26.28	34	18.01	106	53.22	4.86	1.36	0.22	0.23	0.36	0.988
830309	2312	18.04	34	18.41	106	52.87	5.26	0.67	0.24	0.31	0.48	0.606
830309	2325	35.12	34	18.17	106	52.97	4.78	1.62	0.23	0.20	0.35	1.086
830309	2359	00.67	34	18.19	106	52.98	4.39	0.40	0.24	0.29	0.41	0.745
830310	0340	08.58	34	19.13	106	52.46	5.38	0.74	0.23	0.28	0.56	0.944
830310	0747	52.82	34	20.05	106	53.27	5.95	0.28	0.49	0.34	0.66	2.283
830310	0811	54.59	34	17.46	106	52.91	4.37	0.82	0.22	0.22	0.43	0.905
830310	0845	04.65	34	18.36	106	52.46	4.63	0.18	0.32	0.29	0.43	0.775
830310	0958	31.52	34	18.13	106	53.10	4.79	0.38	0.31	0.41	0.39	0.669
830310	1019	25.99	34	18.37	106	51.39	6.37	0.41	0.38	0.33	0.39	1.568
830310	1119	17.07	34	18.57	106	52.09	6.48	0.27	0.28	0.33	0.36	0.629
830311	0755	58.93	34	19.21	106	51.77	6.43	0.23	0.32	0.43	0.49	0.602
830311	0950	32.06	34	18.70	106	52.34	5.77	0.68	0.24	0.32	0.40	0.878
830311	1017	01.55	34	17.84	106	52.60	4.74	1.21	0.29	0.26	0.41	0.411
830311	1046	13.54	34	18.89	106	52.48	5.53	0.87	0.26	0.28	0.43	0.666
830312	0413	53.42	34	17.05	106	52.61	5.11	0.87	0.23	0.33	0.43	0.612
830312	1037	15.87	34	18.88	106	52.49	5.62	0.53	0.21	0.50	0.43	0.881
830312	1221	40.72	34	17.31	106	52.46	4.76	0.12	0.27	0.41	0.55	0.861

yymmdd	hhmm	sec	latitude	longitude	depth	mag	xerr	yerr	derr	R
830312	2108	16.49	34 18.43	106 52.21	4.37	1.21	0.19	0.26	0.45	1.001
830313	1632	19.76	34 18.40	106 52.77	3.32	0.22	0.27	0.48	0.77	0.692
830313	1994	45.42	34 18.40	106 52.41	4.96	0.58	0.40	0.49	0.74	0.932
830313	1955	10.00	34 18.54	106 52.33	6.14	0.14	0.20	0.44	0.43	0.646
830313	2043	08.68	34 18.78	106 52.45	6.11	0.69	0.23	0.47	0.47	0.900
830313	2129	01.56	34 19.37	106 52.71	4.97	0.55	0.27	0.57	0.68	0.597
830315	0748	32.14	34 18.40	106 53.39	4.25	0.55	0.46	0.48	0.52	1.065
830315	0927	02.94	34 17.54	106 52.91	4.20	2.58	0.24	0.29	0.55	0.930
830315	1018	09.89	34 17.89	106 52.15	5.51	0.51	0.26	0.43	0.51	0.931
830316	0830	29.22	34 17.42	106 53.02	4.62	1.73	0.24	0.28	0.77	0.995
830510	0434	56.55	34 03.66	106 57.29	7.25	0.50	0.26	0.34	0.41	0.975
830510	0627	42.49	34 03.53	106 57.19	8.02	0.90	0.26	0.26	0.36	0.935
830510	0657	02.62	34 03.79	106 57.30	7.40	0.40	0.22	0.33	0.33	0.773
830510	0717	27.82	34 02.89	106 56.85	8.93	0.04	0.26	0.46	0.46	1.320
830510	0838	52.99	34 03.69	106 57.47	7.87	1.75	0.24	0.28	0.44	0.853
830510	0814	44.57	34 03.95	106 57.52	7.35	0.30	0.39	0.44	0.35	0.912
930510	1105	46.74	34 03.70	106 57.32	7.45	1.35	0.23	0.27	0.39	0.822
830510	1142	06.88	34 03.42	106 57.63	7.91	0.67	0.28	0.38	0.50	0.791
830510	1157	22.90	34 03.44	106 57.31	7.46	0.02	0.33	0.47	0.48	0.795
830510	1434	37.27	34 03.90	106 57.35	7.87	0.08	0.28	0.41	0.45	0.606
830510	1637	29.38	34 03.59	106 57.24	7.96	0.52	0.24	0.25	0.38	0.907
830511	0557	16.69	34 03.91	106 57.62	7.28	0.06	0.26	0.48	0.48	0.979
830511	0600	21.21	34 03.58	106 57.35	8.48	0.49	0.25	0.36	0.41	0.832
830511	0611	18.51	34 03.78	106 57.39	8.17	0.50	0.22	0.35	0.50	1.308
830511	0616	17.60	34 03.84	106 57.54	7.58	0.90	0.24	0.30	0.35	0.972
830511	1255	30.63	34 03.75	106 57.30	8.49	0.24	0.26	0.46	0.54	1.090
830511	1359	29.83	34 03.79	106 57.83	8.46	0.91	0.29	0.28	0.37	1.150
830511	1430	29.97	34 03.27	106 57.60	8.26	1.19	0.27	0.28	0.38	1.141
830511	1433	07.49	34 03.88	106 57.63	8.57	0.92	0.27	0.34	0.47	1.127
830511	1448	10.10	34 03.87	106 57.56	7.48	0.62	0.52	0.55	0.65	0.782
830511	1452	23.00	34 03.48	106 58.32	7.28	0.89	0.35	0.32	0.41	1.141
830511	1513	44.59	34 02.22	106 58.24	7.12	0.09	0.65	0.66	0.56	1.370
830511	1526	45.18	34 03.65	106 57.27	8.44	1.63	0.25	0.24	0.45	1.324
830511	1549	05.50	34 02.97	106 58.39	6.77	0.22	0.44	0.47	0.39	0.849
830511	1728	53.03	34 03.92	106 57.54	7.35	0.24	0.33	0.41	0.44	0.710
830511	1743	07.69	34 03.77	106 57.54	6.88	0.23	0.26	0.44	0.40	0.596
830513	0813	34.67	34 03.99	106 57.52	7.70	-0.39	0.28	0.45	0.42	0.764
830513	1555	10.59	34 03.77	106 57.29	0.54	0.07	0.24	0.31	0.65	1.162
830513	1613	48.97	34 03.61	106 57.38	6.68	-0.01	0.37	0.49	0.50	0.600
830514	0108	28.34	34 03.56	106 57.88	8.00	0.60	0.22	0.27	0.31	1.220
830514	1443	19.84	34 03.89	106 57.77	8.15	-0.02	0.35	0.35	0.32	0.835
830524	2253	31.24	34 00.58	106 57.50	6.93	0.38	0.34	0.31	0.56	1.028
830530	0745	06.12	34 02.21	106 59.92	8.72	0.91	0.35	0.37	0.56	1.096
8306	9	0839	35.55	34 03.10	106 59.85	6.18	0.23	0.55	0.48	0.62	0.880
830714	0552	25.29	34 04.37	106 57.63	8.39	-0.09	0.49	0.67	0.49	0.967
830714	0649	56.17	34 03.37	106 57.89	8.41	0.09	0.43	0.50	0.40	1.186
830714	0810	15.12	34 04.15	106 57.50	7.78	0.14	0.34	0.47	0.38	1.232
830714	1109	42.47	34 03.79	106 57.65	7.63	0.88	0.35	0.40	0.31	0.829
830714	1123	30.74	34 02.47	106 57.52	7.64	-0.13	0.37	0.60	0.37	1.424
830714	1139	46.61	34 03.99	106 57.40	8.45	0.33	0.29	0.44	0.33	1.014
830714	1242	41.12	34 03.47	106 57.53	7.83	0.06	0.36	0.44	0.32	1.068
830714	1351	25.80	34 02.99	106 57.21	7.68	-0.22	0.36	0.50	0.37	1.379

yymmdd	hhmm	sec	latitude	longitude	depth	mag	xerr	yerr	derr	R
830714	1613	20.78	34 03.88	106 57.60	7.54	-0.06	0.38	0.49	0.42	0.786
830714	1617	53.59	34 03.66	106 57.47	7.60	0.09	0.37	0.50	0.37	0.904
830714	1949	03.04	34 04.26	106 57.56	8.14	0.49	0.39	0.47	0.51	0.889
830715	0432	37.88	34 04.13	106 57.42	7.57	0.71	0.38	0.53	0.40	0.611
830715	0514	09.11	34 03.89	106 57.19	7.56	0.00	0.42	0.49	0.47	0.678
830715	0851	03.71	34 03.58	106 57.24	6.82	0.31	0.25	0.38	0.42	1.319
830716	0328	48.66	34 04.73	106 57.27	7.07	0.43	0.45	0.66	0.40	1.049
830716	0330	25.16	34 04.35	106 57.72	8.17	0.60	0.24	0.38	0.30	0.908
830716	0435	52.25	34 04.21	106 57.34	7.81	0.38	0.33	0.46	0.35	0.840
830716	0436	36.71	34 04.01	106 57.47	8.15	0.27	0.42	0.48	0.43	0.663
830716	0610	26.17	34 03.78	106 57.50	8.55	0.50	0.46	0.67	0.47	1.041
830716	0612	06.38	34 03.61	106 57.88	7.56	0.57	0.27	0.34	0.30	1.366
830716	0632	33.73	34 03.48	106 57.12	7.18	0.51	0.33	0.44	0.39	0.790
830716	0859	48.77	34 03.96	106 57.45	8.26	1.24	0.23	0.27	0.40	1.220
830716	1739	50.03	34 03.67	106 57.42	8.81	0.32	0.25	0.37	0.37	1.062
830716	2150	18.47	34 03.61	106 57.30	7.57	0.17	0.30	0.41	0.34	1.048
830716	2206	12.40	34 03.83	106 57.29	6.52	2.13	0.22	0.24	0.44	1.221
830716	2252	17.85	34 03.32	106 57.34	7.16	0.29	0.43	0.57	0.45	0.890
830716	2300	53.42	34 03.92	106 57.99	6.77	0.03	0.36	0.54	0.41	1.200
830717	0101	26.96	34 03.74	106 57.13	8.03	0.39	0.23	0.37	0.32	0.435
830717	0242	38.23	34 03.90	106 57.46	7.40	0.56	0.25	0.34	0.31	0.873
830717	0244	02.24	34 02.29	106 57.51	7.28	0.22	0.45	0.51	0.42	1.144
830717	0615	10.22	34 02.34	106 57.49	8.55	-0.18	0.62	0.87	0.59	1.040
830717	1132	56.60	34 04.10	106 57.18	7.39	1.67	0.23	0.24	0.45	0.889
830717	1135	43.98	34 05.44	106 57.66	5.94	-0.03	0.48	0.78	0.45	1.043
830717	1427	08.51	34 03.97	106 57.48	7.79	0.43	0.27	0.41	0.40	0.799
830717	2245	29.49	34 03.77	106 57.31	8.29	0.98	0.26	0.38	0.35	1.281
830718	1109	35.96	34 03.92	106 57.14	7.21	0.49	0.34	0.46	0.41	0.429
830718	1756	25.92	34 03.91	106 57.48	7.18	0.66	0.23	0.30	0.31	1.271
830719	0257	04.69	34 03.43	106 57.57	8.12	0.31	0.36	0.45	0.33	1.048
830719	0327	11.28	34 03.97	106 57.56	6.96	0.26	0.31	0.33	0.30	0.837
830719	0340	07.37	34 03.65	106 57.35	7.75	1.92	0.23	0.25	0.35	0.660
830719	0343	22.83	34 03.93	106 57.76	5.72	0.00	0.46	0.58	0.53	0.951
830719	0343	45.22	34 03.80	106 57.46	6.82	0.37	0.36	0.42	0.48	0.881
830719	0440	28.73	34 03.76	106 57.35	8.18	0.68	0.26	0.30	0.35	0.688
830719	0442	47.21	34 03.95	106 57.56	7.86	1.20	0.22	0.25	0.34	0.907
830719	0503	16.29	34 04.00	106 57.61	7.38	0.36	0.25	0.37	0.29	0.799
830719	0753	18.84	34 04.95	106 57.28	6.22	0.11	0.52	0.82	0.45	0.862
830719	0912	54.53	34 03.95	106 57.46	7.73	0.92	0.26	0.35	0.43	1.114
830719	1230	30.39	34 04.40	106 58.21	7.56	0.42	0.28	0.37	0.37	1.536
830719	1332	15.25	34 03.99	106 57.36	7.67	0.44	0.23	0.33	0.33	0.877
830719	1505	16.01	34 04.13	106 57.31	7.51	-0.06	0.42	0.77	0.45	0.471
830719	1622	47.39	34 03.41	106 57.41	7.84	0.02	0.34	0.48	0.41	0.919
830719	2022	59.71	34 03.15	106 57.39	8.06	0.32	0.34	0.49	0.42	1.194
830720	0041	54.52	34 03.71	106 57.54	7.74	1.01	0.22	0.24	0.27	1.002
830720	0130	29.27	34 04.16	106 57.40	7.58	0.00	0.33	0.46	0.41	0.681
830720	0146	06.31	34 03.28	106 57.69	8.18	0.34	0.35	0.43	0.38	0.703
830720	0152	01.48	34 04.32	106 57.32	6.90	0.00	0.28	0.43	0.40	0.758
830720	0411	06.33	34 04.07	106 57.32	7.39	0.22	0.32	0.47	0.37	0.752
830720	1650	26.82	34 04.02	106 57.43	7.64	0.40	0.30	0.43	0.40	0.996
830720	1657	16.12	34 03.94	106 57.37	8.35	1.00	0.27	0.28	0.35	0.940
830720	1658	08.76	34 04.02	106 57.57	7.82	0.39	0.39	0.47	0.49	0.633

yymmdd	hhmm	sec	latitude	longitude	depth	mag	xerr	yerr	derr	R
830720	1722	45.87	34 03.72	106 57.32	8.45	0.41	0.27	0.34	0.29	0.709
830720	1752	40.14	34 03.97	106 57.50	8.60	0.24	0.39	0.46	0.39	0.844
830720	1853	41.31	34 03.33	106 57.26	8.36	0.55	0.45	0.79	0.50	0.868
830722	0702	50.42	34 04.16	106 57.77	8.02	0.06	0.43	0.75	0.48	0.960
950910	1348	15.46	34 06.89	106 49.70	5.60	1.12	0.19	0.23	0.28	0.859
950910	1602	17.05	34 06.99	106 49.72	5.17	1.13	0.16	0.25	0.28	1.078
950910	1902	29.69	34 06.94	106 49.61	5.54	1.09	0.19	0.25	0.27	1.021
950910	2104	49.36	34 07.26	106 49.75	5.47	0.39	0.25	0.53	0.36	0.857
950911	0637	00.74	34 07.10	106 49.61	5.17	0.98	0.19	0.23	0.30	1.234
950911	0759	40.31	34 06.84	106 49.63	4.90	1.01	0.19	0.23	0.31	1.168
950911	0900	58.75	34 06.99	106 49.66	5.81	1.08	0.18	0.25	0.28	1.268
950911	1213	14.67	34 06.65	106 49.60	5.28	1.50	0.19	0.22	0.32	1.004
950911	2122	32.45	34 06.89	106 49.57	5.54	0.92	0.21	0.24	0.32	0.981
950917	1740	17.42	34 06.76	106 49.67	5.34	1.95	0.20	0.22	0.40	0.802
950917	1750	19.45	34 06.89	106 49.68	5.67	1.03	0.20	0.28	0.29	0.897
950918	0310	48.89	34 07.09	106 49.63	5.47	1.18	0.18	0.23	0.28	1.228
950918	0820	55.51	34 06.90	106 49.63	5.08	1.93	0.18	0.22	0.34	1.325
950919	1527	03.49	34 06.87	106 49.59	5.68	1.57	0.20	0.23	0.30	1.053
950920	0909	36.16	34 06.95	106 49.69	5.89	0.84	0.19	0.26	0.29	0.869
950928	2017	04.84	34 06.74	106 49.61	5.72	1.54	0.19	0.22	0.31	0.741
950928	2142	29.66	34 06.79	106 49.62	5.90	1.36	0.19	0.23	0.31	0.801
830329	1756	45.66	34 30.08	107 10.21	5.59	1.53	0.38	0.31	0.57	1.452
830330	0006	53.42	34 29.77	107 10.19	4.22	1.36	0.38	0.32	0.71	1.240
830330	0455	37.23	34 29.41	107 09.36	4.69	1.61	0.35	0.22	0.54	1.241
830331	0907	08.58	34 29.45	107 09.49	4.04	0.55	0.44	0.47	0.71	0.966
830331	0916	50.69	34 29.33	107 09.83	4.36	0.64	0.37	0.39	0.52	1.079
840503	1733	06.88	34 12.57	106 41.41	8.89	0.65	0.40	0.40	0.43	1.135
840503	1803	37.71	34 12.20	106 41.81	9.59	0.64	0.47	0.44	0.43	1.050
840503	2050	52.48	34 12.21	106 42.02	8.19	0.96	0.26	0.25	0.35	0.958
840505	0715	33.36	34 12.41	106 41.95	7.79	0.74	0.27	0.26	0.39	1.066
840505	0849	11.49	34 12.17	106 41.67	9.28	0.75	0.35	0.30	0.52	0.662
860228	0148	16.05	34 35.32	107 09.17	1.22	1.79	0.37	0.23	0.46	1.119
860303	1246	25.41	34 26.77	107 05.01	4.00	0.78	0.37	0.53	0.37	1.411
891125	0024	05.40	33 44.76	106 53.93	8.22	0.84	0.38	0.70	0.97	1.410
900901	0841	24.01	34 18.23	107 06.73	8.25	0.65	0.28	0.30	0.28	1.450
900901	0843	58.72	34 17.96	107 06.97	8.01	1.20	0.26	0.22	0.38	1.373
900901	0921	02.85	34 18.42	107 07.00	8.79	0.90	0.27	0.24	0.28	1.183
900901	0921	14.41	34 17.78	107 06.94	8.07	0.70	0.44	0.42	0.34	1.760
900901	0924	29.32	34 18.42	107 06.69	7.53	0.41	0.31	0.44	0.36	1.164
900901	1047	32.93	34 18.38	107 07.21	8.40	1.33	0.25	0.22	0.32	1.282
900901	2020	26.74	34 18.04	107 06.82	9.44	0.63	0.29	0.33	0.34	1.103
900901	2111	57.38	34 18.26	107 06.91	8.93	0.75	0.26	0.29	0.36	1.025
900901	2131	06.67	34 18.26	107 07.16	9.18	2.06	0.33	0.25	0.49	0.935
900901	2214	20.34	34 18.25	107 07.01	8.96	0.68	0.26	0.27	0.32	0.904
900901	2219	24.97	34 18.04	107 06.81	8.53	0.48	0.32	0.39	0.35	1.081
900902	0115	30.63	34 18.32	107 07.04	8.72	0.91	0.26	0.27	0.32	1.079
900904	0533	35.77	34 18.27	107 07.04	9.60	0.88	0.28	0.29	0.31	1.314
900904	1440	40.15	34 18.39	107 07.36	9.31	2.19	0.31	0.26	0.49	1.349
900904	1722	45.81	34 18.69	107 06.93	9.50	0.72	0.26	0.31	0.32	1.541
900904	1723	42.77	34 18.62	107 06.88	8.68	0.41	0.31	0.35	0.39	1.156
900904	1820	09.66	34 17.99	107 07.21	8.72	0.65	0.28	0.34	0.40	1.194
951014	0423	03.70	34 26.86	107 01.08	4.93	1.43	0.24	0.46	0.48	0.924

yymmdd	hhmm	sec	latitude		longitude		depth	mag	xerr	yerr	derr	R
950904	1759	14.13	34	01.35	106	51.94	4.34	1.40	0.25	0.25	0.58	1.024
950904	1759	14.13	34	01.35	106	51.94	4.34	1.40	0.25	0.25	0.58	1.024
950904	1849	52.10	34	06.04	106	48.29	5.54	2.41	0.23	0.25	0.53	0.627
950914	1607	30.02	34	06.05	106	48.24	4.91	1.14	0.19	0.21	0.32	1.033
950922	1037	57.84	34	18.26	106	55.44	6.35	0.84	0.23	0.29	0.41	1.328
950922	2245	56.25	34	21.30	106	42.58	8.71	1.35	0.33	0.43	0.37	0.914
950924	1603	51.57	34	02.00	107	01.73	7.56	1.37	0.20	0.26	0.26	1.415
950924	1606	44.74	34	02.07	107	01.97	9.22	0.16	0.30	0.36	0.29	0.890
950924	1610	25.43	34	01.94	107	01.91	8.89	0.33	0.29	0.35	0.28	0.887
950924	1758	40.95	34	01.78	107	01.69	7.81	1.57	0.21	0.21	0.28	1.225
950924	1810	55.02	34	01.71	107	01.70	8.80	0.59	0.28	0.26	0.29	0.750
950925	0445	57.79	34	01.76	107	01.67	8.54	1.49	0.21	0.22	0.28	1.192
950828	1556	55.66	34	12.32	106	56.42	3.61	1.52	0.22	0.28	0.35	1.417
950828	1651	25.57	34	12.47	106	56.97	3.51	1.49	0.30	0.37	0.38	1.725
950911	0216	06.20	34	12.31	106	56.25	2.73	2.47	0.21	0.23	0.72	0.945
950911	0218	02.50	34	12.31	106	56.15	2.54	2.11	0.21	0.23	0.70	1.331
950911	1141	15.85	34	12.25	106	56.13	2.10	2.38	0.21	0.23	0.81	0.862
951012	1612	24.60	34	12.16	106	56.73	4.43	1.44	0.20	0.22	0.25	1.541
891130	0008	03.65	34	27.99	106	52.46	6.54	0.97	0.25	0.31	0.51	1.455
891130	0017	18.25	34	27.40	106	53.11	4.35	0.55	0.27	0.47	0.42	1.222
891130	0042	34.46	34	27.52	106	52.97	4.22	0.08	0.26	0.50	0.49	0.837
891130	0152	31.41	34	27.51	106	53.27	3.77	0.48	0.31	0.51	0.74	1.011
891130	0206	29.15	34	27.52	106	52.88	4.48	0.43	0.28	0.54	0.68	0.884
891130	0715	42.11	34	27.51	106	52.74	4.98	-0.25	0.27	0.54	0.64	0.805
891130	1219	59.20	34	27.26	106	52.45	4.54	-0.32	0.27	0.55	0.73	0.839
891130	2009	07.28	34	26.82	106	52.80	5.18	0.61	0.29	0.41	0.49	0.831
891130	2022	49.57	34	26.57	106	52.89	5.13	0.20	0.30	0.45	0.52	0.637
891130	2107	45.10	34	26.96	106	52.92	5.49	0.49	0.30	0.48	0.66	1.183
891201	0033	00.56	34	27.54	106	52.65	5.09	-0.14	0.27	0.54	0.42	0.700
891201	0426	43.41	34	27.20	106	52.83	5.59	-0.09	0.30	0.54	0.46	0.773
891201	0452	22.64	34	26.38	106	52.98	4.57	-0.21	0.29	0.45	0.44	0.702
891201	0520	01.85	34	27.25	106	53.13	6.29	0.44	0.34	0.52	0.48	0.769
891201	0523	09.30	34	26.75	106	52.90	2.53	0.02	0.29	0.42	0.49	1.060
891201	1136	39.98	34	27.37	106	53.32	6.12	0.64	0.31	0.49	0.43	0.840
891201	1441	05.45	34	28.16	106	52.91	3.95	0.27	0.36	0.56	0.50	0.719
891201	1522	35.54	34	27.28	106	52.60	5.55	0.51	0.37	0.52	0.47	0.913
891201	1539	06.96	34	27.33	106	52.90	4.27	-0.17	0.34	0.50	0.49	0.785
900130	0024	28.37	34	27.43	106	52.58	3.83	-0.49	0.26	0.55	0.61	1.118
900130	0148	40.94	34	27.62	106	52.40	4.95	0.19	0.35	0.56	0.42	0.755
900130	0206	15.90	34	26.78	106	52.57	3.00	0.28	0.32	0.52	1.02	0.962
900130	0223	36.15	34	27.76	106	52.94	4.35	0.97	0.30	0.61	0.52	0.883
900130	0313	59.67	34	27.23	106	52.61	5.21	0.07	0.27	0.51	0.56	0.841
900130	0329	17.49	34	27.67	106	52.62	5.62	0.10	0.30	0.58	0.38	1.022
900130	0538	37.36	34	27.36	106	52.39	5.90	0.11	0.28	0.53	0.57	0.915
900130	0642	55.54	34	27.28	106	52.61	5.87	0.38	0.29	0.47	0.50	1.310
900130	0654	54.16	34	26.87	106	52.76	3.35	0.65	0.29	0.50	0.89	1.288
900130	0745	21.33	34	27.30	106	52.73	4.64	-0.18	0.25	0.54	0.74	0.880
900130	0915	13.40	34	26.88	106	53.00	3.60	0.35	0.28	0.48	0.74	0.893
900130	1107	16.24	34	27.89	106	52.12	6.26	1.66	0.23	0.22	0.45	1.905
900130	1429	16.59	34	26.71	106	53.00	4.59	0.57	0.32	0.50	0.52	0.765
900130	1558	46.63	34	27.21	106	52.84	3.61	1.54	0.24	0.34	0.85	1.372
900130	1604	25.71	34	27.54	106	52.73	6.52	1.24	0.25	0.20	0.51	1.601

yymmdd	hhmm	sec	latitude		longitude		depth	mag	xerr	yerr	derr	R
900130	1639	45.68	34	27.46	106	52.38	6.16	1.47	0.26	0.23	0.56	1.490
900130	1750	35.29	34	26.87	106	52.68	3.75	0.19	0.23	0.42	0.54	1.181
900130	1818	57.32	34	27.69	106	52.86	5.98	1.27	0.25	0.29	0.46	1.483
900131	0043	03.10	34	28.11	106	51.91	3.52	0.69	0.31	0.62	0.68	1.027
900131	0115	41.51	34	27.12	106	52.02	5.50	1.19	0.35	0.62	0.77	0.941
900131	0355	52.79	34	26.94	106	52.61	3.87	0.06	0.37	0.53	0.50	0.856
900131	0546	04.50	34	28.19	106	52.69	5.15	0.34	0.32	0.58	0.53	0.854
900131	0711	50.61	34	27.55	106	52.72	5.63	-0.04	0.23	0.57	0.69	1.247
900131	1059	06.34	34	27.99	106	51.93	5.29	0.41	0.28	0.61	0.41	1.148
900131	1726	09.56	34	27.41	106	52.23	4.84	0.20	0.25	0.49	0.60	1.210
900131	1941	22.43	34	27.63	106	52.73	4.73	0.06	0.24	0.61	0.97	0.862
900201	0150	02.61	34	27.78	106	52.99	4.97	0.68	0.25	0.39	0.50	1.135
900201	0208	07.25	34	27.38	106	53.37	4.48	0.63	0.23	0.42	0.68	1.399
900201	0836	07.60	34	27.08	106	52.48	5.27	-0.15	0.29	0.53	0.78	1.373
900201	0836	57.71	34	27.90	106	52.24	5.67	-0.02	0.27	0.55	0.57	1.262
900201	1502	03.08	34	27.46	106	52.21	4.74	0.31	0.30	0.58	0.59	1.019
900321	1756	54.41	34	27.24	106	52.11	6.24	1.41	0.34	0.37	0.82	0.877
900321	1801	36.98	34	26.85	106	52.44	5.17	1.45	0.26	0.38	0.86	1.144
900322	1216	59.55	34	26.80	106	52.79	4.53	1.23	0.26	0.35	0.78	0.933
900422	1525	04.76	34	27.27	106	52.85	6.20	1.64	0.28	0.32	0.66	1.278
900505	1509	15.89	34	26.96	106	53.30	6.20	1.72	0.27	0.37	0.77	0.834
900507	1858	07.70	34	27.09	106	52.63	5.64	1.26	0.25	0.36	0.63	1.073
900514	2241	19.57	34	27.57	106	52.68	5.57	0.64	0.20	0.35	0.77	1.069
900516	1640	30.15	34	27.49	106	52.41	5.46	1.05	0.23	0.25	0.43	1.268
900607	2242	55.60	34	27.38	106	52.69	8.49	2.07	0.30	0.36	0.61	1.003
900610	1842	54.02	34	27.58	106	52.37	7.02	1.34	0.23	0.24	0.75	1.325
900616	0125	09.88	34	27.21	106	52.05	5.23	1.91	0.29	0.26	0.68	1.856
900616	0316	06.58	34	27.42	106	52.26	6.13	1.02	0.23	0.24	0.66	1.375
900704	1803	13.66	34	26.97	106	52.96	4.84	0.79	0.26	0.26	0.77	0.618
900925	0537	25.39	34	27.06	106	51.90	6.67	1.54	0.30	0.23	0.67	1.196
901026	0246	35.86	34	27.06	106	52.21	6.55	1.49	0.25	0.20	0.56	0.934
901108	1124	17.41	34	26.97	106	52.01	6.63	1.24	0.26	0.23	0.62	1.204
901109	2311	42.24	34	27.19	106	51.76	7.07	1.01	0.24	0.22	0.50	1.412
901110	0004	18.69	34	27.29	106	51.34	6.97	1.10	0.24	0.22	0.44	1.355
901111	1004	06.16	34	26.63	106	52.65	6.14	0.39	0.23	0.41	0.55	1.580
901111	1543	52.61	34	26.48	106	52.64	6.28	0.87	0.17	0.39	0.49	1.496
901112	0330	47.14	34	27.24	106	53.09	7.82	2.05	0.23	0.26	0.62	2.092
901112	0407	23.62	34	26.38	106	52.68	7.08	0.94	0.26	0.43	0.73	1.474
901112	0529	44.16	34	26.19	106	52.88	5.27	0.24	0.22	0.42	0.70	2.133
901112	0741	17.02	34	26.59	106	53.31	4.45	0.78	0.20	0.35	0.43	2.145
901112	1323	45.12	34	27.29	106	52.47	9.32	2.04	0.22	0.19	0.49	2.340
901112	2049	45.02	34	26.57	106	52.71	6.58	1.08	0.21	0.37	0.60	1.472
901112	2304	44.95	34	26.99	106	53.01	4.32	0.42	0.25	0.43	0.55	0.980
901113	0301	02.91	34	25.91	106	53.30	3.91	0.17	0.23	0.43	1.00	1.709
901125	0532	16.47	34	27.01	106	52.44	6.88	1.47	0.23	0.21	0.52	1.553
901125	0841	52.91	34	27.20	106	52.15	7.03	1.36	0.22	0.24	0.55	0.936
901126	0610	09.66	34	26.61	106	53.11	7.15	1.87	0.25	0.31	0.48	1.577
901130	1546	36.93	34	27.69	106	52.80	6.05	1.32	0.25	0.29	0.53	1.372
901202	2306	28.85	34	27.50	106	52.14	7.73	0.96	0.24	0.26	0.27	1.172
901203	0002	39.57	34	27.46	106	52.15	6.58	0.87	0.34	0.29	0.55	1.128
901203	0408	43.26	34	27.38	106	51.58	7.37	0.89	0.24	0.28	0.47	1.167
901204	2348	11.15	34	26.72	106	52.19	4.18	0.99	0.28	0.34	0.55	1.463

yymmdd	hhmm	sec	latitude		longitude		depth	mag	xerr	yerr	derr	R
901205	0515	04.10	34	26.92	106	52.41	8.53	2.12	0.30	0.24	0.65	1.219
910306	1817	26.18	34	26.84	106	52.04	5.44	1.03	0.24	0.36	0.51	0.742
910308	0732	27.57	34	26.53	106	52.27	5.40	1.10	0.24	0.25	0.54	1.101
910313	0952	03.77	34	26.72	106	52.85	4.19	1.41	0.24	0.28	0.52	0.806
910326	0101	53.56	34	26.87	106	52.29	6.14	0.84	0.23	0.23	0.48	1.327
910425	1609	21.68	34	27.52	106	53.00	5.35	1.04	0.24	0.23	0.40	1.528
910430	2043	31.07	34	27.06	106	51.64	6.57	1.09	0.23	0.22	0.49	1.015
910519	0043	49.33	34	27.23	106	51.68	6.52	0.86	0.25	0.24	0.58	1.262
910605	0541	05.49	34	27.48	106	51.59	6.61	0.82	0.30	0.29	0.46	0.858
910605	2248	56.54	34	27.33	106	51.49	6.54	0.59	0.23	0.21	0.47	1.311
910606	0034	16.10	34	27.35	106	51.38	5.88	0.58	0.21	0.23	0.45	1.284

This dissertation is accepted on behalf of the
faculty of the Institute by the following committee:

Advisor

April 4, 1997

Date

I release this document to the New Mexico Institute of Mining and Technology.

4/4/97

Student's Signature

Date